UNIVERSITE D'ABOMEY - CALAVI (UAC)

INSTITUT NATIONAL DE L'EAU

Federal Ministry of Education and Research

WASCAL
West African Science Service Center on Climate Change and Adapted Land Use

Registered under N°:3133-17/UAC/VR-AARU/SA

A DISSERTATION

Submitted

In partial fulfillment of the requirements for the degree of

DOCTOR of Philosophy (PhD) of the University of Abomey-Calavi (Benin Republic)

In the framework of the

Graduate Research Program on Climate Change and Water Resources (GRP-CCWR)

By

Mawuli LUMOR

Public defense on: 05/30/2017

======

ESTIMATION OF STREAMFLOW AND SEDIMENT LOADS IN THE WHITE VOLTA BASIN UNDER FUTURE CLIMATE PROJECTIONS

======

Supervisors:

Abel AFOUDA, Professor, University of Abomey-Calavi, Benin
Bernd DIEKKRÜGER, Professor, University of Bonn, Germany
Barnabas AMISIGO, Director of Research, WRI of CSIR, Ghana

======

Reviewers:

Kwasi PREKO, Professor, KNUST-Kumasi, Ghana
Bamory KAMAGATE, Associate Professor, Nangui Abrogoua University, Cote d'Ivoire
Luc SINTONDJI, Associate Professor, University of Abomey-Calavi, Benin

======

JURY

Boukari MOUSSA	Professor, University of Abomey-Calavi, Benin	President
Luc SINTONDJI	Associate Professor, University of Abomey-Calavi, Benin	Rapporteur
Bamory KAMAGATE	Associate Professor, Nangui Abrogoua University, Cote d'Ivoire	Rapporteur
Emmanuel LAWIN	Associate Professor, University of Abomey-Calavi, Benin	Examiner
Abel AFOUDA	Professor, University of Abomey-Calavi, Benin	Supervisor

Dedication

To Jantitri, my Wife and my sons, Elikem, Eyram and Enam.

Acknowledgement

This PhD work is realized in the framework of the West African Science Service Center on Climate Change and Adapted Land use (WASCAL and funded by the **German Ministry of Education and Research (BMBF) in collaboration with the Benin Ministry of High Education and Scientific Research** (MESRS)).

I am most grateful to God Almighty for his grace and mercy and for seeing me through this study. I am indeed indebted to Dr. Barnabas Amisigo, Prof. Dr. Bernd Diekkrüger and Prof. Abel Afouda for accepting to supervise my research. I am indeed highly indebted to Dr. Amisigo for the technical advice and invaluable support he gave me throughout this study. You did not only supervise my work but you held my hand and lifted me up when I was down. I am most grateful.

My heartfelt gratitude also goes to the Federal Government and People of Germany through the German Federal Ministry of Education and Research (BMBF) under the auspices of the West Africa Science Service Centre for Climate Change and Adapted Land Use (WASCAL) for sponsoring my study. My gratitude also goes to the Water Resources Commission, my employer, and the Executive Secretary, Mr. Ben Ampomah, who granted me the permission to take up this award. To the Volta Basin Authority, VBA, special mention of Dr. Jacob Tumbulto, I am most grateful for permitting me to use your hydrometric instruments during my field work. To my tutor and inspirer in the field of hydrology, Mr. Aaron B. Aduna, I simply say "ayekooo".

I am also most grateful to Dr. Boubacar Barry of the Competence Centre, WASCAL who believed in me and encouraged me to take up this challenge. Special thanks also go to Mr. Danladi Anafo of the Volta River Authority (VRA) formerly with the Hydrological Services Department (HSD) in Ghana for assisting me in my field work. I will also want to express my gratitude to the Hydrological Services Department (HSD) for allowing me to use their instruments during this study.

Finally, I wish to dedicate this work to my family, my lovely wife – Patience Jantitiri Tiko-Lumor, my sons – Elikem, Eyram and Enam and not forgetting Awenia for enduring my absence and late nights while undertaking this study. To my Mom, Madam Hilda F.Adda and my Dad, Mr. Charles A. S. Lumor, I am wholly indebted for your love, guidance and support.

Abstract **:**

Among the major sub-catchments of the Volta Basin is the White Volta Basin which is shared between Burkina Faso and Ghana in West Africa. Recent socio-economic developments in the two riparian countries have placed immense pressure on the quantity and quality of the water resources in the basin. Information on streamflow and sediment loads in the basin will therefore play a vital role in sustainably developing and managing the water resources of the basin. This study therefore seeks to estimate long-term time-series of sediment loads by evaluating empirical relationships between turbidity, streamflow and suspended sediment concentration using regression models. An evaluation of the impact of climate projections on streamflows and sediment loads in the White Volta Basin using the Soil Water Assessment Tool (SWAT) coupled with an ensemble of three Regional Climate Models (RCMs) under the CORDEX-Africa Project was also undertaken. Regression analysis showed that a simple linear regression equation derived by relating turbidity and suspended-sediment concentration with a validated model efficiency of 93% was the better model for estimating long-term suspended sediments loads in the White Volta Basin. The SWAT model was calibrated and validated for the periods 1991-2003 and 2004-2013 respectively with Nawuni hydrometric station as the watershed outlet. The model was also spatially validated at Pwalugu and Nasia. Analysis of the water balance of the basin shows that 4.90% of the simulated mean annual precipitation is converted to surface runoff while approximately 85% evapotranspires. The results also show that, based on the period 1990-2010, the White Volta Basin contributes annually an estimated 8.2106 metric tons of sediment load into the Volta Lake barring any deposition between Nawuni and the lake. The RCM-GCMs ensembles were used to downscale precipitation and minimum and maximum temperature for the reference period (1990-2010) and the future period (2031-2050). All the RCM-GCMs ensembles forced by the Representative Concentration Pathways (RCP4.5 and 8.5) projects a rise in temperature by 2.3°C and 2.7°C respectively. The RCM-GCMs however predicted mixed projections for precipitation. The downscaled climate data was then used as inputs into the calibrated SWAT model to simulate and compare the water balance of the study area for the reference and future periods. Similar to the simulated precipitation, projected surface runoff and actual evapotranspiration have mixed results based on the RCM-GCM ensemble used for the simulation. Surface runoff is however projected to increase on average by 23.8% and 27.8% for RCP4.5 and RCP8.5 respectively whereas evapotranspiration is projected to decline on average by 1.5% and 1.0% based on RCP4.5 and RCP8.5 respectively. The results also show that irrespective of the scenario, annual sediment loads in the basin is projected to increase on average by 24.7% and 26.3% under RCP4.5 and RCP8.5 respectively. Finally, extreme value analysis of maximum precipitation for the wet months of July, August and September showed that the magnitude of extreme rainfall events are likely to increase in the future with direct consequence for the generation and transport of sediment loads in the basin.

Key words **:** White Volta Basin, SWAT, streamflow, sediment loads, climate change

Synthesis (Extended abstract in French)

Résumé

La Volta Blanche est l'un des principaux sous-bassins de la Volta. Elle couvre environ 106 000 km^2 et est partagée entre le Burkina Faso et le Ghana en Afrique de l'Ouest. Les récents développements socio-économiques dans les deux pays riverains ont mis une pression énorme sur la quantité et la qualité des ressources en eau dans le bassin. Par exemple, les développements des infrastructures existants dans le bassin, notamment l'hydroélectricité et l'irrigation, ont déjà eu des impacts sur le cycle hydrologique, et les plans de développement futurs pourraient menacer la durabilité des ressources en eau. La connaissance des débits d'écoulement et des transports de sédiments dans le bassin jouera donc un rôle vital dans le développement durable et la gestion des ressources en eau du bassin. Toutefois, les données sur les charges de sédiments en suspension sont limitées dans le bassin de la Volta Blanche en raison du manque de ressources humaines et financières pour la mesure systématique des charges ou concentrations des sédiments. Cette étude vise donc à estimer l'écoulement fluvial et les charges de sédiments dans le bassin de la Volta Blanche à l'aide du model éco-hydrologique SWAT (Soil Water Assessment Tool). Cette recherche permettra également d'améliorer la compréhension de l'impact des changements climatiques sur les débits et les charges des sédiments dans le futur dans le bassin à l'aide du modèle climatique régional de Prévision et Recherche Météorologique (Weather Research Forecasting). Des mesures de terrain ont également été réalisées pour relever les concentrations de sédiments en suspension afin d'étalonner une courbe d'évaluation des sédiments. Sur la base de la relation entre la turbidité et la concentration de sédiments en suspension, un modèle de régression linéaire simple a été développé et utilisé pour calculer à long terme, les charges de sédiments en suspension et qui ensuite ont servir pour le calage et la validation du modèle SWAT. Sur la base des mesures sur le terrain, un facteur de correction de 34% a été appliqué pour corriger la sous-estimation de la mesure de la concentration de sédiments en suspension. Une simple équation de régression linéaire entre la turbidité relative et la concentration en suspension de sédiments a été mise au point avec un coefficient de détermination R^2 de 93%. Cette relation linéaire a été utilisée pour calculer les charges des sédiments en suspension à long terme dans le bassin de la Volta Blanche. Le modèle SWAT a été calibré pour la période de 1991 à 2003 et validé pour la période 2004-2013 à Nawuni comme exutoire du bassin versant de la Volta Blanche. Le modèle a également été validé dans l'espace à Pwalugu et Nasia. L'analyse du bilan hydrique du bassin montre que 4,90% des précipitations moyennes annuelles sont convertis en ruissellement de surface, tandis qu'environ 85% sont transformés en évapotranspiration. Les résultats montrent également que de 1990 à 2010, le bassin de la Volta Blanche produit chaque année 8.2106 tonnes de charges de sédiments qui sont déversés dans le lac Volta sauf en cas de dépôt entre Nawuni et le lac. Un ensemble de trois modèles climatiques régionaux (RCM) et deux modèles climatiques globaux (GCM) dans le cadre du projet CORDEX-Africa a été utilisé pour désagréger les précipitations et températures minimales et maximales pour la période de référence (1990-2010) et la période future (2031-2050). L'ensemble des RCM-MCGs sélectionnés et forcés par RCP4.5 et 8.5 projettent une élévation de température de 2,3°C et 2,7 °C respectivement. Les RMC-GCMs ont prédit cependant des projections mixtes pour les précipitations. Les données climatiques désagrégées ont ensuite été utilisées comme entrées dans le modèle hydrologique calibré (SWAT), pour simuler le bilan hydrique du bassin de la Volta Blanche pour la période de référence (1990-2010) et pour le période futur (2031-2050). Comme pour les précipitations simulées, le ruissellement de surface et l'ETR présentent des résultats mixtes pour les RCM-GCMs utilisés. Les eaux de ruissellement cependant devraient augmenter en moyenne de 23,8% et 27,8% pour respectivement RCP4.5 et RCP8.5, alors que l'évapotranspiration devrait diminuer en moyenne de 1,5% et 1,0% pour respectivement RCP4.5 et RCP8.5. Les résultats montrent aussi que quel que soit le scénario (RCPs), les charges de sédiments annuelles dans le bassin devraient augmenter de 24,7% et 26,3% pour respectivement RCP4.5 et RCP8.5. Enfin, l'analyse des valeurs extrêmes des précipitations maximales pour les mois humides de Juillet, Août et Septembre a montré que l'ampleur des événements de précipitations extrêmes est susceptible d'augmenter à l'avenir avec comme conséquence directe la production et le transport de charges de sédiments dans le bassin.

1 Introduction

Le bassin de la Volta Blanche est l'un des principaux sous-bassins de la Volta situé en Afrique de l'Ouest et couvrant environ 106 000 km2 et est partagé majoritairement entre le Burkina Faso et le Ghana. Le bassin est actuellement confronté à de nombreux défis tels que les inondations, la sécheresse, les variations spatio-temporelles élevées des précipitations, la déforestation, la dégradation des sols, les changements climatiques et le taux de croissance de la population. Ces défis imposent une pression sur la quantité et la qualité des ressources en eau dans le bassin.

Le développement actuel des infrastructures dans le bassin a déjà eu des incidences sur le cycle hydrologique et les futurs plans de développement constitueraient une menace pour la durabilité des ressources si elles ne sont pas correctement gérées. Le barrage de Bagre, situé au Burkina Faso, constitue un stock de l'eau à la fois pour la production d'énergie hydroélectrique et l'irrigation. En aval, la République du Ghana prévoit de développer deux barrages à double usage à Pwalugu et Dobaya pour la production d'énergie hydroélectrique et l'irrigation. Ce développement conjugué à l'évolution du climat a un impact direct sur la qualité et la quantité des ressources en eau dans le bassin.

Le changement climatique, la disponibilité de l'eau et la dégradation de la qualité de l'eau ont déjà été identifiés comme une question importante dans le bassin. En particulier, le transport de sédiments dans les pays riverains constitue une source majeure de dégradation des ressources dans les eaux partagées. Les études de bathymétrie de la morphologie initiale et actuelle du lit de réservoir dans les régions semi-arides du Burkina Faso montrent que les réservoirs ont perdu environ 10-15% de leur capacité de stockage d'origine et plus de 60% de leur volume de stockage inactif au cours des 15 à 20 ans. Au cours de cette période, une couche de sédimentation de 0,3 m à 0,5 m d'épaisseur s'est accumulée sur les lits du réservoir. Néanmoins, des pertinentes questions demeurent à propos de la quantité de charges sédimentaires générées et transportées dans le bassin de la Volta Blanche et de l'impact potentiel d'un climat changeant.

Pour répondre à ces préoccupations, une étude a été effectuée dont les objectifs spécifiques sont: (a) Élaborer et évaluer une relation empirique entre la turbidité et les mesures de la concentration de sédiments en suspension en utilisant des modèles de régression et calculer des séries chronologiques à long terme de charges sédimentaires. (b) Évaluer la capacité du modèle hydrologique SWAT à reproduire les débits d'écoulement et les charges de sédiments dans le bassin de Volta Blanche. (c) Évaluer l'impact du changement climatique sur les écoulements et les charges de sédiments dans le bassin de la Volta Blanche en utilisant SWAT couplé aux modèles climatiques régionaux du projet CORDEX-Afrique et (d) Évaluer l'impact des précipitations extrêmes sur les écoulements et les charges sédimentaires dans le bassin de la Volta Blanche dans un contexte de changement climatique.

2 Domaine d'étude

Le bassin de la Volta Blanc est situé entre les latitudes 8° 50' N et 14° 30' N et les longitudes 0° 06' E et 2° 50' W. Les bassins limitrophes de la zone d'étude sont le bassin d'Oti à l'est, le bassin de la rivière Volta Noir à l'ouest et le Volta principale au sud. Sa limite nord

est le Burkina Faso avec le Ghana couvrant le sud. La Figure 2.2 présente la carte du bassin de Volta Blanche.

Le bassin de la Volta Blanche, le deuxième bassin le plus important du bassin de la Volta, couvre environ 100 148 km^2 à Nawuni et représente environ 26% du bassin versant total de Volta. Au Ghana, le bassin couvre environ 50 000 km^2 et constitue 20% de la superficie totale du Ghana. Environ 47% de la superficie totale du bassin de la Volta Blanche se situe au Ghana et 52% au Burkina Faso avec les 1% restants au Togo. Les rivières Volta Rouge, Nasia, Nabogo et Kulpawn/Sissili sont les principaux affluents du bassin de la Volta Blanche. Les rivières Volta Rouge et Kulpawn/Sissili prennent leurs sources dans les parties centrale et nord-est du Burkina Faso (WRC, 2008).

Le barrage hydroélectrique de Bagre qui couvrant une superficie totale de 33 120 km^2 a considérablement affecté l'hydrologie de la Volta Blanche. Le débit moyen annuel du barrage au cours de la dernière décennie est estimé à 29,7 m^3 / s (WRC, 2008).

3 Matériaux et méthodes

De nombreuses publications sur les modèles de rendement des sédiments, les courbes d'étalonnage des sédiments et des méthodes de mesure de la concentration de sédiments en suspension ont été examinées pour comprendre leurs techniques et leurs applications. Les mérites relatifs et les lacunes de ces approches méthodologiques dans les études sur le transport des sédiments ont été discutés. On a constaté qu'il n'y avait pas de méthode ou d'approche universellement acceptée pour modéliser le rendement des sédiments d'un bassin versant ainsi que pour la collecte des données sur les champs des mesures de décharge des sédiments. Le choix de toute méthodologie dépend de la disponibilité des ressources (données secondaires, financières, équipements, etc.) à la disposition du chercheur.

La collecte de données sur le terrain impliquant des mesures de sédiments en suspension, des mesures de débits d'écoulements de la rivière et des données secondaires, qui comprennent les mesures de turbidité de Ghana Water Company Ltd (GWCL) situé à Nawuni et les débits de sédiments en suspension de l'institut de recherche sur l'eau, (Water Research Institute) de CSIR a été faite pour la zone d'étude. Afin d'inclure les débits critiques dans la collecte de données sur le terrain, un échantillonnage journalier de la concentration de sédiments en suspension a été entrepris en engageant des volontaires locaux qui ont pris des échantillons journaliers d'eau par immersion en surface avec un récipient d'un litre. Les données journalières sur les immersions en surface ont ensuite été améliorées par couplage avec un échantillonnage mensuel intégré en profondeur.

Les méthodes reconnues de collecte des données sur les sédiments en suspension sont fastidieuses, coûteuses et nécessitent beaucoup de main-d'œuvre. De plus, en raison de la variabilité spatiale et temporelle associée au transport de sédiments en suspension dans une rivière, la précision de l'estimation de la concentration de sédiments en suspension (CSS) peut être inconnue. Cependant, l'utilisation de techniques de substitution fournit une estimation plus précise des fluctuations des sédiments en surveillant continuellement la turbidité tout au long d'un événement de tempête. Dans cette étude, l'analyse de régression a été mise à contribution pour développer des relations empiriques entre le débit de la rivière, la concentration de sédiments en suspension et la turbidité dans le bassin de la Volta Blanc. La

méthodologie utilisée dans cette étude suit généralement les techniques décrites par Rasmussen et al., (2009). Les relations dérivées seront ensuite utilisées pour obtenir des charges de sédiments sur le long terme pour calibrer et valider le modèle SWAT.

L'analyse de sensibilité des paramètres du modèle SWAT aux débits d'écoulements et aux charges de sédiments a été faite. Le modèle a ensuite été calibré à Nawuni pour une période de dix ans allant de 1994 à 2003. Une période de trois ans, 1991-1992 a été utilisée comme période de mise en route du modèle. Le calage a été fait en appliquant le programme SUFI2 dans SWAT-CUP en considérant les données (débits et sédiments) au pas de temps annuel, mensuel et journalier observés à la sortie du bassin hydrographique à Nawuni.

Cinq critères de performance ont été utilisés dans SWAT-CUP pour l'évaluation de la performance du modèle : coefficient de détermination (R^2), coefficient de Nash-Sutcliffe (NS) et pourcentage de biais PBIAS. D'autres critères de performances utilisées pendant le calage sont le p-facteur et le r-facteur (Abbaspour, et al., 2007).

L'impact du changement climatique sur les débits et les charges sédimentaires a été analysé en réduisant les séries climatiques projetées pour le futur en utilisant trois modèles climatiques régionaux (MCR) du projet CORDEX-Afrique. Le projet CORDEX-Afrique est la branche Afrique de l'initiative CORDEX qui vise à fournir un ensemble de projections régionales et futures de haute résolution sur le changement climatique sur le domaine africain dans le cadre du cinquième rapport d'évaluation du GIEC (IPCC, 2014). Les MCRs dans le projet CORDEX-Afrique ont une résolution spatiale de 0,44° x 0,44° (système de coordonnées polaires tournées) et utilisent des sorties des projections CMM5 GCM couvrant la période 1950-2100 en tant que conditions aux limites. La simulation des projections futures du changement climatique dans le projet CORDEX-Afrique est basée sur le renforcement de GCM sous les voies de concentration représentatives (scenario RCP) (Vuuren et al., 2011).

Deux scénarios de projection du changement climatique, RCP4.5 et RCP8.5, ont été utilisé dans cette étude. Le RCP4.5 est un scénario d'émissions mondiales à long terme de gaz à effet de serre, d'espèces de courte durée et d'utilisation terrestre-couverture qui stabilisent le forçage radiatif à 4,5 Wm^{-2} en l'an 2100 sans jamais dépasser cette valeur (Thomson et al., 2011). Contrairement à d'autres scénarios, le RCP4.5 est un scénario de stabilisation. En revanche, le RCP8.5 représente un scénario d'émission de haut niveau et correspond à un forçage radiatif croissant à 8.5 Wm^{-2} en l'an 2100 (Moss et al., 2010).

Les trois MRC utilisées dans cette étude et leurs GCM sont : CCLM-MPI-ESM, HIRHAM5-EARTH et RACMO22T-EARTH. Les trois MRC ont été sélectionnés en raison de la disponibilité de séries climatiques traitées couvrant la période 1950 à 2100 pour le projet CORDEX-Afrique. La période d'intérêt retenue pour cette étude était 1991-2010 pour la période référencée et 2031-2050 pour le futur.

4 Résultats

Le meilleur modèle de régression obtenu pour estimer la concentration de sédiments en suspension (CSS) en fonction de la turbidité est le modèle de régression linéaire simple (RLS) obtenu en faisant une transformation logarithmique de la relation (i) ci-après. Le modèle RLS final obtenu pour le bassin de la Volta Blanche à Nawuni sur la base de la turbidité et de la CSS est donné par:

$$CSS = 0.027T^{1.62} \qquad \text{(i)}$$

Où CSS = concentration de sédiments en suspension (mg/l) et T = turbidité (NTU).

Le modèle de RLS le mieux adapté représentant l'intervalle de confiance de 90% est présenté à la Figure i (a). La figure montre que, en tenant compte du niveau de signification de 10%, les informations apportées par les variables explicatives sont significativement meilleures que celles apportées par la moyenne simple. La Figure i (b) montre également les observations de CSS en fonction des valeurs prédites de CSS dans l'espace logarithmique de base 10. La figure montre une répartition uniforme des points autour de la trame individuelle, ce qui implique que le modèle n'a pas de manière significative sur ou sous-estimé le CSS.

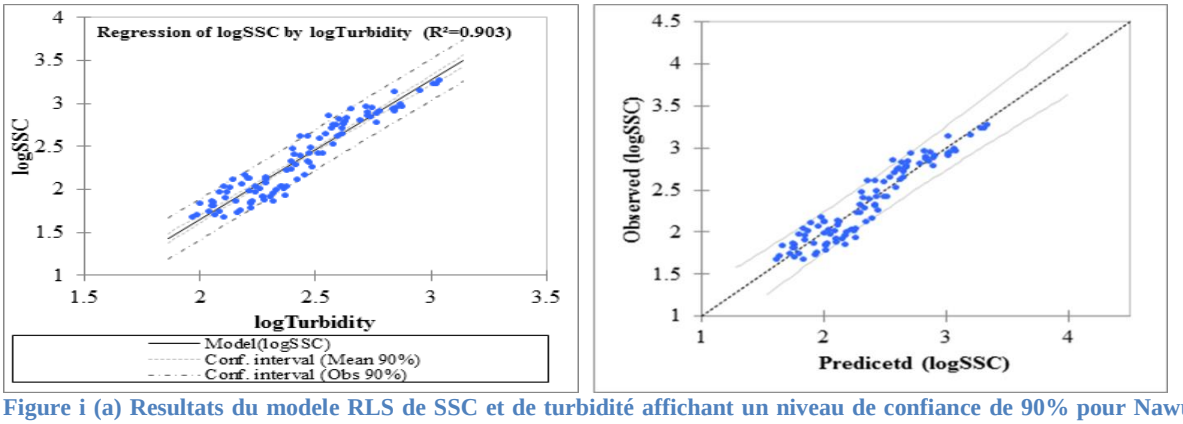

Figure i (a) Resultats du modele RLS de SSC et de turbidité affichant un niveau de confiance de 90% pour Nawuni (sept. 2012-déc. 2013) et (b) Comparaison des valeurs predictes par le modèle RLS par rapport à la CSS observée montrant le niveau de confiance de 90%

Le modèle RLS (équation i) a été utilisé pour estimer CSS en fonction des données de turbidité à long terme obtenues auprès de Ghana Water Company Ltd. Les charges de sédiments à long terme ont ensuite été calculées en utilisant l'équation 3.16 (Horowitz, 2003):

$$SSL = 0.0864 \cdot Q_w \cdot CSS \qquad \text{(ii)}$$

Où SSL=charge sédimentaire quotidienne (tonnes métriques/jour), 0.0864=facteur de conversion, Q_w = débit (m^3/s) et SSC est la concentration en sédiments en suspension (mg/l).

Les résultats du calage du modèle SWAT au pas de temps mensuel pour les débits et les charges de sédiments sont présentés dans la Figure (ii- (a) et (b)) respectivement pour la comparaison visuelle.

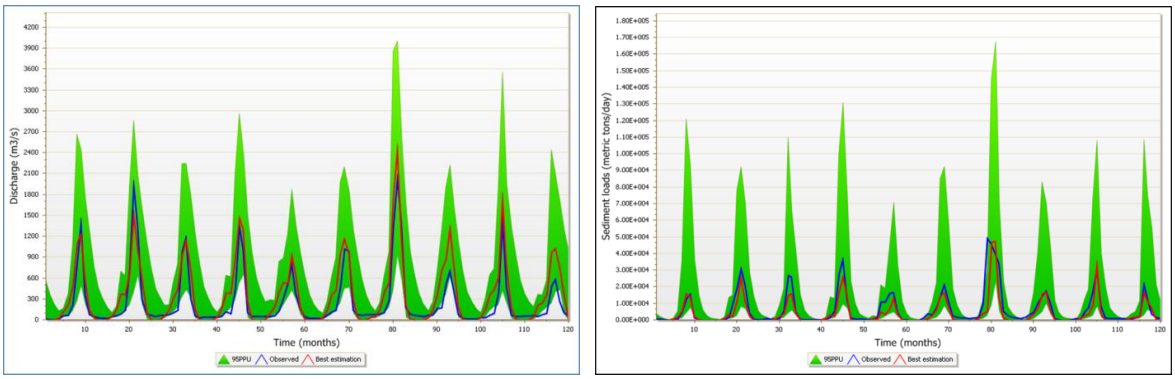

Figure ii 95PPU (vert sombre) dérivé par SUFI-2 avec fonction objectif NS pour les debits mensuels (a) et (b) pendant la période de calage (1994-2003).

La zone ombrée verte de la Figure ii (a) et (b) représente l'incertitude du modèle tandis que les lignes bleue et rouge représentent respectivement les séries temporelles mensuelles

observées et simulées. La performance du modèle pour le débit mensuel et les charges de sédiments peuvent généralement être considérée comme bonnes en fonction des performances générales recommandées pour le temps mensuel par Abbaspour et al. (2007) et Moriasi et al. (2007). Dans la Figure ii (a), on constate que le modèle a sous-estimé les débits maximaux pour les deux premières années, c'est-à-dire avant l'introduction du barrage de Bagre en 1995 et a estimé très bien le pic des quatre suivantes années. Le modèle a ensuite sous-estimé les débits maximaux pour les quatre années restantes, c'est-à-dire entre 2000 et 2003. Le modèle a généralement sous-estimé les débits faibles. En outre, pendant le calage, il y a eu une différence de -13% entre les débits mensuels moyens observés et simulés. De même, au niveau de la Figure ii (b), on constate que la performance du modèle dans l'estimation des charges maximales des sédiments pendant les deux premières années a été satisfaisante, c'est-à-dire avant l'introduction du barrage de Bagre en 1995 et ensuite le modèle a sous-estimé Les pics de charge des sédiments pour les années restantes, sauf en 1996 et 1997. Le modèle a, de manière satisfaisante estimé les faibles charges de sédiments.

Comme pour le calage du modèle, les statistiques d'évaluation des performances du modèle pour les débits mensuels et les charges sédimentaires pendant la validation ont été jugées acceptable aussi bien pour les débits que pour les charges de sédiments en comparaison aux performances générales recommandées pour le temps mensuel par Abbaspour et al. (2007) et Moriasi et al. (2007). Les Figures iii (a) et (b) présentent respectivement les résultats de la validation du modèle pour les débits et les charges sédimentaires.

Le résultat du modèle montre que le bassin de la Volta Blanche contribue environ 42,20 mm de ruissellement et 5,68 x 10^6 tonnes métriques par an de charge de sédiments dans le lac Volta pendant la période de calage.

Les valeurs des critères de performances du modèle pour les périodes de calage et de validation peuvent être considérées comme raisonnablement satisfaisants et que le modèle SWAT est capable de prédire les débits et les charges de sédiments dans le bassin de la Volta Blanche. Cela implique que les paramètres du modèle sélectionnés pendant la période de calage sont représentatifs des paramètres du bassin. Ainsi donc, le modèle SWAT mis en place dans cette étude peut reproduire de manière réaliste le régime hydrologique et les rendements des sédiments dans le bassin de la Volta Blanche et peut donc être utilisé pour les études d'impact futures.

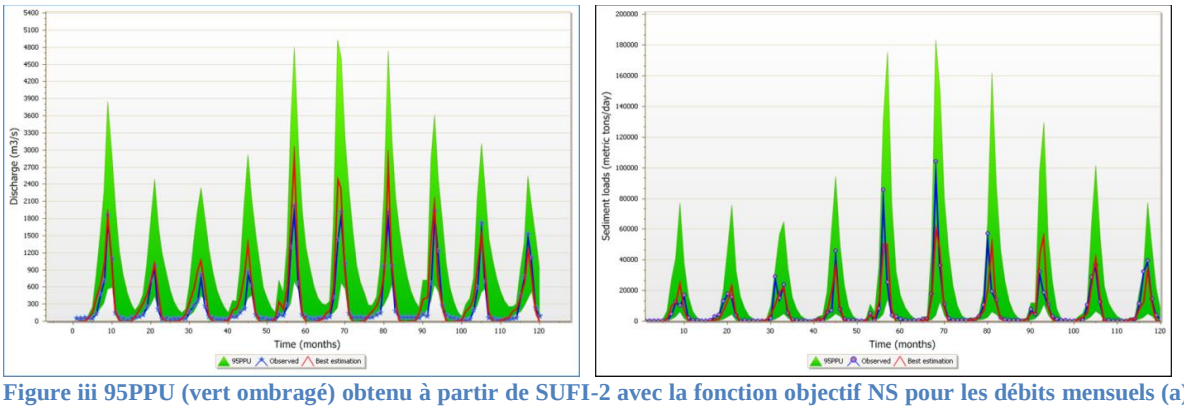

Figure iii 95PPU (vert ombragé) obtenu à partir de SUFI-2 avec la fonction objectif NS pour les débits mensuels (a) et (b) pendant la période de validation (2004-2013).

Les précipitations et la température mensuelles moyennes à long terme pour la période de contrôle (1991-2010) ont généralement été bien simulées par les MRC-GCM (Figure iv (a) et (b)).

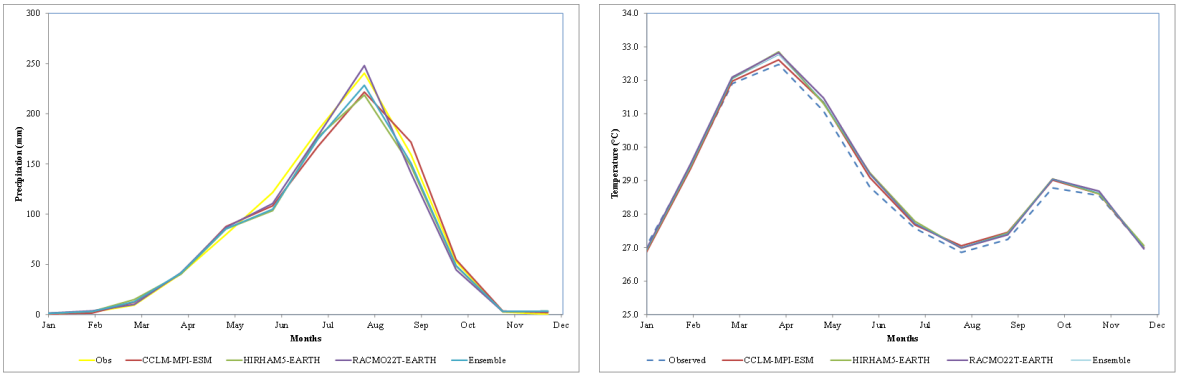

Figure iv Moyenne mensuelle à long terme simulé par les RCM-GCM pour (a) les précipitations et (b) la température par rapport à celle observée pour la période de contrôle (1991-2010) pour le bassin de la Volta Blanche.

Le changement relatif du signal climatique futur peut être calculé comme suit:

$$\Delta = \frac{X_f - X_o}{X_o} \qquad \text{(iii)}$$

Où Δ = variation relative de la variable climatique, X_f = variable simulée pour le future et X_o = observation historique ou variable climatique pendant la période de contrôle. Le changement relatif peut également être exprimé en pourcentage en multipliant de 100%.

La précipitation et la température simulées par les RCM-GCM pour la période de contrôle et le futur en considérant le scénario RCP ont été utilisées pour examiner le comportement futur de chaque RCM-GCM en utilisant l'équation (iii). Tous les RCM-GCM prédisent une augmentation de la température pour le futur (2031-2050) de 2,0 ^{o}C à 2,2 ^{o}C pour RCP4.5 et 2,4 ^{o}C à 2,7 ^{o}C pour RCP8.5. Cependant, dans le cas des simulations de précipitation, HIRMAN5 et RACMO22T prédisent une augmentation des précipitations futures (2031-2050) de l'ordre de 9,4% et 6,3% respectivement pour le RCP4.5 et 14,1% et 8,2% respectivement pour le RCP8.5. Cependant, le CCLM-MPI-ESM prévoit une baisse des précipitations futures (2031-2050) de 6,7% et 10,5% pour RCP4.5 et RCP8.5 respectivement. Ce résultat montre que l'utilisation de la précipitation en tant que modèle de diagnostic peut donc poser problème dans la prévision de la tendance des changements climatiques futurs lorsqu'un seul RCM est appliquée aux études d'impact (Lo et al., 2008).

Après la désagrégation et l'analyse de trois RCM dans le cadre de CORDEX-Afrique, les deux paramètres les plus influençant du cycle hydrologique, les précipitations et la température, ont été utilisés comme entrées dans le modèle hydrologique SWAT pour étudier l'impact du changement climatique sur les débits et les charges sédimentaires du bassin de la Volta Blanche.

Les tendances des projections dans le futur de l'hydrologie de la zone d'étude (flux, écoulement de surface, évapotranspiration réelle, AET, évapotranspiration potentielle, PET et charges sédimentaires) ont été déduites en utilisant Eq (iii) et présentées dans le tableau (i). Les résultats du bilan hydrique pour la projection (2031-2050) montrent une augmentation générale des précipitations annuelles moyennes, du ruissellement de surface et de l'évapotranspiration réelle par tous les MCG-RCM, à l'exception du CCLM-MPI-ESM

(Tableau (i)) qui montre une baisse de tous les composants, à l'exception du PET et des charges sédimentaires.

Table i Changements prévus dans le futur (2031-2050) pour les composantes du bilan hydrique en référence à la période de contrôle (1991-2010).

Water Balance Parameters	CCLM-MPI-ESM		HIRHAM5-EARTH		RACMO22T-EARTH		RCM-GCMs_ESM	
	ΔRCP4.5 (%)	ΔRCP8.5 (%)	ΔRCP4.5 (%)	ΔRCP8.5 (%)	ΔRCP4.5 %)	ΔRCP8.5 (%)	ΔRCP4.5 %)	ΔRCP8.5 (%)
Precipitation	-6.7	-10.5	+9.4	+14.1	+6.3	+8.2	+3.9	+4.8
Water Yield	-11.6	-7.5	+56.5	+76.7	+39.7	+47.4	+31.2	+41.4
Surface Runoff	-4.3	-7.1	+49.3	+54.8	+29.8	+40.4	+32.3	+36.3
AET	-7.1	-11.5	+0.3	+3.8	+0.7	+2.1	-0.1	+1.1
PET	+5.6	+6.9	+4.5	+4.6	+5.2	+6.8	+5.2	+6.1
Sediment loads	+15.5	+11.3	+51.7	+52.9	+5.5	+15.4	+36.0	+32.0

L'effet du changement climatique sur les précipitations en considérant le scénario RCP4.5 et son impact sur les eaux de ruissellement et les charges de sédiments présentés dans le tableau (i) montrent une augmentation des précipitations futures (2031-2050) par rapport à la période de référence (1991-2010). Ce qui entraîne une augmentation du débit de surface et des charges de sédiments pour tous les GCM-RCM, à l'exception du CCLM-MPI-ESM. Le CCLM-MPI-ESM prévoit une baisse de 6,7% des précipitations et une baisse correspondante du ruissellement et de l'évapotranspiration de 4,3% et 7,1% respectivement dans le scénario RCP4.5. Cependant, les charges de sédiments pour le même scénario devraient augmenter de 15,5% par rapport aux conditions actuelles dans lesquelles les charges de sédiments dans la zone d'étude se rapportent directement au ruissellement de surface. De même, sous le scénario RCP8.5, le ruissellement de surface et l'évapotranspiration devraient diminuer de 7,1% et 11,5%, respectivement, tandis que les charges sédimentaires devraient augmenter de 11,3%. Ce rapport contrasté pourrait être attribué au fait que le CCLM-MPI-ESM projette généralement les précipitations extrêmes pour (conditions humides et sèches), ce qui peut entraîner des inondations et des sècheresses. La sècheresse peut provoquer l'assèchement des sols et faciliter l'érosion. Les précipitations résultantes dans la zone d'étude peuvent provoquer l'ensablement des cours d'eau. Par conséquent, une analyse des valeurs extrêmes des précipitations a été effectuée.

L'analyse des probabilités de dépassement (ou des périodes de retour) des précipitations extrêmes a été effectuée en ajustant une distribution de probabilité aux pluies journalières maximales à long terme pour les mois de juillet, août et septembre (JAS) à chaque station climatique dans la zone d'étude. Les quantiles des précipitations extrêmes pour les périodes de retour de 2, 5, 10, 20, 30, 50, 100 et 200 ans ont ensuite été analysés en fonction des changements dans le climat pour la période future. Les quantiles ont ensuite été utilisés pour calculer le Climate Scaling Factor, CSF (Sanderson, 2010). La méthode CSF a été adoptée et appliquée aux quantiles estimés pour les précipitations extrêmes pour les périodes de retour sélectionnées. Cette méthode a été adoptée en raison du fait que le facteur d'échelle, similaire au facteur de perturbation (Boukhris et al., 2008), décrit les différences entre les climats présent et futur et peut être déduit en fonction de leur dépendance à la période de retour (Baguis Et al., 2008). Dans cette étude, les événements de pluie extrêmes

ayant les mêmes périodes de retour pour le présent (19981-2010) et pour le futur (2031-2060) sont utilisés pour calculer les facteurs de mise à l'échelle.

Les résultats obtenus pour la variation future des quantiles pour les périodes de retour sélectionnées sont présentés au niveau de la figure (v) pour la station climatique Babile. Les autres stations climatiques dans la zone d'étude ont généralement montré des tendances similaires à la station climatique Babile. On peut remarquer au niveau de la figure (v) que l'amplitude des hauteurs de précipitations extrêmes augmente généralement pour les périodes de retour par rapport à ce qui est actuellement observé dans la zone d'étude. Le CCLM-MPI a généralement montré la plus petite variation dans les quantiles futurs pour une période de retour donnée. Par exemple, à la période de retour 100 ans à Babile, correspond un quantile de 103,0 mm pour le temps présent alors que le CCLM-MPI-ESM projette un quantile de 105,6 mm (Figure (v)) pour la même période de retour. Cela représente une augmentation de 3% de la quantité future de précipitations extrêmes par rapport au présent. De même, HIRHAM5-EARTH et RAMCO22T-EARTH projettent une augmentation de la hauteur de précipitation extrême future de 17% et 8% respectivement pour tous les intervalles de récurrence à la station climatique de Babile.

Les changements projetés pour l'amplitude et la fréquence des précipitations extrêmes dans la zone d'étude ont un impact direct sur la génération et le transport des charges sédimentaires. Par exemple, alors que CCLM-MPI-ESM prévoit une baisse des précipitations et des eaux de ruissellement futures de 6,7% et 4,3% respectivement (Tableaux (i)), les charges sédimentaires devraient augmenter de 15,5%. Cela s'explique par le fait que les précipitations à haute intensité et de courtes durées ont le potentiel d'augmenter l'érosion des sols dans le bassin. En conséquence, la diminution projetée de la quantité annuelle de précipitations par CCLM-MPI-ESM, conjugué à une augmentation prévue de l'ampleur des précipitations extrêmes pour le même intervalle de récurrence, implique actuellement que plus d'eau sera attendue à l'avenir pour un nombre relativement plus court intervalle. Ces événements pluviométriques de haute intensité mais de courte durée peuvent potentiellement entraîner une augmentation de l'érosion des sols, ce qui entraîne une augmentation des charges sédimentaires dans la zone d'étude.

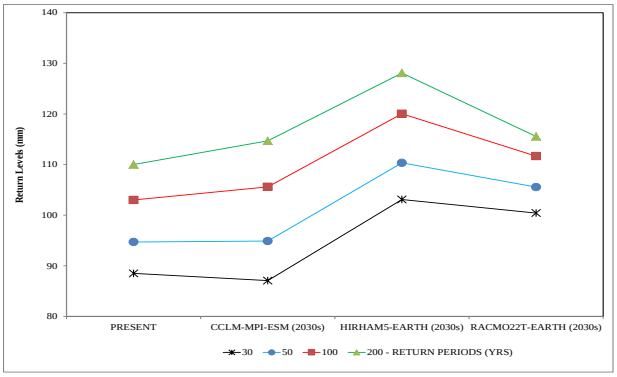

Figure v Changements futurs dans les niveaux de retour extrême JAS pour les périodes de retour sélectionnées à Babile.

5 Conclusion

Un facteur de correction pour la zone d'étude a été déterminé en calculant le rapport de la concentration moyenne d'échantillons en coupe transversale (échantillons intégrés en profondeur) à la concentration moyenne des échantillons de plongée de surface. Un facteur de correction moyen qui peut être appliqué pour tenir compte de la sous-estimation due à l'échantillonnage par la méthode de plongée de surface dans le bassin de Volta Blanc a été estimé à 34%.

Les données de turbidité continue recueillies par GWCL pour l'évaluation de la qualité de l'eau ont été calibrées avec des données SSC mesurées et utilisées pour estimer les séries chronologiques à long terme de charges de sédiments en suspension pour le bassin de Volta Blanche à Nawuni. Une régression linéaire simple, modèle SLR relatif à la turbidité et les données SSC mesurées a été établie. Les charges sédimentaires journalières à long terme pour le bassin de Volta Blanche ont ensuite été calculées en fonction du SSC dérivé du modèle SLR.

Le modèle SWAT calibré pour la Volta Blanche, a montré une bonne performance dans la reproduction des débits annuels, mensuels et journaliers des cours d'eau et des sédiments du bassin. Les résultats du calage et de la validation du modèle ont montré que le modèle SWAT peut prédire avec fiabilité, les débits et les charges de sédiments avec des résultats satisfaisants et peut donc être utilisé comme outil d'analyse des processus hydrologiques et du transport de sédiments dans le bassin de la Volta Blanche.

Comme conséquence du changement climatique, la température en moyenne du bassin devrait augmenter de 2,3 °C ou 2,7 °C en fonction de la direction des voies de concentration représentatives (scénarios RCP). Les précipitations devraient également augmenter en moyenne de 3,2% et 4,0% en fonction des scénarios RCP4.5 et RCP8.5 et, par conséquent, le ruissellement de surface devrait également augmenter de 23,8% et 27,8% respectivement. L'évapotranspiration réelle, l'AET dans le bassin devrait toutefois diminuer en moyenne de 1,5% et de 1,0% en fonction de RCP4,5 et de 8,5 respectivement.

L'analyse fréquentielle des précipitations maximales pour les mois humides de juillet, août et septembre a montré que l'ampleur des précipitations extrêmes risque d'augmenter à l'avenir avec des conséquences directes pour la génération de flux et l'érosion des sols dans le bassin. Par exemple, à la période de retour 100 ans à Babile, correspond un quantile de 103,0 mm pour le temps présent alors que le CCLM-MPI-ESM projette un quantile de 105,6 mm (Figure (v)) pour la même période de retour. Cela représente une augmentation de 3% de la quantité future de précipitations extrêmes pour le même intervalle de récurrence en comparaison à la période actuelle.

Table of Contents

LIST OF ACRONYMS AND ABBREVIATIONS

AGCM	Atmospheric Global Climate Models
AOGCM	Atmosphere-Ocean Global Climate Models
CV	Coefficient of Variation
ECHAM	European Centre Hamburg Model
ET	Actual Evapotranspiration
FAO	Food and Agriculture Organization
GCM	Global Circulation Model
GFDL	Geophysical Fluid Dynamics Laboratory (NOAA US)
GWCL	Ghana Water Company Limited
HADCM	Hadley Center Model
HAP	Hydrological Assessment Project of the Northern Regions of Ghana
HRU	Hydraulic Response Unit
IA	Index of Agreement
IPCC	Intergovernmental Panel on Climate Change
MM5	Mesoscale Model
MoWH	Ministry of Works and Housing
NADMO	National Disaster Management Organisation
NSE	Nash-Sutcliff Efficiency
NTU	Nephelometric Turbidity Units
OGCM	Oceanic Global Climate Models
PBIAS	Percent Bias
PET	Potential Evapotranspiration
PRECIS	Providing REgional Climates for Impacts Studies
r	Correlation Coefficient
R^2	Coefficient of Determination
R^2_a	Adjusted Coefficient of Determination
RCM	Regional Climate Model
RCM-GCM	RCM and GCM Ensemble
REMO	Regional MOdel
RMSE	Root-Mean-Squared Error

SLR	Simple Linear Regression
SRTM	Shuttle Radar Topography Mission
SSC	Suspended-Sediment Concentration
SSL	Suspended-Sediment Load
SWAT	Soil and Water Assessment Tool
TSS	Total Suspended Solids
UNESCO	United Nations Educational, Scientific and Cultural Organization
USGS	United States Geological Survey
USGS	U.S. Geological Survey
VIF	Variance Inflation Factor
WASiM W	Ater flow and balance SImulation Model
WRC	Water Resources Commission
WRI	Water Research Institute

List of Figures

List of Tables

Chapter 1

1 GENERAL INTRODUCTION

Seasonal and annul distribution of streamflow within a watershed can significantly be altered due to urbanization, deforestation and other land-use activities (Alansi et al. 2009). There is the likelihood of such changes also affecting the distribution and pattern of sedimentation (Kasai *et al*., 2005). The impact of climate and land use changes on water, sediment, solutes and nutrients can however be evaluated (Slaymaker, 2003) and understanding how these changes influence stream flow and suspended sediments flow pattern may enable planners in a basin to formulate strategies to minimize the undesirable effects (Alansi et al., 2009).

The Volta Basin which is located in West Africa and shared between six riparian countries is among the 80 internationally shared lake and river basins. The basin has a drainage area of 388,000 sqkm with Burkina Faso draining 43%, Ghana draining 42% and the 15% of the basin being drained by Togo, Cote d'Ivoire, Mali and Benin. The main channel is 1600 km in length and it drains the semi-arid and sub-humid savanna (Photius, 2004) and flows into the Atlantic Ocean through Ghana.

Climate and land use change are expected to have a major impact on water resources and the levels of sedimentation in the Volta Basin. The basin is already experiencing increases in the magnitude and frequency of extreme events which are being attributed to changing climate although large uncertainties still remains. Increasing global temperatures would also have profound impact on evapotranspiration in the basin which could potentially affect atmospheric water storage resulting in changes in the onset of the raining season, temporal and spatial distribution of rainfall as well as the magnitude, frequencies and intensities of the rainfall events. Frequent floods in recent years in the basin, has already caused colossal damage to farmlands, loss of lives and properties, soil erosion and degradation, and disruption of settlement, commerce, and transportation.

According to Andreini and Van de Giesen (2001), the White Volta River basin is experiencing climatic, hydrologic and vegetation changes through its continual usage. Opoku-Ankomah (2000) also pointed out that runoff reductions have been evident in the basin since the 1970s as a result of changes in the frequencies and intensities of rainfall amounts in some of the sub-catchment of the basin. For instance, some sub-catchments of the basin which used to have bi-modal type of rainfall have become uni-modal due to the non-

existence or weakening of the minor raining season resulting in the limitation of rain-fed agriculture to only once a year instead of twice annually.

Furthermore, as the demand for water resources in the basin approached supply, "the tradeoffs between the competing water uses are likely to intensify" (Andreini *et al.*, 2000). Andreini et al., (2000) also observed that, land cover and land use change in the upstream portions of the basin would play an important role in determining the tradeoffs between the demand and supply of water resource in the basin. Predictably, with the recent climatic conditions of highly intense but short duration rainfall patterns and the attendant flooding and prolonged dry seasons in the basin, many inhabitants are finding it extremely difficult to cope with these extreme events.

Surface runoff can be defined as "the flow of water from rain, snowmelt or other sources over the land surface" (Ajayi et al, 2004), and forms an integral component of the water cycle. Significantly, substantial progress has been made in understanding the hydrologic process of rainfall-runoff and how it has affected the water cycle in some parts of the world. However, in the case of sub-Saharan Africa countries, very few examples of detailed hydrological studies exist (van de Giesen et al., 2000).

Sediment yield is a term used to describe "the total sediment outflow from a watershed measurable at a point of reference during a specified period of time" (Cigizoglu, 2002). "Sediment outflow from the watershed is induced by processes of detachment, transportation, and deposition of soil materials by rainfall and runoff" (Boukhrissa, 2013). Accurate measurements of sediment yields in a watershed plays a vital role in minimizing problems related to the loss of water storage volumes and deteriorating water quality in reservoirs resulting from suspended sediment loads transported in rivers. Information on the amount and timing of suspended sediments transported in rivers is therefore vital to the managers of water and land resources. Such information is usually used to judge the health status of watersheds and the success or failure of interventions designed to mitigate adverse impacts of sediments in watersheds (Nolan *et al*., 2005).

Collecting continuous suspended sediment discharge data over a decade can be daunting but necessary in the estimation of sediment yield rates at a catchment level. Several researchers have cautioned that long term monitoring of suspended sediment loads does not necessarily give better results and further suggested that an excellent sediment-rating curve could be constructed from detailed sediment flow data of short period of sampling program (Summer et al., (1992). Information on sediment yields are generally very limited in the Volta Basin, primarily because of limited logistical support for data collection. According to

Akrasi (2005), early sediment studies undertaken in the Volta Basin in Ghana were mainly of short duration and were associated with specific projects. In the 1980s and 1990s, attempts were made to implement the systematic collection of sediment data in Ghana (Akrasi, 2005). However, this initiative failed due to financial constraints (Akrasi, 2005).

Global warming is a term that describes an increase in the median temperature of the earth's surface over a period of time. Global mean surface temperature has been observed to increase by 0.6°C since the late 1950s. The Intergovernmental Panel on Climate Change (IPCC) has projected global temperatures to rise by 1.4–5.8°C during this century. Specifically, the Working Group I of the Fourth Assessment Report of the IPCC project a warming of about 0.2°C for a range of emissions scenarios for the next two decades. According to the report, a warming of 0.1°C per decade is expected assuming greenhouse gases and aerosols concentrations are kept constant at year 2000 levels. In recent years, the accelerating rise in global temperatures however points to the world heading towards the upper boundary of the projected range of increase (IPCC, 2007b).

Climate change is defined as "a change in the state of the climate that can be identified (e.g., using statistical tests) by changes in the mean and/or the variability of its properties, and that persists for an extended period, typically decades or longer" (UNFCCC, 2011). "Climate change may be due to natural internal processes or external forcing, or to persistent anthropogenic changes in the composition of the atmosphere or in land use" (CCFA and FAO, 2012). For instance, natural phenomena such as variations in solar radiation and volcanic activity may significantly contribute to the variability of the climate system. Other contributory effects in composition of the atmosphere are caused by external changes such as human activities like the industrial revolution (IPCC, 2007b).

Climate change is expected to have a major impact on water resources. According to a report of Working Group I of the IPCC (2007b), global monsoon precipitation is projected to strengthen in the 21st century. It is expected to increase in intensity and its area of coverage but with a weaken monsoon circulation. The frequencies of precipitation extremes, such as consecutive dry days, are expected to increase at higher rates than those of the mean (Christensen et al., 2013).

In West Africa, Kunstmann and Jung, (2005) used statistical analysis of historical data (1991-2000) and climate change projection scenarios (2030-2039) of rainfall and streamflow in the Volta Basin and reported a slight reductions in river flow, increase in flood events, increase and intensification of rainfall at the end of the rainy season and increasing duration of the dry season. Several other researchers used GCM-based global climate change scenarios

and predicted significant reduction in river flow and increase of temperature and evapotranspiration in the Volta Basin. These predictions have the potential to impact on erosion and sediment yields in the Volta Basin.

Land use change is a dynamic and complex process that can be exacerbated by a number of human activities. Factors driving land use change include an increase in human population and population response to economic opportunities (Leh *et al.*, 2011). Population in the basin is projected to grow at the rate of 2.5% per annum and national planning studies by the riparian countries predict that the demand for water for irrigation will rise considerably in the near future (Bharati et al., 2008). To overcome the challenges related with inadequate water for irrigation and domestic water supply, several dug-outs, ponds and small dams have been constructed in Northern Ghana and throughout Burkina Faso (Bharati *et al*., 2008).

Despite the social and economic benefits of land use change, the conversion of land use usually has an unintended consequence on the natural environment. For example, land use change has been shown to have negative effects on stream water quality, quantity and stream ecosystem health (Leh et al., 2011). From the foregone, there is therefore the need to study the combined effects of climate and land use changes on the water resources and reservoir sedimentation of the Volta Lake. However, understanding and solving the complex hydrologic processes such as rainfall-runoff, soil erosion, sediment and contaminant transport processes, and their associated problems within a watershed have been quite challenging. These challenges can be attributed to the temporal and spatial variability of the hydrologic processes within a watershed. Scientist and engineers have therefore developed mathematical models as simplified but invaluable tools to analyze these complex hydrologic processes. The models can also be used to evaluate the impact of climate and land use changes on a watershed as well as evaluate best watershed management practices with the aim of minimizing damaging effects of soil erosion, flooding and sedimentation.

1.1 Context and problem statement

Water is the source of life, but also has the potential to be a source of tensions between riparian countries sharing transboundary river basins. One case in point is the Volta basin which is shared between six riparian countries with 85% shared between Ghana and Burkina Faso. According to the IUCN (2008), “populations are set to increase 55% for Burkina and 57% for Ghana by 2025, leading to the expectation that more and more water

will be needed for development". They also projected that demand for water resources is expected to rise up to 128% for Ghana and 429% for Burkina, (IUCN, 2008).

With the population of the Volta Basin projected to grow at the rate of 2.5% per annum (Andah *et al.*, 2003), flood risks and community vulnerability have increased over the last two decades due to the onslaught of development in the river corridors and extreme rainfall events. Without consultation and coordination of investments in infrastructure and agricultural developments, envisaged in Ghana and Burkina Faso, "agreement on shared principles for sustainable management of the Volta River, the controversy on the causes of increased water scarcity and devastating floods in the Volta Basin will only exacerbate" (IUCN, 2008).

Different studies have shown that climate change has already influenced the hydrological cycle and the runoff behavior of the Volta Basin and extreme events have also become a major concern in recent years. Andreini *et al*. (2000) showed that the storage capacity of 132 km³ of the Volta Lake in the 1970's has reduced by 20% to a mean storage capacity of 102 km³ in the 1980's and 1990's. Leemhuis *et al*. (2009) quantified and assessed in comparison with the impact of climate variability on the Volta basin's water resources, the effects on the storage capacity of the Volta Lake as a result of expanding small and medium scale reservoirs in the basin. Andah (2005) also identified water quality degradation as an important issue in the basin. He pointed out that sediment transport across the riparian countries is the major source of degradation of shared water resources. Schmengler (2011) compared the initial and actual reservoir bed morphology in the semi-arid regions of Burkina Faso and found that the reservoirs have lost approximately 10-15 % of their original storage capacity and more than 60 % of their inactive storage volume in the last 15 to 20 years. During that period, a sedimentation layer of 0.3 m to 0.5 m thickness has accumulated on the reservoir beds.

These researched results should be a source of worry to water resources managers and planners in Ghana in general and the Volta River Authority in particular. In the Volta Basin, where hydrological and climatic patterns differ in various regions, it is therefore important to assess both the extent and the spatial distribution of these impacts, as it helps an overall decision making for the basin.

1.2 State of art

1.2.1 Introduction

This section reviews existing literature on sediment transport, methods and approaches for estimating suspended sediment concentration, bed load, sediment yield, and sediment rating curves. The chapter also presents data of previous studies in the study area and examines existing models for predicting sediment transport and sediment yield. Informed by this existing literature, the research methods and materials for the study were designed.

1.2.2 Turbidity and Suspended Sediment Concentration

Turbidity is an expression of the extent to which light is scattered and absorbed by suspended sediment, dissolved organic matter and to some extent plankton and other microscopic organisms (Clesceri, *et al.*, 1994). The presence of suspended sediments, dissolved organic matter, plankton and other microscopic organisms in water makes the water turbid (ASTM International, 2007; Rasmussen *et al.*, 2009). Results from previous studies have shown that turbidity measurements correlate closely with sediment concentrations in streams. According to Lewis (1996) "research conducted by the Pacific Southwest Research Station of the U.S. Forest Service showed that simple linear regression of turbidity and sediment samples provided a more accurate daily prediction of sediment loads than discharge-derived methods, but relationships had to be established separately for samples taken on the rise and fall of event hydrographs" (Lewis 1996). The USGS also conducted similar studies on the Kansas River and found that the relationship between turbidity and suspended sediments was explained by 99% of the model variance (Christensen *et al.*, 2000). Statistical analysis of sediment samples on the Little Arkansas River also showed that 35 to 55 number of data points was adequate to develop a model. Results from the study also showed that outliers exceeding two standard deviations from the mean require further investigation for potential equipment malfunction (Christensen *et al.*, 2000).

Rasmussen *et al.*, (2009) also used continuously monitored streamflow data to analyze the relationships between turbidity and suspended sediment concentration (SSC). They used site specific regression analysis to develop a regression model for estimating specific instantaneous values of SSC based on the turbidity measurements. Jastram *et al.*, (2009) also researched how to measure turbidity in rivers more precisely as a means to estimate SSC. They also used "univariate and multivariate estimations to determine the variables on which SSC depends. In the univariate approach, SSC is only a function of

turbidity" (Jastram *et al.*, 2009). In the multivariate analysis, SSC was related to other hydrologic variables such as turbidity, stage, organic matter, and water temperature. They found that a model including turbidity and stage as independent variables was the most accurate (Jastram *et al.*, (2009).

Wagner *et al.*, (2006) recommended that the estimation of suspended sediment concentration from turbidity measurements should be done by first comparing turbidity measured from a fixed-location to that of cross-section in-stream turbidity measurements

1.2.3 **Sediment Transport**

The transport of sediment is an essential process in an alluvial river, and its understanding, preferably in a quantitative sense, is of paramount importance for adequate morphological modeling. This qualitative classification is according to the ISO-standard 4363-(1977; ISO, 1983; de Vries, 1993).

Water flowing through a riverbed exerts forces on the grains which will start to move at certain critical velocities. With increasing flow velocity, more sediment would move and this is termed sediment transport. Sediment transport can be classified based on the origin of the sediment. Sediment can be transported either as bed load or as suspended load (de Vries, 1993).

Van Rijn (1993) defines bed load transport as the transport of particles by rolling, sliding and siltating. The transport of bed material particles by a flow of water can be of the form of bed load and suspended load. The suspended load may also contain some wash load which is mainly determined by land surface erosion and not by channel bed erosion. The sediment transport in a steady uniform current is therefore assumed to be equal to the transport capacity defined as the quantity of sediment that can be carried by the flow without net erosion or deposition (Van Rijn, 1993).

Suspended load on the other hand is defined as the transport of sediment that is suspended in the fluid for some time. All suspended material finer than the bed material is called wash load. Wash load is generally eroded material from the upstream of a watershed. Transport of wash load depends on the transport capacity of a river and the availability of sediment in the watershed.

By definition, wash load is not determined by the hydraulic characteristics of the river reach considered, hence it cannot be computed. Sediment transport formulae therefore concerns only bed-material transport (de Vries, 1993). According to de Vries (1993), there

are at least two reasons why a quantitative distinction between wash load and bed-material transport is necessary.

1. For the comparison of transport predictions with values measured in the field it is necessary to subtract the wash load component.
2. A reduction of the flow velocity in the direction of the current will make that part of the wash load become bed-material transport (e.g. for sedimentation in reservoirs).

Vlugter (1962) argues that fine particles being moved downstream add part of their potential energy to the river system. On the other hand coarse grains require kinetic energy from the river system to stay in (quasi-) suspension.

Several other authors have derived empirical formulas for estimation of bed load material. For example, Peter-Meyer-Müller (1947) formula for estimating bed load, Engelund-Hansen (1967) formula for estimating total load, and Van Rijn (1993) for estimating suspended and bed load. Generally, "these formulas assume that the amount and grain size of sediment in transport depends on hydraulic parameters (e.g. bed shear stress, velocity) and local bed composition" (de Vries, 1993).

1.3 Sediment Measurements

1.3.1.1 Suspended Sediment Load

Accurate estimation of suspended-sediment concentrations is essential to assess the impact of sediment on the watershed. Generally, suspended sediment constitutes the bulk of sediment transported in several rivers. However, collecting suspended-sediment data using standard techniques is labor intensive and expensive with high degree of uncertainty in estimating the suspended-sediment loads (Gray, 2005).

Suspended sediment load is determined by measuring suspended sediment concentration and discharge. Sediment concentration generally increases with increasing depth. On the other hand, flow velocity decreases with increasing depth. To directly measure suspended sediment concentration, it is vital to consider the fact that interaction of the streamflow and sediment concentration would result in the suspended sediment load profile having a bell shape.

Traditionally, suspended sediment concentration, SSC data is derived by analyzing water samples collected using technics as illustrated by Edwards and Glysson (1999). Several methods have also been employed for the measurement of suspended sediment concentration with mechanical sampling samplers. Among them includes:

- Point-integrated (PI) samplers: these devices measure concentrations in points or portions of the vertical. That way a total sediment profile can be created.
- Depth-integrating (DI) samplers: these are designed to collect one sample over the entire depth, by transiting the stream vertical at a uniform rate.
- Surface dip: this technique collects a sample from the water surface by dipping usually using a 1Liter container. Surface dip is the fastest and cheapest method of collecting sediment samples. However, SSC is usually underestimated with this method since the concentration is lowest near the surface. To overcome this challenge, a correction factor (>1) should be derived. This can be done by comparing surface dip measurements with PI or DI measurements.

Currently, cost-effective surrogate techniques are being developed to augment or in some cases replace the traditional methods for measuring SSC in rivers. Surrogate techniques can produce long-term time-series with quantifiable accuracy for use primarily in sediment-flux computations. Among the methodologies being employed, "turbidity is the most common surrogate technology, and the first to be sanctioned by the U.S. Geological Survey for use in producing data used in concert with water-discharge data to compute sediment concentrations and fluxes for storage in the National Water Information System" (Gray and Gartner, 2010a). According to Gray and Gartner (2010b), "other technologies, including laser-diffraction, digital photo-optic, acoustic-attenuation and backscatter, and pressure-difference techniques are being evaluated for producing reliable sediment concentration and, in some cases, particle-size distribution data".

1.3.1.2 Bed Load

Einstein (1950) defines bed load transport as the transport of sediment particles in a thin layer of two particle diameters thick just above the bed by sliding, rolling and sometimes by making jumps with a longitudinal distance of a few particle diameters (Vries, 1993). The bed layer is considered as the layer in which the mixing due to turbulence is so small that it cannot influence the sediment particles and therefore suspension of particles is impossible in the bed load layer (Vries, 1993).

"Bed load transport can be measured directly using mechanical bed load samplers, like the Helly Smith or the Bed Load Transport Meter Arnhem" (Boiten, 2008). Generally, these instruments trap sediments moving over or close to the river bed by pressing a net on the river bed. The appearance of dunes and ripples in a river can affect the transport of bed load locally. A varying bed form therefore indicates that the bed load also varies both in spatially and temporally. To achieve accurate estimation of bed load, measurement of bed load transport needs to be extensively executed both spatially and temporally (Boiten, 2008). On the other hand, it is sometimes necessary to use dune tracking methods to estimate bed load transport using formulas for dune propagation. Other options such as dredging a river channel and measure the rate of filling or progress of the upstream edge can be used to estimate bed load.

1.3.2 **Sediment Yield**

Accurate estimation of sediment load plays a vital role in the design, construction and management of water resources projects. For example, the economic life of a hydraulic structure can be affected by the amount of sediment load being carried by a river. Sediment load transport also has the potential to affect not only the economic life span of hydraulic structures but may also affect river transport, agriculture and the health sub-sectors of an economy.

Sediment yield is the amount of sediment load flowing through the outlet of a watershed. It is the sediment load normalized for the drainage area of a watershed resulting from erosion and deposition processes in a watershed (Jain and Das, 2010). Sediment yields of river consist of three different kinds of material; dissolved load (consisting of soluble materials transported as chemical ions), suspended load (containing silt and clay in turbulent flows), and bed load (consisting particles moved by saltation, rolling and sliding) (Vries, 1993).

In relatively deep streams of high flows, with bed material that consists of fine sand, the suspended bed material may be 90% or more of the total sediment discharge. However, in shallow streams with medium to coarse sand beds, the unmeasured sediment discharge may represent 50% or more of the total sediment discharge (Andrews, 1981). Various approaches have been developed to determine river sediment yield and these include field measurements and modeling (physical and empirical). Suspended sediment load and bed load are separately measured due to the physical processes that govern their rates of transport which is dependent

on different factors. Total sediment load of a watershed is the sum of suspended load and bed load (Edwards and Glysson, 1999).

Streamflow is generally measured frequently and can be considered as a continuous time-series records. Suspended sediment concentration, on the other hand, are usually measured less frequently. Lack of continuous time-series records on suspended sediment concentration can result in substantial errors in estimating the total sediment load in a river. Because the flow characteristics of a river can quickly change by storm events, infrequent sampling may result in missing these events in time-series records. Even with fair sampling, it is difficult to sample a representative number of events. The method of choice used to estimate sediment load would therefore have a major bearing on suspended sediment concentration estimates derived from infrequently sampled rivers.

1.3.2.1 Field Measurements of Sediment Yield

Several attempts have been made to develop relationships between sediment discharge and other streamflow characteristics such as river discharge, stage, velocity and shear stress. However, no one technic or relationship have received universal acceptance. Generally, the commonly utilized method is to relate sediment discharge or concentration with river discharge. The use of either sediment discharge or concentration has often been used interchangeably (Kisi, 2007). Among the various methods developed to measure suspended sediment yield include the measurement of suspended sediment load and water discharge (Akrasi, 2005), measuring total eroded soil and deposited sediments in small catchments (Verstraeten and Poesen, 2001), and measuring sediment volumes in ponds, lakes or reservoirs (Nichols, 2006). For the measurement of sediment volumes in ponds, lakes and reservoirs, radiometric techniques using ^{210}Pb or ^{137}Cs as tracer elements can be employed to reconstruct sediment budgets over a period of time (Schmengler, 2011).

The ideal situation to estimate the suspended sediment yield of rivers would be to measure suspended sediment concentration and water discharge continuously and use the product function as an estimate of suspended sediment discharge (Lane *et al*., 1997). Obtaining continuous records of concentration however is practically impossible owing to cost, number of samples and sampling frequency among others (Edwards and Glysson, 1999). Alternative to these issues of cost, remoteness of sites, and technical difficulties is to measure water discharge continuously and to take occasional discrete water samples either

manually or using automatic sampling equipment for gravimetric analysis of suspended sediment concentration (Thomas, 1985).

The use of sediment-discharge rating curve to estimate sediment yield is however problematic since suspended sediment concentrations may vary for a given discharge. For example, storm hydrographs are usually, but not always, characterized by high suspended sediment concentrations during the rising limb than the falling limb. These rating curves are usually based on the linear relationship between logarithmic transform of suspended sediment concentration or discharge and streamflow. In the sediment rating curve method, the relationship between sediment discharge or concentration and the streamflow is generally assumed to be constant with time. This assumption may however be problematic since bias may arise as a result of extrapolating the rating beyond the range of the data used in fitting the rating. Extrapolation is sometimes necessary if there are no measured concentrations at extreme events.

Further, the timing between storm events may also influence the availability of fine-grained sediments from the watershed. For instance, an initial storm event following a relatively dry condition may have high suspended sediment concentration than subsequent flows from storms of similar magnitude (Edwards and Glysson, 1999). Consequently, statistical considerations show that "sediment load of a river is likely to be underestimated when concentrations are estimated from water discharge using least squares regression of log-transformed variables" (Asselman, 2000). Also regardless of how the samples are collected, there remain questions of when the measurements of concentration should be made, how they should be used to estimate the total yield, how close can samples be spaced in time and still be meaningful among others (Edwards and Glysson, 1999).

According to Edwards and Glysson, (1999), sediment load transport can be estimated to include the spatial and temporal variations by collecting depth/point-integrated suspended sediment samples. This is achieved by taking the mean weighted concentration in a sample vertical and collecting sufficient verticals to define the mean discharge weighted concentration in the cross section. Verticals of samples could either be taken using Equal-Discharge-Increment or Equal-Width-Increment Methods (WMO-No. 168, 2008). Though both methods have their advantages and disadvantages, if properly used, they yield similar results.

Also the biases in the estimation of sediment loads by rating curves due to the use of log-transformation can be significantly reduced by using nonlinear regression methods. Further improvements can be achieved by identifying seasons and possible breaks in slopes

of the rating curves. Finally, the underestimation caused by using average daily flows with the rating curve can be eliminated by using sub-daily flow data, if available (Singh and Durgunoglu, 1989). The different methods that have been developed for collecting data and estimating suspended sediment yields indicates that each method is characterized by one limitation or the other, and thus the method that one employs is subject to availability of equipment, cost, convenience, the kind of results that is sought among others.

1.3.2.2 Erosion and Sediment Yield Models

To improve the quality of water and restore an impaired watershed, managers of the watershed need data that will enable them make the required decisions (Nangia, 2010). Data collection is however a very expensive, tedious and time consuming process. The use of models can therefore be considered justifiable particularly in the developing countries where institutions mandated to collect data are ill-equipped in terms of technology, personnel, materials as well as financial (Nangia, 2010). Sediment transport models therefore provides invaluable information when applied to ungauged watersheds in predicting the impact of climate change, agricultural activities, land use, stream stabilization and sediment storage in reservoirs (Khanchoul *et al*., 2010). Several models with a wide range of complexities, processes and input data required for model calibration exists for simulating sediment transport and associated pollutant transport. Generally, there is no "one fit all" model for all applications. The model of choice for every application will depend on the watershed characteristics, the purpose and nature of the application and the availability of data (Merritt *et al*., 2003).

Soil erosion models on the other hand represent the relationships between various factors and processes such as land use and land cover, meteorological variables, topography and soil properties occurring on the landscape. One classification of models distinguishes between theoretical or physically based models and empirical models. However, most erosion models are of a hybrid type including both theoretical and empirical components (Haan *et al*., 1994). The emphasis in erosion research on strictly empirically based models is declining. The trend in erosion prediction technology is toward the development of process-based simulation models (Nearing *et al*., 2011). Many physically based upland erosion models in the past have used lumped or semi-distributed techniques for their hydrologic modeling component.

Most of the erosion models are based on the Universal Soil Loss Equation (USLE) (e.g. AGNPS (Young *et al*., 1989), ANSWERS (Beasley *et al*., 1980), EPIC (Sharpley and Williams, 1990), and SWAT (Arnold *et al*., 1998)), on the partition of the watershed in planes and channel elements (i.e. KINEROS (Woolhiser *et al*. 1990), and EUROSEM (Morgan *et al.*, 1998)) or they are not intended for basin-scale use (i.e. CREAMS (Knisel, 1980)).

1.3.2.3 USLE and Modifications

The most widely used and accepted empirical soil erosion model is the USLE (Wischmeier and Smith, 1978) model. The model was developed for sheet and rill erosion based on a large set of experimental data from agricultural plots. Yet, the equation was derived on single agricultural plots and is only valid when applied to an area up to 1 ha. The USLE equation takes into account slope length (L factor), steepness (S factor), climate (R factor), soils (K factor), cropping (C factor) and management (P factor). This model was specifically designed and tested to predict the average annual soil movement from a given field plot under specified land use and management conditions. The USLE has been enhanced during the past 30 years by a number of researchers. MUSLE (Williams and Berndt, 1977), RUSLE (Renard *et al*. 1991), and ANSWERS (Beasley et al., 1980) are all an improvement on the USLE. The USLE and its derivatives are generally limited to the estimation of gross erosion. They lack the capability to compute sediment deposition along depressions, hill slopes and valleys or in channels.

The USLE model is relatively easy to use because of its simplicity and the availability of parameter values (Loch and Rosewell, 1992). The USLE model however has some limitations which include the fact that it is not event-based and therefore unable to identify events which may cause erosion on a large scale (Zhang *et al*., 1995). Ephemeral gully erosion, which can be as extensive as sheet and rill erosion, can occur along the upper reach of a channel and deposition occurs in the lower reaches of the channel (Lane *et al*., 1997).

A number of modifications and revisions to the basic format of the USLE have been proposed in the literature due to its identified limitations. These include the revised USLE (Renard *et al*., 1994), and the USLE-M (Kinnell and Risse, 1998). Generally the continuous improvement of the components of the model has been aimed at making it more process-based. For instance changes to the slope-length factor, *L* in RUSLE allows soil loss from Hortonian overland flow to be estimated in a three dimensional terrain with converging and

diverging slopes (Ryan and McKenzie, 1997). The RULSE has the capability to estimate the cover and management factor, *C* based on vegetation, decay and tillage practices. The RULSE therefore has an advantage over the USLE in which the cover and management factor, *C* is estimated based on data from experimental plots. The USLE-M also directly considers the effect of runoff on erosion with changes to the rainfall erosivity factor, *R* which provides a more complex representation of processes than the USLE (Kinnell and Risse, 1998).

1.3.2.4 Other Models

The KINEROS model (Smith *et al*., 1995) and the EUROSEM model (Morgan, *et al.*, 1998) are single event and physically based models. The KINEROS model uses the Smith/Parlange infiltration model and the kinematic wave approximation to route overland flow and sediment while the EUROSEM model predicts soil erosion by water from fields and small catchments. There are several sediment transport equation options implemented in both models. The watershed in KINEROS and EUROSEM models are represented by a cascade of plane and channel elements and this requires the lumping of some parameters for small areas. The lumping represents a drawback when representing large watersheds such as the White Volta Basin. Additionally, lack of sub-daily data, especially event measuring instrumentation, in the White Volta Basin makes these models not suitable to be applied in that watershed.

SHESED (Wicks and Bathurst, 1996) is based on the European raster SHE model. It simulates soil erosion by raindrop impact, leaf drip and sheet overland flow. Eroded material is transported across the landscape via overland flow. Erosion in channels is modeled as bed erosion. The sediment routine can handle the transport of fine and coarse material. The SHESED model has been applied successfully in Europe and the USA.

The LISEM model (De Roo and Offermans, 1995) is a physically based hydrological and soil erosion model that is completely incorporated in a raster GIS. It can simulate splash erosion and rill and inter-rill erosion. The transport capacity of overland flow is modeled as a function of the unit stream power (Govers and Lock, 1993) and depends on the value of the median grain size.

Developed at CSU, CASC2D-SED (Johnson *et al*., 2000) is a distributed physically-based hydrologic and soil erosion model that simulates the hydrologic response of a watershed for a given rainfall field. Rainfall input in CASC2D-SED can vary in space and time. Additionally, upland sediment production and deposition by size fraction can be

simulated at any point in a watershed. Sediment in CASC2D is transported between cells using the 2-D diffusive wave overland flow routine.

The Soil and Water Assessment Tool (SWAT) model (Arnold *et al.,* 1998) is another effective model used in assessing water resources and nonpoint-source pollution problems for watersheds with a wide range of scales and environmental conditions. SWAT is a basin-scale, physically based and continuous-time model that can run on a daily time-step (Akhavan, 2010). The model is designed to predict the effects of management on water, sediment, and agricultural chemical yields in a watershed (Akhavan, 2010). SWAT main components are weather, hydrology and land management. Other components include soil temperature and properties, plant growth, nutrients, pesticides, bacteria and pathogens. SWAT was chosen because it fulfills the following criteria:

- time-continuous, also suitable for long simulation periods
- spatially distributed (semi-distributed)
- applicable to large-scale catchments (regional scale >10,000 km^2)
- embedded in a GIS interface
- manageable input parameters (freely available input data e.g. DEM, land use and soil data)
- freely available, widespread user group, sufficient documentation and support
- partly process-based, not completely empirical

A complete detailed description of SWAT is presented in Chapter 3.

1.3.3 **Sediment Yield Estimation in the Volta Basin**

Among the numerous methods of estimating SSC from discharge in the absence of actual SSC data is the extrapolation and interpolation, with potential additional modifications using various correction factors such as Duan (1983) and Ferguson (1986) (Horowitz, 2003). Improvement in the estimation of SSC can be achieved by subdividing the calibration data sets into seasonal (e.g. wet and dry) or hydrological (e.g. rising limb and falling limb) groupings (Horowitz, 2003). According to Horowitz *et al.*, (2001), it is possible to estimate SSC for the calculation of annual or longer term suspended sediment fluxes with very good results (errors $\leq \pm 15\%$) using either linear or second-order polynomial sediment rating curves, with and without a 'smearing' correction.

According to Akrasi (2005) the Volta Basin lacks adequate information on sediment yields. This is primarily due to the lack of logistical support for sediment data collection in the basin. Generally, sediment data collections in the basin were mostly associated with specific projects and of short duration (Akrasi, 2005). Akrasi, (2005) therefore developed a simply predictive tool for estimating SSC from discharge using the available limited sediment data obtained from sampling selected rivers in the Volta Basin. The available SSC data obtained for the selected rivers consist of infrequent samples collected at different times of the year over a representative range of river discharges (Amisigo & Akrasi 1996; Akrasi, 2005). Due to the infrequent sampling and limited number of samples the rating curve technique was utilized to compute the mean annual suspended sediment yield for the selected rivers.

A bias correction factor (Ferguson, 1986) was applied to the estimated loads to eliminate possible underestimation due to the log-transformation. Table 1.1 summarized the results obtained for the eight selected sites. Annual sediment yields for the selected stations were then computed from a simple predictive tool which was developed based on multiple regression analysis of the results from the sediment rating curves and summarized in Table 1.2.

Table 1-1: The SSC rating curves for the selected rivers (source: Akrasi, 2005)

Station	**River**	**a**	**b**	**R^2**
Lawra	Black Volta	9.145	1.241	0.95
Bamboi	Black Volta	3.196	1.386	0.98
Pwalugu	**White Volta**	**8.870**	**1.182**	**0.97**
Nawuni	**White Volta**	**3.230**	**1.345**	**0.95**
Ekumdipe	Daka	5.070	1.163	0.97
Saboba	Oti	4.723	1.261	0.97
Aframso	Afram	7.159	0.925	0.66

Table 1-2: Estimated mean annual suspended sediment for the selected rivers (source: Akrasi, 2005)

Station	**River**	**Drainage area (km^2)**	**Sediment yield (t km^{-2} yr^{-1})**
Lawra	Black Volta	90,658	15.20
Bamboi	Black Volta	128,759	25.72
Pwalugu	**White Volta**	**57,397**	**21.65**
Nawuni	**White Volta**	**96,957**	**22.88**
Ekumdipe	Daka	6,586	26.88
Saboba	Oti	54,890	46.56
Aframso	Afram	308	14.84

Opoku-Ankomah and Amisigo (1997), also estimated sediment yields at selected stations in the Volta Basin using flow duration-sediment rating curves based on the Piest duration limits as described. The annual specific suspended sediment yield for the selected stations in the Volta Basin were found to vary from 8 to about 28 t/km^2/yr and decrease with catchment area (Opoku-Ankomah and Amisigo, 1997). The sediment yield values compare with values of 3.9 to 85 t/km^2/yr obtained for some major rivers in various parts of West Africa (Walling, 1983; Opoku-Ankomah and Amisigo, 1997).

As part of the prefeasibility studies of the White Volta Development Scheme for the Volta River Authority, Coyne et Bellier, (1993) developed sediment rating curves for the White Volta basin based on limited sediment measurements. Two sediment rating curves were developed for the Pwalugu station on the White Volta by splitting the data based on the rising and falling limbs of the hydrograph. Coyne et Bellier (1993) applied the derived sediment rating curves to the monthly discharges at Pwalugu which resulted in an average sediment transport of 61.7 kg/s which is equivalent to 1.95x10^6 metric tons/yr.

1.3.4 **Climate Change**

Global climate change caused by continuous greenhouse (GHG) emissions has the potential to adversely impact and trigger large-scale irreversible and catastrophic changes that will exceed the adaptive capacity of natural and social systems (IPCC, 2007a). Climate change is a global systemic risk that poses serious threats to life and properties and the socio-economic well-being of many countries. According to the Working Group I of the Fourth Assessment Report of IPCC, a warming of about 0.2 degree Celsius is projected for a range of emissions scenarios for the next two decades (IPCC, 2007b). A number of methods are widely reported for estimating climate change. An extensive review of the several techniques involved in representing regional and local scale processes when using climate models is given by Fowler and Kilsby (2007).

Climate change has the potential to alter regional hydrological cycles with consequences of changing the quantity and quality of streamflows. The "importance of water in both society and nature underscores the necessity of understanding how a change in climate could affect regional water supplies" (Xu and Singh, 2004). This change can be studied using a hydrological model that is driven with the output from a general circulation model (GCM). GCMs have been developed to simulate the present climate and predict potential changes in the future climate.

GCMs are generally developed to incorporate a large proportion of the complexity of the global system and operate at the continental and hemispheric spatial scales thereby making them unfit to represent local sub-grid scale features and dynamics (Ghosh and Misra, 2010). To overcome these challenges, Regional Climate Models, (RCMs) capable of generating the high-resolution meteorological inputs required for modeling eco-hydrological processes have emerged. RCMs can relate large-scale atmospheric predictor variables to local- or station-scale meteorological series. The boundary and sea-surface conditions of RCMs are generally derived from GCMs. Their high resolution makes them very suitable for resolving challenges posed by small-scale features such as topography and land use. These features have major impact on climate parameters such as rainfall in a climate model.

The emergence of downscaling technics has provided the process of linking local/station scale meteorological time series to large-scale atmospheric predictor variables. Presently, there are two main techniques of downscaling. These are; dynamic and statistical downscaling. Dynamic downscaling technique involves the explicit solving of the process-based physical dynamics of the system (Chong-yu, 1999) whereas the statistical downscaling technique utilizes identified system relationships derived from observational data (Chong-yu, 1999).

Dynamic downscaling uses RCMs to simulate high resolution (typically 50 km) physical processes that are consistent with large scale climate projection from a GCM (Mearns *et al.*, 2006). Due to the high resolution of RCMs they are ideal in capturing the variability of regional rainfall. Examples of RCMs are WRF, REMO, MM5 and PRECIS.

Statistical downscaling on the other hand consists of deriving statistical relationships between local/station climate variables such as precipitation and surface air temperatures and large-scale predictors such as pressure fields (Mearns *et al.*, 2006). The developed statistical relationship is then usually applied to the output of a GCM experiment to simulate local climate characteristics in the future. Statistical downscaling methods such as multiple linear regression, nonlinear regression (e.g. artificial neural networks) and stochastic weather generators are easier and less costly to implement as compared to dynamical downscaling technique which requires limited-area models (LAMs) or regional climate models (RCMs) (Khan et al., 2006). One major drawback of statistical downscaling is the assumption that the relationships between large and local-scale processes will remain the same in the future (stationarity assumptions) (Trzaska and Schnarr, 2014).

1.4 Justification of the Research Methodology

Many published sediment yield models, sediment rating curves, and suspended sediment concentration measuring methodologies were reviewed to understand their techniques and applications. Relative merits and shortcomings of these methodological approaches in sediment transport studies were discussed. It was realized that there is no universally acceptable method or approach to modeling a catchment's sediment yield as well as field data collection of sediment discharge measurements. The choice of any methodology depends on the availability of resources (secondary data, financial, equipment etc) at the disposal of the researcher.

In-situ field data collections involving suspended sediment discharge measurements, river discharge measurements and secondary data, which include turbidity measurements from the Ghana Water Company Ltd, GWCL treatment plant at Nawuni and suspended sediment discharge from the Water Research Institute, WRI of CSIR, were obtained for the study area. In order not to miss critical flows in the in-situ field data collection, daily sampling of suspended sediment concentration was undertaken by engaging local volunteers who took daily water samples by surface dipping with a one liter container. The daily surface dip data was then enhanced by coupling with monthly depth-integrated sampling.

The sediment loads model of choice selected for this study was the Soil and Water Assessment Tool, SWAT. SWAT was chosen because it fulfills the following criteria:

- time-continuous, also suitable for long simulation periods
- spatially distributed (semi-distributed)
- applicable to large-scale catchments (regional scale >10,000 km^2)
- embedded in a GIS interface
- manageable input parameters (freely available input data e.g. DEM, land use and soil data)
- freely available, widespread user group, sufficient documentation and support
- partly process-based, not completely empirical.

This research was conducted by calibrating, validating and deploying the SWAT2009 version in the ArcGIS 10 User Interface.

1.5 Objectives of the Research

1.5.1 Main Objective

The main objective of this study is to contribute towards sustainable integrated water resources management of the White Volta Basin by studying the impact of future climate change on the streamflows and sediment yields in the basin.

1.5.2 Specific objective

In this context, four specific objectives will be addressed.

- To develop and evaluate an empirical relationship between turbidity and suspended sediment concentration measurements using regression models and compute long-term time-series of sediment loads.
- Evaluate the ability of the Soil and Water Assessment Tool (SWAT) to reproduce streamflows and sediment loads in the White Volta Basin.
- Assess the impact of climate change on streamflows and sediment loads in the White Volta basin using SWAT coupled with Regional Climate Models under the CORDEX-Africa project.
- Assess the impact of extreme precipitation under climate change on streamflows and sediment loads in the White Volta basin

1.6 Research questions and hypothesis

This research seeks to link sedimentation, an important component of the hydrology of the White Volta Basin, with the effects of climate change on the water resources of the basin. This will be achieved by answering the following research questions:

- Can modern methods of surrogate sediment monitoring and measurements be applied in the White Volta Basin to estimate long-term sediment loads?
- How can the Soil and Water Assessment Tool (SWAT) coupled with Regional Climate Models (RCMs) be used as a tool to realistically reproduce the hydrological regime and sediment yields in the White Volta Basin and predict the impact of future climate change in the basin?
- How will the impact of climate change and climate variability in the White Volta Basin affect streamflows and sediment loads?
- Will extreme precipitation under a changing climate exercibate the impact of climate change on the runoff and sediment loads in the White Volta Basin?

1.7 Novelty of this Research

Numerous Researchers have undertaken research in Volta Basin on the impact of climate change and land use changes largely on availability of water resources. Although, sediment loads, which is generally required to judge health of watershed, plays a pivotal role in the sustainable management of water resources of a river basin. However, appropriate policy measures informed by empirical evidence of climate change impacts on water resources and sediment loads in the Volta Basin has not been developed.

The novelty in this research is therefore the attempt to link sediment loads, an important component of the hydrology of the White Volta Basin, a sub-catchment of the Volta Basin, with the streamflows. Additionally, the effects of climate change and extreme precipitation on streamflows and sediment loads in the White Volta Basin will be undertaken to provide policy makers an informed and empirical evidence of climate change impacts on water resources and sediment transport in the basin.

1.8 Scope of the thesis

A coefficient/correction factor to correct underestimation associated with surface dip suspended sediment concentration sampling in the White Volta was developed. Long-term suspended sediment loads based on turbidity measurements undertaken by GWCL in the White Volta Basin at Nawuni was computed. The impact of projected climate change scenarios on streamflows and sediment loads in the White Volta Basin was investigated. However, the variability of land-use/land-cover which is known to play a vital role in the hydrology and sediment transport of a watershed was not included in this study. The impacts of the Bagre dam in Burkina Faso and the proposed Pwalugu dam in Ghana were also not investigated.

1.9 Expected results and benefits

The development of a coefficient/correction factor to correct underestimation associated with surface dip suspended sediment concentration sampling in the White Volta Basin can be used to minimize errors associated with surface dipping. The application of the correction factor can also reduce cost associated with the use of the kinematic depth-integrated sampler in the White Volta Basin. This study will also provide the opportunity to compute long-term suspended sediment loads based on surrogate techniques by relating

suspended sediment concentration to turbidity which is consistently monitored by Ghana Water Company Limited at all its water treatment and production sites. Appropriate policy and legistilative measures informed by empirical evidence of climate change impacts on water resources and sediment transport can be developed by the Volta Basin Authority and the riparian countries, based on the projected climate change scenarios in this study, to formulate adaptation strategies to mitigate the effects of climate change for sustainable utilization of the water resources in the basin.

1.10 Structure of the thesis

This thesis is organized into eight (8) chapters. The first chapter gives background information on other research related to the impact of climate and land use change on runoff and sediment loads and the underpinning issues that are of focus in the study area. This chapter also discusses the problem under study and outlines the objectives of the study. The chapter also presents a review of existing literature on methods and approaches for estimating turbidity, suspended sediment concentration, sediment yield, sediment rating curves and also presents data of previous studies in the study area. The chapter also examines existing models for predicting sediment transport and sediment yield. Chapter 2 introduces the physical settings of the study area by stating the geographical position of the study area and the underlying physical, demorgraphic and socio-economic factors prevailing within the basin. Chapters 3 focus on the materials and methods used to undertake this research and the models used are also explained in this chapter. Chapter 4, here the results of the development and evaluation of empirical relationships between turbidity, streamflow and suspended sediment concentration are presented. This chapter also presents the computation of long-term sediment loads time-series. Chapter 5 discusses the result of the SWAT sensitivity analysis, model calibration, uncertainty and validation. Chapter 6 dwells on the trends in future climate projections and its impact on streamflows and sediment loads in the study area. Chapter 7 examines the impact of future projected extreme precipitation on streamflows and sediment loads in the study area and chapter 8 presents a general discussion relating all the findings of the study, stating the significance of the results to decision making and policy formulation, drawing conclusions and making recommendations for informed decision making and for future studies.

Chapter 2

2 THE STUDY AREA

2.1 Introduction

Although this research was undertaken in the White Volta sub-catchment of the Volta Basin, this chapter also provides a general description of the whole Volta Basin since information presented in most literatures focuses more on the Volta Basin. However, wherever available, information on the White Volta Basin is included in this chapter.

2.2 Location, topography and river network

The Volta basin is one of the major rivers in the west tropical zone of Africa and presents several peculiar characteristics. For example, unlike the Niger, Logone and Chari Rivers which originates from the southern humid tropical zones and flows north towards the borders of the Sahara, the Volta River presents a different aspect altogether. The Volta River takes its source from several rivulets that originate in the Sahelian areas with less than 1,000 mm of mean annual precipitation and flows slowly southwards towards the humid tropical zones of West Africa (Volta-HYCOS, 2006). The West Coast (Figure 2.1) comprises several rivers that flow into the Gulf of Guinea. It covers 13 countries from Senegal to Nigeria and covers 4.7% of the African continent (FAO, 1997). The Volta Basin extends from latitude 5° 30' N to 14° 30' N and longitude 5° 30' W to 2° 00' E covers 28% of the West Coast and is shared by Burkina Faso, Ghana, Mali, Benin, La Cote d'Ivoire and Togo. The river's length is estimated to be 1,600 km with a basin area of 388,000 km² (Photius, 2004) and flows into the Atlantic Ocean. The basin covers most parts of southern Burkina Faso and a greater part of Ghana. Some minor portions also cover almost all the northern part of Togo, some fringes of Benin, Côte d'Ivoire and Mali. Table 2.1 shows the percentage of area of the basin covered by each riparian country.

The flow in the Volta basin becomes significant in its lower reach in Ghana after receiving considerable inflows from its tributaries, the Oti, Black and White Volta. The Volta Lake, created in 1964, with storage capacity of 148 billion m^3 has become the hub of Ghana's development. "Further north, increasing needs of populations of the pre-Sahelian zone have led to intense research for means of optimal use of water in spite of its scarcity. The Bagré, Kompienga and Ziga dams have been built in this framework. The total storage volume in Burkina Faso is less than 4 billion m^3" (Volta-HYCOS, 2006).

The Volta Basin is drained by three main sub-basins namely: the Black Volta (Mouhoun), the White Volta (Nakambé) and its tributary the Red Volta (Nazinon) and the Oti, which flows from Togo and Benin. The Oti is considered the main tributary of the Volta basin. The focus of this research is however limited to the White Volta sub-basin of the Volta Basin.

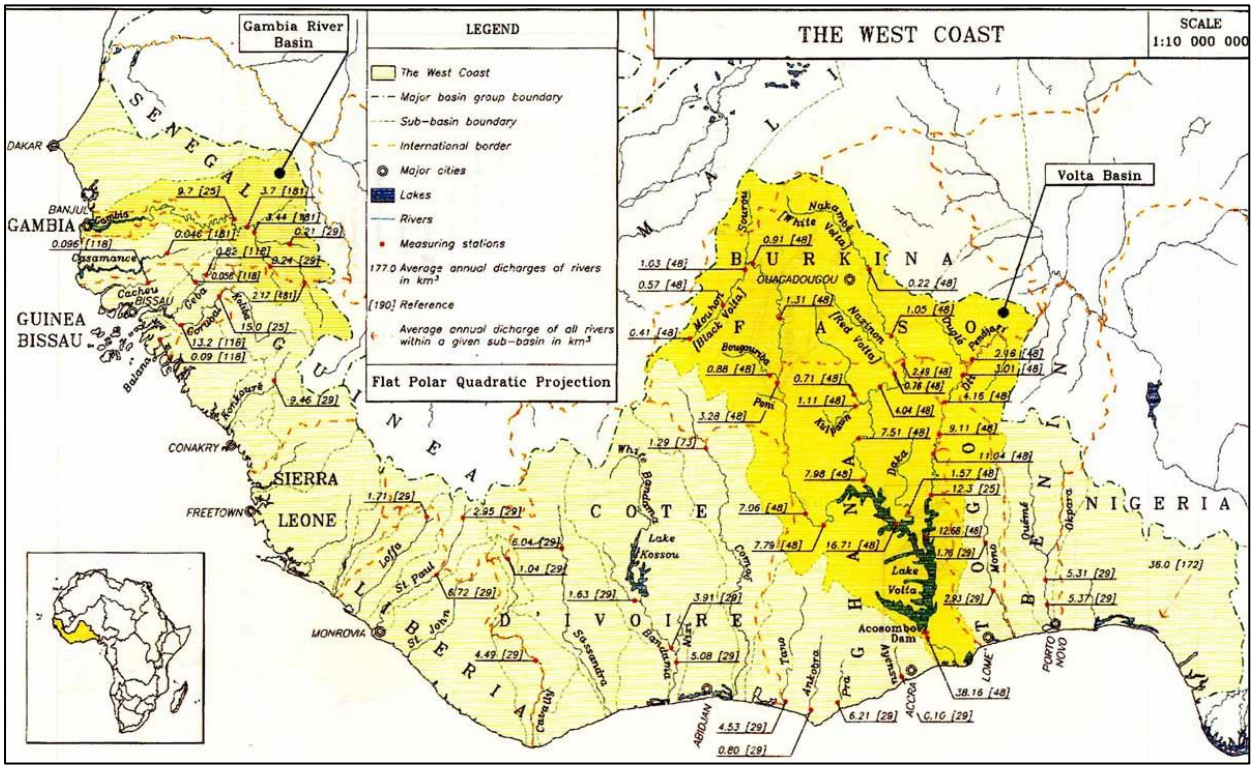

Figure 2-1: Map showing the extend of the West Coast (Source: FAO, 1997)

Table 2-1: Percentage of total area of the Volta Basin covered by the riparian countries (Source: FAO, 1997)

Country	Country Size (km^2)	Extent of Country in the Basin (km^2)	Percentage of Basin Area (%)	Percentage of Country Size (%)
Benin	112,620	16,000	4.06	14.21
Burkina Faso	274,000	183,000	46.42	66.79
Côte d'Ivoire	322,462	7,000	1.78	2.17
Ghana	238,540	152,000	38.56	63.72
Mali	1,240,190	9,496	2.41	0.77
Togo	56,785	26,700	6.77	47.02

The White Volta Basin (Figure 2.2) is located between latitudes 8° 50' N and 14° 30' N and longitudes 0° 06' E and 2° 50' W. The basin shares boundary with the Oti Basin in the east, the Black Volta River Basin in the west and the Main/Lower Volta in the south. Burkina Faso forms its northern boundary with Ghana covering the south.

The White Volta Basin, the second largest catchment of the Volta Basin, covers about 100,148 km^2 at Nawuni and represents approximately 26 % of the total Volta catchment area. The basin area in Ghana is approximately 50,000 km^2 and constitutes 20% of Ghana's total land area. Approximately 44% of the total area of the White Volta Basin falls within Ghana with the remaining 56% in Burkina Faso. The Red Volta, Nasia, Nabogo and the Kulpawn/Sissili rivers are the main tributaries of the White Volta Basin. The Red Volta and the Kulpawn/Sissili rivers take their sources in the central and north-eastern portions of Burkina Faso (WRC, 2008).

The Bagre hydroelectric dam which covers a total area of 33,120 km^2 has significantly impacted on the hydrology of the White Volta. The annual average flow from the dam within the last decade is estimated at 29.7 m^3/s (WRC, 2008).

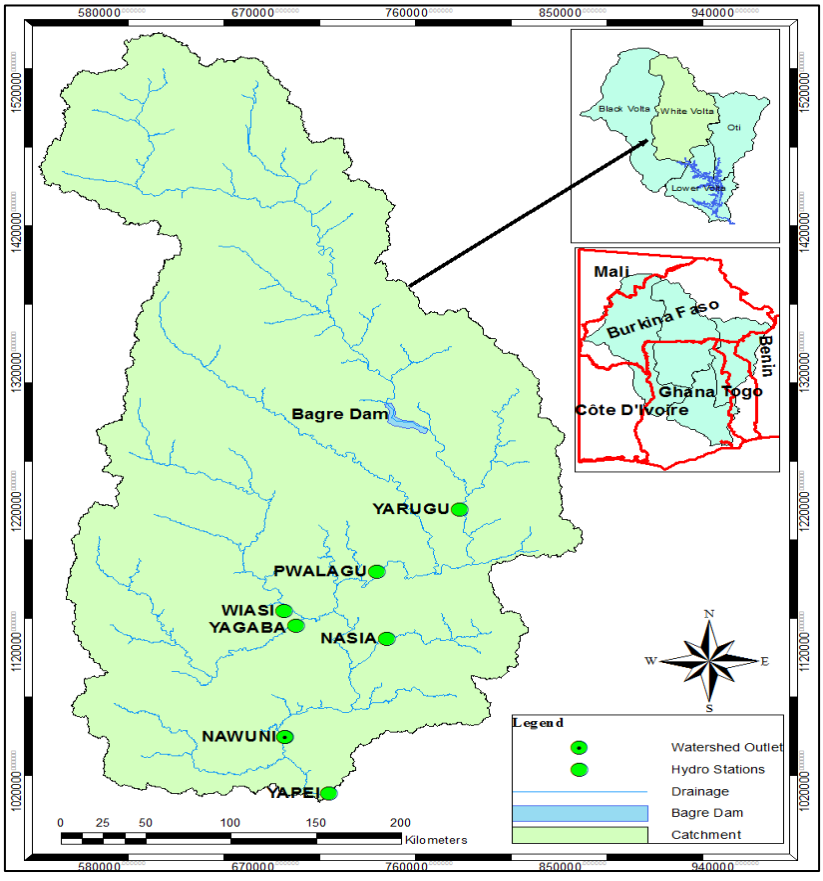

Figure 2-2: Map of the White Volta Basin showing Volta Basin, the six riparian countries, Bagre dam and watershed outlet for this study.

2.3 Climate

The Volta Basin climate is generally regulated by the shifting of the Inter Tropical Convergence Zone, ITCZ between the south and north of the basin (Amisigo, 2005). The ITCZ is a region in which the monsoon and harmattan converges. The harmattan is a dusty,

dry and hot tropical continental air mass that flows from the Sahara in the north towards the Atlantic and the monsoon on the other hand is a warm and moist tropical maritime air mass from the Atlantic in the south towards the Sahara (Amisigo, 2005).

The region is marked by two main seasons, the wet and dry seasons, generated by the oscillation of the ITCZ. The ITCZ oscillates across the region and often times passes the lower latitudes twice resulting in two rainy seasons in such areas (Amisigo, 2005). The complex oscillation of the ITCZ also creates 3 main climatic zones. These include; the humid southern zone, the tropical transition zone and tropical northern zone which covers most parts of the basin. The tropical northern zone has one rainy season and one dry season. The rainy season starts from April and ends in October, with a peak rainfall in September. The dry season on the other hand starts from November and ends in March (Amisigo, 2005).

The White Volta Basin climate is generally characterized as tropical continental, or savanna, with a uni-modal rainy season. The onset of the rainy season starts from May and ends in October, followed by a prolonged dry season. Peak rainfall usually occurs around late August or early September. It is estimated that 60% of the total rainfall amount occurs within the three months of JAS (July, August and September) with torrential rains creating serious water related problems. The interior savanna environment of northern Ghana is constituted by two different ecologies namely the Guinea and Sudan savanna and is regulated by the distribution and amount of rainfall.

The Guinea savanna ecological zone has an annual total rainfall ranging between 1000 to 1300 mm. The rainy season ranges from 140-190 days in duration with an average number of rain days between 60 and 90 days. The reference evaporation (ETo Penman) is estimated at about 2000 mm/annum, causing a deficit every dry season. Generally, absorptive capacity of the soils is unable to contain the amount and intensity of the rainfall in the basin. This creates high amounts of runoff and causes soil erosion which has direct impact on agricultural production in the area. Evapotranspiration in the basin is however considerably less than precipitation during the main rainy season.

2.4 Rainfall

Rainfall in the Volta Basin is highly variable in both space and time. The isohyets increases southwards with mean annual rainfall ranging from less than 500 mm in the extreme north in Burkina Faso to more than 1600 mm in southern Ghana (Amisigo, 2005). Figure 2.3 presents the annual rainfall distribution in the Volta basin

The White Volta River Basin falls under the tropical continental or interior savannah climatic zone characterized by a uni-modal rainfall regime. The rainy season extends from April to October, peaking in August or September. This is followed by a prolonged dry season from November to March. These features can be observed in Table 2.2, which is a summary of monthly rainfall data at the Navrongo and Tamale meteorological synoptic stations (WRC, 2008).

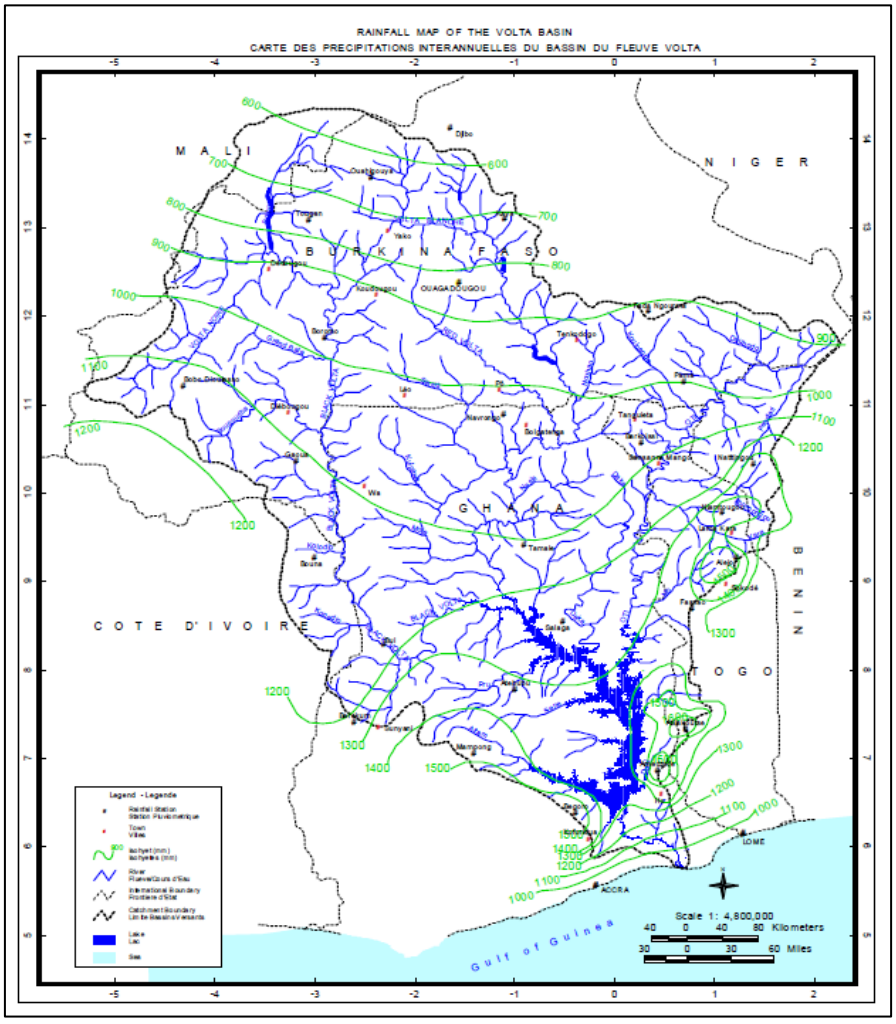

Figure 2-3: Annual rainfall distribution in the Volta Basin (Source: VBRP, 2002; cited in Amisigo, 2005)

Table 2-2: Mean monthly rainfall (mm), Navrongo and Tamale (1961-2005) (Source: WRC, 2008)

Station	Jan	Feb	Mar	Apr	May	Jun	Jul	Aug	Sep	Oct	Nov	Dec	Total
Navrongo	1	3	15	53	100	132	189	270	165	51	4	2	985
Tamale	4	9	44	84	122	154	159	201	219	86	10	3	1,095

2.5 Temperature

Temperatures in the Volta Basin generally decrease from the north to the south. Average monthly temperatures ranges from 36 °C to 27 °C in the north and from 30 °C to 24 °C in the south (Obuobie, 2008). Maximum daily temperatures could rise to 44 °C and usually occurs between March and April whereas minimum daily temperatures could fall as low as 14 °C usually recorded between December and February (Obuobie, 2008).

Similar to the Volta Basin, the White Volta Basin is characterized by uniformly high temperatures throughout the year with a mean annual temperature of about 28 °C. The months of March and April are the hottest periods with a temperature of about 32 °C. August is the coolest month with a mean temperature of about 26°C. Diurnal variations of 5 ^{o}C-7 ^{o}C from the mean are observed in the basin (WRC, 2008).

2.6 Evaporation

Mean annual potential evaporation in the Volta Basin is estimated to exceed 2,500 mm in the north whereas the south is estimated to be approximately 1,500 mm per annum. Approximately 80% of annual precipitation in the basin is removed by evapotranspiration (Kasei, 2009). Monthly rainfall generally exceeds potential evaporation mostly for only 2–3 months per year (Figure 2.4). Similar to the Volta Basin, the mean annual potential evapotranspiration of the White Volta sub-basin exceeds mean annual rainfall in the entire basin. It varies from about 1,950 mm in the northern part of the basin to approximately 1,650 mm in the south (WRC, 2008).

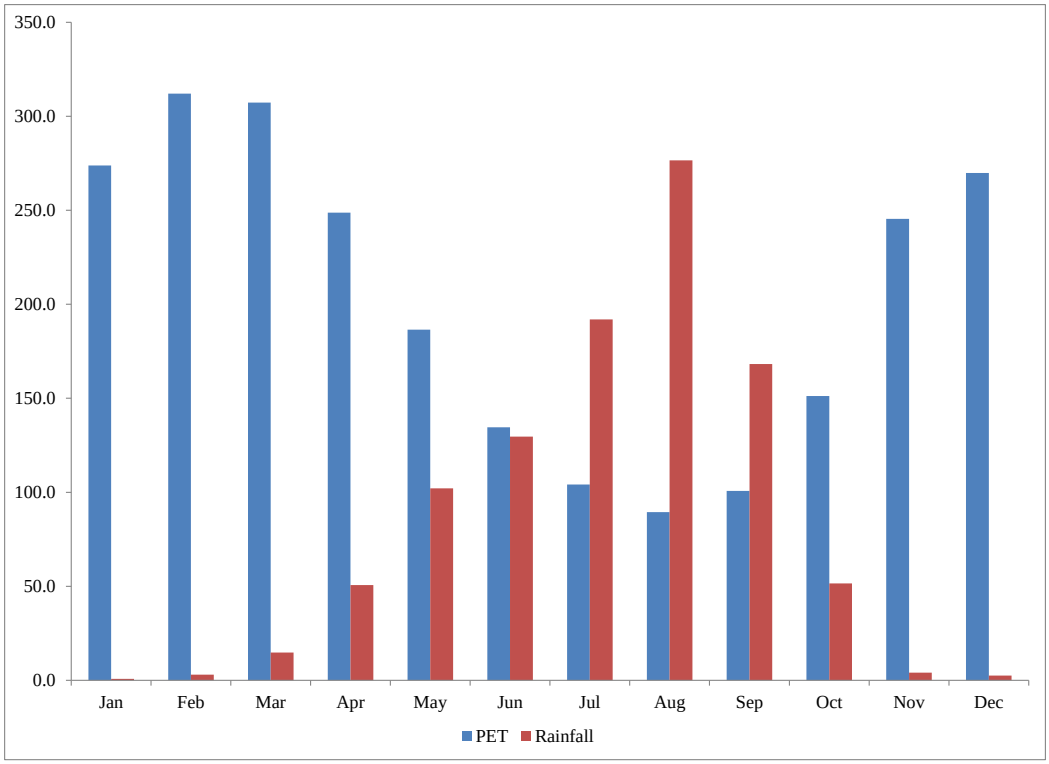

Figure 2-4: Long-term mean monthly precipitation and potential evapotranspiration (PET) for the Navrongo (1961-2003) synoptic station. (source: Ghana Meteorological Agency)

2.7 River Runoff

Runoff in the Volta Basin accounts for approximately 9 % of annual precipitation (Andreini *et al.*, 2000). Annual variability of runoff in the basin is higher than precipitation. This can be attributed to the non-linear response of runoff to precipitation (Obuobie, 2008).

The White Volta Basin has a mean annual flow ranging from a minimum of 0.2 km^3 downstream of its sources in northern Burkina Faso to approximately 8 km^3 before it confluence with the Black Volta in Ghana. The mean annual flow entering Ghana from Burkina Faso is approximately 2.2 km^3 and increases to 4.0 km^3 downstream of the confluence with the Red Volta (Amisigo, 2005).

The flow regime of the river exhibits a marked variability in the seasonal runoff within the year as well as in the annual flows. These features are highlighted below using streamflow data from the Daboya gauging station in the downstream section of the White Volta River. The discharge record used represents the flow regime after commissioning of the Bagré Dam in Burkina Faso in 1995.

Table 2.3 shows the average monthly runoff as well as the average monthly maximum and minimum values. The distinct, skewed temporal distribution of the White Volta River

runoff within a year is clearly detected from these presentations. It is worthwhile noting that statistically about 80%-85% of the total annual runoff occurs during a span of only 3 months, i.e. from August to October.

Figure 2.5 provides a graphical representation of the annual runoff as recorded at Daboya. The average annual volume of flow at Daboya during the 1997 to 2007 period is recorded as 6,335 million m^3, equivalent to 201 m^3/sec. It can be derived from the graph that widespread flooding in the White Volta River system occurs when the annual runoff approaches 10,000 million m^3, as it happened in 1999 and 2007 (WRC, 2008).

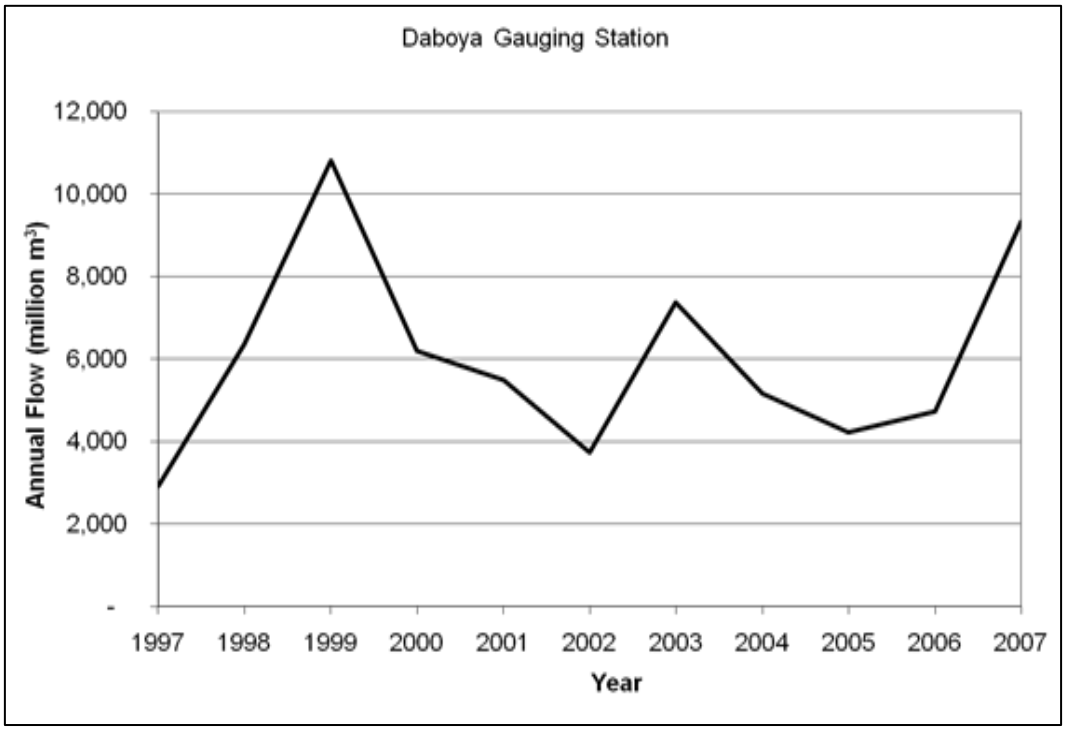

Figure 2-5: White Volta River annual runoff (1997-2007) at Daboya (source: WRC, 2008)

Table 2-3: White Volta River mean monthly flows (1997-2007) at Daboya (m^3/sec) (source: WRC, 2008)

	Jan	Feb	Mar	Apr	May	Jun	Jul	Aug	Sep	Oct	Nov	Dec
Mean	26.8	25.4	24.7	31.5	42.6	84.6	151.1	469.2	910.8	518.0	71.2	35.1
Max	48.7	52.7	37.5	45.6	89.0	189.2	309.9	903.8	1612.4	1028.5	151.8	56.1
Min.	6.8	7.2	5.5	19.3	19.7	43.7	59.0	182.3	479.3	168.5	36.9	18.2

2.8 Flooding

Flooding has been identified as one of the major water management problems in the basin (WRC, 2008). Recent devastating floods in the basin include the 1994, 1999 and 2007 floods. For examples 52 people were reported to have lost their lives in the 1999 floods. Moreover, an estimated USD21 million was required to rehabilitate the affected flood victims. The floods experienced in September 2007 have been the most widespread and devastating of the recent floods in the basin (WRC, 2008).

According to UN Integrated Regional Information Networks and the National Disaster Management Organization (NADMO) under the Ministry of Interior in Ghana, an estimated 266,000 people in the 3 northern regions were affected by the 2007 floods. 22 people were reported to have lost their lives with over 11,000 homes and more than 12,000 ha of farmland destroyed. Government estimates for immediate aid to the 3 regions were reported to be nearly USD48 million. Additionally, in all these floods the threat to human health through pollution of potable water sources such as boreholes/wells have also been significant (WRC, 2008).

2.9 Geology and Hydrogeology

The dominant geology of the Volta Basin is the basement crystalline rocks which are of Precambrian age. They made up of the Tarkwaian, Birimian, Dahomeyan, Buem and Togo formations (Figure 2.6) (Obuobie, 2008).

Palaeozoic consolidated sedimentary formation, commonly known as the Voltaian system, is the dominant geological formation in the southern part of the basin. It consists of shales, sandstones, arkose, limestones, mudstones, sandy and pebbly beds (Obuobie, 2008). The dominant geological formations in the northern part of the basin are made up of thick layers of sandstones, schist and carbonates (Martin, 2005).

The geological formation of the White Volta Basin on the other hand consists of 45% crystalline rocks of the Birimian formation with some isolated patches of the Tarkwaian formations. The Voltaian system, consisting of the Upper Voltaian sandstone, Obosum and Oti beds and Basal sandstone, forms 55% of the geology of the basin (WRC, 2008).

The Voltaian systems comprise of sandstones, shales and mudstone beds, and rest on the Birimian, the Granite and Tarkwaian formations. They extend over a large part of the central, eastern and southern portions of the basin and are considered to be of late

Precambrian to Paleozoic age. Three main stratigraphic subdivisions of the Voltaian systems occur in the basin - the Basal sandstone, the Upper Voltaian and Obosum beds.

The Birimian formation and its associated granite intrusions as well as the Voltaian formation are characterized essentially by little or no primary porosity. Therefore, groundwater occurrences are associated with the occurrence of secondary porosities caused by fracturing, faulting, jointing and weathering.

It has been estimated that in most parts of the basin, current groundwater production is less than 1% of estimated recharge (WRC, 2008). Production is still less than 5% of recharge even in areas such as the north-eastern part of the basin, where groundwater abstraction is relatively high (Martin and van de Giesen, 2005). The mean yield as calculated from a total of more than 1,400 existing boreholes with yield data available in the White Volta River Basin is 3.7 m^3/hour (HAP, 2008). Table 2.4 below summarizes the statistical evidence related to occurrence and potential rate of groundwater abstraction in the White Volta Basin.

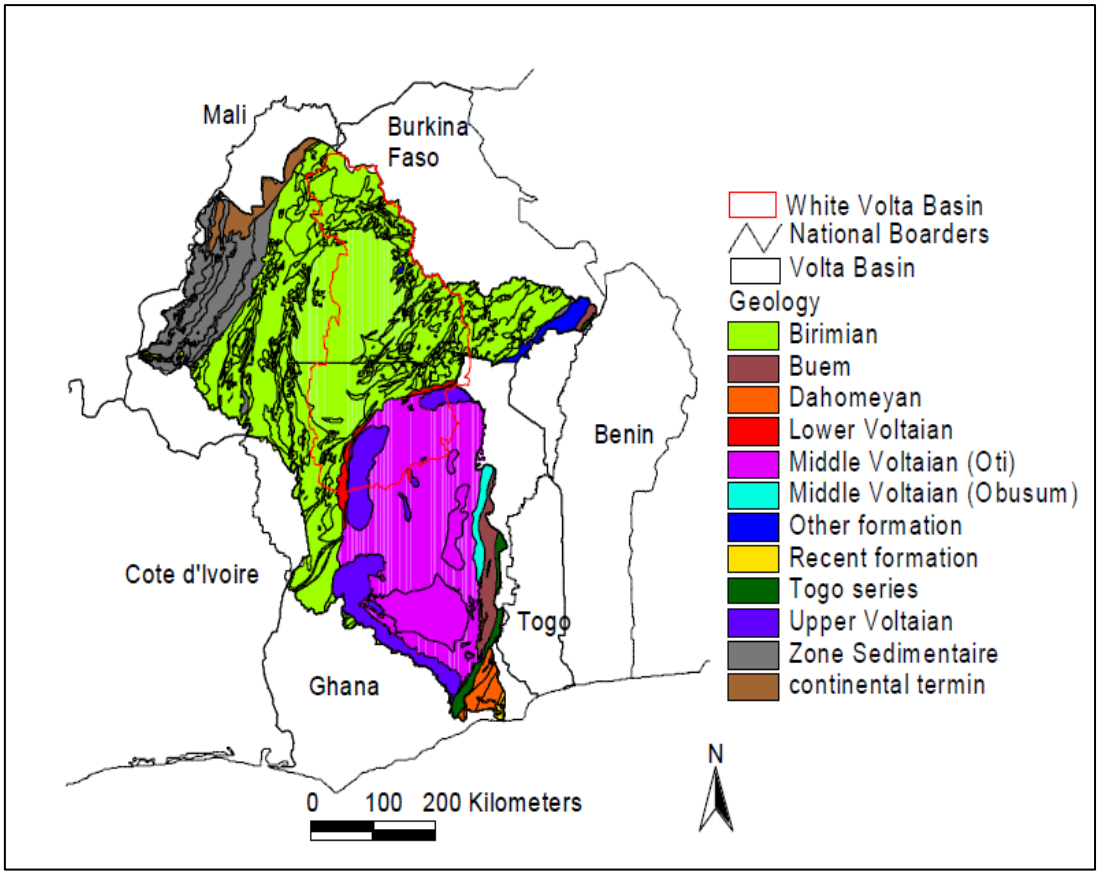

Figure 2-6: Geology map of the Volta Basin (source: Obuobie, 2008)

Table 2-4: Borehole characteristics in White Volta Basin (Source: HAP, 2008)

Geological zone	Depth of borehole (m)		Depth to aquifer top (m)		Borehole yield (m^3/hour)	
	Range	Mean	Range	Mean	Range	Mean
Birimian Formation	10 – 104	43.6	1 – 81	24.5	0.6 – 12.0	3.1
Voltaian Formation	6 – 180	54.2	1 – 72	17.3	0.5 – 18.0	4.1

2.10 Land-use/Land-cover

The savannah, which comprises grassland interspersed with shrubs and trees, is the predominant type of land cover in the Volta Basin. It covers approximately 86% of the basin's catchment area with settlement/industrial, croplands, wetlands and forest cover making up the remaining 14% of the land cover type in the basin (WRI, 2003). Figure 2.7 presents the land use map of the Volta Basin.

Short bush fallow cultivation along the river banks and less intensive bush fallow cultivation in other parts of the basin constitute the main land use in the White Volta basin. Animal grazing is common in the basin (Andah, 2005).

The original ecology of the White Volta River Basin was moist Guinea savannah with a considerable cover of broad-leaved trees forming closed canopy of branches in some places. It was relatively rich in species of flora and fauna (teeming game of browsing and grazing animals that were in ecological balance with the vegetation). Human activities through time have significantly modified this fragile ecology. A marked deterioration in the ecology has been realized in the basin within the past 10-20 years (WRC, 2008). The forested area and tree cover has thinned considerably leading to significant increase in the area coverage of what is classified as open savannah woodland. Table 2.5 summarizes the development in area coverage of the forested land and other zones as it has occurred during the period 1990-2000.

At present the vegetation of the basin consists of shorter grasses and a few fire-resistant trees. This kind of vegetation has resulted mainly from prolonged grazing, burning and cultivation. Two physiognomic types of savannah may be recognized in the White Volta Basin. The north-eastern corner of the basin has been so disturbed by intensive farming that few trees remain apart from the baobab (*Adansonia digitata*).

The traditional savannah woodland with light canopy which characterized the greater part of the area has gradually been replaced with a type of open savannah with scattered trees that rarely form closed canopy. Annual bushfires have acted to influence the dominance of

grasses to the detriment of the former woodland. What remains of the original vegetation occurs along the wetter banks of rivers and streams as gallery forest and in fire protected forest reserves.

"Predominant land use of the White Volta is extensive land rotation cultivation two to six miles away from the village with widespread grazing of large numbers of cattle and other livestock" (Andah, 2005) and compound cropping (home gardening) around the house (Andah, 2005). Analysis of the 1989 land use and land cover showed that in the northern portions of the basin, an estimated 50% of the land was being cultivated at the compound and bush fallow scale (Andah, 2005). Furthermore, pasture is also very poor and usually under natural conditions with annual bush burning.

From various perspectives, the water resources are under pressure in the dry, low-flow season. Original people settled in the valley bottoms where adequate supplies of water ensured plentiful harvests. Soil fertility in the valley bottoms declined over time, forcing the populations to settle on watersheds placing the water resources under siege.

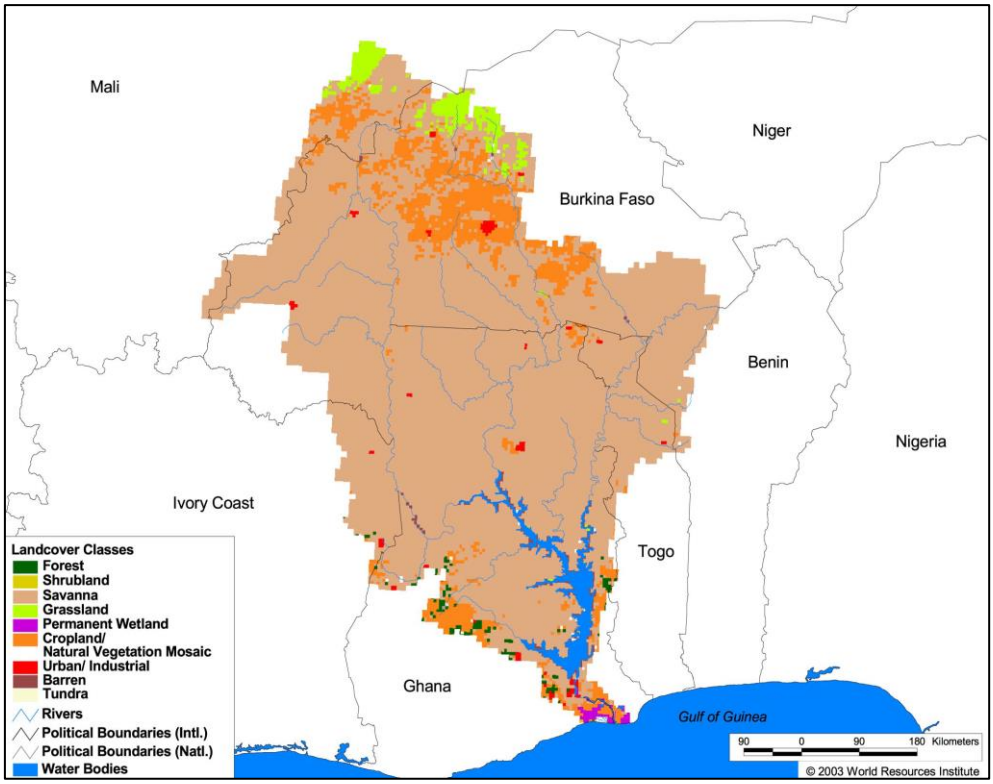

Figure 2-7: Land cover and use types in the Volta Basin (source: WRI, 2003)

Table 2-5: Development in land use/cover of the White Volta River Basin (1990-2000) (source: WRC, 2008)

Year	Forested area	Savannah woodland	Arable land	Settlements and build-up (bare) areas	Unclassified and water bodies
1990	18%	29%	51%	0.2%	1.8%
2000	8%	40%	51%	0.5%	0.5%

2.11 Soils

The soils found in the Volta Basin of Ghana are predominantly Lixisols, Leptosols, Plinthosols, Acrisols and Luvisols. Figure 2.8 presents the soil map of the Volta Basin. The soils formed from the Voltaian sediments vary widely in terms of soil texture and productivity and generally have low inherent soil fertility compared to the granite derived soils. Furthermore, the groundwater table in the Voltaian sediments is shallow as compared to that of the granitic soils (Agyare, 2004).

Luvisols, Regosols and Arenosols are the major soil types found in the Volta Basin with Luvisols being the dominant soil type. Regosols and Arenosols are generally found at the extreme northern part of the basin. Luvisols are soils having an argic horizon which has a cation exchange capacity equal to or greater than 24cmol (+) kg^{-1} clay throughout (ISRIC, 2016).

Regosols are soils of medium and fine texture without distinctive horizon other than an ochric horizon at the surface (ISRIC, 2016). The Regosols found in the basin are sensitive to drought due their high permeability and low water holding capacity. Arenosols in the basin also have low water holding capacity due to their high clay content. They are generally low in soil fertility and are poor in crop production (Obuobie, 2008).

The soils in the northern part of the basin are largely lateritic compared to soils in the southern part which are of the lixisol type. The "weathered soils are usually a composition of kaolinite clays and have high contents of iron, aluminum and titanium oxide and the aggregate stability at the surfaces is usually low, and soils with low vegetation cover are prone to erosion" (Kasei 2009).

The soil textures of the basin comprise of sandy loam to sandy clay loam (Bharati et al., 2008). Generally, the upper part of the soil profile contains high clay contents and coarse textures at the lower parts. On average, weathering reaches a depth of 30-40 m (Bharati et al., 2008). A study on soil properties conducted by Agyare (2004) revealed high discrepancies between subsoil and topsoil at two different climatic zones in the basin. The high

discrepancies were attributed to the fact that there was less soil disturbance in the subsoils. The computed saturated hydraulic conductivity was also found to be highly variable in space for the soil layers considered.

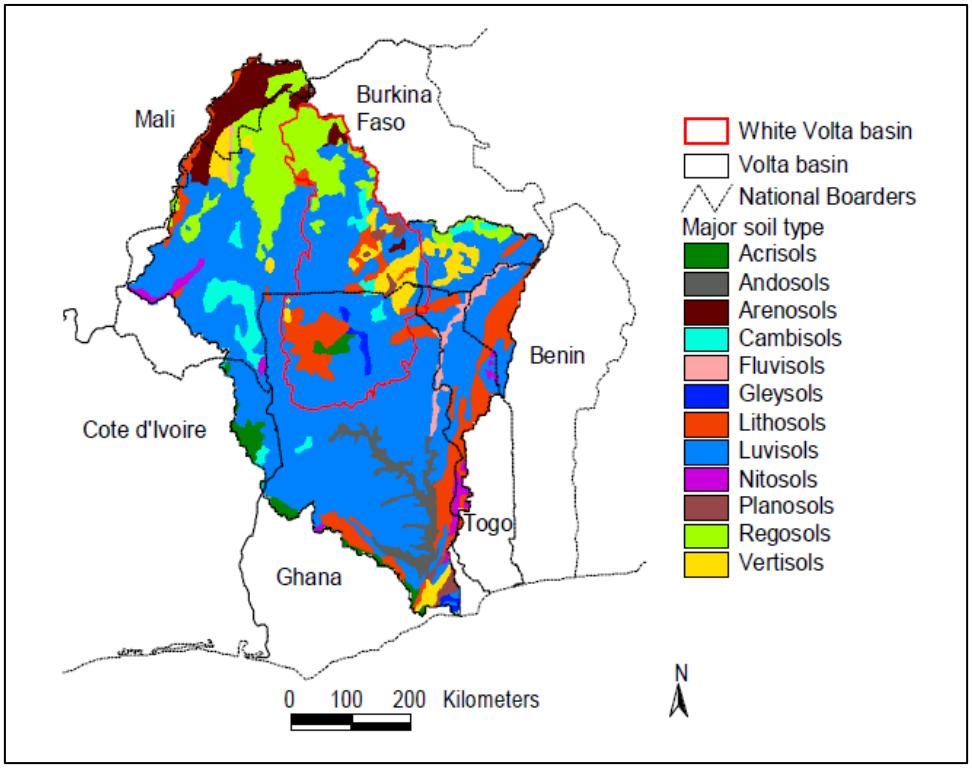

Figure 2-8: Soil map of the Volta Basin (source: Obuobie, 2008)

2.12 Demography

Among other demographic characteristics, the size of the population, its growth rate, density, and rural/urban distribution have strong bearings on Basin-wide productivity and livelihood security outcomes. The countries with the largest population are Ghana (20 million), Côte d'Ivoire (16 million), and Burkina Faso and Mali (around 11 million each), while Benin (6 million) and Togo (5 million) have the lowest populations.

The countries within the basin have one of the fastest growing populations in the world, although annual population growth rates vary considerably: Benin, Burkina Faso, and Togo between 2.4 and 2.6%; Côte d'Ivoire and Mali between 2.2 and 2.5%; and Ghana, the only country with a growth rate below 2% (Andah, 2005). Rural population growth rates are consistently lower than the national rate, that is urban, which points to rapid urbanization and rapid increases in the urban areas. With an average basin growth rate of 2.54%, the population is projected to grow to an estimated 35 million by the year 2025 and represents a

90% increment over a 25 year period (Barry *et al*., 2005). Majority of the basin's inhabitants reside in Ghana and Burkina Faso (Table 2.6).

The main economic activity in the basin is agriculture which is mostly subsistence farming (Rodgers *et al*., 2006). Tamale and Bolgatanga in Ghana and Ouagadougou in Burkina Faso are among the few cities located in the White Volta Basin.

Table 2-6: Volta Basin demographic characteristics (source: Barry et al., 2005)

Basin Country	Basin population in country			Growth Rate (%) (2000)	Pop. density (pers./km2) (2000)	Rural (%)
	1990	2000	2025			
Burkina Faso	7,014,156	887,4148	1,599,7351	2.4	41.53	77.4
Ghana	5,198,000	667,4376	1,169,6054	2.5	26-104	84.0
Togo	1,189,900	1,594,446	3,385,266	2.8	66	70.0
Mali	380,000	625,000	1,260,000	2. 8	45-75	87.8
Benin	382,328	476,775	820,000	2.3	43.4	64.0
Côte d'Ivoire	no data	397,853	717,672	2.5	8-22	77.0

2.13 Conclusion

The White Volta Basin, the second largest catchment of the Volta Basin, covers about 100,148 km^2 at Nawuni and represents approximately 26 % of the total Volta catchment area. The Red Volta, Nasia, Nabogo and the Kulpawn/Sissili rivers are the main tributaries of the White Volta Basin. The Bagre hydroelectric dam is the major hydraulic infrastructure in the basin.

The White Volta Basin climate is generally characterized as tropical continental, or savanna, with a uni-modal rainy season. The onset of the rainy season starts from May and ends in October, followed by a prolonged dry season. Peak rainfall usually occurs around late August or early September. Annual total rainfall in the basin ranges between 1000 to 1300 mm and a mean annual temperature of about 28 °C.

Chapter 3

3 DATA, MATERIALS AND METHODS

3.1 Overview of Data Collection

A significant amount of spatial and temporal data is available in the White Volta Basin for the development and calibration of a SWAT model. The data for the model development, calibration, and validation originated from numerous sources and include spatial information such as DEM, soils and land use. Temporal data such as climate measurements, river discharge and sediment discharge derived from turbidity measurements were also obtained through field measurements and desktop analysis.

Hydro-meteorological data were obtained from the Hydrological Services Department in Ghana, the Ghana Meteorological Agency and the Direction de la Météorologie Nationale, Burkina Faso. Climatological data such as daily rainfall, minimum and maximum air temperature, relative humidity, wind run (converted to wind speed), and sunshine hours (converted to solar radiation) was obtained for 22 weather stations located within and around the White Volta Basin and covers the period 1990 to 2013.

3.1.1 Turbidity Data

3.1.1.1 Historical Turbidity Data

Daily turbidity data spanning the period 1993-2013 was collected from the Ghana Water Company Limited, GWCL. GWCL abstracts raw water for treatment from the White Volta River at Nawuni for Tamale and its environs. As part of the standardization process, the GWCL has been monitoring the raw water quality at their abstraction point in Nawuni since 1993. The GWCL has collated daily and monthly water quality parameters such as pH, color, alkalinity and turbidity from 1993 to date. The quality of the raw water is monitored at least three times daily and at most twelve times daily.

3.1.1.2 Field Measurements of Turbidity

According to Rasmussen *et al.,* (2009), different meter configurations, measurement methods, and color effects may affect the relationship between turbidity and SSC. These effects may be minimized by obtaining comparable measurements for a specific site using consistent measurement techniques and appropriate instruments. Wagner *et al.*, (2006) therefore recommended that an evaluation of the turbidity records should be undertaken by

comparing in-stream turbidity in the cross-section with the turbidity as measured at the fixed-location (Rasmussen *et al*., 2009).

The abstraction point for the GWCL was considered as the fixed-location. GWCL has over the period collected the raw water samples for water quality analysis from the same intake point. Approximately 50 m downstream of the intake point; discharge measurements were undertaken with a Rio Grande Workhorse ADCP mounted on a Zodiac inflatable boat (Plate 3-1b). At the discharge measuring cross-section (Plate 3-1a), concomitant turbidity and suspended sediment samples were taken using the equal-width increment method (Gray *et al.*, 2008). The cross-section turbidity measurements were periodically collected at three different depths (0.2, 0.6, 0.8 of total depth) as recommended by Anderson (2005) (Plate 3-1a). These measurements were then averaged and used in evaluating the representativeness of the turbidity as measured at the fixed-location.

Plate 3-1: Cross-section turbidity measurements with (a) Quanta Lab at Nawuni and (b) fixing Rio Grande ADCP to Zodiac inflatable boat at Daboya

3.1.2 Suspended Sediment Concentration Measurements

3.1.2.1 Historical Suspended Sediment Concentration Data

The available suspended sediment concentration data for Nawuni and Pwalugu were obtained from the Water Research Institute, WRI of the Council for Scientific and Industrial Research, CSIR. The data which was part of measurements of suspended sediment concentrations of water samples collected from six rivers (Amisigo & Akrasi 1996) covers the period July 1994-March 1995. The surface dip sampling method was used in collecting the data at a sampling interval of 3 days on average. To correct for the underestimation of surface dip sampling, a correction factor of 25% was used to provide mean concentration values for the cross-section area (Akrasi, 2005).

3.1.2.2 Field measurements of suspended sediment concentration

To determine the annual variability in sediment yields for the study area, suspended sediment samples were collected from September 2012 to December 2013 at eight (8) selected monitoring stations (Figure 2.2). As a result of the high variability of suspended sediment concentration in rivers (Lawler et al., 2006), gauge readers of the selected stations were engaged to take daily water samples by surface dipping. Daily surface dip samples (Plate 3-2 (a)) were sampled concurrently with kinematic depth-integrated sampling (Plate 3-2 (b)) during monthly field visits. A correction factor was developed by correlating the surface dip samples with the depth-integrated samples. The derived correction factor was then used to correct the bias associated with the surface dip samples taken by the gauge readers (Moshe, 1982; Edwards and Glysson, 1999; Akrasi, 2005). To account for lateral and vertical variability in sediment concentration, the cross-section was divided using the equal width increment method and sampling undertaken with a depth-integrated sampler (DH-48 during low flows and DH-76 during high flows). The cross-section was divided into five sections and samples were taken at the midpoints of the intervals (Edwards and Glysson, 1999). Prior to sampling, the gauge height at the station was read and river discharge measured with the Rio Grande WorkHorse ADCP (Plate 3-1b). Depth-integrated samples were taken simultaneously with turbidity measurement with the Quanta HydroLab (Plate 3-1a).

Plate 3-2: Sampling with the (a) depth-integrated sampler at Yapei and (b) surface dip at Nasia.

The suspended sediment samples were transported to Accra and analyzed in the WRI Laboratory, using the evaporation method (Porterfield, 1972). This involves flocculating the suspended sediment samples using magnesium chloride ($MgCl_2$), settling for 24 hours and decanting the supernatant solution. The settled sediments were emptied into dishes of known

tare weights and oven dried at 85°C. The dishes were then cooled in a desiccator after which their gross weights were taken. The weight of each sediment sample was obtained by deducting the tare weights of dishes from gross weights. The suspended sediment concentration of the sample was then obtained by dividing the weight of the sediment by the weight of the mixture of sediment and water and multiplied by one million converting it to parts per million. The sediment concentration for the cross-section was obtained by adding the samples taken at each point interval. The daily suspended sediment load was computed using Equation 3.1 (Porterfield, 1977; Horowitz, 2003):

$$SL = 0.0864 \cdot Q \cdot SSC \qquad (3.1.1)$$

where *SL* is the daily sediment load (metric tonnes/day), *0.0864* is a conversion factor, *Q* is the instantaneous river discharge (m^3/s) and *SSC* is the instantaneous suspended sediment concentration (mg/l).

The computed instantaneous river discharge and the water level at the station were entered into a hydrological database (Hydata v4.2 by Institute of Hydrology, Wallingford, UK) for analysis. Hydata is the database being used by the Hydrological Services Department (HSD), Ghana. The existing rating curves obtained from HSD were updated with the new discharge measurement.

The time of sampling the suspended-sediment concentrations were matched to the closest time of turbidity measurement recorded by GWCL. Data points with a standardized residual exceeding three standard deviations from the regression were considered outliers and removed from the data set. Regression models were then developed with the measured data and validated using the 1994/1995 historical data.

Monthly, annual, mean monthly and mean annual suspended sediment load as well as annual sediment yield for the period was computed from the daily sediment discharge data of each sampled site. Mean monthly suspended sediment load is the average of the daily suspended sediment discharge per month (metric tonnes/day) whiles the monthly sediment load is the sum of the daily sediment load in a month (metric tonnes/month). Annual suspended sediment load is the sum of monthly sediment load for the year (metric tonnes/yr). The annual specific sediment yield was obtained by dividing annual suspended sediment yield by catchment area (metric tonnes/ km^2/yr) (Akrasi, 2005).

3.1.3 **Digital Elevation Model (DEM)**

The first step in setting up the ArcSWAT model for the study is the physiographic analysis based on catchment topography. The ArcSWAT automatically delineates a watershed into sub-watersheds based on the digital elevation model (DEM) to account for catchment heterogeneities. A pre-processed 90 m resolution DEM of the study area was derived from the Shuttle Radar Topography Mission (SRTM) and obtained through the Glowa Volta Project (Figure 3-1). The DEM was supplied as an input to the ArcSWAT for topographic analysis, delineation of sub-watershed and stream network generation.

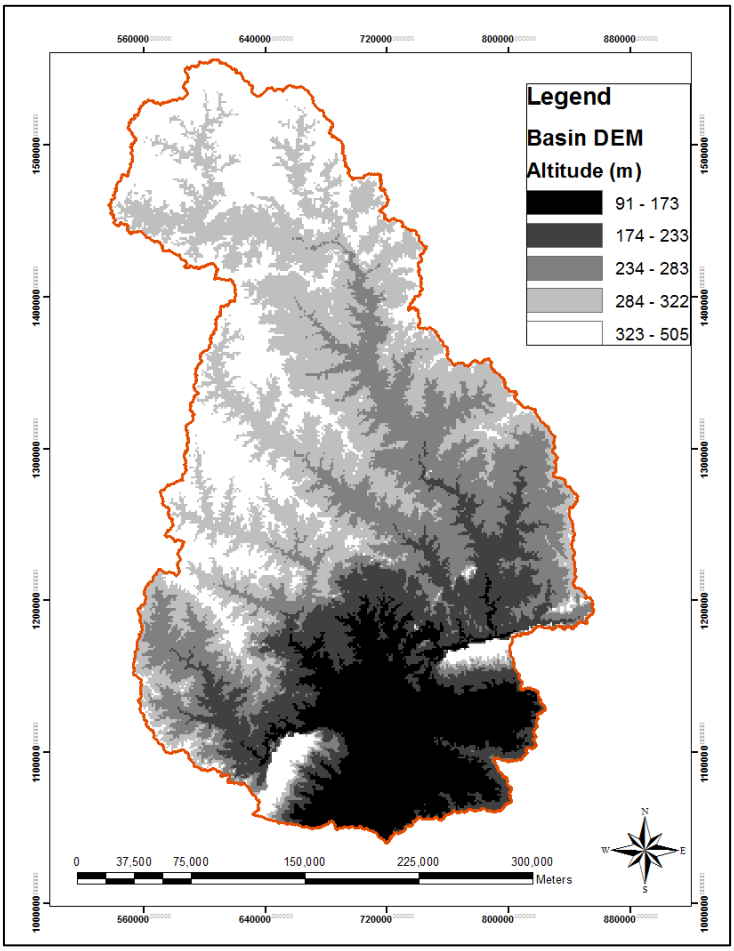

Figure 3-1: DEM of the White Volta Basin
(source: delineated from Volta Basin SRTM DEM, GVP)

3.1.4 **Climate Data**

Climatological time-series data such as daily precipitation, daily maximum and minimum air temperature, relative humidity, wind speed, and solar radiation were used as input to the SWAT model in this study. The climate data was obtained for twenty-two (22) weather stations located within and around the White Volta Basin (Figure 3-2) and generally

covers the period 1970 to 2013. The climate time-series data for the period 1991 to 2013 was however used in this study.

The climatological data obtained for this study was not uniformly distributed in the study area. The data consist of sixteen (16) weather stations obtained from the Ghana Meteorological Agency with the other 6 from the National Meteorological Directorate of Burkina Faso. Of the sixteen (16) weather stations in Ghana, four (4) are synoptic stations (Wa, Tamale, Yendi and Navrongo), seven (7) are climate/agro-meteorological stations and the rest are rainfall measuring points. On the other hand, four (4) of the stations in Burkina Faso are synoptic stations (Ouagadougou, Ouahigouya, Fada-Ngourma and Po), and the other two (2) being rainfall measuring points. The time-series data coverage is summarized in Table 3-1.

Table 3-1: Weather stations and time-series in the White Volta used in the SWAT model

No.	Station	Station Type	X_coords	Y_coords	Rainfall	Temperature	Relative Humidity	Wind Run	Sun Shine
1	Babile	Agromet	-2.82	10.52	1960-2013	1960-2013	1983-2013	1972-2013	2002-2013
2	Bole	Agromet	-2.42	9.02	1960-2013	1961-2013	1961-2013	1961-2013	1961-2013
3	Daboya	Rainfall	-1.38	9.57	1990-2013				
4	Damongo	Agromet	-1.80	9.07	1960-2013	1960-2013			
5	Lawra	Rainfall	-2.88	10.47	1960-2013				
6	Manga Bawku	Agromet	-0.27	11.02	1979-2013	1960-2013	2011-2013		
7	Navrongo	Synoptic	-1.10	10.90	1960-2013	1960-2013	1970-2013	1960-2013	1960-2013
8	Pong Tamale	Agromet	-0.83	9.67	1960-2013	1960-2013			
9	Tamale	Synoptic	-0.88	9.42	1960-2013	1960-2013	1970-2013	1960-2013	1960-2013
10	Tumu	Rainfall	-1.98	10.87					
11	Vea	Agromet	-0.85	10.87	1972-2013	1972-2013	1989-2013		1989-2013
12	Wa	Synoptic	-2.50	10.07	1975-2013	1980-2013	1980-2013	1980-2013	1980-2013
13	Yapei	Rainfall	-1.15	9.15	1975-2013				
14	Zuarungu	Agromet	-0.80	10.78	1960-2013	1960-2013	1993-2013		2004-2013
15	Funsi	Rainfall	-1.98	10.28	1960-2013				
16	Yendi	Synoptic	0.02	9.45	1960-2013	1960-2013	1977-2013	1980-2013	1960-2013
17	Ouahigouya	Synoptic	-2.43	13.58	1980-2010	1980-2010	1980-2010	1980-2010	1980-2010
18	Po	Synoptic	-1.15	11.17	1980-2010	1980-2010	1980-2010	1980-2010	1980-2010
19	Ouagadougou	Synoptic	-1.52	12.35	1980-2010	1980-2010	1980-2010	1980-2010	1980-2010
20	Fada Ngourma	Synoptic	0.36	12.03	1980-2010	1980-2010	1980-2010	1980-2010	1980-2010
21	Kaya	Rainfall	-1.08	13.10	1980-2010	1980-2010	1980-2010	1980-2010	1980-2010
22	Tenkodogo	Rainfall	-0.38	11.77	1980-2010	1980-2010	1980-2010	1980-2010	1980-2010

Some of the weather stations have missing data in their time-series ranging from several days to years. The WXGEN weather generator model offered in SWAT was used to fill in the gaps in the measured time-series. The WXGEN model requires at least twenty (20) years of records to be able to fill in missing data. For this study, twenty-three (23) years climate statistics from the six (6) synoptic stations in the study area were used for generating the missing data in all the climate records.

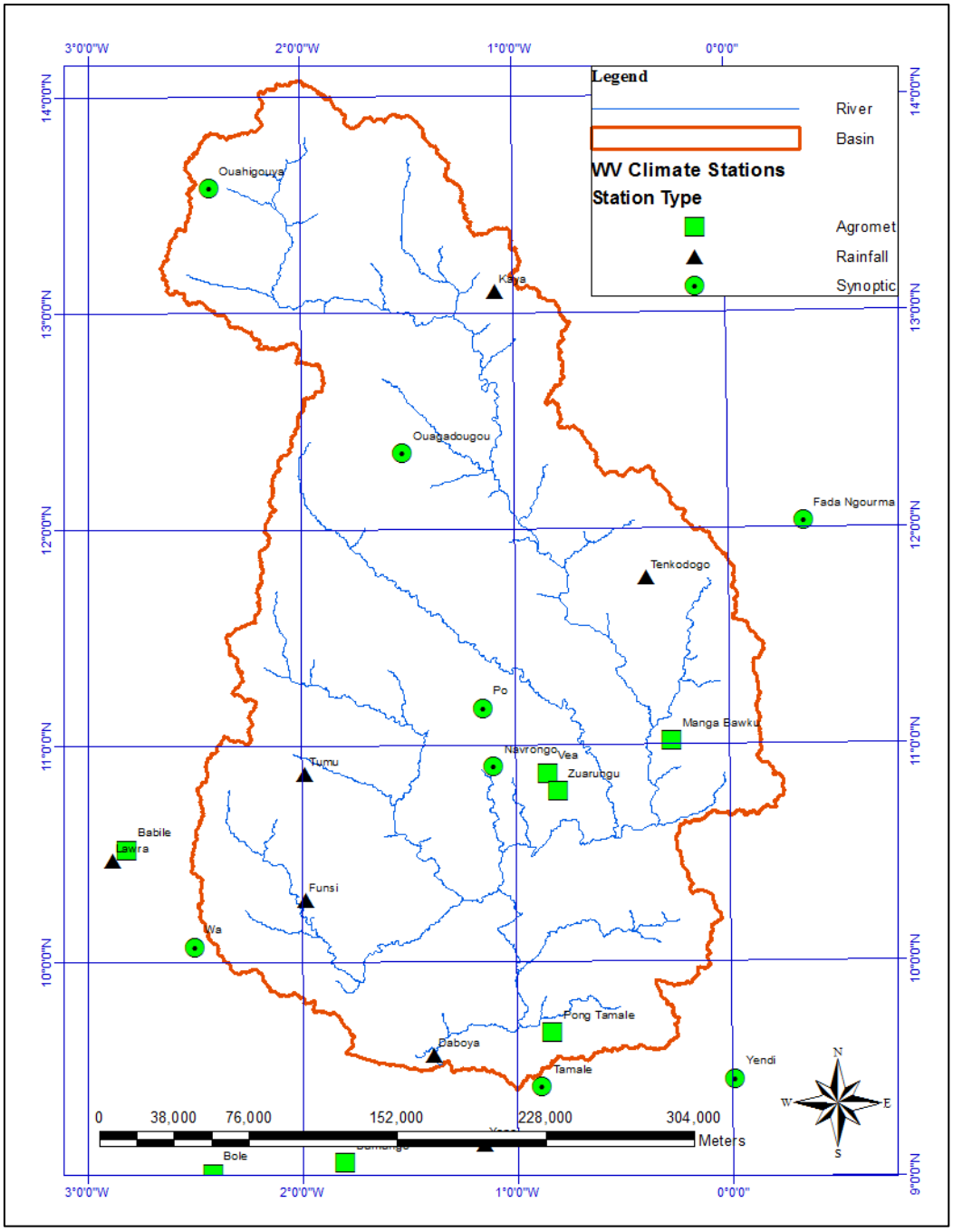

Figure 3-2: The White Volta Basin showing the locations of climate stations

3.1.5 **Soils**

Soil hydraulic properties play a pivotal role in determining the water budget for the soil profile, surface runoff and erosion in distributed hydrologic models. SWAT requires the textural, physical and chemical properties of each the soil layers. The soil data used in this study was obtained from the Food and Agriculture Organization (FAO) digital soil map of the world and derived soil properties (FAO/UNESCO, 2003). The digital soil map of the world

incorporates approximately 5000 mapping units and more than 200 soil-units for two layers (0-30 cm and 30-100 cm depth) (Schuol *et al.*, 2008). The datasets comprises of digital map layers with associated attribute tables of soil properties. The map covers the entire world and is presented in ArcInfo GIS export format. The soil map of the world is a compilation of soil data from individual countries which also used a variety of local soil data. The data was therefore generalized for the entire world. The map scale is 1:5,000,000 with a spatial resolution of 10 km.

The FAO soil map is made up of polygonal mapping units which are linked with unique numbers in the feature attribute tables. The attribute tables are referenced as SNUM and ranges from 1 to 1972 for Africa. The attribute table also contains the FAO soil identifier name and number, and the soil-units contained within the mapping unit. The soil classification map of the study area according to FAO/UNESCO Soil Classification System is presented in Figure 3-3 with the percent coverage areas in Table 3-2. Seven different soil textures were identified in the study area and dominated by sandy loam with 35.93% of the total catchment area with the least dominant soil being sand with just 0.01% of coverage area (Table 3-2).

Table 3-2: Soil texture in the White Volta Basin and percent area covered

Texture	Area Covered (sqkm)	Percent Coverage (%)
Sandy Loam	35986	35.93
Sandy Clay Loam	25665	25.63
Loam	15712	15.69
Loamy Sand	11413	11.40
Clay	10006	9.99
Clay Loam	1361	1.36
Sand	6	0.01

To integrate the digital soil map within the SWAT model, a Soil Lookup Table was created to link the digital soil map with the usersoil table in SWAT. The usersoil table in SWAT contains the textural and physical-chemical properties for each soil layer (Table 3-3). In addition to the digital soil map other physical properties of soils in the study area were obtained from other sources including the FAO-derived soil properties and literature (Agyare, 2004; Obuobie, 2008).

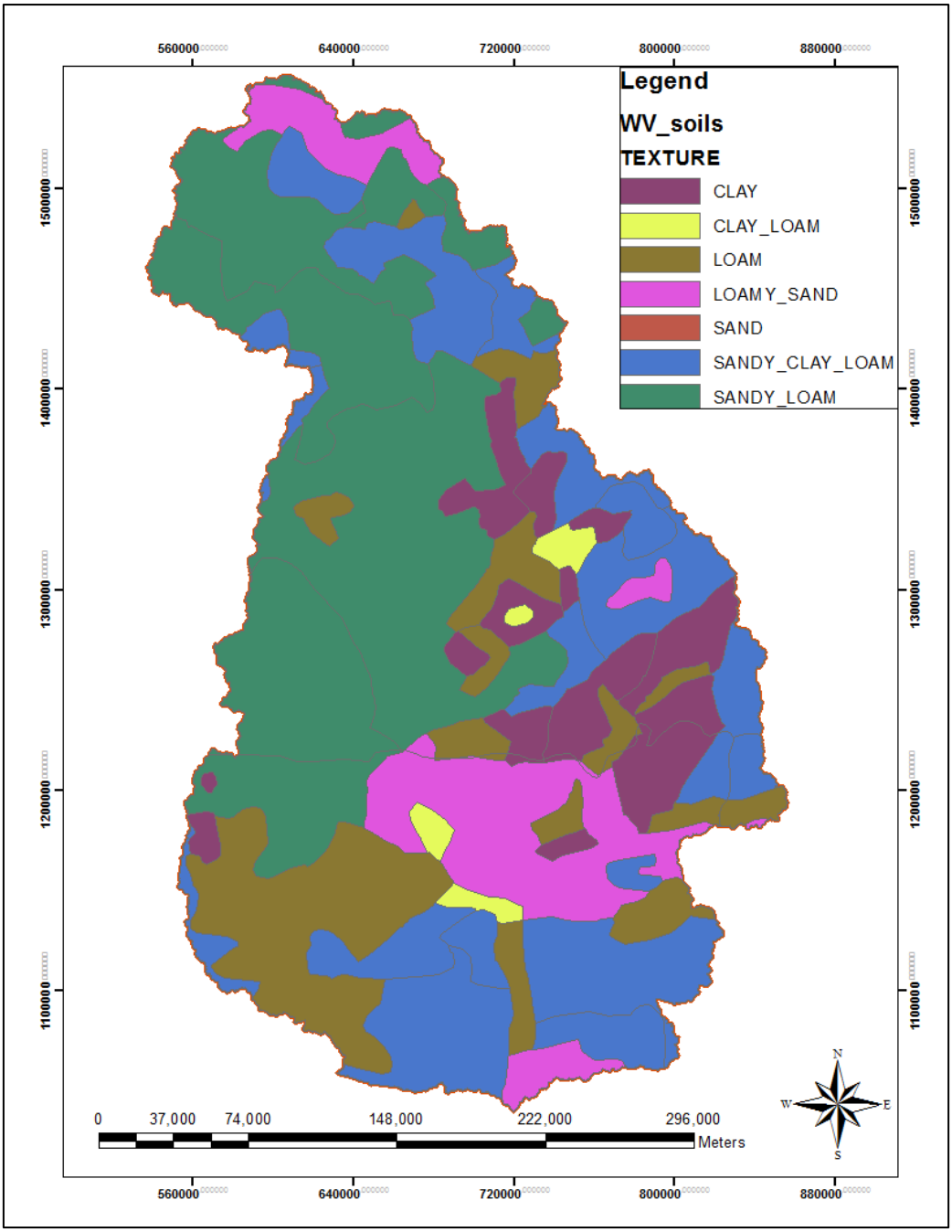

Figure 3-3: Soil map of the White Volta Basin (source: FAO/UNESCO, 2003)

Table 3-3: Soil properties required in the SWAT model (Neitsch *et al.*, 2011)

Soil Parameter	Description
NLAYERS	Number of layers in the soil (min 1, max 10)
HYDGRP	Soil hydrologic group (A, B, C, D)
SOL_ZMX	Maximum rooting depth of soil profile
ANION_EXCL	Fraction of porosity from which anions are excluded
SOL_CRK	Crack volume potential of soil [optional]
TEXTURE	Texture of soil layer [optional]
SOL_Z	Depth from soil surface to bottom of layer
SOL_BD	Moist bulk density
SOL_AWC	Available water capacity of the soil layer
SOL_K	Saturated hydraulic conductivity
SOL_CBN	Organic carbon content
CLAY	Clay content
SILT	Silt content
SAND	Sand content
ROCK	Rock fragment content
SOL_ALB	Moist soil albedo
USLE_K	Soil erodability factor

3.1.6 **Land use/Land cover**

Land use/land cover affects surface runoff, erosion, sediment transport and evapotranspiration in a catchment. In SWAT the classification of HRU is determined by soil types, land use conditions, and elements related to vegetation and landscape characteristics. The land-use/land-cover map used in this study is the GlobCover 2009 (Arino *et al.*, 2012) land cover product (Figure 3-4) (http://dup.esrin.esa.it/invitations.asp). The GlobCover 2009 land cover product is the second 300-m global land cover map produced from an automated and regionally-tuned classification of MERIS (Medium Resolution Imaging Spectrometer Instrument) Fine Resolution (FR) surface reflectance mosaics time series for the year 2009 (Arino *et al.*, 2012). The map was produced, from the bimonthly and annual MERIS FR mosaics for the year 2009 that were geometrically corrected using the AMORGOS tool (Bourg and Etanchaud, 2007), by the European Space Agency (ESA) and the Université catholique de Louvain (UCL). The Digital Elevation Model (DEM) used for the ortho-

rectification is based on the ACE DEM and is called Getasse 30 (Arino *et al.*, 2012). The GlobCover land use/land cover map has twenty-two (22) classes as defined by the United Nations (UN) Land Cover Classification System (LCCS).

For the purposes of this study, the FAO-LCCS codes used in the GlobCover land cover map were redefined to be compatible with the SWAT land cover/plant codes. The corresponding land cover categories and the area covered under each category for the White Volta basin are presented in Table 3-4. Based on the reclassifications, Agricultural Land-Row Crops was found to be the major land use/land cover category with 37.03% of the total catchment area and Forest Evergreen with 0.01% of the total catchment area being the least land use/land cover category.

Table 3-4: Spatial distribution of GlobCover 2009 land use/land cover classes and SWAT codes in the White Volta Basin

Code	GlobCover (LCCS)	SWAT Code	SWAT Land/Plant Classification	Area (sqkm)	Area (%)
14	Rainfed croplands	AGRL	Agricultural Land-Generic	22,744	22.71
20	Mosaic Croplands/Vegetation	AGRR	Agricultural Land-Row Crops	24,626	24.59
30	Mosaic Vegetation/Croplands	AGRR	Agricultural Land-Row Crops	12,458	12.44
40	Closed to open broadleaved evergreen or semi-deciduous forest	FRSE	Forest Evergreen	10	0.01
60	Open broadleaved deciduous forest	FRSD	Forest Deciduous	4,487	4.48
110	Mosaic Forest-Shrubland/Grassland	FRST	Forest Mixed	9,905	9.89
120	Mosaic Grassland/Forest-Shrubland	FRST	Forest Mixed	190	0.19
130	Closed to open shrubland	RNGB	Range Brush	21,842	21.81
140	Closed to open grassland	RNGE	Range Grasses	1,763	1.76
150	Sparse vegetation	RNGE	Range Grasses	1,362	1.36
190	Artificial areas	URBN	Residential	140	0.14
200	Bare areas	BARE	Barren Areas	300	0.3
210	Water bodies	WATR	Water Bodies	320	0.32

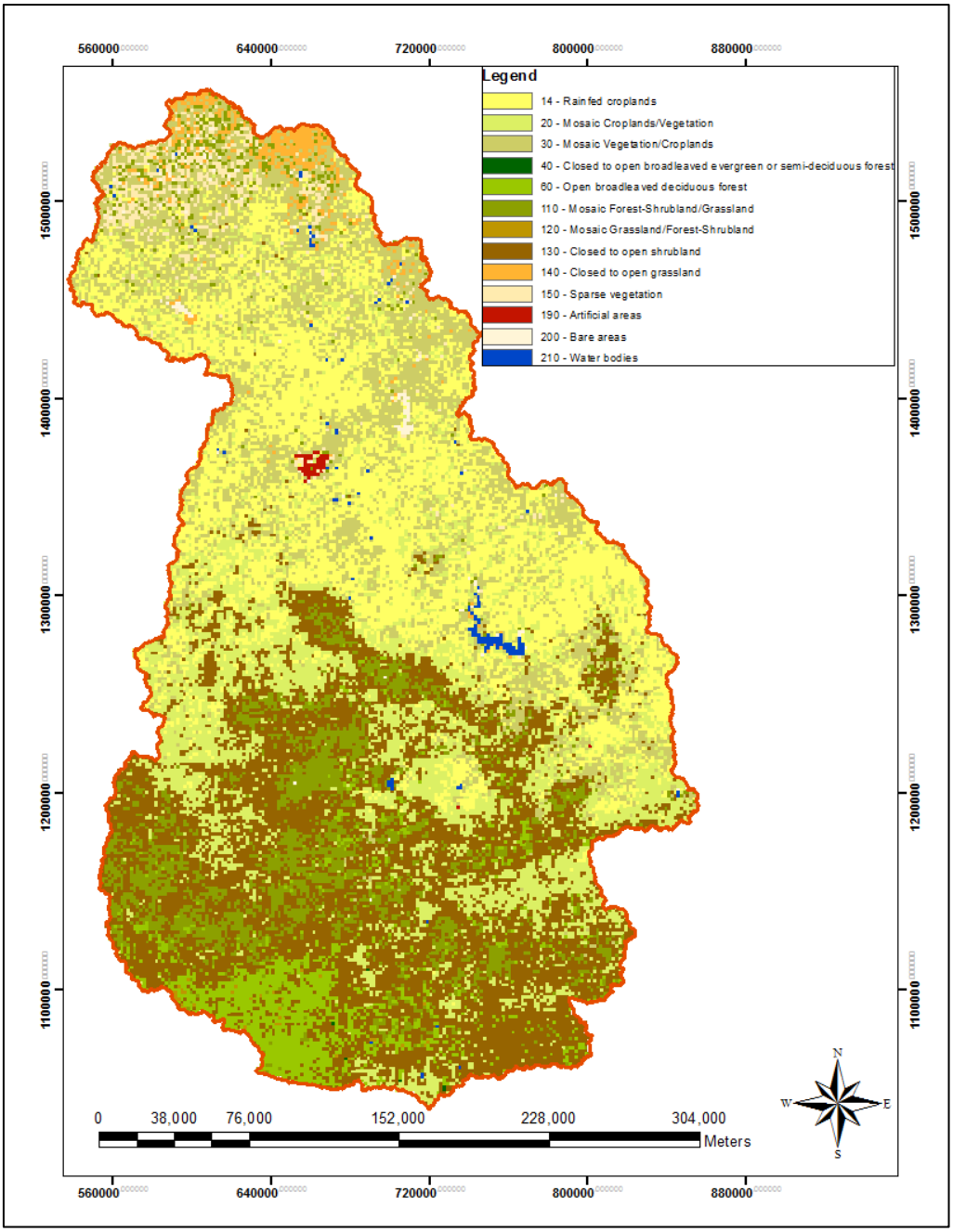

Figure 3-4: Land-use/land-cover map of the White Volta Basin (GlobCover2009, 2011)

3.1.7 **The Bagre Dam**

The Bagre dam is the only major reservoir sited on the main river course of the study area (see Figure 2.2). The Bagre dam was incorporated as reservoir in the White Volta SWAT model. SWAT requires data on the reservoir characteristics and reservoir management for simulating the reservoir water balance. Data on the reservoir characteristics were obtained from literature (Table 3-5) (Obuobie, 2008). According to Nii Consult (2007), data on the reservoir management obtained from Société Nationale d'Électricité du Burkina

(SONABEL) were difficult to predict since the data essentially depend on the demand fluctuations.

The reservoir characteristics used in simulating the water balance in the White Volta SWAT model are presented in Table 3-5. The data on monthly turbine flows for the Bagre dam used in this study were obtained from Nii Consult (2007) and SONABEL for the period 1995-2006 and 2007-2012 respectively. The Bagre reservoir became operational in February 1995.

Table 3-5: Characteristics of the Bagre dam in the White Volta Basin (source: Obuobie, 2008)

Parameter	Description	Value	Unit
MORES	Month the reservoir became operational	February	-
IYRES	Year of the simulation the reservoir became operational	1995	-
RES_ESA	Reservoir surface area when the reservoir is filled to the emergency spillway	43900	ha
RES_EVOL	Volume of water needed to fill the reservoir to the emergency spillway	$336300*10^4$	m^3
RES_PSA	Reservoir surface area when the reservoir is filled to the principal spillway	25200	ha
RES_PVOL	Volume of water needed to fill the reservoir to the principal spillway	$168900x10^4$	m^3
RES_VOL	Initial reservoir volume	$168900x10^4$	m^3

3.1.8 **Streamflow Data**

The streamflow used in this study were mainly obtained from the Hydrological Services Department (HSD) of Ghana is the only source of the since the hydrological stations required for calibrating and validating the model were mainly within Ghana. HSD has established 124 hydrological monitoring stations in the Volta Basin since its establishment. Over the years, the numbers of these hydrological monitoring stations in the basin have declined by 48%. Unfortunately, only 38% of the operating hydrological stations have stage-discharge measurement and none of the hydrological stations has 30 years of continuous data which is generally considered a basic requirement for hydrological and water resources management analysis.

The model was calibrated and validated with daily, monthly and annual streamflow data obtained for Nawuni hydrometric gauging station (see Figure 2.2). The model was further spatially validated with daily streamflows from the Pwalugu and Nasia hydrometric gauging stations. The White Volta River flows into the Volta Lake with Yapei being the last hydrometric gauging station. In this study however, Nawuni was used as the watershed outlet due to the availability of continuous streamflow and turbidity time-series as well as over one year of systematic daily sediment data collected in 1994/95 and 2012/13. Nawuni has a drainage area of approximately 100,000 km^2.

3.2 Development of Sediment Rating Curves

3.2.1 Introduction

Estimation of sediment loads typically requires frequently sampling streamflow and analyzing the total suspended solids, TSS in a laboratory. The resulting TSS is used concomitantly with river discharge to compute suspended sediment concentrations, SSC along the entire storm hydrograph. Sediment loads for the watershed can then be estimated from the computed SSC. Accepted methods of collecting suspended sediment data are however tedious, expensive and labor intensive. Moreover, due to the spatial and temporal variability associated with suspended sediment transport in a river, the accuracy of estimating SSC may be unknown. The use of surrogate techniques however provides a more accurate estimate of sediment fluctuations by continuously monitoring turbidity throughout a storm event. This chapter therefore presents the development of the relationship between sediment and turbidity as a cost effective estimation of sediment loads at Nawuni in the White Volta Basin using linear regression analysis. The methodology employed in this study generally follows the techniques as reported by Rasmussen *et al.,* (2009). The derived relationships was then be used to obtain long-term sediment loads for calibrating and validating the SWAT model.

3.2.2 Correlation of Surface Dip and Depth-Integrated Sampling (Correction Factor)

Generally, SSC obtained from water samples collected from the water surface by dipping will invariably underestimate the mean concentration in the vertical and subsequently

the overall cross-section. This can be attributed to the fact that sediment concentrations are generally less at the water surface but increases towards the river channel bed (Akrasi, 2005).

In order to correct possible underestimation by the surface dip sampling, suspended-sediment samples were collected at the gauge reader's single vertical near the river bank using the 1 liter sampling container before and after each cross-section sample were taken with the depth-integrated sampler. These samples then form the basis for the derivation of a correction factor that was used to adjust the concentration of the surface dip samples at the single vertical.

The correction factor was determined by computing the ratio of the average concentration of cross-section samples (depth-integrated samples) to the average concentration of surface dip samples (Edwards and Glysson, 1999) for each monitoring station. A mean correction factor was then obtained for the entire White Volta Basin by computing the average of all the sampling stations. The quality of the application of the correction factor to the surface dip was evaluated using the Nash-Sutcliffe efficiency, NSE (Equation 3.2.13) and the relative error.

3.2.3 **Regression Analysis**

The fundamentals for estimating time-series of suspended sediment concentration (SSC) from periodic measurements of SSC, turbidity, and streamflow data are the type and goodness-of-fit of the derived regression model for the estimation (Gray and Gartner, 2010a).

A simple linear regression (SLR) model relating turbidity to suspended-sediment concentration (SSC) is usually considered adequate for estimating SSC time-series (Gray and Gartner, 2010a). However, based on the criteria for determining the adequacy of a SLR model, a multiple regression (MR) model relating two or more other explanatory variables such as stage, turbidity and streamflow to SSC could be employed to significantly improve the regression model (Rasmussen *et al.*, 2009).

In this study, the time-series (i.e. turbidity, stream and SSC) collected during the period September 2012 to December 2013 were used as the calibration data set. All the data sets were transformed using the base-10 logarithmic transformation. Transformation of the data sets prior to regression analysis makes the residuals more symmetric, linear, and homoscedastic (Rasmussen *et al.*, 2009).

A SLR and MR models relating turbidity to SSC and turbidity and streamflow to SSC respectively were then developed and validated for the White Volta Basin. The models were

validated with the 1994-1995 data sets. Diagnostic statistics were used to analyse the performance of the derived models during the validation period. The appropriate model equation was selected and subsequently used to estimate long-term suspended sediment concentration and loads for the White Volta Basin.

3.2.3.1 Relationship between Turbidity, Streamflow and Suspended Sediment Concentration

The relationship between the river discharge, suspended sediment concentration and turbidity at Nawuni in the White Volta was evaluated by plotting the time series of the 2013 calendar year. The plot was used to evaluate the variability of the turbidity and streamflow and their relationship with SSC in the White Volta Basin.

3.2.3.2 Analysis of In-Stream Cross-Section and Fixed-Location Turbidity

The development of the regression analysis was preceded by an evaluation of the relationship between the fixed-location turbidity as measured by GWCL and the in-stream turbidity as measured with the Quanta HydrolabSonde. The relationship between the fixed-location turbidity and the in-stream turbidity was evaluated to check the representativeness of turbidity time-series as measured by GWCL. A plot of turbidity at the fixed-location and the in-stream turbidity was made and a one-on-one plot, i.e. y = x line was then drawn through the points on the plot.

3.2.3.3 Identifying Outliers

Prior to the development of the SSC regression model, a scatterplot of the turbidity and SSC time-series was used to evaluate and identify possible outliers in the data set. The data was further examined by analyzing the residuals. Residuals that exceeded three (3) standard deviations from the predicted line were considered insufficient for the regression analysis and therefore eliminated from the data set. An extreme outlier is one for which the standardized residual is greater than three (3). The standardized residual is given by (Helsel and Hirsch, 2002):

$$e_{si} = \frac{y_i - y_m}{\sqrt[s]{1 - h_i}} \qquad (3.2.1)$$

where y_i and y_m are the ith and mean of the response variable h_i is the leverage and is given by:

$$h_i = \frac{1}{n} + \frac{(x_i - x_m)^2}{\sum_{i=1}^{n}(x_i - x_m)^2} \qquad (3.2.2)$$

where x_i and x_m are the ith and mean of the explanatory variable and n is the number of samples.

and s is the standard error of the regression and is given by:

$$s = \sqrt{\sum_{i=1}^{n} \frac{(y_i - y_m)^2}{(n-2)}} \qquad (3.2.3)$$

3.2.3.4 Correlation Analysis

Correlation coefficient is a "measure of the strength of association between two continuous variables" (Helsel and Hirsch, 2002). Pearson's r, which measures the linear association between two variables, is the most commonly used measure of correlation (Helsel and Hirsch, 2002). Pearson's r is given by:

$$r = \frac{1}{n-1}\sum_{i=1}^{n}\left(\frac{x_i - x_m}{S_x}\right)\left(\frac{y_i - y_m}{S_y}\right) \qquad (3.2.4)$$

where n is the number of data points, x_i and y_i are the ith observation for the variables, x_m and y_m are the means and S_x and S_y are the standard deviation of the variables. If the data lie exactly along a straight line with positive slope, then $r = 1$ (Helsel and Hirsch, 2002). In this study, the relationship between explanatory and response variables was evaluated by computing the Pearson's correlation coefficient and plotting the time series. The scatter plots and correlation coefficient helps to identify which variables are statistically related. Helsel and Hirsch (2002) suggest that before applying multiple linear regressions to any variables, it is important to understand the causes and consequences of multicollinearity. Multicollinearity is the condition where at least one explanatory variable is closely related to one or more other explanatory variables. In this study, variance inflation factor (VIF) was computed and used for measuring multicollinearity. The VIF is given by (Helsel and Hirsch, 2002):

$$VIF_j = \frac{1}{\left(1 - R_j^{\,2}\right)} \qquad (3.2.5)$$

where R_j^2 is the coefficient of determination (R^2) from a regression of the *jth* explanatory variable on all of the other explanatory variables. In this study, the VIF for the

explanatory variables, turbidity and streamflow, was computed by estimating the R^2 from the regression of turbidity on streamflow.

3.2.3.5 Simple Linear Regression, SLR Analysis

After the correlation analysis, the SLR was used to establish a relationship between turbidity and SSC as a power function.

$$SSC = aT^c \qquad (3.2.6)$$

SSC is the suspended sediment concentration (mg/l), and *T* is the turbidity (NTU), *a* and *c* are transport curve parameters (Gray and Simoes, 2008). Equation 3.2.6 was formulated as a linear model in base-10 logarithmic space to find a solution for transport-curve parameters.

The t-statistics, the p-value and the 90% confidence intervals were used to evaluate the performance of the SLR model. For a statistically significant linear relationship between turbidity and SSC, the absolute value of the t-statistics should be greater than 2 (Helsel and Hirsch (2002)).

The diagnostics statistics used to evaluate the SLR were the coefficient of determination adjusted (R^2_a) and the model standard percentage error (*MSPE*). The R^2_a for the turbidity shows the fraction of variability in the SSC that is explained by the regression model (Rasmussen et al., 2009). RMSE expressed as a percentage is referred to as the model standard percentage error (*MSPE*) (Rasmussen *et al*., 2009). For *RMSE* expressed in base-10 logarithmic units, the *MSPE* is given by:

$$\text{Upper } MSPE = \left(10^{RMSE} - 1\right) \times 100 \text{ and}$$
$$\text{Lower } MSPE = \left(1 - 10^{-RMSE}\right) \times 100 \qquad (3.2.7)$$

The *MSPE* and the 90% prediction intervals determine the uncertainty range associated with each estimated SSC value. Generally, a SLR model is preferable for a site where turbidity is the explanatory variable highly correlated with SSC or where *MSPE* is less than 20 percent (Rasmussen *et al.*, 2009).

The model residuals were also used to further evaluate the performance of SLR model. Ordinary residuals can be expressed as the difference between the measured and model estimated values (Moriasi *et al.*, 2007). In theory, the residual error (e_i) for the computed SSC should be random and normally distributed with a mean residual value of zero and a constant variance (Helsel and Hirsch, 2002). A model residual value of zero shows that

the estimated SSC value is equal to the observed SSC value. A positive model residual value shows that the observed SSC value is greater than the estimated SSC value. A negative residual value, on the other hand, indicates that the model estimated value is greater than the measured value (Rasmussen *et al.*, 2009). In this study, the residual variance were then analyzed by plotting the residuals against the model computed SSC.

3.2.3.6 Nonlinear Multiple Regression, NMR Analysis

Generally, it is recommended that an additional explanatory variable should be added to a SLR model in a multivariate regression analysis if the p-value of the partial F-statistic is less than 0.025 (Rasmussen *et al.*, 2009). A nonlinear multiple regression model was used to fit a 3rd order polynomial function of the form:

$$\log SSC = a + c\log T + b_n \log Q_w^n \qquad (3.2.8)$$

where *SSC* is the suspended sediment concentration (mg/l), Q^n_w is streamflow (m^3/s), *T* is the turbidity (NTU), and *a*, b_n ,and *c* are transport curve parameters (Gray and Simoes, 2008). After obtaining a solution, Eq. , was retransformed into a power function of the form:

$$SSC = aQ_w^{\ b}T^c \qquad (3.2.9)$$

The NMR was evaluated using the coefficient of determination (R^2), sum of square errors (SSE). The SSE estimates the total within-group noise using departures from the sample group mean. Error in this context refers not to a mistake, but to the inherent variability within a group (Helsel and Hirsch, 2002). The smaller the SSE, the better the model fits the sample with zero as the optimal best fit.

3.2.3.7 Bias Correction Factor, BCF

The derived regression equations were retransformed from the logarithmic space to linear space. This approach usually introduces a bias in the computed SSC (Rasmussen *et al.*, 2009). The bias usually occurs due to the fact that the regression estimates are the average of the SSC for a given explanatory variable in logarithmic space. Retransforming the model estimates from the logarithmic space to linear space may deviate from the mean of the SSC for a given explanatory variable in linear space.

The nonparametric bias correction factor proposed by Duan (1983) was therefore used to correct the bias due to the retransformation. The BCF is given by:

$$BCF = \frac{\sum_{i=1}^{n} 10^{e_i}}{n} \qquad (3.2.10)$$

Where n is the number of samples, and e_i is the residuals in logarithmic units.

3.2.3.8 Regression Model Validation

Model validation is the process of estimating the suspended sediment concentration using the developed models for different time spans. The purpose of validating the model in this study was to establish whether the model has the ability to predict the measured suspended sediment concentrations at Nawuni for a different time period.

The derived models were validated by comparing the model estimated SSC with measured daily suspended sediment concentration sampled from July 1994 to March 1995.The performances of the derived models were then evaluated using the coefficient of determination (R^2), mean absolute error (MAE), percent bias (PBIAS) and the Nash-Sutcliffe efficiency (NSE). The R^2 measures the degree to which two variables are linearly related and ranges from 0 to 1, with higher values indicating less error variance (Moriasi *et al.*, 2007). MAE presents a more balanced perspective of the goodness-of-fit at average SSCs and range from 0 to +∞. A MAE value of 0 indicates a perfect fit (Kisi, 2007). The NSE on the other hand defines the relative magnitude of the residual variance compared to the measured variance. The NSE is a normalized statistic and ranges from -∞ to 1. The optimal value of NSE is 1.0 (Moriasi *et al.*, 2007). The R^2, RMSE, MAE and NSE are respectively defined by:

$$R^2 = \left[\frac{\sum_{i=1}^{N} (O_i - O_{mean}) \cdot (P_i - P_{mean})}{\left[\sum_{i=1}^{N} (O_i - O_{mean})^2 \right]^{0.5} \cdot \left[\sum_{i=1}^{N} (P_i - P_{mean})^2 \right]^{0.5}} \right]^2 \qquad (3.2.11)$$

$$MAE = \left[\frac{1}{N} \sum_{i=1}^{N} |O_i - P_i| \right] \qquad (3.2.12)$$

$$NSE = 1 - \left[\frac{\sum_{i=1}^{N} (O_i - P_i)^2}{\sum_{i=1}^{N} (O_i - O_{mean})^2} \right] \qquad (3.2.13)$$

3.3 Streamflow and Sediment Load Estimation using Soil and Water Assessment Tool (SWAT)

3.3.1 Introduction

This chapter focuses on the application of the Soil and Water Assessment Tool (SWAT) model to simulate the hydrology and sediment loads of the study area. The chapter also presents the sensitivity analysis, calibration, validation, and performance evaluation of the SWAT model.

Among the large collection of hydrological modeling systems available, the Soil Water Assessment Tool (SWAT) (Arnold *et al.*, 1998; Arnold and Fohrer, 2005) was selected as the model of choice for this study. SWAT has been used extensively to assess quantity and quality of water resources in a wide range of spatial and temporal scales, climatic and hydrological conditions worldwide (Gassman *et al.*, 2007). The model is developed in a modular structure in which various watershed processes (e.g., sediments, nutrients, and pesticides) can be run depending on the purpose and availability of data. SWAT is public domain, open source software coded in FORTRAN that can be further customized. Current versions of SWAT include a series of tools which are key elements when assessing model performance. In this chapter a detailed description of the Soil and Water Assessment Tool (SWAT) is presented. The modeling of watershed hydrology and sediment loads using the SWAT model is also presented. Results and discussions of the model sensitivity analysis, calibration, validation and model performance evaluation are also presented.

3.3.2 Overview of SWAT

The Soil and Water Assessment Tool (SWAT) model is a physically based, spatially semi-distributed and computationally efficient model that can be used to simulate a single basin or a system of multiple basins that are hydrologically connected (Di Luzio *et al.*, 2002). It is a continuous time series model with a GIS interface and that uses readily available input data. The main components of the model include climate, soil erosion, soil temperature, plant growth, nutrients, land management, channel and reservoir routing. Watersheds in SWAT are divided into subbasins (van Griensven *et al.*, 2013). Each subbasin is further divided into Hydrologic Response Units (HRUs) and connected through stream channels. HRU is a unique combination of a soil and vegetation type in a sub-catchment (van Griensven *et al.*, 2013). SWAT simulates hydrology, vegetation growth and management practices at the HRU level. With its capability of subdividing a watershed, the model can reproduce the differences

in evapotranspiration for different soils and crops. Furthermore, subdividing the subbasins into HRUs makes it possible to account for the impact of varying land use types, soil properties and management practices on the hydrology of a watershed. Water, sediment, nutrients and other pollutants are determined in a sub-watershed from each HRU and routed through the stream network to the outlet of the watershed. The hydrologic simulation in the SWAT model is underpinned by the soil water balance (van Griensven *et al.*, 2013).

SWAT has been widely used to evaluate the effects of various land management practices as well as the impact of climate change projections on the hydrology and sediment yields of many watersheds in the United States. Several studies have reported its use for hydrological simulation in the US (Arnold and Allen, 1996; Arnold *et al*., 2000; FitzHugh and Mackay 2000). Other publications also reported its application for simulating sediment and nutrients loads (White and Chaubey 2005; Arabi *et al.*, 2007; Jha *et al.*, 2007). SWAT results have also been reported on studies focusing on the effects of climate change using information derived from projections downscaled with regional climate models (RCMs) coupled with general circulating models (GCMs) (Bouraoui et al. 2002; Boorman 2003; and Jha *et al*., 2006). Several authors have also reported the use of SWAT to study land use impacts (Miller *et al.*, 2002; Heuvelmans *et al*., 2005; and Lorz *et al*., 2007).

SWAT is widely used in the United States by several States and institutions to perform Total Maximum Daily Load (TMDL) analyses (Borah *et al*., 2006) which must be performed for impaired waters as mandated by the 1972 U.S. Clean Water Act (USEPA, 2006). The model has also been used to study the effectiveness of conservation practices within the USDA Conservation Effects Assessment Program (CEAP, 2007) initiative (Mausbach and Dedrick, 2004) and wide range of other water use and water quality applications. SWAT has also being widely applied in other regions such as Europe (Conan *et al*., 2003 and Gikas *et al*., 2005); Asia (Hao *et al*., 2004; and Huisman *et al.*, 2004) and Africa (Sintondji, 2005; and Govender and Everson, 2005).

In SWAT the spatial heterogeneity of the watershed is taken into account, considering information from climate, elevation (DEM), soil and land use maps. The climate time-series required by SWAT as input to the drive the model include precipitation, solar radiation, wind speed, relative humidity, and maximum and minimum air temperature. These data are provided at the subbasin level and grouped into HRUs, climate, reservoirs, groundwater, runoff in the main channel draining the subbasins etc.

3.3.3 **Development of SWAT**

The SWAT model development is based on the continuation of USDA Agricultural Research Service (ARS) modeling experience and can be originally traced to previously developed USDA-ARS models (Figure 3-5). These includes; the Chemicals, Runoff, and Erosion from Agricultural Management Systems (CREAMS) model (Knisel, 1980; Gassman *et al.*, 2007), the Groundwater Loading Effects on Agricultural Management Systems (GLEAMS) model (Gassman *et al.*, 2007), and the Environmental Impact Policy Climate (EPIC) model (Izaurralde *et al*., 2006), which was originally called the Erosion Productivity Impact Calculator (Williams, 1990; Gassman *et al*., 2007). SWAT was designed to simulate management impacts on water and sediment movement for ungagged rural basins and is derived from the Simulator for Water Resources in Rural Basins (SWRRB) model (Arnold and Williams, 1987; Gassman *et al.*, 2007).

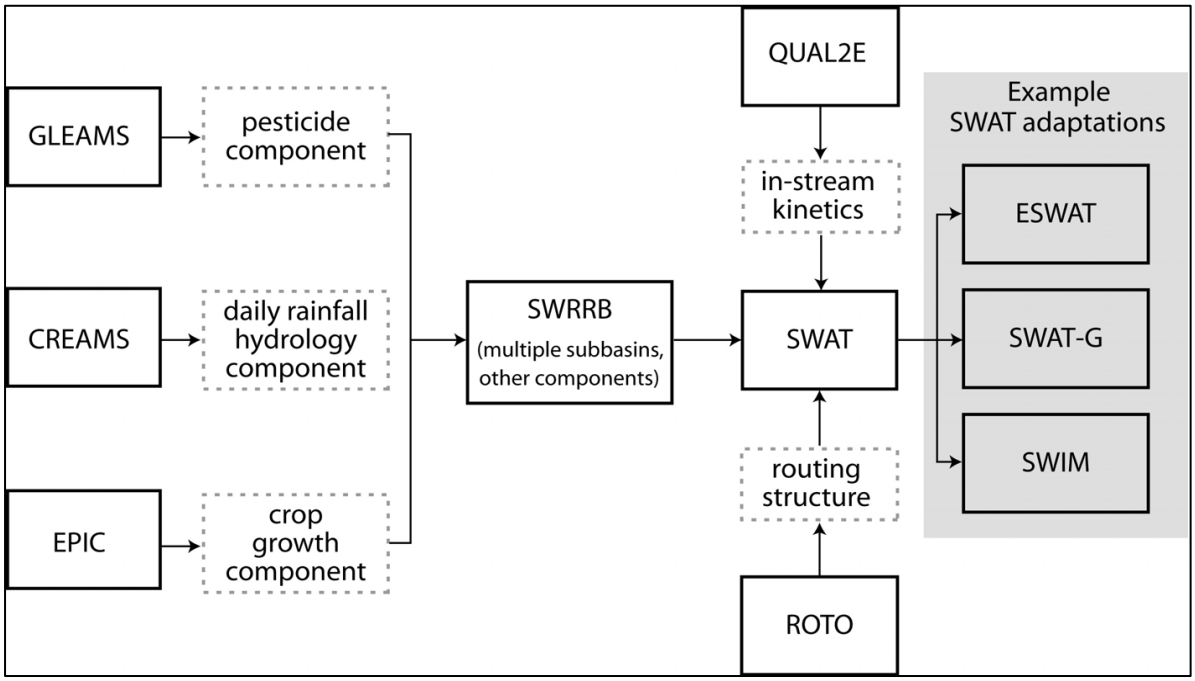

Figure 3-5: Flow chart of SWAT developmental and adaptations (source: Gassman *et al.*, 2007).

The Routing Outputs to Outlet (ROTO) model (Arnold *et al.*, 1995) was developed to assess the impact of downstream water management practices in the Indian Reservation Lands in Arizona and New Mexico which covers several thousand square kilometers (Gassman *et al.*, 2007). Multiple SWRRB runs were performed in the Reservation Lands and their outputs linked and routed through reservoirs and channels using a reach routing

approach in ROTO. SWRRB and ROTO were subsequently merged into a single module and called SWAT model (Figure 3-5).

3.3.4 **Components of SWAT**

The main computational components of SWAT can be categorized into eight major divisions. These are; weather, hydrology, sedimentation, nutrients, soil temperature, crop growth, pesticides and agriculture. Since the SWAT model is physically based, its computation is run based on physical inputs such as weather variables, topography, soil properties, vegetation and land-management practices within a watershed. The flow of water, sediment transportation, crop growth and nutrient cycling are directly modeled by SWAT using the concomitant physical processes (Neitsch *et al.*, 2011).

3.3.4.1 Hydrological Component

The water balance in SWAT is the driving force behind flow components in the watershed. SWAT simulates hydrology as a two-component system which is composed of land hydrology and channel hydrology (Neitsch *et al.*, 2011). The first process in the hydrological component is the land phase of the hydrological cycle (see Figure 3-6). The quantity of water, sediments and nutrient and pesticide loadings in the main channel and in each sub-basin is controlled by the land phase of the hydrologic cycle. The second phase in the hydrological component is the routing phase in the hydrologic cycle. The routing phase can be defined as the flow of water, sediments and nutrients and pesticide loadings through the channel network to the outlet of the watershed.

SWAT simulation of the land phase in the hydrologic cycle is based on the mass water balance of a watershed. The primary process simulated by SWAT in each HRU is the soil water balance and is represented by Equation 3.15 (Arnold *et al.*, 1998; Neitsch *et al.*, 2011).

$$SW_f = SW_o + \sum_{i=1}^{t} (R_d - Q_{sr} - E - w_s - Q_g) \qquad (3.3.1)$$

where SW_f = final soil water content (mm), SW_0 = initial soil water content (mm) on day i, t = time in days, R_d = precipitation (mm H_2O) on day i, Q_{sr} = surface runoff (mm) on day i, E = evapotranspiration (mm) on day i, w_s = water entering the vadose zone from the soil profile (mm) on day i, and Q_g = return flow (mm) on day i.

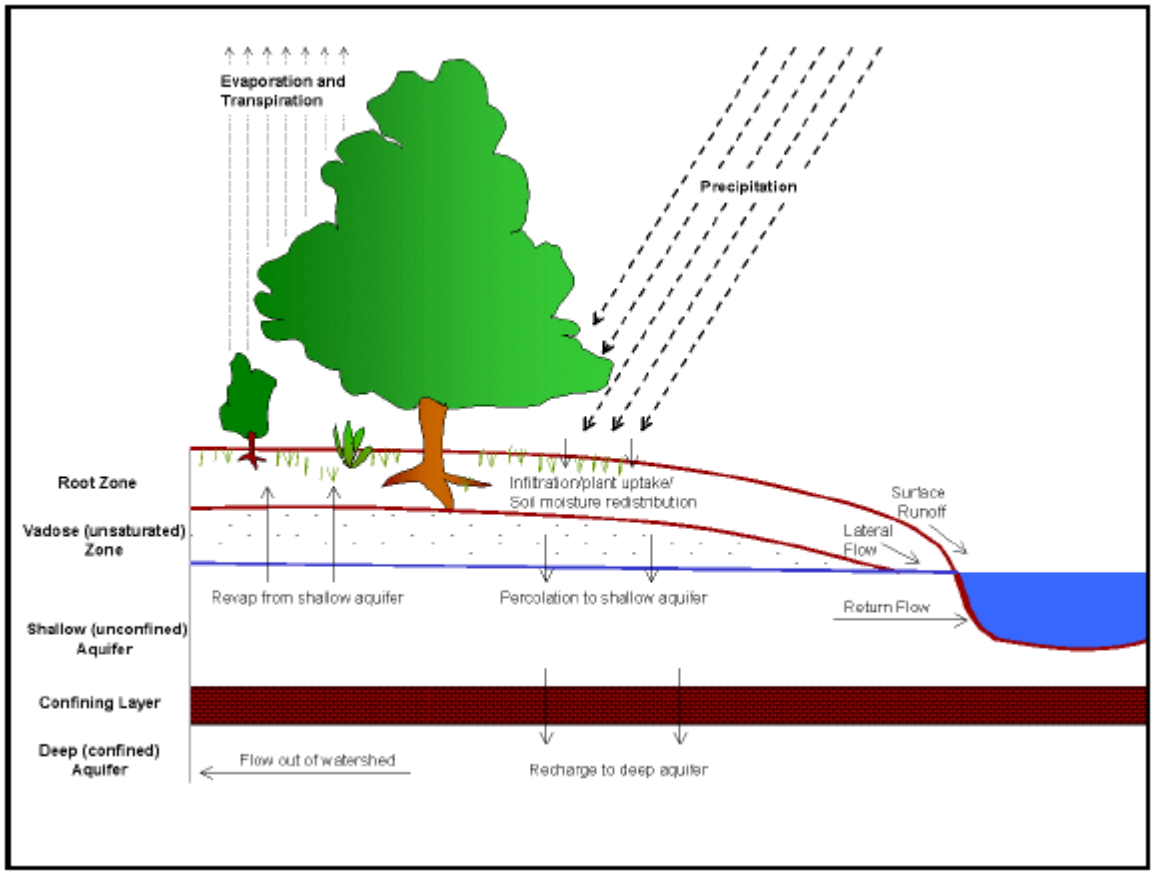

Figure 3-6: Schematic representation of the hydrological cycle (Neitsch *et al.*, 2011).

3.3.4.1.1 Climate

The water balance in a watershed is controlled by the climate which drives the moisture and energy inputs and determines the importance of the different components of the hydrologic cycle (Neitsch *et al.*, 2011). The climate parameters needed to run SWAT includes; daily rainfall, minimum and maximum air temperature, wind speed, solar radiation and relative humidity. SWAT permits daily climatic variables to be input from records of observed data or generated during simulation using the WXGEN weather generator model (Sharply and Williams, 1990; Neitsch *et al.*, 2011). Generally, SWAT ability to simulate the observed hydrograph of a river is enhanced when observed input data is used (Neitsch *et al.*, 2011).

A rainfall event on a given day has a direct effect on the variation of temperature, relative humidity, and solar radiation for the day (Neitsch *et al.*, 2011). The water balance of a watershed is therefore controlled by precipitation which is the mechanism by which water enters the land phase of the hydrologic cycle. Observed rainfall data are not sufficiently

available in the study area due to various reasons. Even where long-term time series is available, there may be missing gaps ranging from a day to decades that require filling.

The equation used for computing the amount of precipitation on a wet day with the skewed distribution model is given by (Neitsch *et al.*, 2011):

$$R_d = \mu_{mth} + 2 \cdot \sigma_{mth} \cdot \left(\frac{\left[\left(SND_d - \frac{k_{mth}}{6} \right) \cdot \left(\frac{k_{mth}}{6} \right) + 1 \right]^3 - 1}{g_{mth}} \right) \quad (3.3.2)$$

where: R_d = rainfall (mm), μ_{mth} = mean daily rainfall (mm) for the month, SND_d = standard normal deviateion computed for the day, σ_{mth} = standard deviation of daily rainfall (mm) for the month and k_{mth} = skew coefficient for daily rainfall in the month.

The SND for the day is computed as:

$$SND_d = \cos(6.283 \cdot rnd_2) \cdot \sqrt{-2\ln(rnd_1)} \quad (3.3.3)$$

where: rnd_1 and rnd_2 are random numbers between 0.0 and 1.0.

The exponential distribution is often used in areas where data on rainfall events are limited. With this distribution, daily rainfall is calculated using the equation (Neitsch *et al.*, 2011):

$$R_d = \mu_{mth} \cdot (-\ln(rnd_1))^{r\exp} \quad (3.3.4)$$

where: R_d = amount of rainfall (mm); μ_{mth} = mean daily rainfall (mm H_2O) for the month; rnd_1 is a random number between 0.0 and 1.0; and *rexp* is an exponent that should be set between 1.0 and 2.0.

In this study, daily observed climate data were available for the simulation albeit with gaps in some of the stations. The WXGEN weather generator in SWAT was therefore used to fill-in the gaps using the skewed normal distribution option for calculating the amount of rainfall on a wet day.

3.3.4.1.2 Surface Runoff

Surface run-off in SWAT is determined by the modified SCS curve number (USDA Soil Conservation Service) or the Green and Ampt infiltration method (Neitsch *et al.*, 2011). The SCS curve number is a function of permeability of the soils, land use and land cover and the antecedent soil water conditions in a watershed (Neitsch *et al.*, 2011).

The Green Ampt method requires sub-daily precipitation data which is not available in the study area. The SCS curve number method on the other hand was developed to provide consistent bases for estimating empirically the amounts of runoff under varying land use and soil types (Neitsch *et al.*, 2011). The SCS curve number option was therefore used for estimating the runoff in this study.

The SCS curve number equation is given by (Neitsch *et al.*, 2011):

$$Q_{sf} = \frac{(R_d - I_a)^2}{(R_d - I_a + S)} \qquad (3.3.5)$$

where Q_{sf} = accumulated runoff or rainfall excess (mm), R_d = rainfall depth (mm), I_a = initial abstraction (surface storage, interception and infiltration) prior to runoff (mm) and S = retention parameter (mm). S is computed as:

$$S = 25.4\left(\frac{100}{CN} - 10\right) \qquad (3.3.6)$$

where CN = curve number. The initial abstractions, I_a, is commonly approximated as $0.2S$ and Equation 3.3.5 becomes:

$$Q_{surf} = \frac{(R_{day} - 0.2S)^2}{(R_{day} + 0.8S)} \qquad (3.3.7)$$

Runoff will only occur when $R_{day} > I_a$. A graphical solution of Equation 3.3.7 for different curve number values is presented in Figure 3-7 (Neitsch *et al.*, 2011).

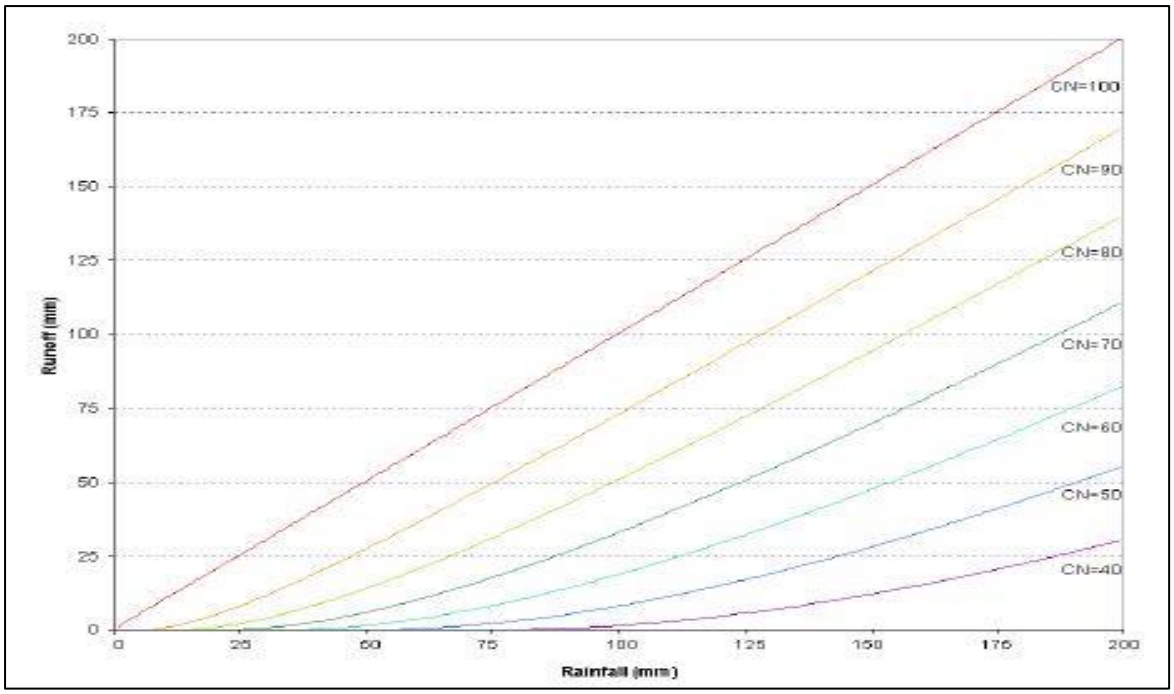

Figure 3-7: Graphical presentation of the relationship between runoff and rainfall in SCS curve number method (source: Neitsch et al., 2011)

3.3.4.1.3 Peak Runoff Rate

Peak runoff rate is defined as the maximum runoff that occurs for a given rainfall event and provides the erosive power of a storm which predicts sediment loss. SWAT determines the peak runoff rate with a modified rational method (Neitsch *et al.*, 2011).

The most widely used empirical formula for the design of storm water drainage, ditches and channels is the rational formula. The modified rational formula is however given by (Neitsch et al., 2011):

$$q_p = \frac{C \cdot i \cdot A}{3.6} \qquad (3.3.8)$$

where q_p = peak runoff rate (m^3/s), C = runoff coefficient, i = rainfall intensity (mm/hr) and A = sub-catchment area (km^2) with 3.6 being a unit conversion factor.

The time of concentration can be calculated by summing the overland flow time and the channel flow time (Neitsch *et al.*, 2011). That is:

$$t_{conc} = t_{ov} + t_{ch} \qquad (3.3.9)$$

where t_{conc} = time of concentration, t_{ov} = overland flow time, and t_{ch} = channel flow time.

The overland flow time of concentration tov, can be computed as:

$$t_{ov} = \frac{{L_s}^{0.6} \cdot n^{0.6}}{18 \cdot s^{0.3}} \qquad (3.3.10)$$

where L_s = average sub-catchment slope length (m), s = average sub-catchment slope (m/m), and n = Manning's roughness coefficient for the sub-catchment.

The channel flow time of concentration, t_{ch}, can be computed as:

$$t_{ch} = \frac{0.62 \cdot L \cdot n^{0.75}}{Area^{0.125} \cdot {slp_{ch}}^{0.375}} \qquad (3.3.11)$$

where t_{ch} = time of concentration (hr) for the channel flow, L = channel length (km) from the furthermost point to the sub-catchment outlet, n = channel Manning's roughness coefficient, $Area$ = sub-catchment area (km^2), and slp_{ch} = channel slop (m/m).

3.3.4.1.4 Evapotranspiration

Evapotranspiration is defined as the process by water at the earth's surface is converted to water vapor. It consist of evaporation from the soils and plant canopy, transpiration and sublimation (*Neitsch et al.*, 2011). It is the primary process through which water is removed from a watershed.

In SWAT, there are three available possibilities of computing the potential evapotranspiration (PET) in a watershed. These are; the Hargreaves method (Hargreaves *et al.*, 1985), Priestly-Taylor method (Priestly and Taylor, 1972) and the Penman-Monteith method (Monteith, 1965). The Hargreaves method requires only air temperature as input data, the Priestly-Taylor method requires solar radiation, air temperature and relative humidity, and the Penman-Monteith method requires solar radiation, air temperature, relative humidity and wind speed (Neitsch *et al.*, 2011). In this study, the Penman-Monteith method for estimating the PET was applied.

3.3.4.1.5 Soil Water

When water enters the soil, the water may move in different directions and may also be removed through evaporation or plant uptake. The water may also be removed through groundwater recharge by percolation through the bottom of the soil profile. The water may also move laterally in the soil profile and contribute to streamflow (Neitsch *et al.*, 2011).

In SWAT, a storage routing methodology is used to estimate the amount of water that moves from one layer to the other. The equation used to estimate percolation in SWAT is given by (Neitsch *et al.*, 2011):

$$w_p = SW_l \cdot \left(1 - \exp\left[\frac{-\Delta t}{TT_p}\right]\right) \qquad (3.3.12)$$

where w_p = amount of water percolating (mm), SW_l = volume of water (mm) drained in the soil layer, Δt = time step (hrs), and TT_p = time (hrs) it takes for water to percolate. Percolation does not occur if the HRU has a seasonal high water table and this is determined by:

$$SW_{l+1} \leq FC_{l+1} + 0.5 \cdot (SAT_{l+1} - FC_{l+1}) \qquad (3.3.13)$$

where SW_{l+1} = water content (mm) of the underlying soil layer, FC_{l+1} = water content (mm) of the underlying soil layer at field capacity, and SAT_{l+1} = amount of water (mm) in the underlying soil layer when completely saturated. The time it takes for water to percolate TT_p in Equation 3.3.12 is unique for each layer and is determined by:

$$TT_p = \frac{SAT_l - FC_l}{Ksat} \qquad (3.3.14)$$

where TT_p = time (hrs) it takes for water to percolate, SAT_l = saturated water content (mm) in the soil layer, FC_l = water content (mm) of the soil at field capacity and K_{sat} = saturated hydraulic conductivity (mm/hr) for the layer. The vadose zone is the unsaturated zone between the bottom of the soil profile and the top of the aquifer (Neitsch *et al.*, 2011).

Water can exit the ground again as lateral flow from the upper soil layer after infiltration or as a return flow that exits the shallow aquifer and flow into the nearest stream network. It is usually considered in a 2D flow domain (Figure 3-8).

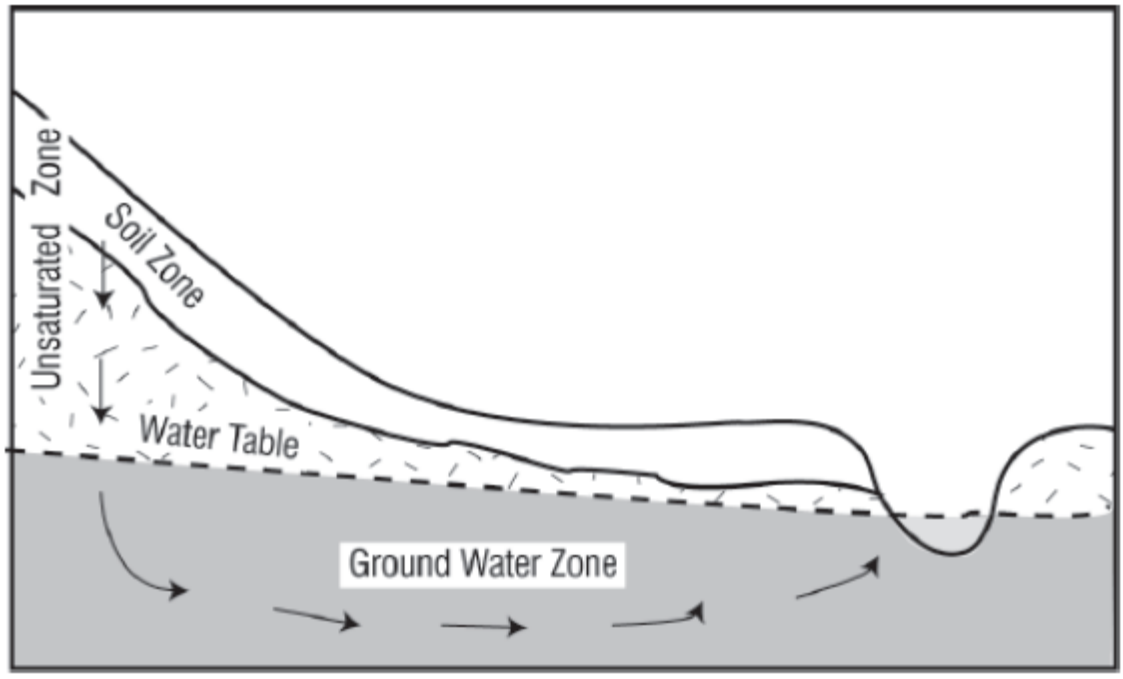

Figure 3-8: Schematic diagram of the sub-surface water fluxes

In SWAT, when rain falls on soils with high hydraulic conductivity in the top layers and an impermeable or semi-permeable layer at a shallow depth, the water percolates vertically to impermeable layer and forms a perched water table. The perched water table is the source for lateral subsurface flow (Neitsch *et al.*, 2011).

SWAT incorporates a kinematic storage model for subsurface flow developed by Sloan *et al.*, (1983) (Neitsch *et al.*, 2011) and summarized by Sloan and Moore (1984) (Neitsch *et al.*, 2011) (Figure 5.5). The equation for estimating the kinematic storage model is given by (Neitsch *et al.*, 2011):

$$Q_{lt} = 0.024 \cdot \left(\frac{2 \cdot SW_{ly,excess} \cdot K_{sat} \cdot slp}{\phi_d \cdot L_{hill}} \right) \qquad (3.3.15)$$

where Q_{lt} = lateral flow (mm/d), $SW_{ly,excess}$ = volume of soil water drained (mm), K_{sat} = saturated hydraulic conductivity (mm/hr), slp = slope (m/m), φ_d = drainable porosity (mm/mm) and L_{hill} = hillslope length (m).

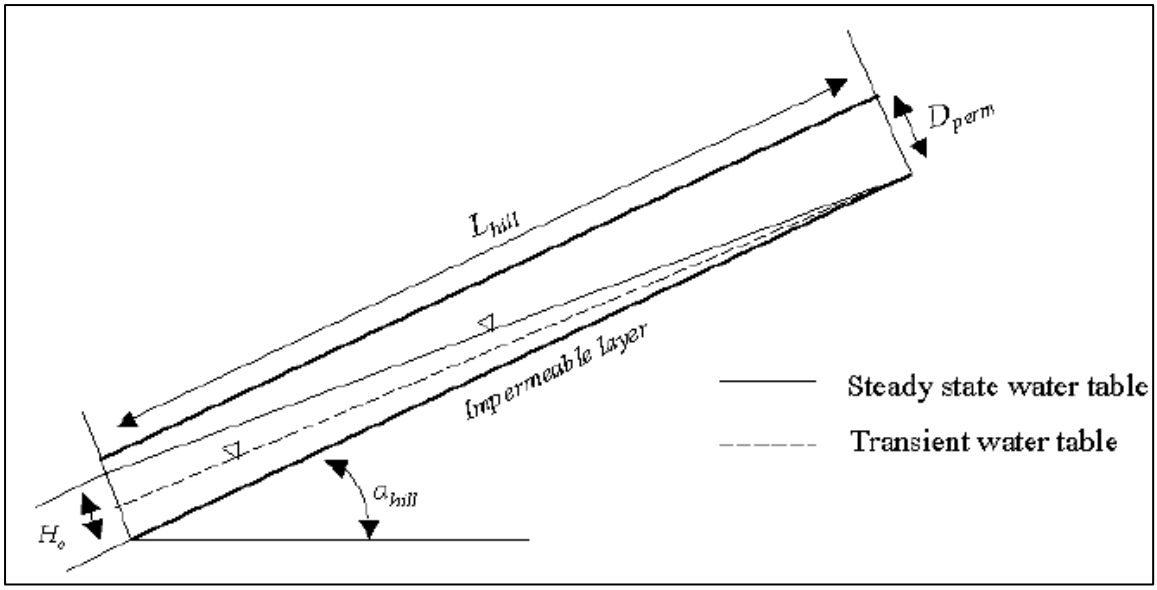

Figure 3-9: Behavior of the water table as assumed in the kinematic storage model (Neitsch et al., 2011)

In large watersheds, a portion of lateral flow is lagged and released to the main channel and is determined by (Neitsche *et al.*, 2011):

$$Q_{lt} = (Q'_{lt} + Q_{lts,i-1}) \cdot \left(1 - \exp\left[\frac{-1}{TT_l}\right]\right) \qquad (3.3.16)$$

where Q_{lt} = lateral flow discharged (mm) to the main channel, Q'_{lt} = amount of lateral flow (mm) generated in the sub-catchment, $Q_{lts,i-1}$ = lateral flow (mm) stored or lagged from the previous day, and TT_l = time (days) it takes for lateral flow to travel.

If drainage tiles are present in the HRU, lateral flow time is calculated by (Neitsche *et al.*, 2011):

$$TT_{lag} = \frac{tile_{lag}}{24} \qquad (3.3.17)$$

where TT_{lag} is the time it takes for lateral flow to travel (days), and $tile_{lag}$ is the drain tile lag time (hrs). Lateral flow travel time in HRUs without drainage tiles is calculated as:

$$TT_{lag} = 10.4 \cdot \frac{L_{hill}}{K_{sat,mx}} \qquad (3.3.18)$$

where TT_{lag} is the time it takes for lateral flow to travel (days), L_{hill} is the hillslope length (m), and $K_{sat,mx}$ is the topmost layer saturated hydraulic conductivity (mm/hr).

3.3.4.2 Sediment Component

Erosion occurs on a landscape when soil particles are detached, transported and deposited by the erosive forces of raindrops and surface flow of water (Neitsch *et al.*, 2011). Erosion and sediment yield in SWAT are estimated for each HRU using MUSLE, Equation 3.3.19 which improves the prediction of sediment yields and removes the requirement for delivery ratios. It permits the application of the equation to individual storm events by replacing the rainfall energy factor with a runoff factor (Neitsch *et al.*, 2011).

SWAT uses the amount of runoff to simulate erosion and sediment yield. The hydrology module determines the runoff erosive energy and depends on the peak runoff, runoff rate and the subbasin areas. The crop management factor which is a function of the soil surface residues, the minimum crop factor for plants and aboveground biomass is re-computed each day that runoff occurs (Neitsch *et al.*, 2011).

$$SY = 11.8 \cdot (Q_s \cdot q_p \cdot A_{hru})^{0.56} \cdot K_{se} \cdot C_m \cdot P_{sp} \cdot L_{sf} \cdot C_{ff} \qquad (3.3.19)$$

where SY = sediment yield (metric tons per day), Q_s = surface runoff volume (mm/ha), q_p = runoff peak rate (m^3/s), A_{hru} = area of the HRU (ha), K_{se} = soil erodibility factor (0.013 metric ton m^2 hr/(m^3-metric ton cm)), C_m is the cover management factor, P_{sp} is the support practice factor, L_{sf} is the topographic factor and C_{ff} is the coarse fragment factor.

Sediment in the surface runoff is also lagged and the amount released to the main channel is calculated by (Neitsch *et al.*, 2011):

$$sed = \left(sed' + sed_{s,i-1}\right) \cdot \left(1 - \exp\left[\frac{-surlag}{t_c}\right]\right) \qquad (3.3.20)$$

where sed = sediment discharged (metric tons/day) to the main channel, sed' = sediment load (metric tons/day) generated, $sed_{s,i-1}$ = sediment (metric tons) stored or lagged from the previous day, $surlag$ = surface runoff lag coefficient, and t_c = time of concentration (hrs).

The sediment transport in the channel consists of two components; namely deposition and degradation, which operates simultaneously (Setegn *et al.*, 2008). Landscape and channel components regulate the transportation of sediments in the watershed. In SWAT, particle size distribution of eroded sediments are tracked and routed through channels and reservoirs from the landscape component. The amount of sediments reaching a stream channel is therefore defined by the difference between the total sum of sediment yield computed by MUSLE and the lagged and trapped sediments in the landscape of a watershed (Neitsch *et al.*, 2011).

In the stream channel, SWAT determines the deposition and degradation process by calculating the maximum amount of sediment that can be transported from a reach segment by using following equation:

$$sc_{ch,mx} = c_{sp} \cdot v_{ch,pk}^{\ spexp} \qquad (3.3.21)$$

where $sc_{ch,mx}$ = maximum sediment concentration transported by the water (ton/m^3 or kg/L), c_{sp} = a user defined coefficient, $v_{ch,pk}$ = peak channel velocity (m/s), and *spexp* = exponent parameter for determining sediment re-entrained in channel. The exponent parameter varies between 1 and 2. The peak channel velocity, $V_{ch,pk}$, is calculated by:

$$v_{ch,pk} = \frac{prf \cdot q_{ch}}{A_{ch}} \qquad (3.3.22)$$

where *prf* = peak rate adjustment factor, q_{ch} = channel flow (m^3/s), and A_{ch} = channel cross-sectional area (m^2). The maximum concentration of sediment, $sc_{ch,mx}$ that is calculated from Equation 3.3.21 is compared to the sediment concentration in the channel at the initial time step, $sc_{ch,i}$. If $sc_{ch,i} > sc_{ch,mx}$, then the dominant process in the channel segment is sediment deposition and the net amount of sediment deposited is calculated as:

$$sed_{dep} = \left(sc_{ch,i} - sc_{ch,mx}\right) \cdot V_{ch} \qquad (3.3.23)$$

where Sed_{dep} = sediment deposited in the reach segment (metric tons), $sc_{ch,i}$ = initial sediment concentration (kg/L or ton/m^3) that can be transported by the water, and V_{ch} = volume of water in the channel (m^3).

If $sc_{ch,i} < sc_{ch,mx}$ then the dominant process in the river segment is degradation and the net amount of sediment reentrained is estimated by:

$$sed_{\deg} = \left(sc_{ch,mx} - sc_{ch,i}\right) \cdot V_{ch} \cdot K_{\sec} \cdot C_{chf} \qquad (3.3.24)$$

where sed_{deg} = sediment re-entrained in the channel (metric tons), K_{sec} = channel erodibility factor, and C_{chf} = channel cover factor. Once the amount of deposition and degradation is calculated, the final amount of sediment in the channel is determined by:

$$sed_{ch} = sed_{ch,i} - sed_{dep} + sed_{\deg} \qquad (3.3.25)$$

where sed_{ch} = suspended sediment in the channel (metric tons), $sed_{ch,i}$ = initial suspended sediment in the channel (metric tons), sed_{dep} = sediment deposited in the channel (metric tons), and sed_{deg} is the sediment reentrained in the channel (metric tons).

Sediment loads transported out of the channel is determined by:

$$sed_{out} = sed_{ch} \cdot \frac{V_{out}}{V_{ch}} \qquad (3.3.26)$$

where sed_{out} = sediment load (metric tons) transported out of the channel, sed_{ch} = suspended sediment load (metric tons) in the channel, V_{out} = volume of outflow (m^3) during the time step, and V_{ch} = volume of water (m^3) in the channel.

3.3.4.3 Flow Routing Component

The flow routing component is the routing phase of the hydrological cycle in SWAT that simulates the hydrology of a watershed. The routing component is utilized in SWAT to simulate the movement of water, sediments, nutrients and pesticides (Neitsch *et al.*, 2011). Two options are available to route the flow in the channel network in SWAT. These are; the Muskingum and variable storage channel routing techniques. The Muskingum channel routing technique simulates the storage volume in a river channel length using a combination of wedge and prism storage. The variable storage channel routing technique however simulates the storage volume using a simple continuity equation. In this study the variable storage routing method was adopted.

3.3.4.4 Impoundments Component

In SWAT, water ponding structures such as ponds, reservoirs and wetlands have been incorporated in the watersheds being modeled. SWAT simulates a reservoir as an impoundment situated on the main channel network of a watershed. The model does not differentiate between natural and man-made impoundments. The water balance of a reservoir in SWAT is calculated by (Neitsch *et al.*, 2011):

$$V = V_{st} + V_{fin} - V_{fout} + V_{pcp} - V_{evap} - V_{seep} \qquad (3.3.27)$$

where V = volume of water in the impoundment (m^3), V_{st} = initial volume of water (m^3) stored in the water body, V_{fin} = volume of water (m^3) flowing into the water body, V_{fout} = volume of water (m^3) exiting the water body, V_{pcp} = amount of rainfall (m^3) on the water body, V_{evap} = amount of water (m^3) evaporated, and V_{seep} = amount of water (m^3) removed by seepage.

Although there are several ponds and dams in the upper parts of the study area, only the Bagre dam was incorporated as a reservoir in this study.

3.3.5 **Model Sensitivity, Calibration and Performance Evaluation**

3.3.5.1 Hydrologic Response Units (HRUs) Analysis

HRU is a unique combination of a soil and vegetation type in a sub-catchment (Gassman *et al.*, 2007). SWAT simulates hydrology, vegetation growth and management practices at the HRU level. Generally, SWAT uses a threshold level to eliminate minor land use in each subbasin, minor soil within a land use and minor slope classes within a soil type on specific land use. With the elimination of minor soil types, land use and slopes, the area of the remaining soil types, land use and slopes are redistributed to achieve 100% coverage of their respective areas. The HRU Analysis Menu on the ArcSWAT Toolbar was used to characterize the soil types, land use and slope classes. This tool permits the loading of soil and land use maps, evaluation of slope characteristics and the determination of the land use/soil/slope class combinations in the delineated sub-watersheds.

Two options are available in defining HRU distribution. In the first option, a single HRU is assigned to each sub-watershed whereas in the second option, multiple HRUs are assigned to each sub-watershed based on a given threshold values. In this study, the multiple HRU option which accounts for various scenarios of land use, soil and slope threshold combinations were tested.

3.3.5.1.1 Evaluation of Rainfall Input and Density of HRU

Rainfall input is generally considered the driving force in runoff generation in hydrologic modeling. The output of a hydrologic model can therefore be affected by the number of rainfall gauges available within and around a watershed. Furthermore, in SWAT, the number of subbasins modeled has a direct influence on the number of rainfall stations used in modeling the output of a watershed. Generally, the higher the number of subbasins modeled in a watershed, the higher the number of rainfall stations utilized by the model (Obuobie, 2008).

The starting point in setting up the White Volta SWAT model was to delineate the watershed based on the DEM (Fadil *et al.*, 2011). The watershed was then divided into multiple subbasins based on the outlets generated by intersection of reaches and the seven selected discharge outlets. Thereafter, each subbasin was sub-divided into homogeneous hydrologic response units (HRUs) which are derived from overlaying the slope, land use and soil layers. Generally, the accuracy of a model output increases with increasing the number of HRUs in a watershed with diverse land use and land cover.

Therefore, prior to undertaking the model sensitivity analysis to identify and rank the most sensitive model parameters, the effects of the number of rainfall stations and land-use/land cover units on the model output were assessed. Ten (10) scenarios were developed from five (5) subbasin thresholds and two (2) land-use and soil thresholds within each of the subbasin thresholds. The model was then run for the period 1991 to 2013.

3.3.5.2 Parameter Sensitivity Analysis

Sensitivity analysis is a process that demonstrates a model response to changes in a model input parameter and can be performed with different methods (Veith and Ghebremichael, 2009). SWAT adopts a combination of Latin Hypercube (LH) and the One-factor-At-a-Time (OAT) sampling techniques (Van Griensven, 2005). Sensitivity analysis in SWAT is performed by running a simulation (p+1)*m times, where p is the number of parameters being evaluated and m is the number of LH loops. For every loop, a unique area of the parameter space is sampled for a selected set of parameter values and a baseline simulation is performed for that unique area. The OAT technique is then used to randomly select a parameter, and a user-defined percentage is used to change its value from the previous simulation. SWAT simulation run is then performed with the new parameter set and then a different parameter is selected randomly and varied. Once all the parameters have been varied, the LH algorithm subsequently detects a new unique area to sample by making changes to all the parameters (Veith and Ghebremichael, 2009).

The sensitivity analysis tool in SWAT has the capability of performing two types of analyses. The first type of analysis uses only modeled data to identify the impact of adjusting a parameter value on some measure of simulated output, such as average streamflow. The second type of analysis uses measured data to provide overall "goodness of fit" estimation between the modeled and the measured time series (Veith and Ghebremichael, 2009).

The hydrologic simulation by SWAT is generally based on more than 30 parameters that have to be calibrated by adjusting the parameters to achieve a desired output. In this regard, the calibration process becomes complex, time consuming and computationally extensive. The automatic sensitivity analysis tool therefore aids in identifying and ranking the parameters that have significant impact on the model outputs, in this case flow and sediment concentration, and needs to be given high priority during model calibration.

In this study, all the twenty-six (26) default parameters that govern the streamflow component and the six (6) default parameters that control the sediment component in SWAT

were selected for the sensitivity analysis. Sensitivity analysis was run for two scenarios. In the first scenario, streamflow and sediment loads were simulated without observed data. The second scenario utilized observed monthly streamflow and sediment data at Nawuni. The sensitivity analysis for the two scenarios was run with the following criteria; ten (10) number of intervals within Latin hypercube, 5% parameter change for OAT, 203 random seed number, and the sum of squared residuals as the objective function. The first fifteen (15) ranked sensitive parameters for both model outputs were selected for further sensitivity and uncertainty analyses and calibration in SWAT-CUP.

3.3.5.3 SWAT-Calibration and Uncertainty Procedures (SWAT-CUP)

SWAT-CUP (SWAT-Calibration and Uncertainty Procedures) is a module that incorporates several calibration and uncertainty analysis programs for SWAT (Figure 3-10). The module affords a semi-automated approach that comprises both manual and automatic calibration and incorporates sensitivity and uncertainty analysis (Abbaspour *et al*., 2007).

Currently the program can run SUFI-2-Sequential Uncertainty Fitting (Abbaspour, *et al.*, 2007), GLUE-Generalized Likelihood Uncertainty Estimation (Beven and Binley, 1992), and ParaSol-Parameter Solution (van Griensven and Meixner, 2006), and MCMC-Markov Chain Monte Carlo procedures. SWAT-CUP has been applied to analyze the effects of blue-green water in Africa and Iran respectively by Schuol *et al.*, (2008b) and Abbaspour *et al.*, (2007). All the parameters in SWAT can be included during calibration process in SWAT-CUP. Additionally, precipitation and temperature can also be treated as random variables and fitted during the calibration process.

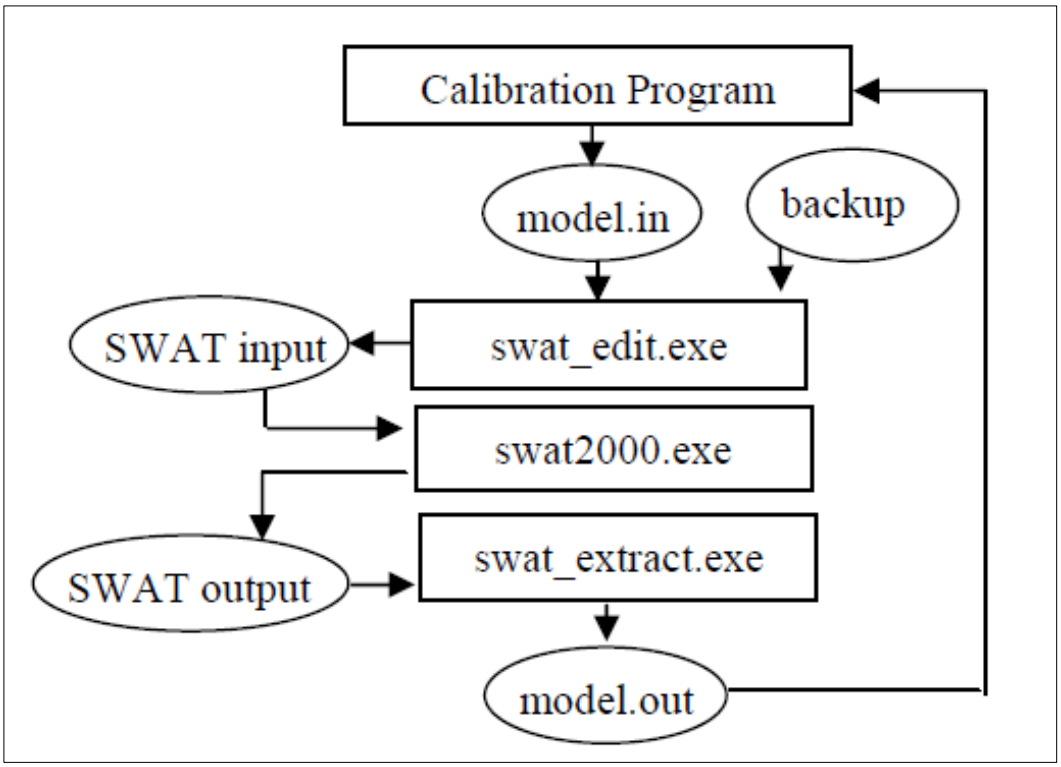

Figure 3-10: Interaction between a calibration program and SWAT in SWAT-CUP (source: Abbaspour et al, 2007)

For this study, the fifteen (15) ranked SWAT parameters relating to streamflow and sediment load were analyzed using the SUFI-2 optimization technique. SUFI-2 was selected in this study because it incorporates parameter uncertainty which accounts for all sources of uncertainties in SWAT (Schuol *et al.,* 2008b). The P-factor which is the percentage of measured data bracketed by the 95% prediction uncertainty (95PPU) accounts for all uncertainties in the model. According to Schuol *et al.*, (2008b) breaking down the total uncertainty into its various components is of some interest, but quite difficult to do and no reliable procedure yet exists to break down the uncertainties into the various components.

Another measure quantifying the strength of a calibration/uncertainty analysis is the R-factor (Schuol *et al.*, 2008b). R-factor is the average thickness of the 95PPU band divided by the standard deviation of the measured data and is calculated by (Yang *et al*, 2008):

$$R-factor = \frac{\frac{1}{n}\sum_{t_1=1}^{n}\left(y_{t_1,97.5\%} - y_{t_1,2.5\%}\right)}{\sigma_{obs}} \qquad (3.3.28)$$

where, $y_{t_1,97:5\%}$ and $y_{t_1,2:5\%}$ represent the upper and lower boundaries of the 95PPU, t_1 is the observed data and σ_{obs} symbolizes the standard deviation of the measured data. The *P-factor* is the percentage of observed data bracketed by the 95PPU band, and the *R-factor* stands for

thickness of the uncertainty band (Yang et al., 2008). SUFI-2 therefore brackets most of the measured data with a large *P-factor* (100% being the maximum) and a small *R-factor* (0 being the minimum).

The flowchart of the SUFI-2 algorithm for the uncertainty analysis is graphically illustrated in Figure 3-11. From Figure 3-11 it can be seen that a single parameter value (depicted by a point) results in a single model response (see Figure 3-11a), whereas an uncertain parameter (depicted by a line) results in the 95PPU (depicted by the shaded area) in Figure 3-11b. Generally, increasing the parameter uncertainty results in increasing output uncertainty and this may not necessarily be linear (see Figure 3-11c). SUFI-2 therefore usually starts with a large physically meaningful parameter uncertainty range which allows the observed data to initially fall within the 95PPU. The uncertainty range is then decreased in steps while observing the *P* and *R* factors. At each step, the sensitivity matrix (equivalent to Jacobian) is calculated and used to update the previous parameter ranges. This is then followed by the computation of the covariance matrix, the 95% confidence intervals and the correlation matrix. An update, centered on the best simulation, is then made to the parameters using new but smaller ranges as compared to the previous ranges. The goodness-of-fit and uncertainties in a calibrated model are assessed by the *P and R-factors*. A *P-factor* of 100% and an *R-factor* close to zero represents the ideal model simulation. When the *R-an*d *P-factors* are acceptable, then the parameter uncertainties are the desired parameter ranges. Additionally, the R^2 and/or Nash–Sutcliff (NS) coefficient between the measured data and the predicted can be used to measure the goodness-of-fit (Abbaspour, *et al.*, 2014).

In this study, the initial parameter range for the selected parameters for the White Volta Basin were set based on literature (as reported by Obuobie, 2008) and the Absolute SWAT Values file in SWAT-CUP. The Absolute SWAT Values file is a text file incorporated in the SWAT-CUP program that contains almost all the SWAT parameters with their suggested physically meaningful minimum and maximum value ranges. The threshold for distinguishing the behavioral and non-behavioral simulation was also set to 0.5 for the Nash–Sutcliff (NS) coefficient. Optimal calibration and parameter uncertainty for both methods were measured on the basis of proximity of the P-factor to 100% and R-factor to 1 (SWAT-CUP 2012 user manual).

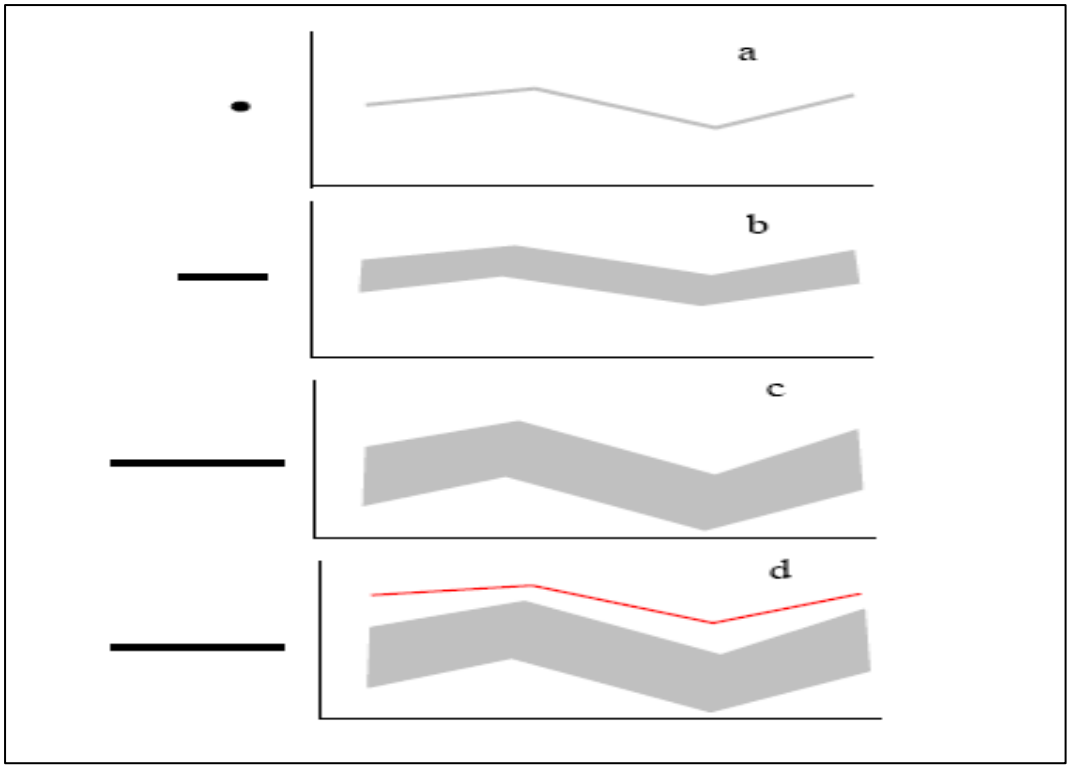

Figure 3-11: A graphical representation of the relationship between parameter uncertain and output uncertainty

3.3.5.4 Model Parameter Sensitivity Analysis in SWAT-CUP

Sensitivity analysis can be described as the process of determining the response of a model output with respect to changes in model parameters (Ma *et al.*, 2000). The input parameters in SWAT are process based and their range of uncertainty should therefore be within realistic limits. Prior to the calibration and validation in SWAT, it is important to determine the most sensitive parameters for the watershed being simulated. The modeler is usually required to determine which variables to adjust based on expert judgment or on sensitivity analysis. In this study, the one-at-a-time, OAT sensitivity analysis was performed using the SWAT_CUP 2012 interface and following the procedures outlined in the user manual (Abbaspour *et al.*, 2014). The OAT sensitivity analysis, also referred to as local sensitivity analysis, is performed by changing parameter values one-at-a-time. The OAT sensitivity analysis was necessary in helping to select reasonable parameter ranges for the selected parameters.

3.3.5.5 Model Calibration and Validation

In SWAT, the modeler defines which parameters to modify depending on knowledge of the physical characteristics of the watershed or on the results of the parameter sensitivity

analysis. After the model was set up and sensitivity analysis performed to select the most sensitive parameters for calibration, the model was calibrated for the period 1994-2003 at the Nawuni outlet of the watershed using the semi-automated procedure in SWAT-CUP.

Firstly, the hydrology was calibrated at a yearly time step using mean annual discharge measurements. This was then followed by annual sediment load calibration at a yearly time step using annual values of sediment loads derived from sediment rating curves relating turbidity and suspended sediment concentration (see Section 3.2). In that sequence, the model was calibrated at monthly and daily time steps. Figure 3-12 shows the applied semi-automated calibration procedure and the criteria for model evaluation. SWAT-CUP was setup with the selected fifteen (15) model parameters following the procedure outline in the SWAT-CUP 2012 user manual. The model was run with 500 simulations as one iteration. The model goodness of fit and efficiency was inspected in the 95ppu plot and the summary_stat.txt file respectively under the calibration outputs module. When the model performance is considered as poor according to the performance criteria used in this study, which is based on Moriasi *et al.*, (2007), the suggested new parameters ranges set out in the *New_par.txt* file in SWAT-CUP is copied to *Par_inf.txt* file and SWAT-CUP run again for 500 simulations. The parameter range for any of the parameters may be manually edited if the suggested new parameters are considered not to be physically acceptable. Figure 3-13 presents the detailed procedure in running SUFI2 in SWAT-CUP.

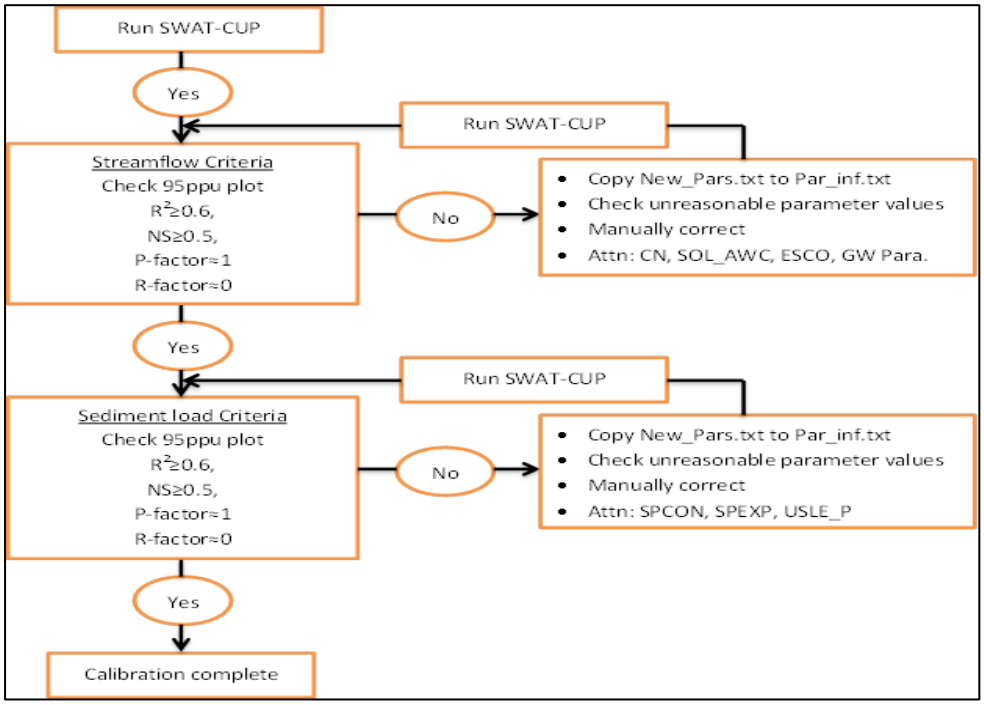

Figure 3-12: Applied procedures for semi-automated calibration of hydrology and sediment load in SWAT-CUP.

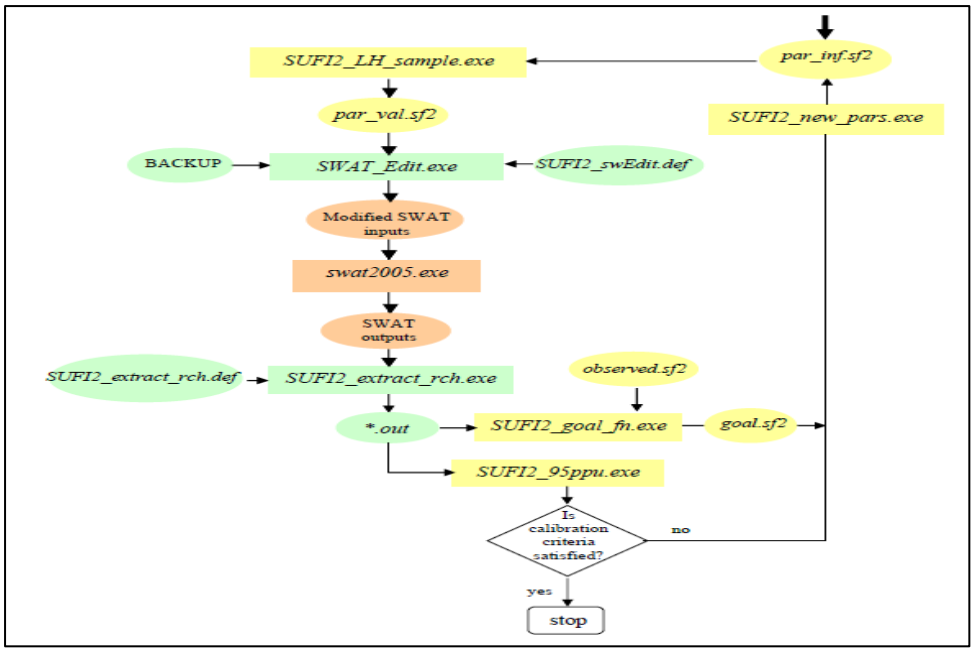

Figure 3-13: Flow chart of SWAT (orange), iSWAT (green), and SUFI2 (yellow). Modules are run by two batch files: SUFI2_pre.bat and SUFI2_post.bat.

3.3.5.6 Model Performance Evaluation

The White Volta Basin SWAT model performance was evaluated using graphical and quantitative statistical techniques. The graphical method of evaluating a model provides the first overview of the model performance through visual comparison of the observed and simulated time series and is pivotal for model evaluation (Moriasi *et al.*, 2007). Other methods of evaluating a model performance are the quantitative statistics.

Quantity statistics can be divided into three main categories. These are:

i. The standard regression statistic which determine the strength of the linear relationship between the observed and simulated time series.
ii. The dimensionless statistic which provide a comparative model evaluation.
iii. The error index statistic which measures deviation of simulated from observed (Legates and McCabe, 1999).

Based on recommendations by ASCE (1993) and Legates and McCabe (1999), Moriase *et al.*, (2007) recommend that both graphical techniques and quantitative statistics be used in model evaluation.

3.3.5.6.1 Standard Regression (Coefficient of Determination, R^2)

The coefficient of determination, R^2 (Equation 3.2.11) was used to describe the degree of co-linearity between the observed and simulated time series. R^2 ranges from 0 to 1, with 1 being the ideal simulation. Generally, R^2 values higher than 0.5 are considered acceptable (Santhi *et al.*, 2001, Van Liew *et al.*, 2003; Moriasi *et al.*, 2007). Although R^2 is a widely used performance statistic, it has been found to be oversensitive to high extreme values (outliers). The R^2 has also been found to be insensitive to additive and proportional differences between model simulation and observed data (Legates and McCabe, 1999; Moriasi *et al.*, 2007).

3.3.5.6.2 Dimensionless (Index of Agreement, IA and Nash-Sutcliffe Efficiency, NSE)

The index of agreement, *IA* assesses the quality of the temporal simulation of the observed data by the SWAT model. *IA* (Willmott, 1981) is a standardized measure of the degree of model prediction error and varies between 0 and 1 (Moriasi *et al.*, 2007). An *IA* value of 1 indicates an excellent agreement between the observed and simulated values, and 0 indicates no agreement (Willmott, 1981; Moriasi *et al.*, 2007). *IA* is very sensitive to extreme values as a result of the squared differences but can detect additive and proportional differences in the observed and simulated means and variances (Legates and McCabe, 1999; Moriasi *et al.*, 2007). IA is calculated by (Willmott, 1981):

$$IA = 1 - \frac{\sum_{i=1}^{N}(O_i - P_i)^2}{\sum_{i=1}^{N}\left(|P_i - O_{mean}| + |O_i - O_{mean}|\right)^2} \qquad (3.3.29)$$

where, O_i is the *ith* observed value, P_i is the *ith* predicted value, O_{mean} is the mean of observed time series and N is the total number of observations. Other studies have used the Index of Agreement (IA) as an additional statistic to evaluate the performance of the SWAT model (Sintondji, 2005; Chekol, 2006; Obuobi, 2008).

Another dimensionless quantitative statistics used in this study to evaluate the model performance is the Nash-Sutcliffe, *NSE* (Equation 3.2.13). The *NSE* is a normalized statistic which describes the relative magnitude of the residual variance compared to the observed data variance (Nash and Sutcliffe, 1970; Moriasi *et al.*, 2007). The *NSE* explains the goodness of fit on a plot of observed versus simulated time series on a 1:1 line. A perfect model would produce an *NSE* of 1, however, Moriasi et al., (2007) indicate that the

performance of a model is considered to be "good" if the *NSE* is between 0.65 and 0.75 and "satisfactory" when the *NSE* is above 0.5.

3.3.5.6.3 Error Index (Percent Bias, PBIAS)

The predictive performance of the White Volta SWAT model was also evaluated using the Percent bias, *PBIAS*. *PBIAS* evaluates the average inclination of the simulated time series to be greater or less than their respective observed time series (Gupta *et al*., 1999; Moriasi *et al*., 2007). The perfect *PBIAS* value is 0.0 with lower absolute values representing ideal model performance. Positive and negative values show model underestimation and overestimation bias respectively (Gupta *et al*., 1999). *PBIAS* is calculated by:

$$PBIAS = \frac{\sum_{i=1}^{N}(O_i - P_i)}{\sum_{i=1}^{N}(O_i)} \cdot 100 \qquad (3.3.30)$$

where, O_i is the *ith* observed value, P_i is the *ith* predicted value, and N is the total number of observations. PBIAS values between ±10 and ±15 indicate a "good" model simulation, whereas values greater than ±25 indicate an "unsatisfactory" model simulation (Moriasi *et al*., 2007).

3.3.6 **White Volta Basin SWAT Setup**

This study was conducted using the ArcSWAT2009 version of SWAT (Soil and Water Assessment Tool) to model runoff and sediment outflow at Nawuni in the White Volta Basin. The data required to setup the White Volta Basin SWAT model included a digital elevation model (DEM) of the White Volta Basin, climate data, soil and land-use maps, and reservoir data. Calibration and validation of the model was undertaken using observed streamflow and sediment data.

3.4 Climate Change Impact Analysis

3.4.1 **Introduction**

This section examines the impact of future climate change on the streamflows and sediment loads in the study area. The emergence of downscaling technics has provided the process of linking local/station scale meteorological time series to large-scale atmospheric

predictor variables. The Quantile Mapping (QM) downscaling technique (Boe et al., 2007), a statiscal downscaling technique, was adopted to downscale and bias correct the climate series for this study.

3.4.2 **Climate Change Projections and Downscaling**

For the purpose of this study, three RCMs under the frame work of the Coordinated Regional Climate Downscaling Experiment (CORDEX) (Giorgi et al., 2009) were used to downscale future projected climate series for the study area. CORDEX is a program sponsored by the World Climate Research Program with the aim of designing a set of standardized experiments for downscaling GCMs from the family of the Coupled Model Intercomparison Project phase 5 (CMIP5) (Taylor *et al.*, 2012).

The CORDEX-Africa Project is the Africa branch of the CORDEX initiative which aims at providing an ensemble of high-resolution historical and future regional climate change projections over the African domain within the framework of the IPCC Fifth Assessment Report (IPCC, 2014). The RCMs in the CORDEX-Africa Project are set at a spatial resolution of 0.44° x 0.44° using a rotated pole coordinate system and uses outputs from the CMIP5 GCMs projections covering the period 1950-2100 as boundary conditions. The simulation of future climate change projections in the CORDEX-Africa Project are based on GCM forcing under the Representative Concentration Pathways, RCPs (Vuuren et al., 2011).

The RCPs projections cover a wider range of scenarios than the Special Report on Emissions Scenarios (SRES) used in previous assessments. The RCPs generally represent climate scenarios that include climate policies. In comparable terms, RCP8.5 is broadly comparable to the SRES A2/A1FI scenario, RCP6.0 to scenario B2 and RCP4.5 to scenario B1. The RCP2.6 however has no equivalent scenario in SRES (IPCC, 2016). RCP4.5 and RCP8.5 are the two climate change scenarios implemented in the CORDEX-Africa Project.

RCP4.5 is a scenario of long-term, global emissions of greenhouse gases, short-lived species, and land-use-land-cover which stabilizes radiative forcing at 4.5 Wm^{-2} (approximately 650 ppm CO_2-equivalent) in the year 2100 without ever exceeding that value (Thomson et al., 2011). Contrary to other scenarios developed by the IPCC, which examined possible greenhouse-related emissions in the absence of measures designed to limit anthropogenic climate change, the RCP4.5 is a stabilization scenario. It assumes that climate policies, such as the introduction of a set of global greenhouse gas emissions prices, are

invoked to achieve the goal of limiting emissions and radiative forcing. RCP8.5 on the other hand represents a high-level emission scenario and corresponds to a rising radiative forcing at 8.5 Wm^{-2} (approximately 1370 ppm CO_2-equivalent) in the year 2100 (Moss et al., 2010). Nikulin *et al.*, (2012) presents a detailed description of the physical parameterization and model dynamics of the RCMs implemented in the CORDEX-Africa Project.

The three RCMs used in this study and their driving GCMs and their institutions/modeling centers are presented in Table 3-6 below. The three RCMs were selected due to the availability of processed climate series spanning the period 1950 to 2100 for the CORDEX-Africa project. Other available RCMs e.g. the RCA4 (Rossby Centre regional Atmospheric model, version 4) driven by several GCMs ICHEC-EC-EARTH have gaps covering the period 2006-2050 in the climate series. The selected period of interest for this study was however 1991-2010 for the referenced period and 2031-2050 for the future which the RCA4 has gaps in the data sets.

Table 3-6: Details of the RCMs their driving GCMs under the CORDEX Framework

RCMs			**GCMs**		
Short Name	Full Name	Institution	Short Name	Full Name	Institution
CCLM4	CLMcom COSMOCLM	Climate Limited-Area Modelling (CLM) Community	MPI-ESM-LR	Max Planck Institute Earth System Model, low resolution	Max Planck Institute for Meteorology, Germany
HIRHAM5	DMI HIRHAM5	Danmarks Meteorologiske Institut (DMI), Danmark	ICHEC	ICHEC-EC-Earth	Irish Centre for High-End Computing-EC-EARTH consortium
RACMO22T	KNMI Regional Atmospheric Climate Model, version 2.2 (RACMO2.2T)	Koninklijk Nederland's Meteorologisch Instituut (KNMI), Netherlands	ICHEC	ICHEC-EC-Earth	Irish Centre for High-End Computing-EC-EARTH consortium

The CORDEX-Africa framework was chosen for this study due to the fact that, numerous studies can be found in the literature showing that the overall performance of the CORDEX RCMs in simulating the regional climate of the respective domains is very encouraging. Over the continental African domain, (Laprise et al., (2012); Nikulin et al.,

(2012); Kim et al., (2014); Dosio and Panitz (2015)) all reported reasonable results of CORDEX simulated climate variables whereas (Paeth et al., (2011); Owusu and Klutse, (2013); Gbobaniyi et al., (2014); Klutse et al., (2014)) also reported good performance of the CORDEX RCMs in the West African sub-region. For instance, Nikulin et al., (2012) assessed an ensemble of ten (10) RCMs to simulate the climatology of the entire African continent and observed that all the models performed reasonably well in predicting the seasonal means and annual cycle of precipitation whereas Gbobaniyi et al., (2014) also assessed the ability of the RCMs to simulate the occurrence and movement of the West African monsoon. Specifically in the study area, Owusu and Klutse, (2013) simulated the rainfall regime over Ghana, north of latitude 8° N, using the CORDEX framework and observed a good agreement between the simulated and observed climate series. Owusu and Klutse, (2013) and Gbobaniyi et al., (2014) however reported that some of the RCMs exhibited some level of biases.

3.4.2.1 Downscaling and Bias Correction

To improve the biases associated with the future projection of climate variables by the RCMs as reported by Owusu and Klutse (2013) and Gbobaniyi et al., (2014), the Quantile Mapping (QM) downscaling technique (Boe et al., 2007) was adopted in this study for the removal of the RCMs model bias in the projected future climate series. The QM technique was selected due to its flexibility, less computational demand and simplicity. The procedure employed in the QM downscaling technique involves the generation of a correction function (*f*) between the observed and the RCM model simulated distributions and the application of same to remove the biases.

Historical observed precipitation and minimum and maximum air temperatures spanning the period (1991-2010) for eleven (11) selected climate stations (see Appendix B for the list of stations), and the outputs from the control run of the three CORDEX-Africa RCMs spanning the period (1950-2100) were obtained and applied for the QM as described by Sarr et al., (2015). The QM was applied on a monthly integrals to develop a statistical distribution function which is close to the statistical distribution of the observed period for a given climate variable. The procedure can be explained as follows:

i. The observed climate time series were split into two parts, one part for calibration and other part for validation. To eliminate non-stationarity in the climate series, the calibration time series consists of odd years whereas the validation is based on even years. Daily time series of the month were then

extracted for both calibration and validation periods from observed and RCM simulated data.

ii. Two empirical cumulative distribution functions, f_o (statistical distribution for the observed time series) and f_m (distribution for the RCM simulated time series) were then developed for the calibration period.

iii. The RCM simulated time series were then corrected on the validation and future projected periods using the transformation:

$$X_C = f_o^{-1}(f_m(X_m)) \qquad (3.4.1)$$

where X_c *and* X_m are the corrected and uncorrected variable extracted from the RCM simulations.

iv. The probability mass function (PMF) of, e.g. precipitation occurring, defined as rainfall intensity exceeding 1mm/day, and the probability density function (PDF) of precipitation intensity on rainy/wet days are built. The QM technique was then applied to generate a biased corrected future projected climate series of a particular variable if the PDF or PMF of the corrected variable was closer to the PDF of the observation than the PDF of the uncorrected variable.

v. A two-sample Kolmogorov-Smirnov (KS) test is then applied to compare the PDFs of the observations and the corrected variable during the calibration and validation periods. The null hypothesis is that the two sets of data are from the same continuous distributions or alternatively they are from different continuous distribution (Sarr et al., 2015).

Sufficiently long term historical observed time series are required to downscale and biased correct the climate change scenarios within the CORDEX-Africa framework. In this study, historical time series of daily rainfall and maximum and minimum air temperatures spanning the period 1991-2010 for 11 selected climate stations (see Appendix B) were used for the downscaling. The selected stations and time frame were chosen due to the fact that the time series had fewer gaps, generally less than 5% of the time frame. The downscaling process consists of the extraction of a climate variable from a selected RCM-GCM ensemble for a selected scenario. The extracted variable is downscaled to a station specific location by specifying the latitude and longitude of the local climate station. The RCM-GCM downscaled climate variable is then biased corrected using the QM technique and comparing with the historical observations using the Q-Q, PDF, CDF and P(rain/no rain) plots.

3.4.2.2 Evaluation of Climate Change Scenarios

According to Lo *et al.*, (2008), precipitation is a model diagnostic field which is more difficult to simulate. This section therefore focuses on the performance of the three RCMs and their ensemble mean in simulating precipitation and temperature for the study area. Precipitation and temperature plays a major role in the hydrological cycle since they are considered to be the main drivers of moisture into the system. It is therefore very important not only to ensure that the simulated precipitation in the study area represents the annual amounts and temporal distribution, but also ascertain that the frequency statistics of the climate series are consistent with the long-term observed mean (Obuobie, 2008).

After downscaling and bias correction, statistical tools were utilized to examine the performance of the RCM-GCM models and to also check for possible trends. The objective of this process is to examine if the removal of bias associated with the RCM-GCM model outputs are consistent with the model outputs during the control run. It is generally expected that bias correction will minimize variation in the outputs of the RCM-GCMs during the control period and consequently the future scenarios. To achieve this objective the climate series covering the periods 1991-2010 defined as the control period in this study and 2031-2050 considered as the future were extracted from the RCM-GCMs simulations. Statistical analysis such as the mean, maximum, minimum and the coefficient of variation were computed and compared. Additionally, comparison plots of long-term mean monthly precipitation and temperature were plotted. Furthermore, to assess possible clusters and the detection of dry and wet scenarios, the mean values of the mean air temperature was plotted against the mean values of the precipitation in the basin for each scenario.

3.4.2.3 Trends in Future Climate

As indicated earlier, a plot of the RCM-GCMs simulated mean monthly precipitation against the mean temperature for the study area can provide a statistical means of detecting which RCM-GCM is predicting a future warmer/colder and drier/wetter climate scenarios. The relative change in the future climate signal was computed by:

$$\Delta = \frac{X_f - X_o}{X_o} \qquad (3.4.2)$$

where Δ represents the relative change of the climate variable, X_f is the simulated future variable and X_o is the historical observation or the climate variable during the control period. The relative change can also be expressed in percentages by multiplying by 100%.

The use of precipitation or temperature as a diagnostic field in predicting the future climate was evaluated by scattered plots of the RCM-GCMs simulated mean temperatures and mean monthly precipitation. Further examination of the individual points in the scatter plots of the mean precipitation and temperature can indicate whether the future climate will be warmer/colder and drier/wetter as simulated by the individual RCM-GCMs under the two RCPs.

3.4.3 **Impact of Climate Change on Streamflows and Sediment Loads**

In this section, the impact of climate change on the streamflows and sediment loads in the White Volta Basin was assessed using the calibrated SWAT model driven by the RCM-GCMs downscaled temperature and precipitation time series under the RCPs forcing.

First, the calibrated SWAT model was used to simulate the hydrology of the catchment for the controlled period (1991-2010) using precipitation and temperature from the historical observations as input. The output of the SWAT model i.e. streamflow and sediment loads was then extracted and used as the basis of comparing the impact of climate change in the study area. The downscaled climate series for the controlled period for each RCM-GCM and the RCM-GCMs Ensemble mean were also used as inputs into SWAT to simulate the streamflows and sediment loads and the output compared with the extracted streamflow and sediment loads from the historical observation simulation. Performance statistics such as R^2, NSE, P- and R-values and PBIAS were then used to assess how well the hydrological model predicted the streamflow and sediment loads.

The output of the SWAT simulations for the control period using the climate series from the historical observations and the RCM-GCMs simulated series forced by RCP4.5 were compared. The results of the SWAT simulation using the historical and all the RCM-GCMs downscaled climate series for the control period were then are summarized. A comparison of the long-term mean monthly streamflow and sediment loads are also presented.

3.4.3.1 Trends in Future Hydrology

In other to assess the impact of the projected changes in the RCM-GCMs downscaled precipitation and temperature on streamflow and sediment loads in the study, the downscaled future (2031-2050) climate data was applied as inputs into the hydrological model, SWAT to

simulate the impact of climate change on the hydrology of the White Volta Basin relative to the baseline period (1991-2010). The trend in the projected future hydrology (streamflow, surface runoff, actual evapotranspiration, AET, potential evapotranspiration, PET and sediment loads) of the study area was computed using the relative change in future signal, Equation 3.4.2.

3.5 Analysis of Extreme Precipitation

The impact of climate change on sediment loads can be directly linked to the intensities of extreme precipitation in the study area. This is generally due to the fact that the generation of runoff, and consequently sediment loads, in the catchment is highly influenced by the intensities and amounts of precipitation. This section therefore focuses on analyzing the exceedance probabilities (or return periods) of extreme rainfall amounts by fitting a probability distribution to the long-term maximum daily rainfall for the peak months of July, August and September (JAS) at each climate station in the study area. The return levels of extreme precipitation precipitations for some selected return periods are then analyzed with regards to changes in the future climate.

3.5.1 Maxima Precipitation for July, August and September (JAS)

The annual rainfall amounts in the study area usually occur between May and October and peaking in August/September (Section 2.5). For the purpose of analyzing the extreme rainfall events in the study area, the maximum daily rainfall amount for each month in the July, August and September (JAS) period for each year was extracted from the historical observations using the peak-over threshold (POT) method. The POT threshold was set using a 1-year and a 2-year return period. This implies that for the 20 year record (1991-2010), the highest extreme rainfall amount for each month in the period JAS in each year is selected and additionally the 10 next highest extreme rainfall amounts for each month are also retained. In other to eliminate inter-dependence of the extreme rainfall events, an independent criteria which was set to be equal to the temporal aggregation, was applied to make sure rainfall extreme events are separated by more than the temporal aggregation which is one day. This procedure would result in the selection of at least 60 and at most 90 highest rainfall amounts for the JAS in the historical observations.

Similarly, the maximum daily rainfall amounts for the months of JAS were extracted from the RCM-GCMs-simulated precipitation for the present (1981-2010) and future (2031-2060) periods under the RCP4.5 scenario. Overall, 90 maximum rainfall values were extracted per station for each period and RCM-GCM ensemble.

3.5.2 **Homogeneity Test**

Prior to fitting the probability distribution, the time series were tested for randomness and homogeneity in the annual extreme rainfall events. Generally, it is required that time series are homogeneous and independent to be used in frequency analysis. In this study, the adjusted partial sum proposed by Buishand (1982) method of homogeneity test was used.

The adjusted partial sum is given by:

$$S_0 = 0, \& S_n = \sum_{i=1}^{n} (X_i - X_m) \tag{3.5.1}$$

where X_m = mean of the series $X_{i=1}$, X_2, ….X_k and n=1, 2,…,k. Generally, S fluctuates around zero for a homogeneous and independent series. On the other hand, S_n can either be positive or negative shift when there is a break in the series. The homogeneity of the time series is evaluated by rescaling S_n by dividing by the standard deviation and computing the maximum, M and range, R of the rescaled S_n. M and R can be computed by:

$$M = \max\left(\frac{S_n}{\sigma}\right) \tag{3.5.2}$$

$$R = \max\left(\frac{S_n}{\sigma}\right) - \min\left(\frac{S_n}{\sigma}\right) \tag{3.5.3}$$

where σ = standard deviation.

A test of significant departure from homogeneity is given by:

$$\pm p_{\alpha/2} / \sqrt{k} \tag{3.5.4}$$

where p= percent point function of the standard normal distribution, k = sample size and α = significance level. Equation 3.5.4 depends on the sample size and is used to generate the confidence bands in the plot.

3.5.3 **Fitting the Generalized Extreme Value, GEV Distribution**

The next step after testing the homogeneity of the climate series is to select the best probability distribution that best fit the time series for each climate station. For the purpose of this study, four 3-parameter probability distributions namely; the generalized extreme value,

GEV, the Pearson Type III, the Log-Logistic (3) and Lognormal (3P) probability distribution models were fitted to the annual extreme precipitation of the historical observations of all the 11 climate stations used in this study. The probability density functions for the selected distributions are presented in Table 3-7.

The parameters of the probability distribution were estimated using the L-moment (Hosking and Wallis, 1997) estimation method. The L-moment method of estimation has an advantage over ordinary distribution moments in that; L-moments always maintain the mean of the probability distribution. Furthermore, the sample estimates of L-moments are unbiased and less sensitive to random outliers and gross observational errors than sample estimates from ordinary moments (Gubareva and Gartsman, 2010). The sample estimates of L-moments is computed by:

$$l_{r+1} = \sum_{k=0}^{r} P_{r,k}^{*} b_k \quad \text{r} = 0, 1, \ldots, \text{n-1}, \tag{3.5.5}$$

where

$$P_{r,k}^{*} = \frac{(-1)^{r-k}(r+k)!}{(k!)^2 (r-k)!} \tag{3.5.6}$$

and

$$b_r = n^{-1} \sum_{j=r+1}^{n} \frac{(j-1)(j-2)...(j-r)}{(n-1)(n-2)...(n-r)} x_{j:n} \tag{3.5.7}$$

where x_j = ordered sample, n = sample size and l_{r+1} = *(r+1)-th* sample L-moment.

The sample L-moment ratios of the rth order are given by

$$t_r = l_r / l_2 \tag{3.5.8}$$

where t_r = sample coefficient of L-variation, t_3 = sample coefficient of L-asymmetry (skewness) and t_4 = sample L-kurtosis.

The Anderson-Darling test (Stephens, 1974) was used to test the goodness-of-fit at the 0.05 significance level and the best fitted probability distribution model was selected for that particular station. The Anderson-Darling test statistic is a modification of the Kolmogorov-Smirnov test which tends to give more weight to the tails than the Kolmogorov-Smirnov test. The Anderson-Darling test statistic has the advantage of allowing a more sensitive test since it uses the applied distribution in estimating the critical values. The Anderson-Darling test statistic is given by:

$$A^2 = -n - \frac{1}{n} \sum_{i=1}^{n} (2i-1)(\ln F(X_i) + \ln(1 - F(X_{n-i+1}))) \tag{3.5.9}$$

The following null hypothesis is tested at the specified significance level:

Ho: the maximum daily precipitation time series follow the selected distribution

Ha: the maximum daily precipitation time series does not follow the selected distribution.

Additionally, quantile-quantile, Q-Q plots were also plotted to aid in visual observation of how well a specific probability distribution is able to fit the input time series. The Q-Q plots are generally linear when the selected probability distribution fits well with the input time series.

Table 3-7: Probability density functions for the selected distributions

Distribution	Probability Density Function	Parameters
GEV	$f(x)=\frac{1}{s}\exp(-(1+kz)^{-1/k})(1+kz)^{-(k+1)/k}$ For $k\neq 0, 1+k\frac{(x-m)}{s}>0$ *and* $K=0$, $-\infty<x<+\infty$	k-continuous shape parameter s-continuous scale parameter m-continuous location parameter
Pearson Type III	$f(x)=\frac{1}{x\mid b\mid \Gamma(a)}\left(\frac{\ln(x)-g}{b}\right)^{a-1}\exp\left(-\frac{\ln(x)-g}{b}\right)$ *for* $b<0$, $0<x\leq e^{g}$ $e^{g}\leq x<+\infty$	a-continuous parameter (a>0) b-continuous parameter (b≠0) g-continuous parameter
Log-Logistic (3P)	$f(x)=\frac{a}{b}\left(\frac{x-g}{b}\right)^{a-1}\left(1+\left(\frac{x-g}{b}\right)^{a}\right)^{-2}$ *For* $g\leq x<+\infty$	a-continuous shape parameter (a>0) b-continuous scale parameter (b>0) g-continuous location parameter (g≡0 yields 2P Log-Logistic)
Lognormal (3P)	$f(x)=\frac{\exp\left(-\frac{1}{2}\left(\frac{\ln(x-g)-m}{s}\right)^{2}\right)}{(x-g)s\sqrt{2\pi}}$ *For* $g<x<+\infty$	s-continuous parameter (s > 0) m-continuous parameter g-continuous location parameter (g≡0 yields 2P Lognormal)

3.5.4 **Exceedance Probability (Return Period)**

After determining the best fitted probability distribution for the selected climate stations in the study area, the probability of occurrence, which is defined as the probability of an event of a specified magnitude being equaled or exceeded during the specified period, was computed. If n is the sample size and r is the ordered rank of the sample x where $x_1>x_2\ldots>x_r$, then the probability of exceeding the r^{th} largest value, x_r is given by:

$$P(X\geq x_r)=\frac{r}{n} \qquad (3.5.10)$$

For a given return period, T the probability of exceeding a given return level, x_T can be generally computed by:

$$x_T = F^{-1}\left(1-\frac{1}{T}\right) \quad (3.5.11)$$

where F = cumulative density function.

Having selected the best fitted distribution for the extreme precipitations for the selected climate stations in the study area, the return levels of rainfall events where estimated for return periods between 2 and 200 years from the historical observations and the RCM-GCMs-simulated precipitation forced by the RCP4.5 scenario. The return periods were computed for the present (1981-2010) and future (2031-2050) in the case of the RCM-GCMs and (1991-2010) for that of the historical observations.

3.5.5 **Climate Scaling Factor**

In this study, the climate scaling factor method as described by Sanderson (2010) was adopted and applied to the estimated extreme return levels of rainfall for the selected return periods. This method was adopted due to the fact that the scaling factor, similar to the perturbation factor (Boukhris et al., 2008), describes the differences between the present and future climates and can be derived based on their dependency on the return period (Baguis et al., 2008). In this study the extreme rainfall events having the same return periods in the present (19981-2010) and future (2031-2060) are used to compute the scaling factors.

The level of change in the future return periods can be calculated by estimating the climate scaling factor which is the ratio of the precipitation return levels in the future period over that of the control period as simulated by the RCM-GCMs. The scaling factor (similar to the perturbation factor), F is computed by (Willems and Vrac, 2011):

$$F(p) = \frac{S_f(p)}{S_r(p)} \quad (3.5.12)$$

where $S_f(p)$ = future (2031-2060) precipitation (return level) quantile and $S_r(p)$ = reference (1981-2010) precipitation (return level) quantile. $Q_f(p)$ and $Q_r(p)$ are both associated to the return period, T.

To be able to compare the impact the RCM-GCMs projection had on future surface runoff and sediment loads in the study area, the future return levels for all the return periods were estimated by multiplying the climate scaling factor derived from the RCM-GCMs with the return levels calculated from the historical observations. Generally, it is expected that the magnitude of extreme rainfall events will change, either by increasing or decreasing in the future for a given return period.

3.5.6 **Spatial Distribution of Changes in Return Levels**

A second analysis of the changes in the future projected extreme precipitation amounts was performed to evaluate the spatial variability of the changes in the return periods in the study area. Spatial analysis of the changes can provide detail information about the patterns and direction of the future extreme rainfall events and its impact on sediment loads in the study area. The spatial distribution of the 30-year return period was analyzed by taking the relative difference between the return levels as projected by the RCM-GCMs and that of the historical observations using the relative change in future signal, Equation 3.4.2. The spatial pattern of the future changes in return levels for the 30-year return period as projected by the RCM-GCMs was analyzed by performing a simple kriging.

3.6 Conclusion

This chapter summarises all the data required to undertake this research work. The chapter also describes the models used in this study. Section one provides an overview of all the data collected during this study whereas section two describes the methology employed in estimating long-term sediment loads in the study area. The hydrological and climate models used in this research were also described in sections three and four respectively. Finally, section five shows how extreme value analysis of precipitation under climate change was carried out.

Chapter 4

4 DEVELOPMENT OF SEDIMENT RATING CURVES

4.1 Introduction

The use of surrogate techniques relating suspended sediment concentrations, SSC and turbidity and/or riverchage discharge can provides accurate estimates of sediment fluctuations in a river. This technique is a cost effective method of estimating SSC in a river because turbidity and river discharge are easily measured compared to SSC and can also be continuously monitored throughout a storm event. This chapter therefore presents the development of the relationship between SSC and turbidity and/or river discharge as a cost effective estimation of sediment loads at Nawuni in the White Volta Basin using regression analysis.

4.2 Correlation of Surface Dip and Depth-Integrated Sampling (Correction Factor)

Prior to undertaking the regression analysis, statistical parameters such as the mean, standard deviation, coefficient of variation and skewness of the measured data were computed and presented in Table 4-1.

Table 4-1: Statistical parameters of the river discharge, turbidity and SSC data at Nawuni

Variable	Mean	S_x	C_v	C_{sx}	Min	Max	Max/ Mean
Discharge (m^3/s)	429.26	414.80	0.97	1.66	40.8	1319.2	3.07
Turbidity (NTU)	322.66	219.18	0.68	0.97	93.0	1082.0	3.35
SSC (mg/l)	375.88	405.99	1.08	1.50	47.8	1908.0	5.08

S_x: standard deviation; C_v: coefficient of variation; C_{sx}: coefficient of skewness.

From Table 4-1, it can be seen that the river discharge, turbidity and SSC data show a significantly low skewed distribution and this is confirmed by the low coefficient of variation and the ratio between the maximum and mean. These statistics potentially minimizes the variation of the model estimated SSC from the measured.

Table 4-2 presents the computation of the correction factor for Nawuni. From Table 4-2, a correction factor of 1.41 was obtained for the Nawuni sampling stations. The efficiency of the correction factor to the surface dip was found to be 82.16% according to the Nash-Sutcliffe efficiency, NSE (Equation 3.2.13) whereas the relative error was found to be 16%. Table 4-3 also presents the results of the computed correction factors for all the stations in the study site. From Table 3-3, the average correction factor that can be applied to account for

underestimation due to sampling by the surface dip method in the White Volta Basin was found to be 1.34 (i.e. 34%). The correction factor of 34% is of the same magnitude as that assumed by Akrasi (2005).

Table 4-2: Computation of the correction factor for Nawuni in the White Volta Basin

Date	S1	S2	S3	S4	S5	SSC_DI	SSC_SD
15-09-12	80	73.4	77.1	80.1	74.7	**77.1**	54.4
29-10-12	49.6	52.8	57.5	47.9	53.2	**52.2**	31.9
22-11-12	54.4	36.4	46.9	43.1	37.2	**43.6**	27.6
12-12-12	97.7	94.4	89.7	92.8	99.5	**94.8**	60.8
17-01-13	79	68.9	67.7	68.2	77.6	**72.3**	35.9
22-04-13	52.3	47.9	53.4	49.5	54.1	**51.4**	23.6
15-05-13	161	164	147.1	170.1	164.7	**161.4**	95.7
06-06-13	71.2	69.2	67.5	72	65.2	**69**	41.4
24-07-13	155.4	146.4	136.9	173.1	186.7	**159.7**	98.5
13-08-13	202.3	197.1	213.4	197.3	190	**200**	169.8
06-09-13	152	178.9	167.2	149.3	157.1	**160.9**	137.2
08-10-13	82.3	79.2	91.4	78.9	80.5	**82.5**	70.5
27-12-13	142.7	127.8	133.4	121.8	126.9	**130.5**	112.7
24-01-14	72.3	69	63.4	70.2	84.6	**71.9**	50.3
Mean						**102.0**	**72.2**

S1,..,S5 are the sampling sections (S1–same as gauge reader's single vertical), SSC_DI–sampling by depth-integrated sample (mg/l), SSC_SD–sampling by surface dip (mg/l) and SSC_SD_corr–corrected surface dip suspended-sediment concentration (mg/l).

Akrasi (2005) applied a correction factor of 25% to account for the underestimation by the surface dip sampling method based on results of similar studies by Roosebom and Annandale (1981) in South Africa.

Table 4-3: Computed correction factors for the sampled stations in the White Volta Basin

Station	Correction Factor	NSE (%)	RE (%)
Nawuni	1.41	82	16
Nasia	1.23	86	11
Pwalugu	1.35	92	13
Yarugu	1.37	82	11
Wiasi	1.39	89	15
Yagaba	1.34	94	9
Yapei	1.29	87	12

4.2.1 Evaluating the relationship between Turbidity, Suspended Sediment Concentration and River Discharge

The measured turbidity, streamflow and SSC for the 2013 calendar year (Figure 4-1) was plotted and evaluated. The figure illustrates the variability of turbidity observations, and demonstrates the close correlation between turbidity and SSC at Nawuni in the White Volta Basin. The plot shows a sharp rise and declines for the turbidity and SSC in May but the trend in the river discharge generally remains flat. These sharp peaks of turbidity and SSC recorded in the month of May can be attributed to the early rains which wash off sediments that have accumulated during the dry season and loose top soils from agricultural lands which are usually ploughed in May. The early rains however usually contribute insignificant runoff to the watershed outlet due to dry antecedent moisture conditions during that period. Additionally, bush burning, which damages vegetation, is rampant around this period in the basin and therefore presents little resistance to sediment transport into the river.

On the other hand, the figure also shows that while the turbidity and SSC peaks in late August, the streamflow peaks in late September. This can be attributed to the fact that, with increasing rainfall in the basin, the re-growth of the vegetative cover improves and provides resistance to sediment transport into the river. As runoff reaches its peaks, the basin becomes lush with vegetation thereby impeding the transport of sediments into the river. . This also implies that, the main source of sediments in the study area is mainly driven by upland erosion and sediment transport.

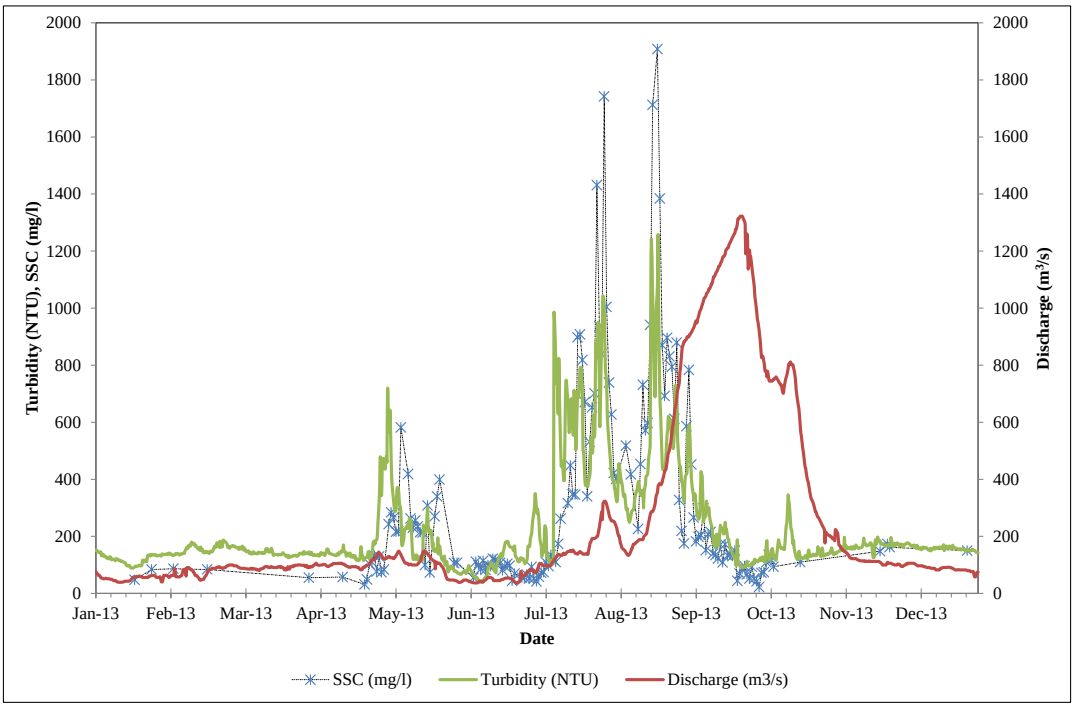

Figure 4-1: A plot of river discharge (m3/s), turbidity (NTU) and SSC (mg/l) at Nawuni for 2013

4.2.2 Relationship between Fixed-Location and Cross-Section Turbidity

Results of the evaluation of the relationship between the turbidity as measured at the fixed location by the GWCL and the mean cross-section turbidity measured with the Quanta HydrolabSonde is presented in Figure 4-2. The figure shows that the measured turbidity at the fixed-location overestimates the mean cross-section turbidity for the high turbidity values. This can be attributed to the fact that at high flows the flow velocities at the river banks are very low compared with that of the mid-section causing a semblance of laminar flow at the river bank. The velocity gradient thus tends to force fine and other microbial materials to settle at the river banks resulting in high turbid waters compared to the mid-sections. The deviations from the 1:1 line (Figure 4-2) are however minimal indicating a fairly harmonized data between the GWCL turbidity measurements at the fixed-location and the mean cross-section measurements by the Quanta HydrolabSonde.

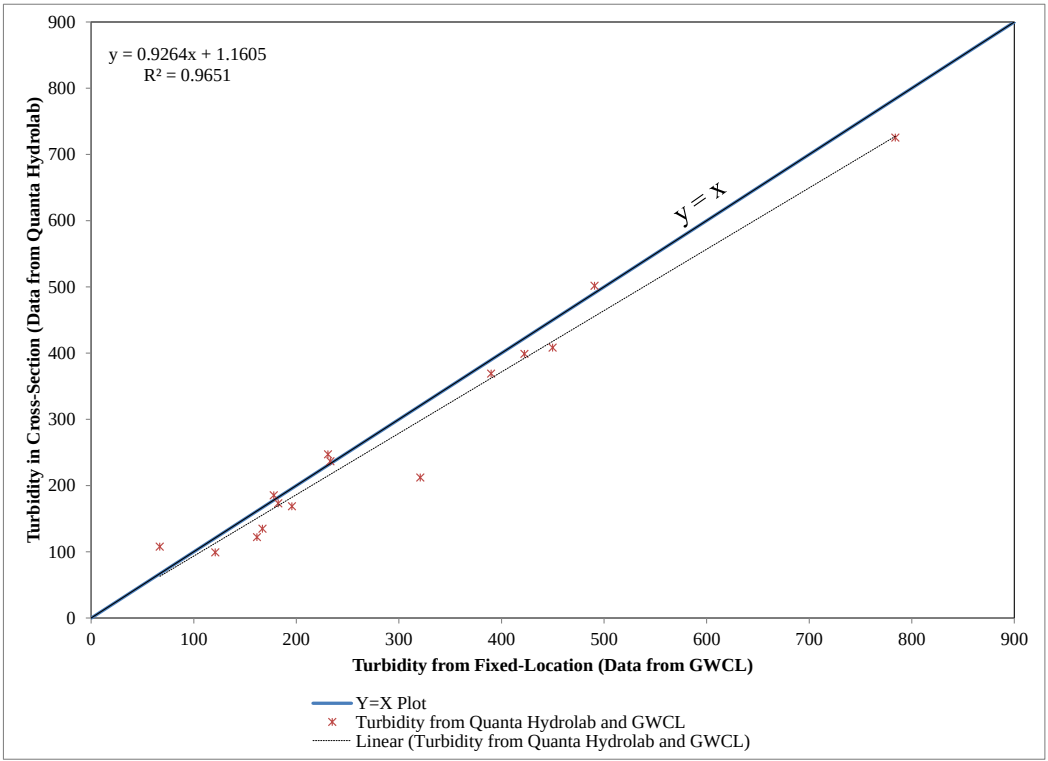

Figure 4-2: Comparison of Turbidity from Fixed-Location (GWCL, Nawuni Headworks) and In-Stream Cross-Section Measurements (Quanta Hydrolab)

4.2.3 Identification of Outliers

Figure 4-3 presents the scatter plot of turbidity versus the suspended sediment concentration at Nawuni. In this study, no outlying data points were identified in a scatter plot of turbidity versus suspended sediment concentration consisting of all the time-series data used in the regression analysis. The standardized residuals were computed for the data

and the maximum deviation from the predicted line found to be 2.14 which is less than the recommended value of 3. All the 155 time-series data points were therefore considered sufficient for the regression analysis

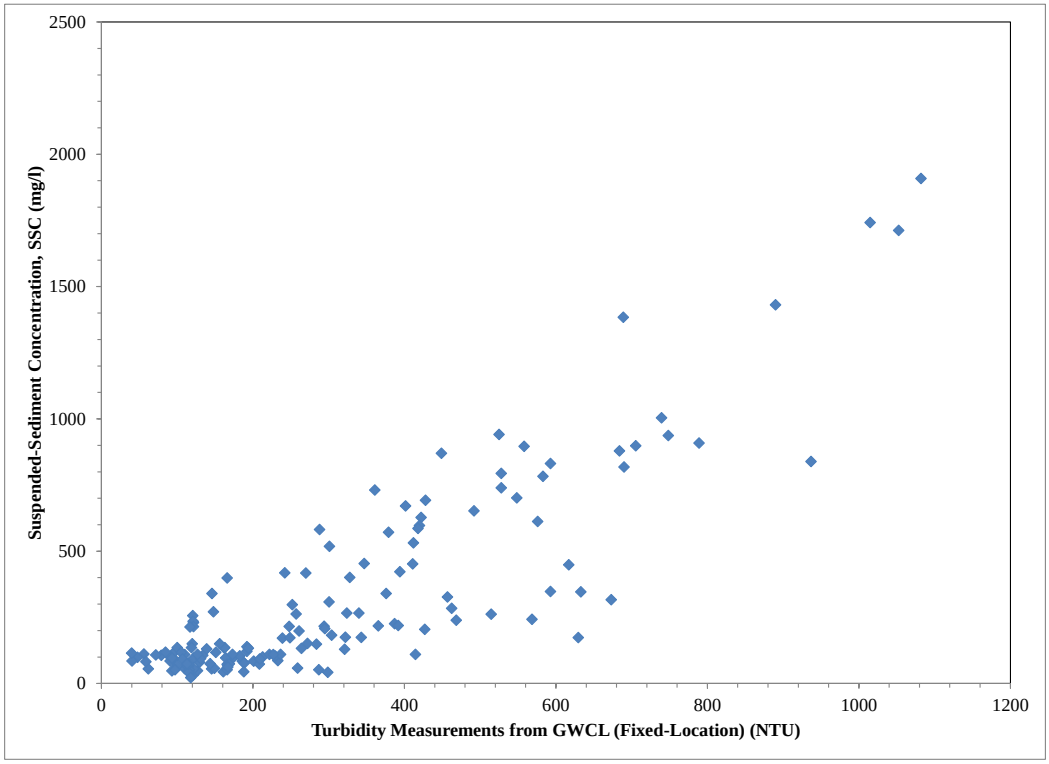

Figure 4-3: A scatter plot of turbidity (NTU) from GWCL and SSC (mg/l)

4.2.4 **Correlation Analysis**

In this study, scatter plots and correlation coefficients in logarithmic space were used to evaluate the relationship between turbidity, streamflow and SSC. Figure 4-4 presents a scatter plot of turbidity versus suspended sediment concentration in base-10 logarithmic transform space. The relationship shows a strong association with a correlation coefficient of 0.95. The plot showed a linear relationship between the turbidity and the SSC implying a linear regression model can be developed between them (Lee *et al.*, 2008).

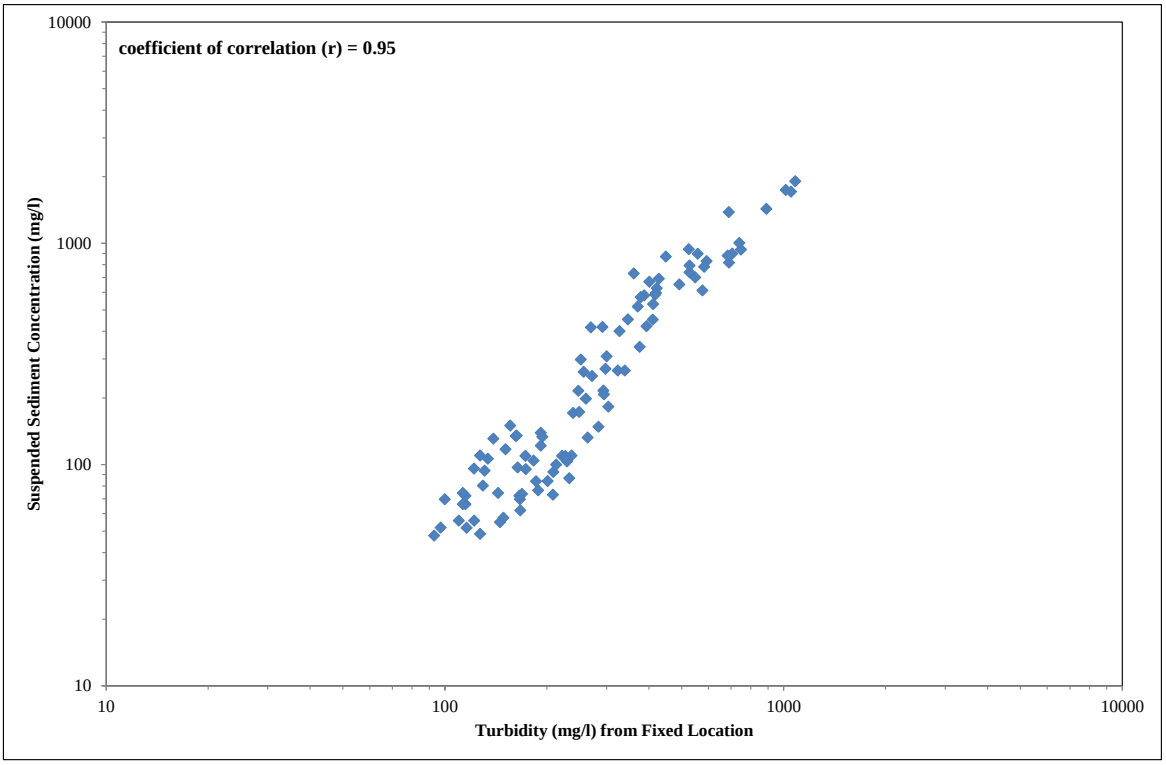

Figure 4-4: A plot of turbidity (NTU) and SSCmg/l) in log-10 space at Nawuni.

The relationship between the streamflow and SSC in log-10 transform space however shows a parabolic shape (Figure 4-5). An observation from Figure 4-1 and 4-5 shows that the SSC peaked in the 3rd week of August as streamflow just begins to rise. The plots also show that beyond this period, every incremental streamflow correspond with a decline in SSC. This period also concedes with the peak of the rainfall. As the soil moisture reaches saturation and the vegetative cover becomes lush, less sediment are being eroded from the uplands and transported to the watershed outlet.

With the cessation of rainfall in the basin, streamflow eventually decline in magnitude below the SSC. This suggests that the river remained turbid over a wide range of flows, and the suspended sediment concentrations remain relatively high during low flows (Akrasi, 2005). This implies that a nonlinear multiple regression model relating turbidity and streamflow to SSC would be applicable.

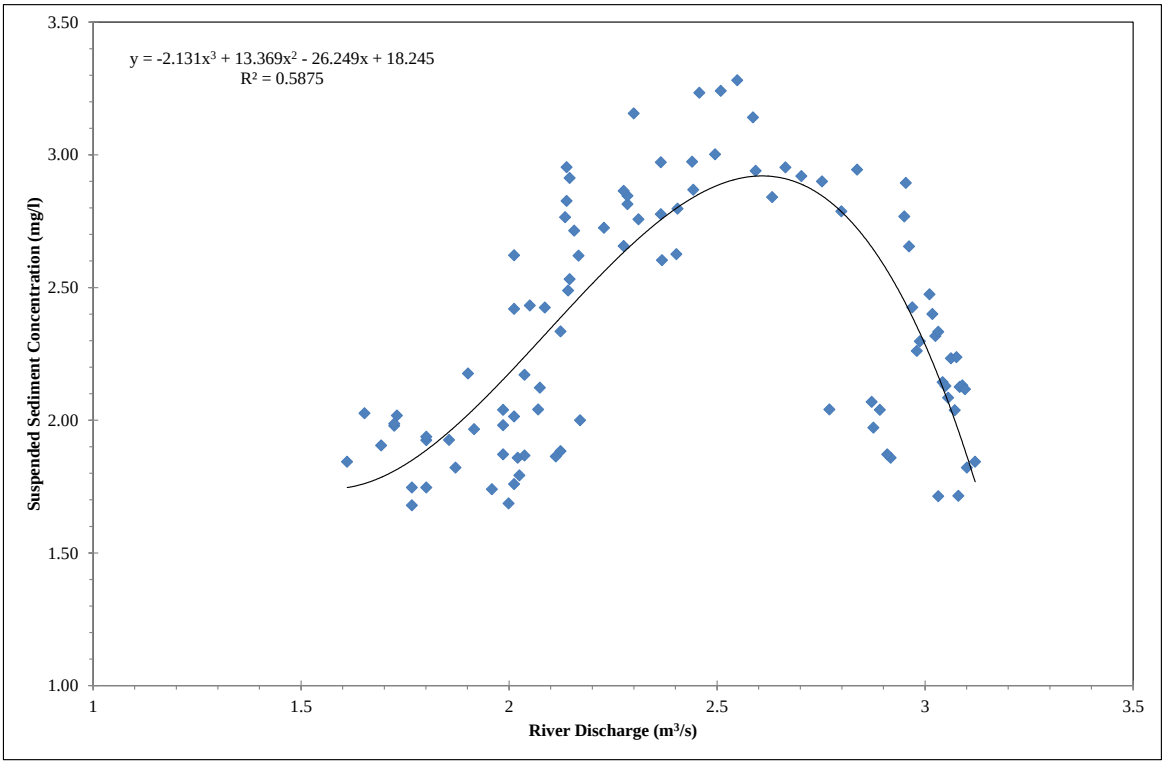

Figure 4-5: A plot of discharge (m3/s) and SSC (mg/l) in log-10 space at Nawuni.

4.2.5 **Regression Analysis**

4.2.5.1 Simple Linear Regression Model (SLR)

Analysis of the regression residual plots for turbidity and SSC in linear space shows a heteroscedastic pattern (Figure 4-6). Heteroscedasticity occurs when the residual variance increases with increasing computed SSC implying the need for variance stabilizing transformation of the response variable. In this study, the turbidity and SSC were therefore transformed using the base-10 logarithmic transform function.

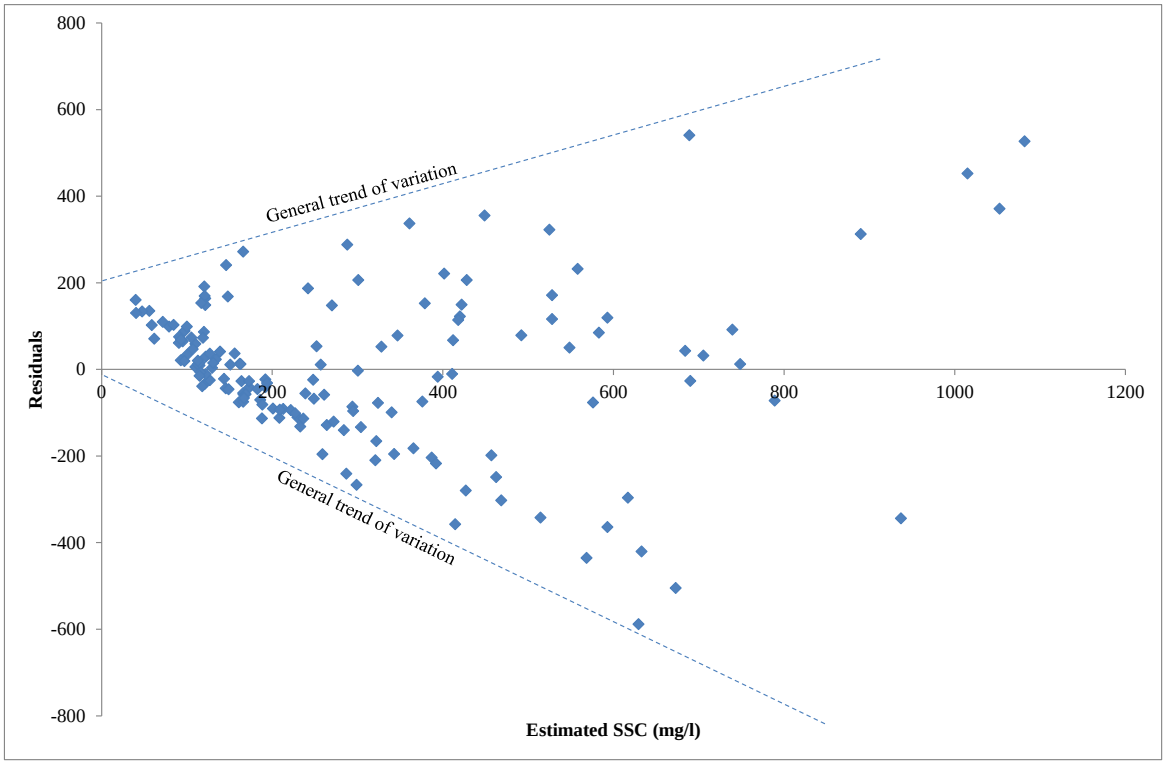

Figure 4-6: Computed suspended-sediment concentrations and regression residuals in linear space showing heteroscedasticity.

A plot of the residuals (Figure 4-7) resulting from the regression based on the log-10-transformation however shows a pattern of homoscedasticity (i.e. constant variance). The residuals were also evaluated for normality by plotting the residuals on a normal-probability plot (Figure 4-8) and determining the probability plot correlation coefficient (PPCC). According to Helsel and Hirsch (2002), the ideal transformation maximizes the probability plot correlation coefficient (PPCC) for the regression residuals and optimizes the normality of residuals. According to Rasmussen *et al.*, (2009), residuals which are not normally distributed will not be linear or evenly distributed on a normal probability plot and have a smaller PPCC (Rasmussen *et al.*, 2009). From Figure 4-8, the probability plot for the regression based on the log-10 transformation shows a linear, evenly distributed residuals and a high PPCC of 0.97.

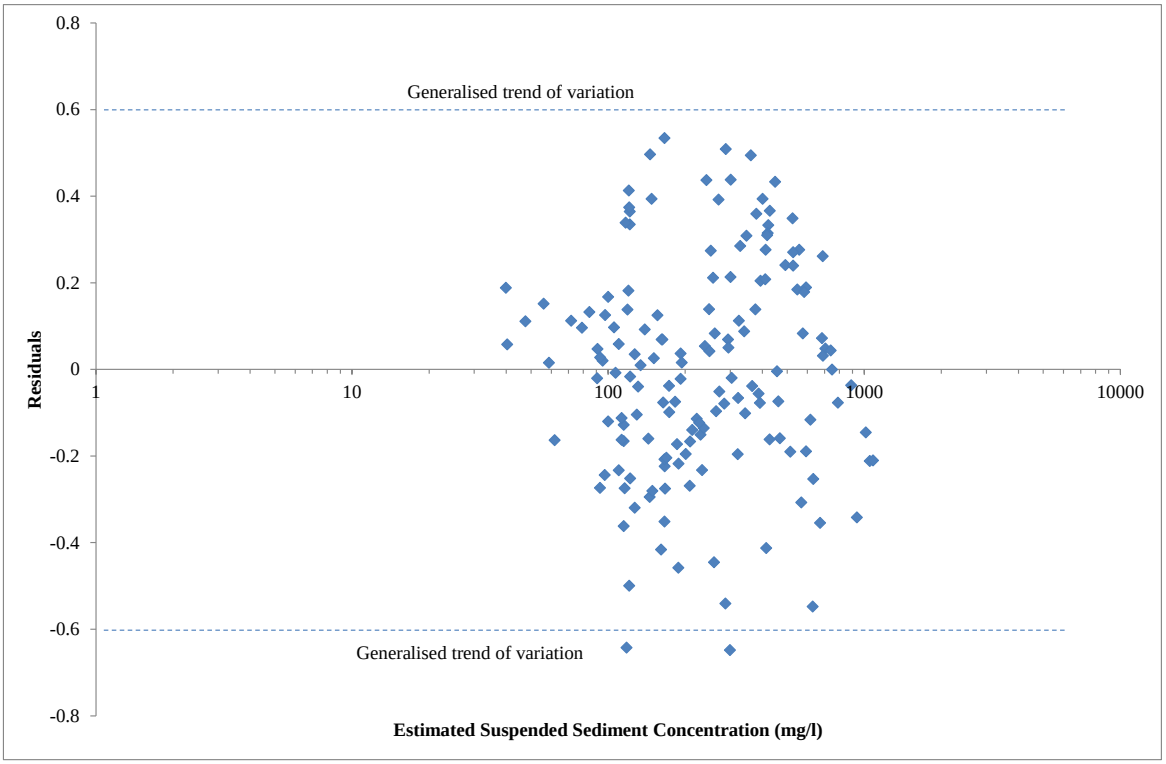

Figure 4-7: Plot of computed suspended-sediment concentrations and regression residuals

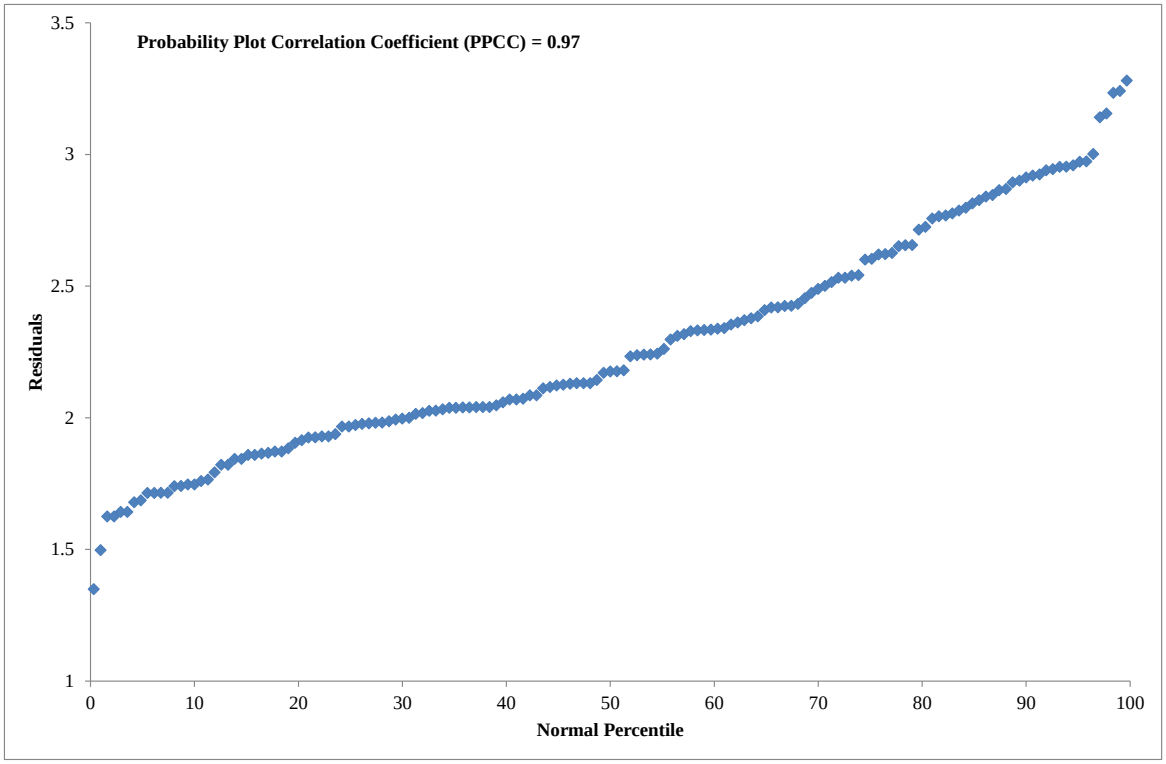

Figure 4-8: Normal probability plot of the regression residuals

The SLR model in base-10 logarithmic space for the White Volta at Nawuni is given by:

$$\log_{10}SSC = 1.62\log_{10}T - 1.58 \qquad (4.1.1)$$

where *SSC* is the suspended-sediment concentration (mg/l) and *T* is the turbidity (NTU). Table 4-4 presents the model basic information, regression coefficients, and model diagnostic statistics. The best fit SLR model plot showing the 90% confidence interval is presented in Figure 4-9. The figure shows that given the significance level of 10%, the information brought by the explanatory variables is significantly better than what a basic mean would bring. Figure 4-10 also shows a plot of the predicted versus the observed SSC on a one-on-one plot in base-10 logarithmic space. The figure shows a uniformly distribution points around the one-on-one plot implying that the model did not significant over or underestimated the SSC.

Table 4-4: SLR model coefficients and diagnostic statistics

Variable	Coefficients	Standard Error	t-Statistics	P-value	Lower 90.0%	Upper 90.0%
Intercept	-1.58	0.13	-12.03	< 0.0001	-1.80	-1.36
Log-10(Turbidity)	1.62	0.05	30.07	< 0.0001	1.53	1.71

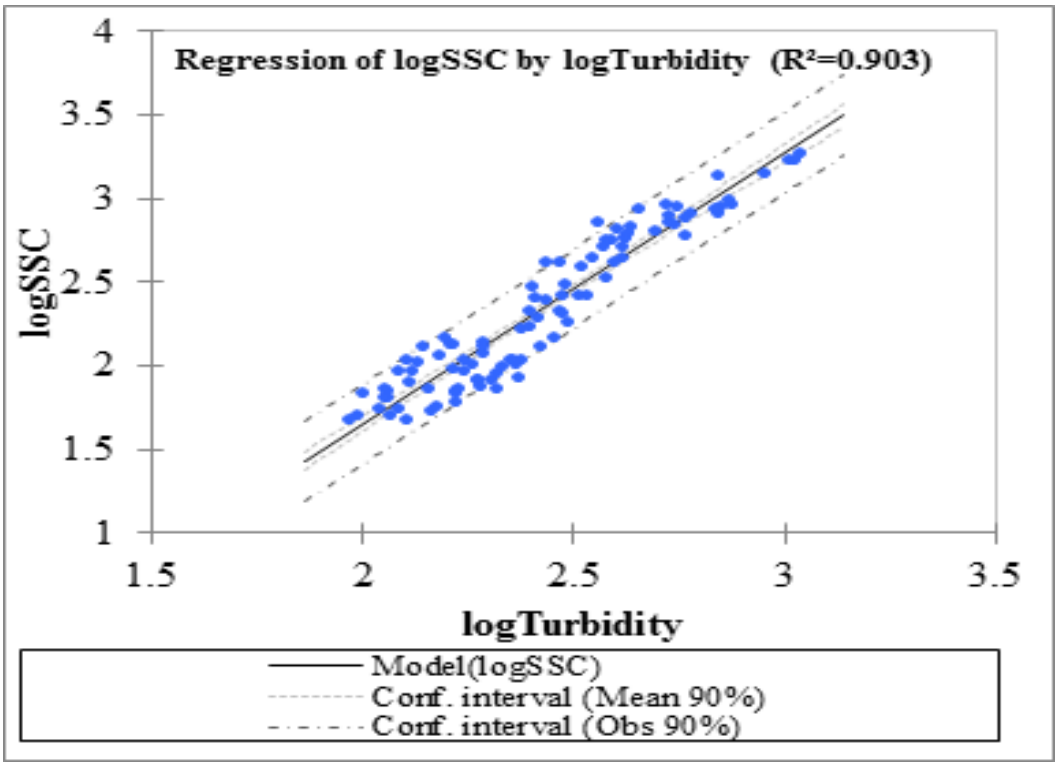

Figure 4-9: A plot of SLR of SSC and turbidity showing 90% confidence level for Nawuni (Sept. 2012-Dec. 2013)

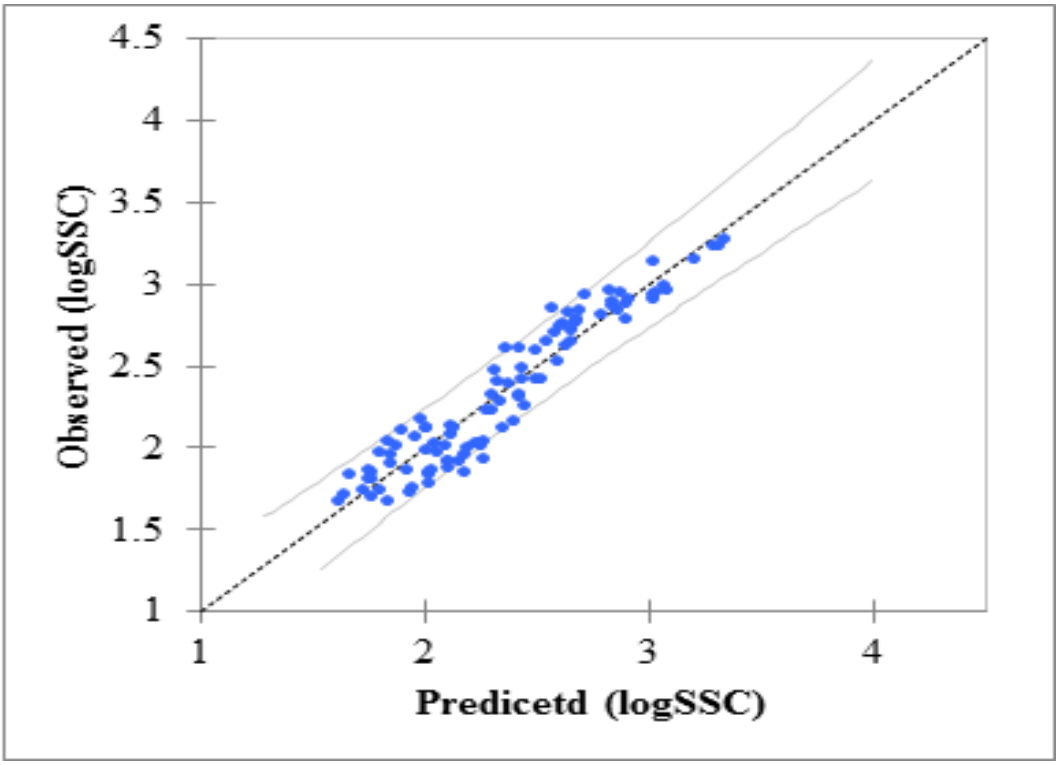

Figure 4-10: Comparison of SLR model predicted versus observed SSC showing the 90% confidence level at Nawuni (Sept. 2012-Dec. 2013).

The absolute values of the t-statistics of 12.03 and 30.07 for the intercept and turbidity respectively (Table 4-4), are greater than 2 and can be considered significant to be included in the SLR model. The p-values for the intercept and turbidity were all less than 0.0001 satisfying the null hypothesis at 90% confidence level. A standard error of 0.032 for the turbidity also shows less dispersion of the data around the regression line.

The diagnostics statistics used to evaluate the SLR model are also presented in Table 3-5. The R^2_a value of 0.902 indicates that the SLR model explains 90.2% of the variability in the SSC.

Table 4-5: SLR Model diagnostics for the White Volta Basin at Nawuni

No. of Measurements	RMSE	R^2	Adjusted R^2_a	*Lower MSPE*	*Upper MSPE*
155	0.141	0.903	0.902	27.7%	38.3%

From Table 4-4, the 90% prediction interval was found to be 1.53 and 1.71 percent for the lower and upper significant levels respectively. This implies that, for every given turbidity value, there is a 90% certainty that the actual SSC value occurs within 0.18 interval.

The bigger the 90% prediction interval, the higher the uncertainty associated with the estimated SSC (Rasmussen *et al.*, 2009).

From Table 4-5, the Upper and Lower MSPE were found to be 38.3% and 27.7% respectively which are greater than the recommended 20%. This implies that, an additional explanatory variable such as the river discharge may improve the estimation of SSC in a multiple linear regression model.

The bias correction factor (*BCF*) was estimated using Equation 3.2.10 and found to be 0.027. Applying the BCF and retransforming Equation 4.1.1, the final SLR model for the White Volta Basin at Nawuni on the basis of turbidity and SSC is given by:

$$SSC = 0.027T^{1.62} \qquad (4.1.2)$$

where *SSC* is the suspended-sediment concentration (mg/l) and *T* is the turbidity (NTU).

4.2.5.2 Nonlinear Multiple Regression (NMR) Model

The MSPE for the SLR model for the White Volta at Nawuni was found to be greater than 20% indicating that an additional explanatory variable such as streamflow in a NMR model may improve the model estimation of SSC.

In this study, the applicability of the NMR was initially analyzed by computing the variance inflation factor (VIF) (Equation 3.2.5) for turbidity and streamflow using the R^2 from the regression of turbidity on streamflow. The R^2 was found to be 0.014 resulting in a VIF of 1.00 which is considered ideal for the development of a NMR model. A VIF of 1.00 implies that turbidity and streamflow are not strongly multicollinear and can therefore be used as explanatory variables in the development of a multiple regression model.

The NMR model in base-10 logarithmic space relating turbidity and streamflow to SSC for the White Volta is given by:

$$\log SSC = -1.73 + 1.49\log T - 0.25\log Q_w + 0.42\log Q_w^2 - 0.09\log Q_w^3 \qquad (4.1.3)$$

where *SSC* is the suspended sediment concentration (mg/l), Q_w is streamflow (m^3/s) and *T* is the turbidity (NTU).

The NMR model equation in base-10 logarithmic space shows a linear relationship between turbidity and SSC and a polynomial relationship between the streamflow and SSC as confirmed in the correlation analysis.

The diagnostics statistics used to evaluate the NMR model are presented in Table 4-6. The R^2 value of 0.915 indicates that the NMR model explains 91.5% of the variability in the

SSC. The sum of square errors (SSE) was found to be 1.704 indicating that the model estimated SSC did not significantly depart from the measured mean and hence, it is a very good fit.

Table 4-6: NMR Model diagnostics for the White Volta Basin at Nawuni

No. of Measurements	RMSE	R^2	SSE	*Lower MSPE*	*Upper MSPE*
155	0.135	0.915	1.704	26.66%	36.35%

The upper and lower MSPE for the NMR were found to be 36.35 and 26.66% respectively which are greater than the recommended 20%. This implies that, the additional explanatory variable, the streamflow, may not sufficiently improve the estimation of SSC by the NMR model.

The bias correction factor (*BCF*) was found to be 0.55 and the final retransformed NMR model for the White Volta Basin at Nawuni on the basis of turbidity, streamflow and SSC is given by:

$$SSC = 0.010 Q_w^{0.30} T^{1.42} \qquad (4.1.4)$$

where *SSC* is the suspended-sediment concentration (mg/l), Q_w is the river discharge (m^3/s) and *T* is the turbidity (NTU). The low magnitude of the streamflow exponent (<1) implies that SSC in the White Volta tends to decrease during rising streamflow.

A plot of the NMR model predicted versus the observed SSC in base-10 logarithmic space is presented in Figure 4-11. The figure shows a uniformly distribution points around the one-on-one plot implying that the model did not significant over or underestimated the SSC.

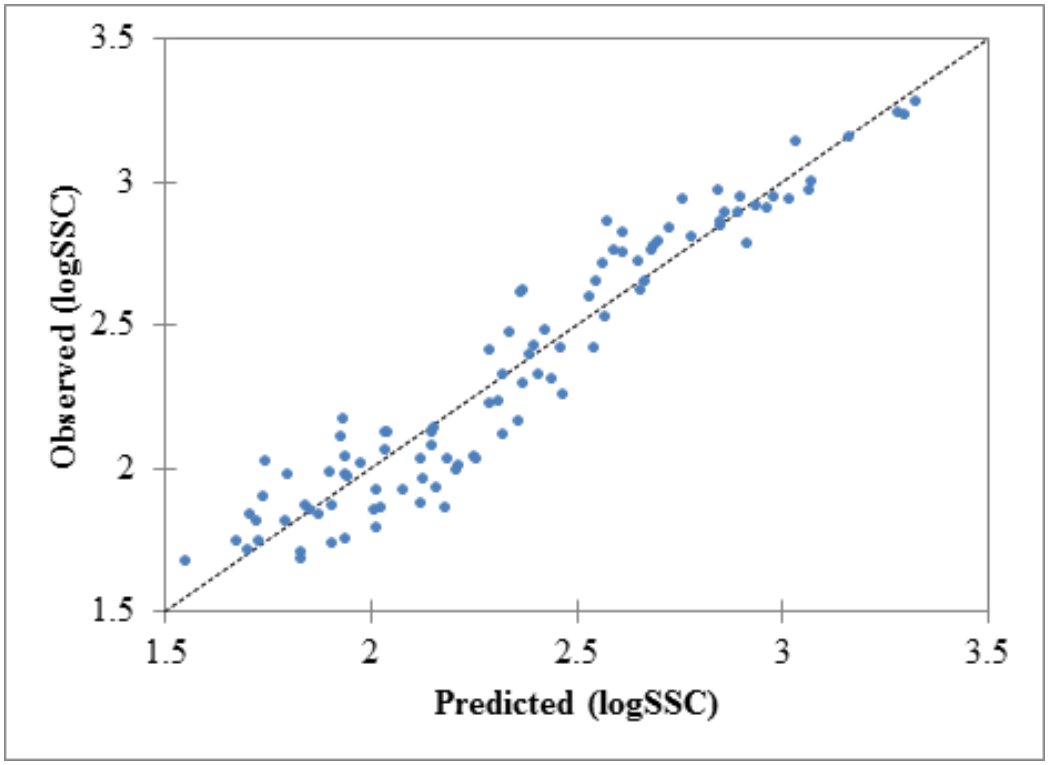

Figure 4-11: Comparison of NMR model predicted versus observed SSC at Nawuni (Sept. 2012-Dec. 2013)

4.2.6 Model Validation

To evaluate the reliability of the derived linear regression models, the models were used to estimate SSC and compared with measured SSC at the Nawuni hydrological gauging station for the period of July 1994-March 1995. The ability of the models to accurately estimate the SSC was then evaluated using model performance statistics such as the R^2, MAE, and NSE. Table 4-7 presents the model performance statistics for the Nawuni station.

Table 4-7: Model Performance Statistics for the SLR and NMR of the White Volta Basin for the validation period (1994-1995)

Model Type	R^2	MAE	NSE
SLR	0.93	3.29	0.93
NMR	0.79	1.65	0.66

The coefficient of determination, R^2 was found to be 0.93 and 0.79 for the SLR and the NMR models respectively. This indicates that the turbidity alone explains the variability of the SSC in the White Volta Basin than a combination of turbidity and streamflow. Figure 4-12 shows a plot of predicted SSC versus observed SSC on a one-on-one plot. For a perfect estimate, the data fitting a function should fall along the 1:1 line, where the model estimates

are equal to the observed. The plot shows that both the SLR and NMR predicted very well the observed SSC at Nawuni during the validation period. The NMR model however tends to overestimate the high SSC in the basin. The model efficiencies and mean absolute errors were also found to be very good with values of 0.93 and 3.29 for the SLR and 0.66 and 1.65 for the NMR respectively.

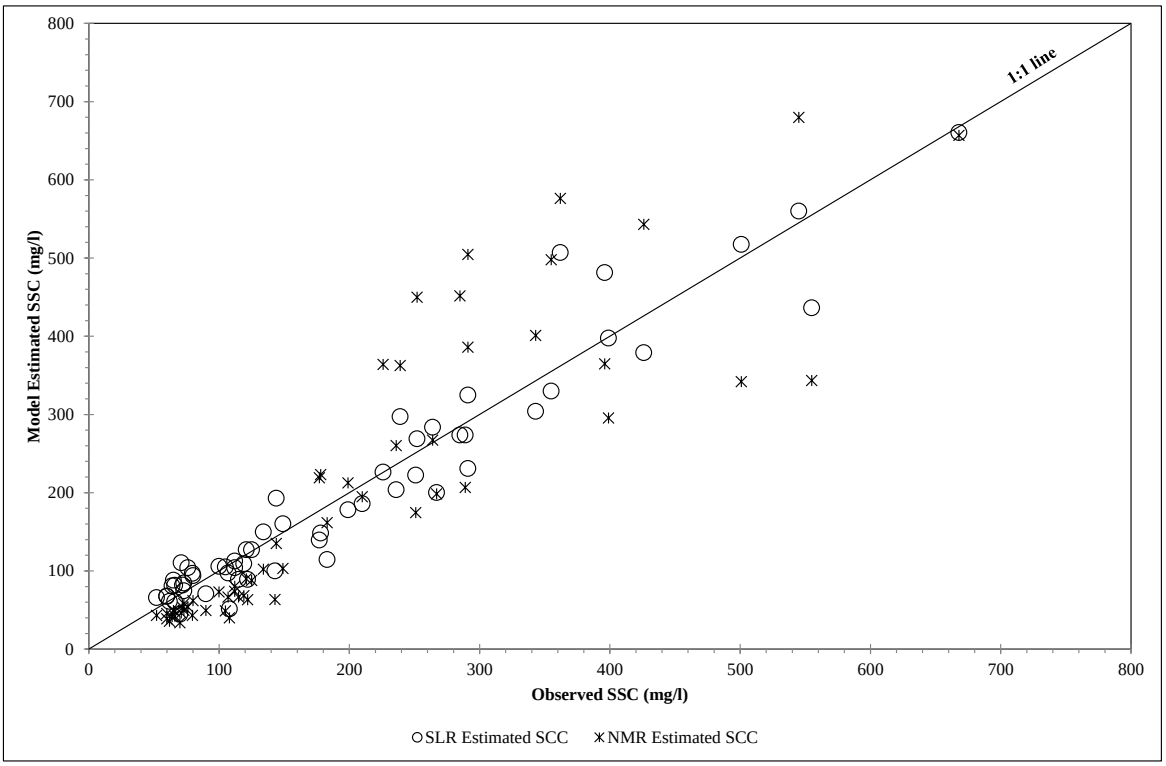

Figure 4-12: Comparison of Observed and Model Estimated SSC (mg/l) for the White Volta at Nawuni

Overall, the performance statistics indicates that the SLR model can be considered the better option for estimating long-term time series of SSC for the White Volta Basin. The addition of streamflow as an explanatory variable in the MLR did not improve the estimation of the SSC and this is reflected in the magnitude of the streamflow exponent.

Based on the above results, it is evident that monitoring turbidity in conjunction with limited sediment sampling will provide a reasonable surrogate method for estimating SSC on a daily or sub-daily time scale. The derived SLR model was subsequently used to estimate long-term time series of sediment loads in the White Volta Basin.

4.2.7 Estimation of Suspended Sediment Load (SSL) for the White Volta Basin

The SLR model was used to estimate SSC based on long-term turbidity data obtained from the Ghana Water Company Ltd. Long-term sediment loads were subsequently computed using Equation 3.1.1 (Horowitz, 2003). With Equation 3.1.1, the daily sediment loads of the White Volta Basin at the Nawuni hydrological station was computed based on the estimated SSC and streamflow. Monthly and annual sediment loads were also computed and used in the calibration and validation of the Soil and Water Assessment Tool (SWAT). A plot of the long-term monthly computed SL is presented in Figure 4-13.

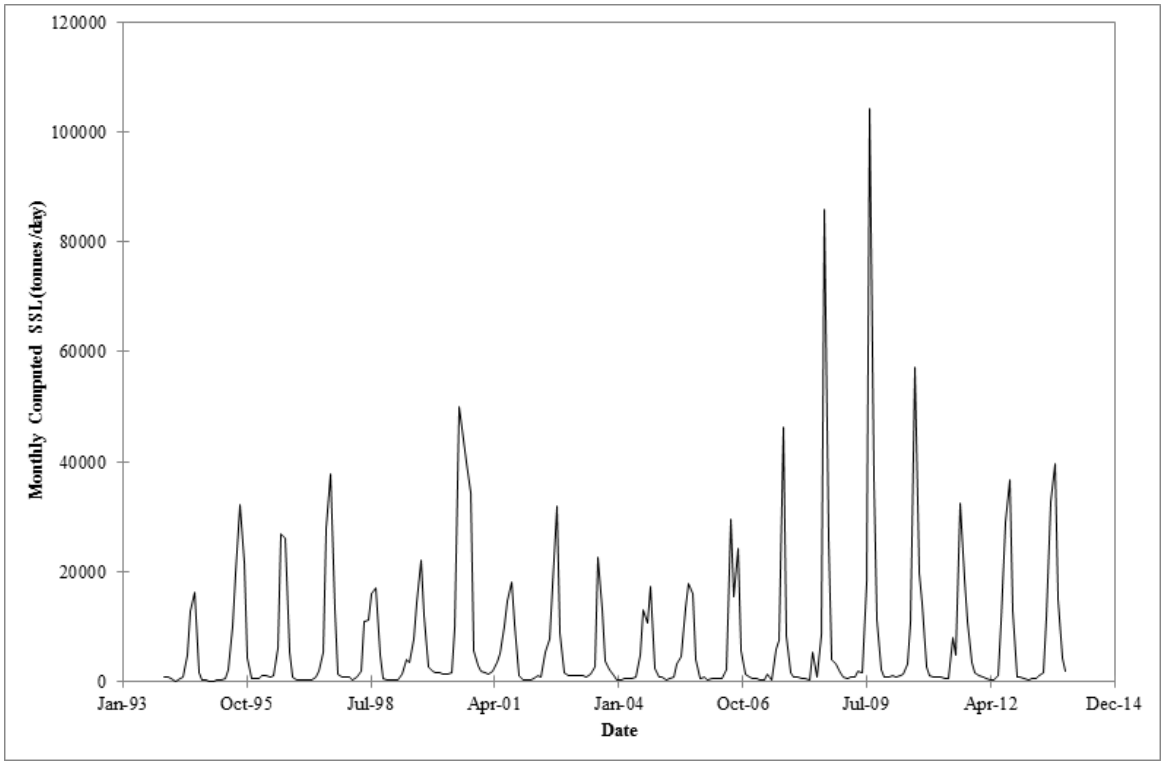

Figure 4-13: Long term monthly computed SSL (tonnes/day) for the White Volta Basin at Nawuni (1994-2013).

4.3 Conclusion

Generally, the results obtained in this chapter shows that, underestimation of suspended-sediment concentration resulting from the use of the surface dip sampling technique in the White Volta Basin can be corrected by applying a correction factor of 34%.

Continuous turbidity data collected by GWCL as part of their water quality assessment requirement was calibrated with measured SSC data and used to estimate long-term time-series of suspended sediment loads for the White Volta Basin at Nawuni using

regression models. A simple linear regression, SLR model relating turbidity and the measured SSC data was found to be the best fitted model.

The mean annual suspended sediment load for the White Volta Basin at Nawuni was estimated to be 5.68x106 metric tonnes per annum. Although the estimated sediment loads for the White Volta Basin can be considered to be relatively low compared with other rivers, the results provide a valuable basis for assessing the potential impact of climate change on sediment transport in the White Volta using the Soil and Water Assessement Tool (SWAT) coupled with Regional Climate Models (RCMs).

Chapter 5

5 CALIBRATION, UNCERTAINTY ANALYSIS AND VALIDATION OF SWAT

5.1 Introduction

This chapter presents the results of the application of the Soil and Water Assessment Tool (SWAT) model to simulate the hydrology and sediment loads of the White Volta Basin. The chapter also presents the results of the sensitivity analysis, calibration, uncertainty analysis, validation, and performance evaluation of the SWAT model.

5.2 Hydrologic Response Units (HRUs) Analysis

The results of evaluating the HRUs showed that reducing the threshold of 1,500 km^2 to 500 km^2 as the minimum drainage area for delineating the watershed in scenarios 150-A/B to 50-A/B respectively led to no change in the number of rain gauges utilized (Table 5-1). However, the results show an increase in the mean annual areal rainfall from 874.7 mm to 894.4 mm and consequently an increase in the mean annual streamflow from 255.64 mm to 266.12 mm respectively.

Table 5-1: Model performance for different subbasins and HRU scenarios for the White Volta Basin (1991-2013)

Scenario	Subbasin threshold (km^2)	No. of subbasins	No. of HRUs	Land-use/Soil threshold/ Slope	No. of Rain gauges used	Mean Annual Rainfall (mm)	Mean Annual Discharge (mm)	Total Sediment Loading (T/km^2)
150-A	1,500	36	459	15/10	12	874.7	255.64	17.798
150-B	1,500	36	510	10/10	12	874.7	254.43	18.174
100-A	1,000	48	519	15/10	12	875.0	257.77	17.963
100-B	1,000	48	579	10/10	12	875.0	256.76	18.401
50-A	500	114	1032	15/10	12	894.4	264.95	19.319
50-B	500	114	1125	10/10	12	894.4	266.12	19.532
30-A	300	204	1590	15/10	13	886.5	261.83	20.036
30-B	300	204	1767	10/10	13	886.5	261.34	20.051
10-A	100	604	3767	15/10	14	886.2	260.87	19.971
10-B	100	604	4022	10/10	14	886.2	260.64	19.989

The results also show that increasing the number of subbasins from 114 to 204 and 604 in scenarios 50-A/B to 30-A/B and 10-A/B respectively led to the number of rain gauges utilized increasing from 12 to 13 and 14 respectively (see Table 5-1). This however resulted in a decline in the annual rainfall from 894.4 mm to 886.5 mm and 884.2 mm and a corresponding decrease in the annual discharge from 266.12 mm to 261.34 and 260.64 mm respectively. Although increasing the number of subbasins from 114 in scenario 50-B to 604

in scenario 10-B resulted in a corresponding increase in the number of rain gauges from 12 to 14 used in the simulation, there was a decrease in the annual rainfall and discharge suggesting that there is a limit to which an increase in the number of subbasins can influence the model output. That is, the additional two rain gauges in the simulation did not add to the total annual rainfall in the basin and subsequently annual discharge. This implies that the influence of the two additional rain gauges on the model output is insignificant.

The results also indicate that there is a limit to which the number of land-use units could affect streamflow. For instance, increasing the number of HRUs from 459 in scenario 150-A to 510 in scenario 150-B resulted in an increase in the number of land-use types from 6 to 7. This however, resulted in a slight decrease in the mean annual streamflow from 255.64 mm to 254.43 mm. Increasing the number of HRUs from 1032 in scenario 50-A to 1125 in scenario 50-B resulted in an increase in the number of land-use types from 6 to 7. The resultant mean annual streamflow however showed a significant increase from 264.95 mm to 266.12 mm for the same amount of mean annual rainfall of 894.4 mm.

Based on the scenario analysis, scenario 50-B was selected because it provided a better physical characterization of the watershed than scenarios 50-A, 100-A and B, and 150-A and B and less demand on computational resources than 30-A and B and 10-A and B. Selecting scenario 50-B implies that land uses and soil types which forms at least 10% of the sub-catchment area and at least 10% of the area within each selected land use respectively would be included in the definition of each HRU.

5.2.1 **Parameter Sensitivity Analysis**

Having considered the effects of the number of subbasins and HRUs on the model output and model run efficiency, scenario 50-B was selected for the sensitivity analysis. The White Volta SWAT model was subsequently set up by delineating the watershed with a drainage area threshold of 500 km^2. This resulted in 114 subbasins with minimum and maximum catchment areas of 1.81 km^2 and 7796 km^2 respectively. Thereafter, 1125 HRUs were generated by overlaying the subbasins, land-use, soil and slope layers based on a minimum threshold of 10%, 10% and 5% dominant land-use, soil, and slope respectively.

The SWAT model was then setup and executed using the Runoff Curve Number method for simulating the rainfall-runoff processes, the Penman-Monteith method for computing the potential evapotranspiration and the variable-storage method for simulating the channel routing. A period spanning January 1991 to December 2013 was selected for

simulation and sensitivity analysis with the first three years i.e. from 1991 to 1993 considered as the warm-up period.

For the combined model outputs, 32 default parameters were selected and the sensitivity analysis tool executed first without observed data and secondly with monthly observed streamflow and sediment load data. Results of the sensitivity analysis show that the 10 most sensitive parameters and their ranking were the same for the two scenarios. Results of the parameter ranking and the average percentage change in the objective function value are presented in Table 5-2. According to Veith and Ghebremichael (2009), the parameter producing the highest average percentage change in the objective function value is ranked as most sensitive.

In this study, the first 10 most sensitive parameters were selected for each model output and this resulted in 15 parameters overall (Table 5-3). The results in Table 5-3 indicate that the streamflow was sensitive, from most to least, to CN, GWQMN, ESCO, SOL_Z, CH_K2, SOL_AWC, ALPHA_BF, GW_REVAP, REVAPMN and CANMX. On the other hand, the sediment load was sensitive, from most to least, to CH_N2, CH_K2, SPCON, CN2, USLE_P, SOL_Z, SPEXP, ALPHA_BF, SURLAG and ESCO. Based on the selected 10 sensitive parameters criteria, the streamflow and sediment loads were found not to be sensitive to SOL_K (Soil hydraulic conductivity), USLE_C (minimum value of USLE C factor applicable to land cover/plant), CH_COV (channel cover factor), CH_EROD (channel erodibility factor), SOL_ALB (moisture soil albedo), GW_DELAY (Groundwater delay), among others as listed in Table 5-2.

Table 5-2: A listing of the parameter ranking in the SWAT sensitivity analysis

No.	Streamflow			Sediment load		
	Parameter	Rank	Mean	Parameter	Rank	Mean
1	Cn2	1	1.08	Ch_N2	1	5.08
2	Gwqmn	2	0.84	Ch_K2	2	3.17
3	Esco	3	0.80	Spcon	3	2.59
4	Sol_Z	4	0.35	Cn2	4	2.38
5	Ch_K2	5	0.33	Usle_P	5	1.24
6	Sol_Awc	6	0.20	Sol_Z	6	0.60
7	Alpha_Bf	7	0.12	Spexp	7	0.60
8	Gw_Revap	8	0.09	Alpha_Bf	8	0.56
9	Revapmn	9	0.06	Surlag	9	0.55
10	Canmx	10	0.06	Esco	10	0.44
11	Blai	11	0.04	Gwqmn	11	0.40
12	Ch_N2	12	0.04	Slope	12	0.31
13	Epco	13	0.02	Blai	13	0.27
14	Gw_Delay	14	0.02	Sol_Awc	14	0.21
15	Sol_K	15	0.01	Epco	15	0.07
16	Surlag	16	0.00	Gw_Revap	16	0.06
17	Slope	17	0.00	Canmx	17	0.05
18	Biomix	18	0.00	Slsubbsn	18	0.03
19	Slsubbsn	19	0.00	Gw_Delay	19	0.03
20	Sol_Alb	20	0.00	Revapmn	20	0.02
21	Usle_P	21	0.00	Biomix	21	0.01
22	Ch_Cov	33	0.00	Sol_K	22	0.01
23	Ch_Erod	33	0.00	Usle_C	23	0.01
24	Sftmp	33	0.00	Sol_Alb	24	0.00
25	Smfmn	33	0.00	Ch_Cov	33	0.00
26	Smfmx	33	0.00	Ch_Erod	33	0.00
27	Smtmp	33	0.00	Sftmp	33	0.00
28	Spcon	33	0.00	Smfmn	33	0.00
29	Spexp	33	0.00	Smfmx	33	0.00
30	Timp	33	0.00	Smtmp	33	0.00
31	Tlaps	33	0.00	Timp	33	0.00
32	Usle_C	33	0.00	Tlaps	33	0.00

Table 5-3: The 15 sensitive parameters selected for the White Volta Basin SWAT model

Parameter Description	Variable Name	Ranking	
		Flow	Sediments
SCS runoff curve number	Cn2	1	4
Threshold depth of water in the shallow aquifer required for return flow to occur (mm)	Gwqmn	2	11
Soil evaporation compensation factor	Esco	3	10
Depth from soil surface to bottom of layer	Sol_Z	4	6
Effective hydraulic conductivity in main channel alluvium	Ch_K2	5	2
Available water capacity of the soil layer	Sol_Awc	6	14
Baseflow alpha factor (days)	Alpha_Bf	7	8
Groundwater "revap" coefficient	Gw_Revap	8	22
Threshold depth of water in the shallow aquifer for "revap" to occur (mm)	Revapmn	9	20
Maximum canopy storage	Canmx	10	13
Surface runoff lag time	Surlag	16	9
Manning's "n" value for the main channel	Ch_N2	12	1
Linear parameter for calculating the maximum amount of sediment that can be reentrained during channel sediment routing	Spcon	33	3
Exponent parameter for calculating sediment reentrained in channel sediment routing	Spexp	33	7
USLE equation support (USLE practice factor)	Usle_P	21	5

In contrast to other studies in the study area (e.g., Obuobie, 2008), the streamflow was found not to be sensitive to SOL_K and SURLAG. This may be attributed to the fact that the SCS curve number approach does not consider SOL_K in the calculation of surface runoff. The results of the sensitivity analysis however confirm the high sensitivity of the SWAT model to changes in CN2, groundwater parameters such as GWPMNN and SOL_AWC as reported in a previous study (e.g., Obuobie, 2008).

5.2.2 **One-at-a-time Sensitivity Analysis**

The “one-at-a-time sensitivity shows the sensitivity of a variable to the changes in a parameter if all other parameters are kept constant at some value” (Abbaspour *et al*., 2014). The 15 selected model parameters which were changed one-at-a-time following the ranking as presented in Table 5-3 above aided in obtaining reasonable parameter ranges for the semi-automated model calibration.

After executing the SWAT-Cup with three (3) simulation runs and parameter range of -25% to 25% of the initial CN2 values, a plot of the observed flow (the dotted line) and the model output for three values of CN2 within the specified range is presented in Figure 5-1 and 5-2 for the streamflow and sediment loads.

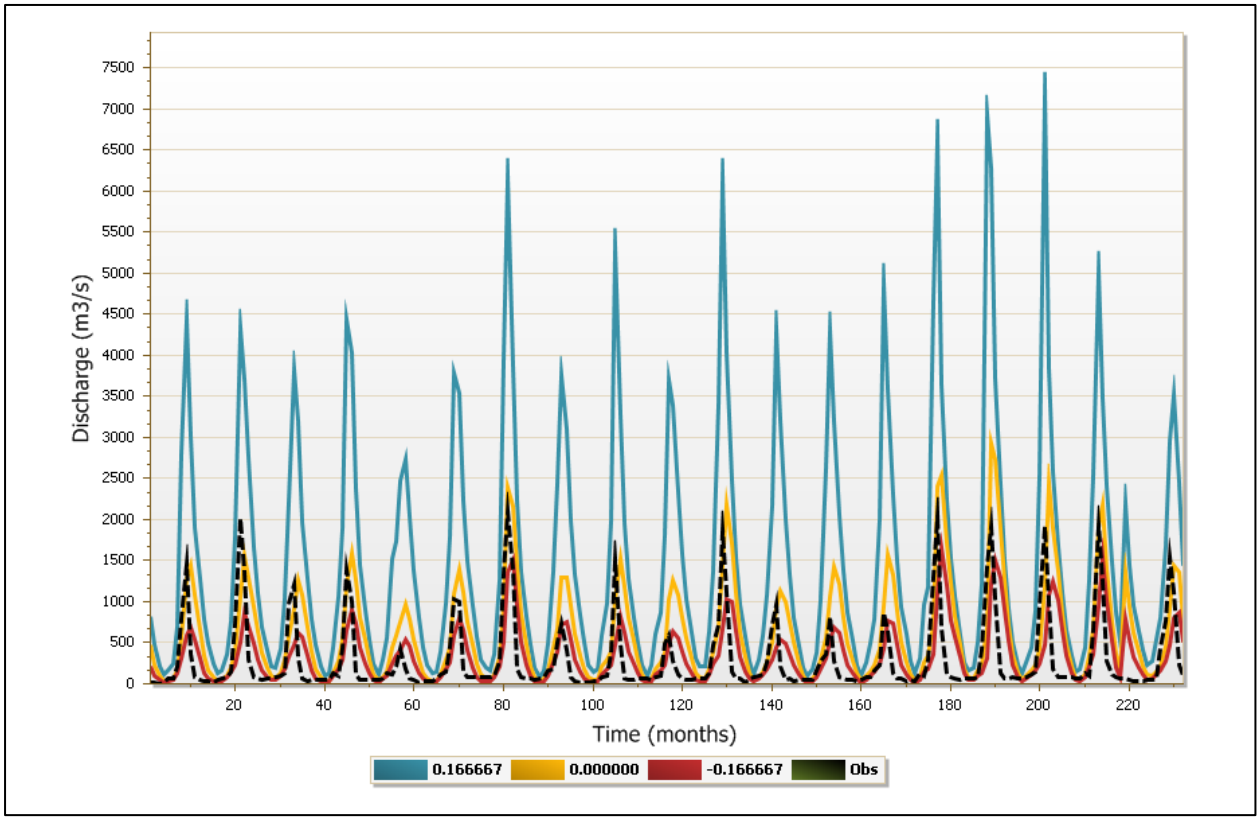

Figure 5-1: Sensitivity of streamflow on CN2 for the White Volta Basin SWAT Model. The dashed line represents the observed streamflow at Nawuni

Clearly, it can be seen in Figure 5-1 that CN2 falls within -16% to 0 of the initial CN2 values. On the other hand, in Figure 5-2, the sensitivity of sediment load to CN2 after the three simulations shows that the simulated sediment loads for the specified range generally has higher peaks than that of the observed sediment load. The specified range of CN2 will therefore require further reduction to adequately simulate the sediment load. It is however important to recognize from Table 5-3 above that CN2 was found to be the fourth ranked sensitive parameter to the sediment load. Adjusting the range of CN2 in this case may not necessarily result in achieving the desired changes in the sediment load but may affect the streamflow simulation.

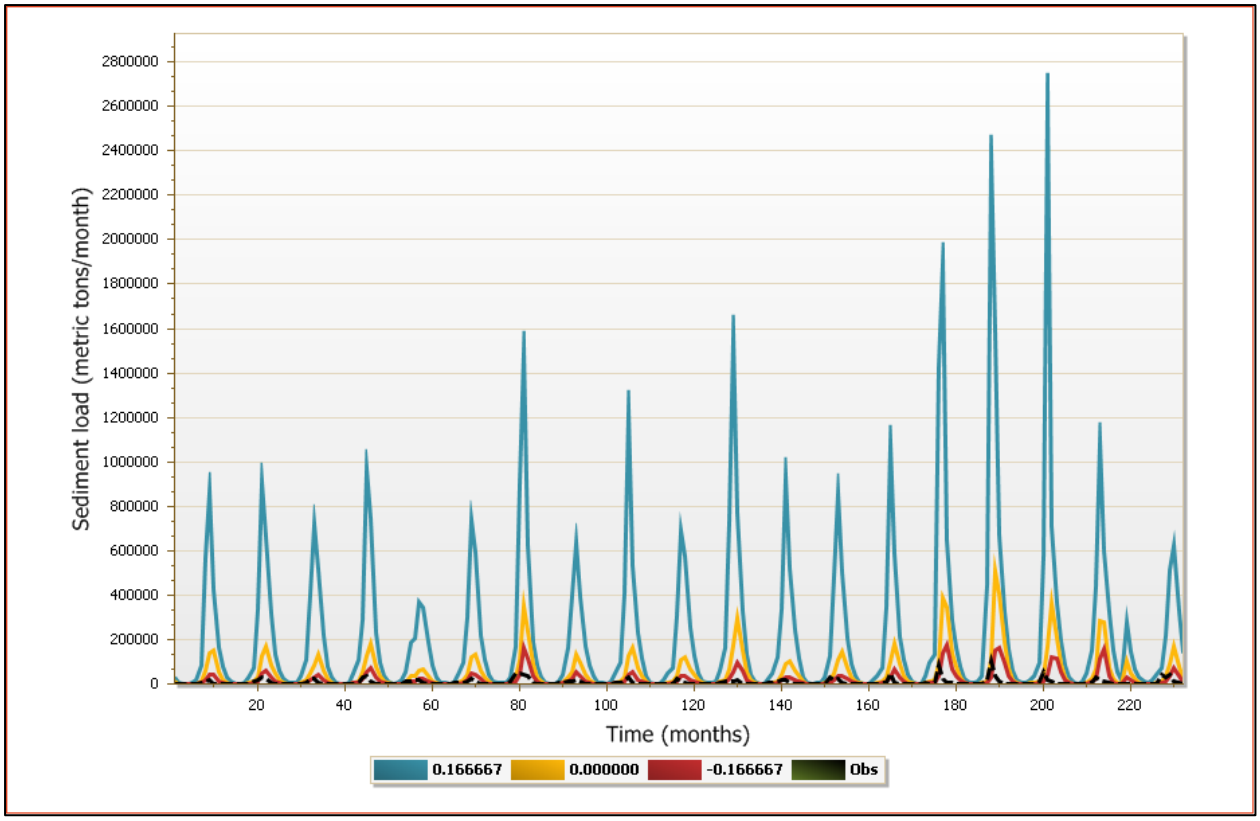

Figure 5-2: Sensitivity of sediment load on CN2 for the White Volta Basin SWAT Model. The dash line represents the observed sediment loads at Nawuni.

Figure 5-3 present the plot of the observed streamflow (the dotted line) and the simulated streamflows for three simulations with CH_N2 values within a range of -0.01 to 0.3. In this case too, all other model parameters were held constant except the CH_N2 which was varied within the specified range. It can be observed in Figure 5-3 that the sensitivity of the streamflow to changes of CH_N2 resulted in the model underestimating the peak streamflows for the specified parameter range of CH_N2. This implies that the range of CH_N2 values will have to be increased to increase the simulated peak flows. From Table 5-3 above, it is however noted that CH_N2 was not sensitive to the streamflows according to the parameter selection criteria used. Adjusting the range of CH_N2 in this case may not necessarily result in achieving the desired changes in the streamflow.

From Figure 5-4 on the other hand, the sensitivity of sediment load to CH_N2 after the three simulations shows that the simulated sediment loads for the specified range is generally within 0.145 and 0.248. This implies that decreasing the range of CH_N2 below 0.145 will result in overestimation of the high peaks for the sediment load.

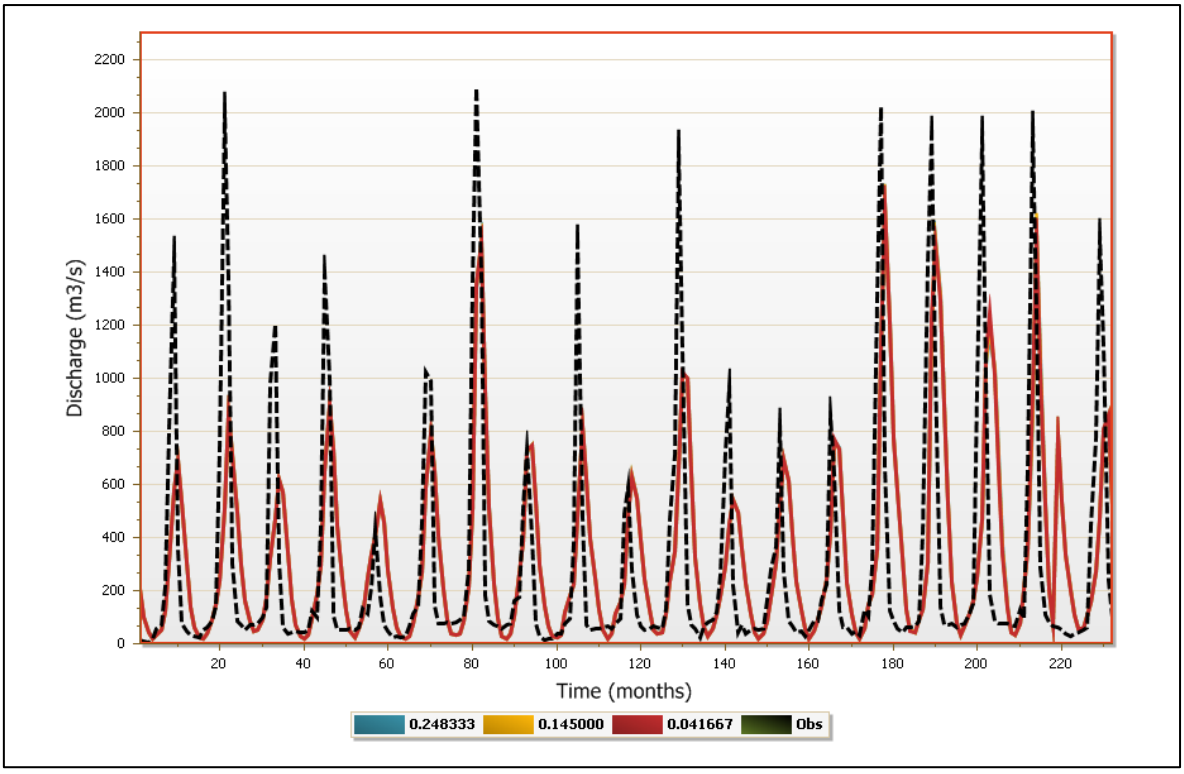

Figure 5-3: Sensitivity of streamflow on CH_N2 for the White Volta Basin SWAT Model. The dash line represents the observed streamflow at Nawuni.

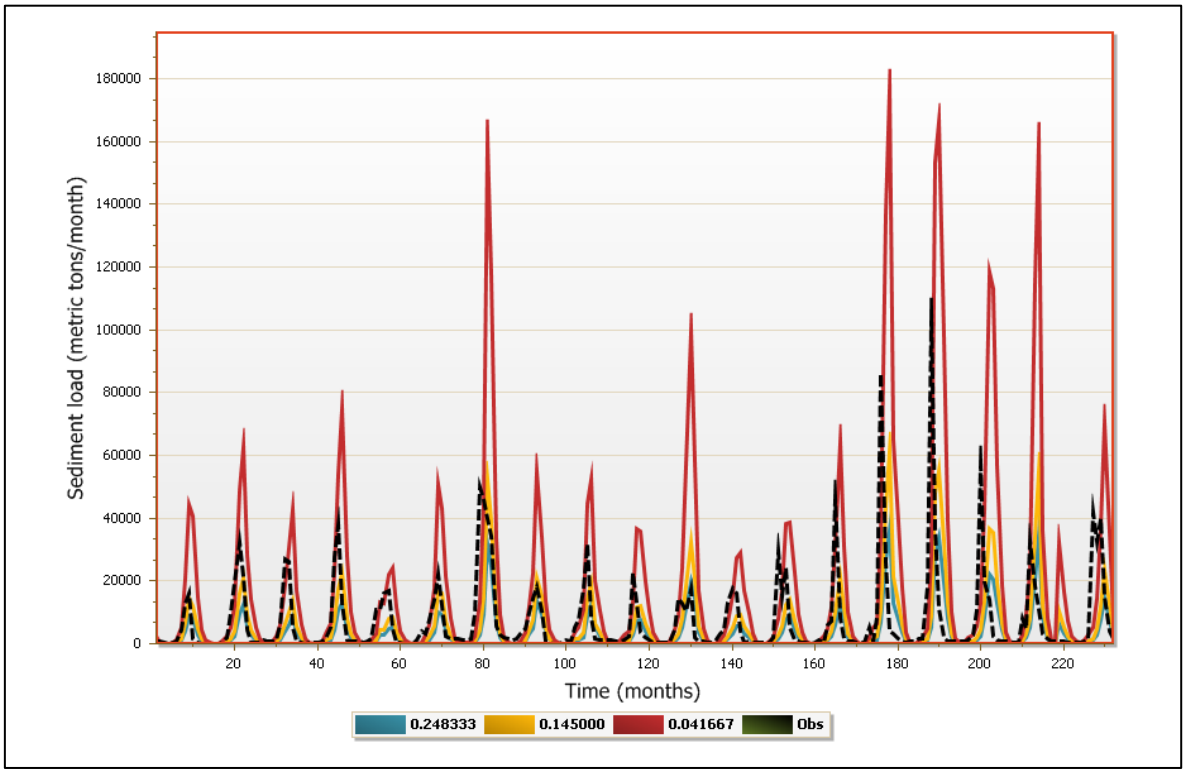

Figure 5-4: Sensitivity of sediment load on CH_N2 for the White Volta Basin SWAT Model. The dash line represents the observed sediment loads at Nawuni.

5.3 Model Calibration and Uncertainty Analysis

After setting up the White Volta SWAT model and analyzing the sensitivities of the streamflow and sediment loads to the model parameters, the model was then calibrated at Nawuni for a ten year period spanning from 1994 to 2003. A three year period, 1991-1992 was used for warming the model. The calibration was done by applying SUFI2 in SWAT-CUP to the White Volta Basin outlet at Nawuni. The calibration was based on annual, monthly and daily observed stream discharge and sediment loads at the watershed outlet at Nawuni.

The model calibration was performed following the procedure outlined in Figure 3-12 and 3-13, Section 3.3.5.3. The model was first run with 500 simulations and the goodness-of-fit of the simulated model outputs and the observed measured compared by visual inspection in the 95ppu plots. The efficiency of the model was further analyzed with five performance evaluation coefficients in the *summary_stat.txt* file in SWAT-CUP. These coefficients includes; coefficient of determination (R^2), Nash–Sutcliffe (NS) coefficient of efficiency and Percent Bias, PBIAS. The other measure of the goodness of calibration is the *P-factor* (percent data bracketed) and the *R-factor* (a measure of the thickness of the 95PPU band). The *R-factor* quantifies the thickness of the 95PPU (Equation 5.28) and the smaller this number, the smaller the uncertainties and the better the calibration. A desirable value for the *R-factor* is 1 with a *P-factor* also close to 1 (Abbaspour, *et al.*, 2007).

The hydrology component of the model was calibrated with total streamflow (m^3/s) as a composition of surface runoff, baseflow and lateral flow measured as daily discharged at the watershed outlet at Nawuni. The sediment component of the model was also calibrated as sediment loadings (metric tons/day) of the HRUs that reach the channel outlet at Nawuni as suspended sediment. In-stream sediment deposition and bank erosion were not considered due to insufficient knowledge about these processes in the White Volta Basin. Thus, the dynamic geomorphology of the natural river beds in the catchment was not addressed. Table 5.4 summarizes the final calibrated parameters for the White Volta SWAT model.

Table 5-4: White Volta SWAT model parameters included in the final calibration and their initial and final ranges

Parameter Description	Parameter Name	Method	Initial Parameter Range	Final Parameter Range
SCS runoff curve number	CN2	Relative	-0.25 - 0.25	0.12 - 0.38[a]
Available soil water capacity	SOL_AWC	Relative	0 - 1	0.18 - 0.60[a]
Manning's "n" value for the main channel	CH_N2	Replace	-0.01 - 0.3	0.084 - 0.088
Threshold depth of water in the shallow aquifer for "revap" to occur (mm)	REVAPMN	Replace	0 - 500	1.97 - 8.95
Effective hydraulic conductivity in main channel alluvium	CH_K2	Replace	0 - 500	134.04 - 231.21
USLE equation support (USLE practice factor)	USLE_P	Relative	0 - 1	0.07 - 0.27
Surface runoff lag time	SURLAG	Relative	0 - 24	7.66 - 13.91
Baseflow alpha factor (days)	ALPHA_BF	Replace	0 - 1	0.19 - 0.76
Depth from soil surface to bottom of layer	SOL_Z	Relative	0 - 3000	187.17 - 592.33
Linear parameter for calculating the maximum amount of sediment that can be reentrained during channel sediment routing	SPCON	Relative	0.0001- 0.01	0.0014 - 0.0018
Soil evaporation compensation factor	ESCO	Absolute	0 - 1	0.04 - 0.16
Threshold depth of water in the shallow aquifer required for return flow to occur (mm)	GWQMN	Replace	0 - 500	7.41 - 18.98
Exponent parameter for calculating sediment reentrained in channel sediment routing	SPEXP	Relative	1 - 1.5	1.073 - 1.093
Maximum canopy storage	CANMX	Absolute	0 - 100	0 - 20
Groundwater "revap" coefficient	GW_REVAP	Replace	0.02 - 0.2	0 - 0.038

[a] Ranges vary depending on the hydrologic soil group within one land use or soil type.

Annual calibration of the model was performed by analyzing the mean annual streamflow (m^3/s), water yield (mm) and sediment loadings (metric tons/yr) for the period

1994-2003. Results of the model calibration show good agreement between simulated and observed mean annual water yield, streamflow and sediment loadings. Table 5-5 presents the statistics and the indicators of the goodness of fit for the annual water yield, streamflow and sediment loadings. Figures 5-5, 5-6 and 5-7 present a comparison plot between the simulated and observed mean annual water yield, streamflow and sediment loadings respectively. In Figure 5-5, it can be seen that the model overestimated the mean annual water yield in eight out of the calibrated ten year period and underestimated in the other two years. The difference between the simulated and observed mean annual water yield was found to be -17% which is very high. This is due to the fact that the mean annual water yield was not a target variable during the calibration process. The coefficient of determination (R^2), Nash-Sutcliffe model efficiency (NSE) and the index of agreement (IA) were found to be 0.87, 0.47, and 0.87 respectively for the mean annual water yield indicating a satisfactory agreement between the observed and simulated variables.

Table 5-5: Annual Statistics and goodness-of-fit analysis at Doboya (1994-2003)

Variable Name	Mean Annual		Standard Deviation		Performance Indicators		
	Observed	Simulated	Observed	Simulated	R^2	NSE	IA
Water Yield (mm)	78.87	76.97	27.08	22.51	0.87	0.47	0.87
Streamflow (m^3/s)	250.48	244.42	40.08	49.27	0.87	0.80	0.93
Sediment loadings ($x10^3$ metric tons/day)	17.18	15.56	9.06	8.66	0.78	0.67	0.88

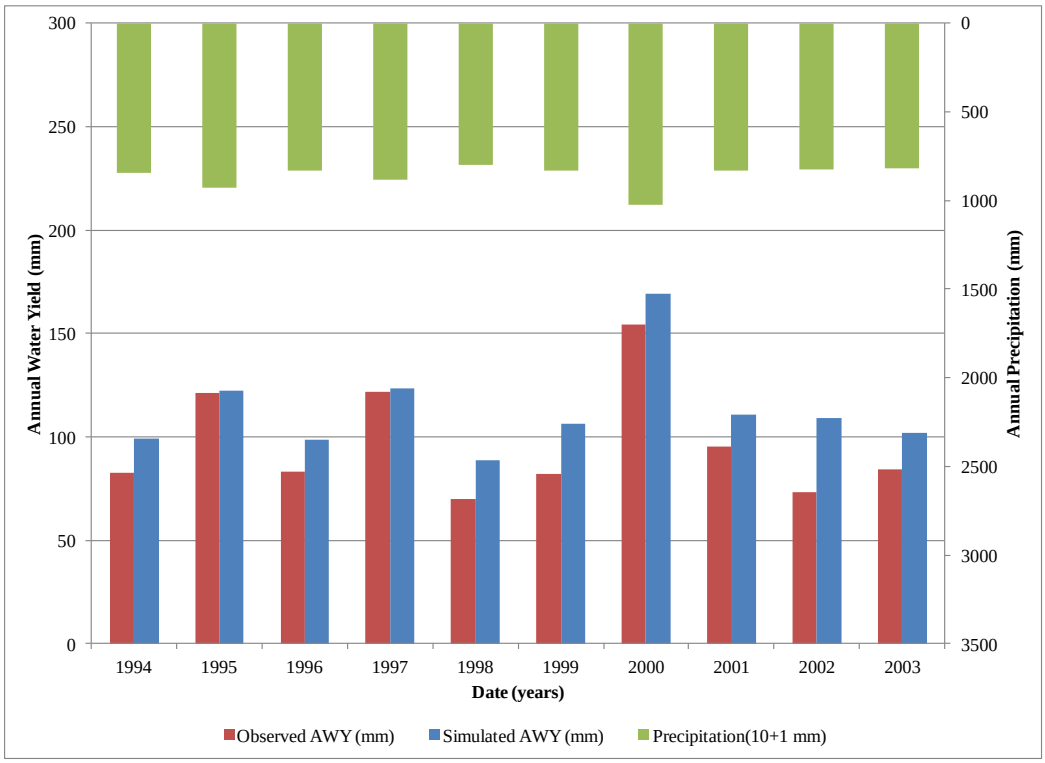

Figure 5-5: Comparison of observed and simulated annual water yield at Nawuni

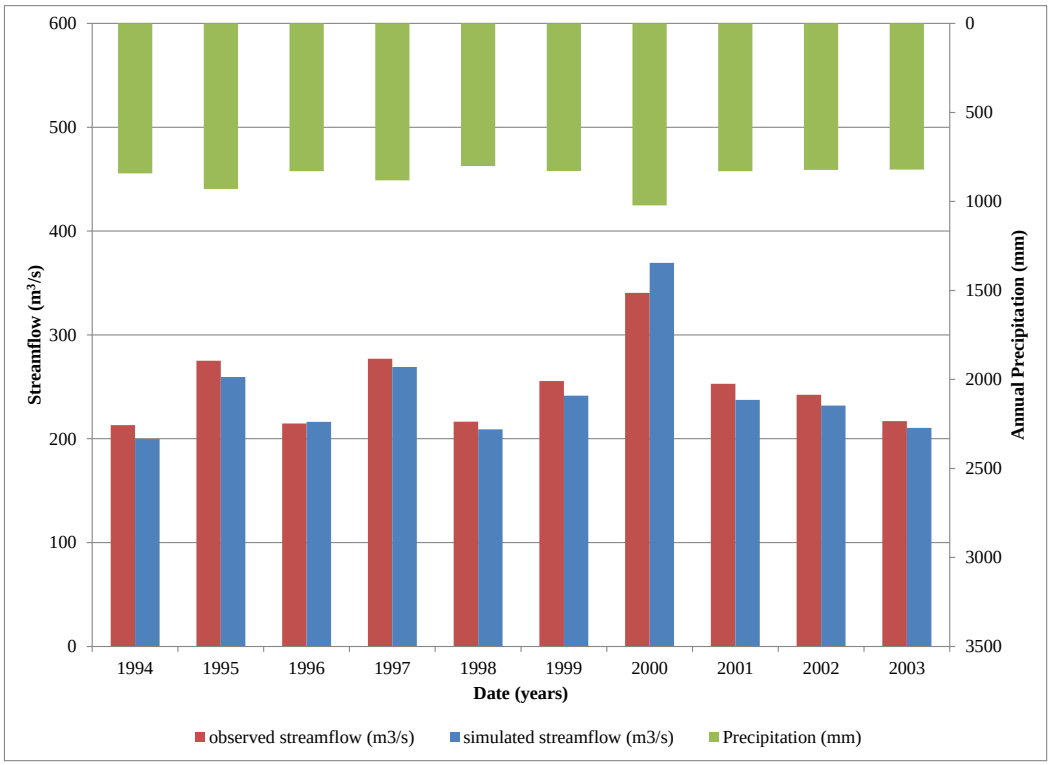

Figure 5-6: Comparison of observed and simulated annual streamflow at Nawuni

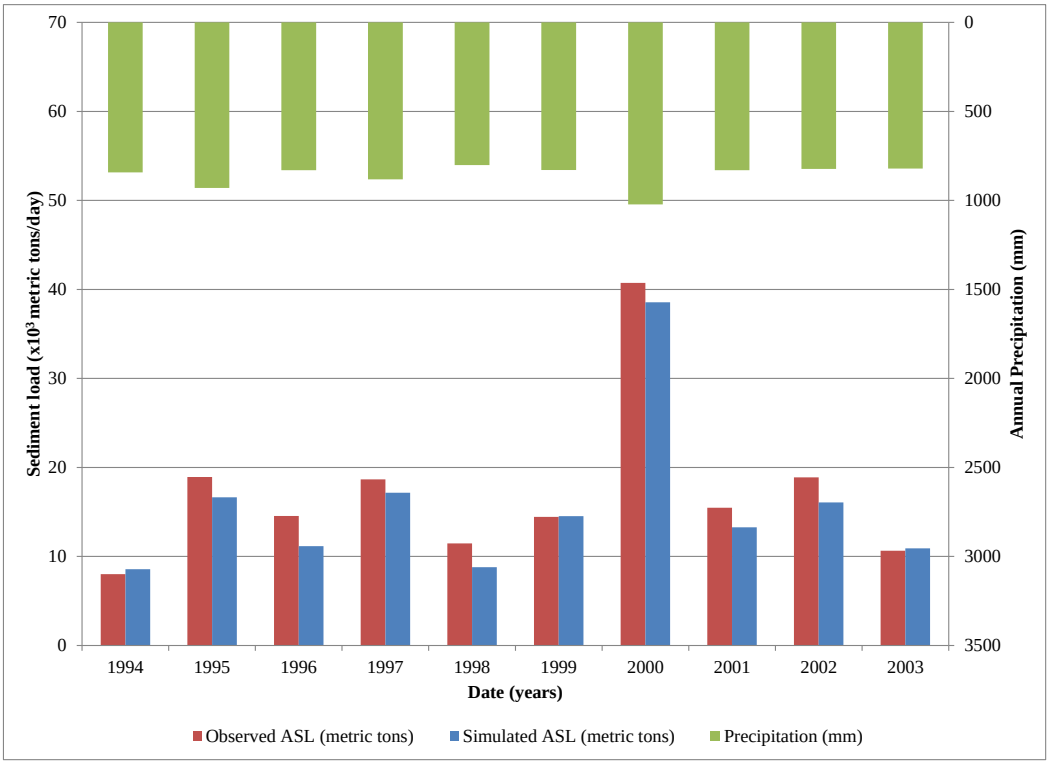

Figure 5-7: Comparison of observed and simulated annual sediment loads at Nawuni

In Figure 5-6, the model overestimated the mean annual streamflow in one, i.e. 2000, out of the calibrated ten year period and generally underestimated in the remaining years. The difference between the simulated and observed mean annual streamflow was found to be -0.2 % which is under 1% indicating a much focus calibration of the hydrology component of the model. The coefficient of determination (R^2), Nash-Sutcliffe model efficiency (NSE) and the index of agreement (IA) were found to be 0.87, 0.80, and 0.93 respectively indicating a very good agreement between the observed and simulated annual streamflows.

In Figure 5-7, the model generally underestimated the mean annual sediment loads in seven out of the calibrated ten year period and slightly overestimated in two of the calibrated years. The difference between the simulated and observed mean annual sediment loads was found to be 11%. The coefficient of determination (R^2), Nash-Sutcliffe model efficiency (NSE) and the index of agreement (IA) were found to be 0.78, 0.67, and 0.88 respectively showing a good agreement between the simulated and observed mean annual sediments loads at Nawuni.

With exceptions in years 2000 and 2001 in Figure 5-7, Figures 5-5 through to 5-7 generally indicates a linear relationship between the annual areal mean precipitation in the basin and the mean annual water yield, streamflow and sediment loads. From Figure 5-7, the difference between the observed and simulated sediment loads for years 2000 and 2001 is

23% and 45% respectively. This can be attributed to the fact that years 2000 and 2001 recorded the highest rainfall in the basin for the calibration period and could impact heavily on the turbidity measurements which is used to derive the suspended sediment loads.

Similarly, just as outlined in Section 3.3.5.3, the model was also calibrated at monthly and daily time scales for the streamflows and sediment loads. To achieve the best model efficiency between the observed and simulated streamflows and sediment loads, the SUFI2 in SWAT-CUP was run with the Nash-Sutcliffe objective function for several iterations consisting of 500 simulations each till the best parameter ranges were obtained. The goodness-of-fit and efficiency of the simulations were analyzed by using a combination of five performance evaluation coefficients in SWAT-CUP, i.e. R^2, NSE, PBIAS, bR^2, *P-factor* and *R-factor*. These five performance evaluation indicators were analyzed for the monthly and daily time steps. The results of the simulations are presented in Figure 5-8 and 5-9 and Figure 5-10 and 5-11 for visual comparison for the monthly and daily time step respectively. Table 5-6 and 5-7 summarized the model evaluation statistics for monthly and daily time step respectively.

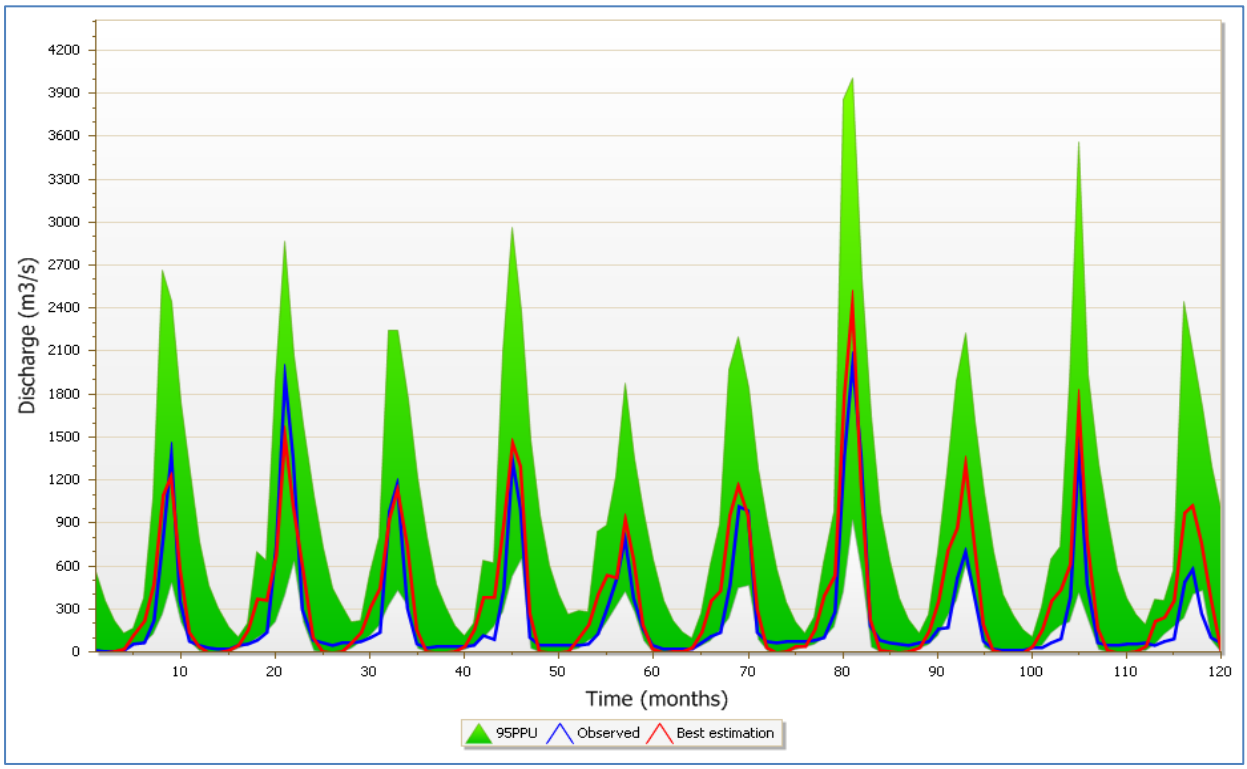

Figure 5-8: 95PPU (shaded green) derived by SUFI-2 with NS objective function for the monthly streamflow during the calibration period (1994-2003).

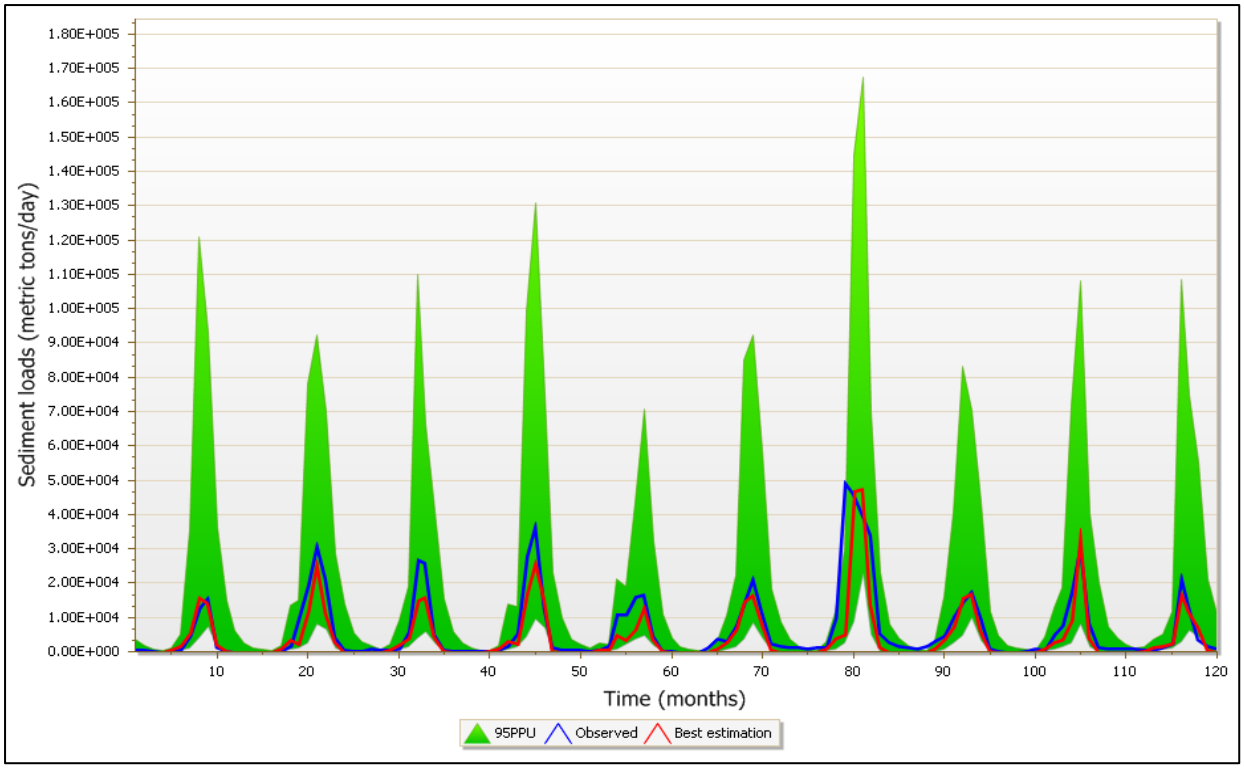

Figure 5-9: 95PPU (shaded green) derived by SUFI-2 with NS objective function for the monthly sediment loads during the calibration period (1994-2003).

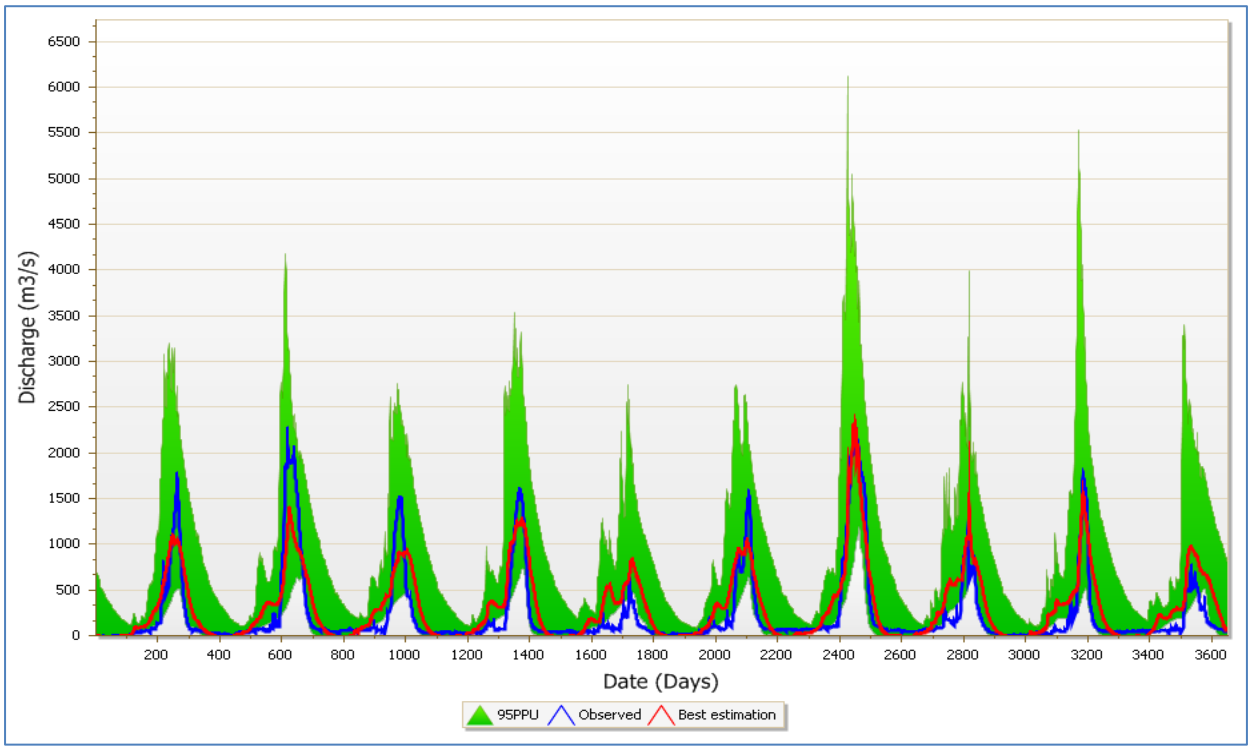

Figure 5-10: 95PPU (shaded green) derived by SUFI-2 with NS objective function for the daily streamflow during the calibration period (1994-2003).

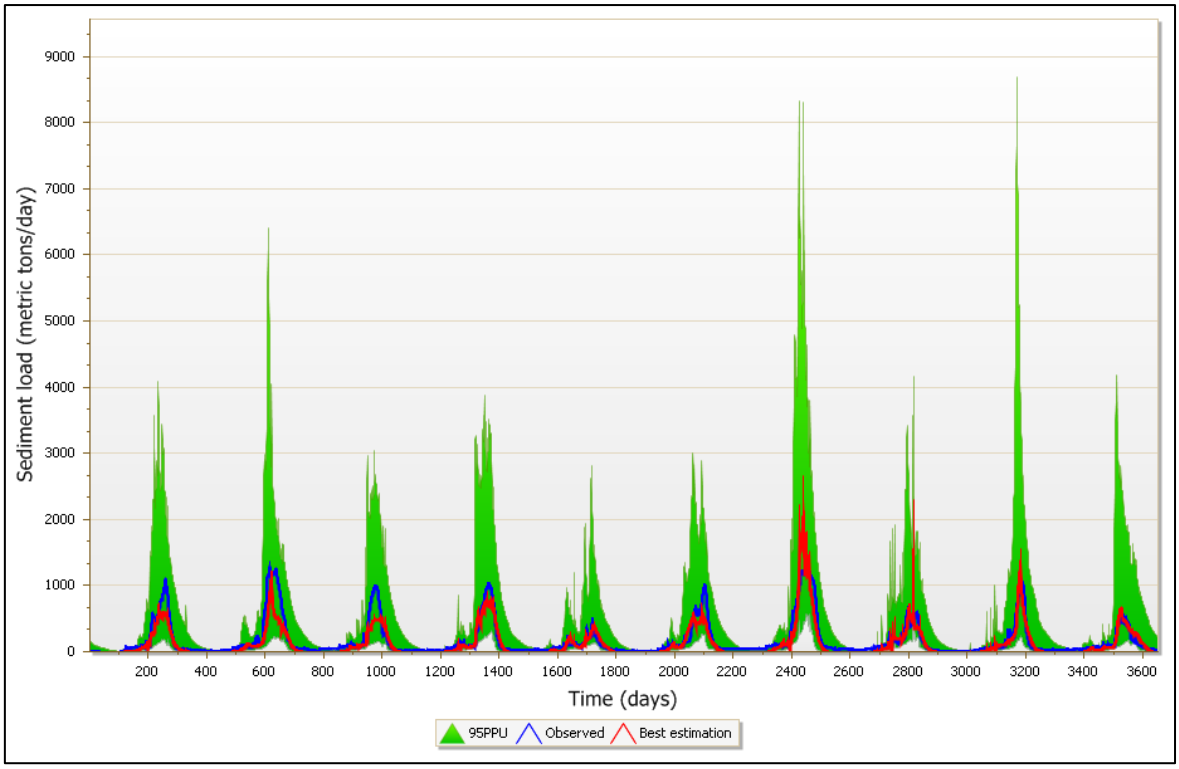

Figure 5-11: 95PPU (shaded green) derived by SUFI-2 with NS objective function for the daily sediment loads during the calibration period (1994-2003).

Table 5-6: Model performance evaluation statistics for monthly streamflow and sediment load calibration at Nawuni (1994-2003).

Goal type= Nash-Sutcliff No. of simulations=500 Best simulation no.=159 Best goal= 0.78						
Variable	P-factor	R-factor	R^2	NSE	bR^2	PBIAS
Streamflow	0.90	1.44	0.83	0.82	0.6852	-13.6
Sediment Load	0.80	1.03	0.75	0.74	0.6028	17.2

Table 5-7: Model performance evaluation statistics for daily streamflow and sediment load calibration at Nawuni (1994-2003).

Goal type=Nash-Sutcliff No. of simulations=500 Best simulation no.=276 Best goal= 0.76						
Variable	P-factor	R-factor	R^2	NSE	bR^2	PBIAS
Streamflow	0.84	1.35	0.78	0.76	0.6118	-25.3
Sediment Load	0.72	1.16	0.80	0.77	0.6713	23.1

The result for the monthly streamflow and sediment load calibration with the Nash-Sutcliffe coefficient of efficiency as the objective function with a behavioral threshold set at 1% in SUFI-2 is presented in Figure 5-8 and 5-9 respectively and the performance evaluation

statistics summarized in Table 5-6. The green shaded area in Figure 5-8 and 5-9 represents the model uncertainty whereas the blue and red lines represent the observed and simulated monthly time series respectively. From Table 5-6, 90% of the observed streamflow data was found to be bracketed by the 95PPU (*P-factor*) with an *R-factor* value of 1.44, which is an excellent result considering the recommended values of 100% and 1 for the P-factor and R-factor respectively (Abbaspour, *et al.*, 2007). Similarly, the performance evaluation statistics of 0.78, 0.82 and -13.6% for the R^2, NSE and PBIAS in Table 5-6 can be classified as good according to the general performance ratings recommended statistics for monthly time step by Moriasi *et al*. (2007). In Figure 5-8, it can be seen that the model underestimated the peak flows for the first two years, that is, prior to the introduction of the Bagre Dam in 1995 and estimated very well the peak flows for the next four years. The model then underestimated the peak flows for the remaining four years, i.e between 2000 and 2003. The model however, generally underestimated the low flows. In addition, the streamflow calibration results displayed a -13% difference between the observed and simulated average monthly flows.

Similar to the monthly streamflow, the observed monthly sediment load in Figure 5-9 and Table 5-6 was found to be 80% bracketed by the 95PPU (P-factor) with an R-factor of 1.03, which are very close to the suggested values of 100% and 1 respectively. The model performance can therefore be considered as excellent according to Abbaspour, *et al.*, (2007). The performance evaluation statistics for the monthly sediment calibration display Nash–Sutcliffe (NSE) efficiency and PBIAS of 0.74 and 17.2% respectively which are classified as good for sediment loads according to the general performance ratings recommended statistics for monthly time step by Moriasi *et al.* (2007). Additionally, the sediment calibration results displayed a 17% difference between the observed and simulated average monthly load. In Figure 5-9, it can be observed that the model performance in estimating the peak sediment loads for the first two years was satisfactory, that is, prior to the introduction of the Bagre Dam in 1995 and thereafter the model underestimated the peak sediment loads for the remaining years except in 1996 and 1997. The model however, generally estimated the low sediment loads satisfactorily.

The results of the daily calibration for streamflow and sediment loads are presented in Figure 5-10 and 5-11 respectively. The green shaded areas represent the model uncertainty whereas the blue and red lines represent the observed and simulated monthly streamflow. The statistics of the performance evaluation for the daily calibration is summarized in Table 5-7.

From Table 5-7, with the graphical presentation in Figure 5-10, 83% of the observed daily streamflow data was found to be bracketed by the 95PPU (P-factor) with an R-factor

value of 1.94, which can be classified as very good according to Abbaspour, *et al.*, (2007). The goodness of fit indicators also shows good agreement between the simulated and observed daily streamflow at Nawuni with the R^2, NSE, bR^2 and PBIAS found to be 0.78, 0.76, 0.61 and -25.3 respectively. In Figure 5-10, it can be observed that the model performance in estimating the peak streamflows for five out of the ten year calibration period was satisfactory. The model however, performed poorly in estimating the peak flows in the other five years but generally performed satisfactorily in estimating the low daily streamflows.

Figure 5-11 presents the results of the daily calibration of sediment loads. From Table 5-7 and Figure 5-11, about 81% of the observed daily sediment loads data was found to be bracketed by the 95PPU (P-factor) with an R-factor value of 2.26, which can be classified as a satisfactory result. The goodness of fit indicators also shows satisfactory agreement between the simulated and observed daily sediment loads at Nawuni with the R^2, NSE and bR^2 and PBIAS found to be 0.80, 0.77, 0.67 and 23.1 respectively. In Figure 5-11, it can be seen that the model generally underestimated the daily sediment loads except in the years 2000 and 2001 where the model overestimated the peaks. The model however estimated satisfactorily the low sediment loads.

Although the statistical evaluation of the model performance showed a satisfactory simulation for the calibration period for both the streamflow and sediment loads, the model tended to underestimate the peak flow in the wet years. This could be partly because the curve number, which is the most sensitive parameter, was unable to generate accurate runoff prediction for a day that experience several storms within the catchment. When several storms occur during a single day, the soil moisture level and the corresponding runoff curve number vary from storm to storm (Kim and Lee, 2008). However, SCS-CN methods define a rainfall event as the sum of all rainfall that occurs during one day, and this might lead to underestimation of runoff (Choi et al., 2002).

The obtained results showed that the observed and simulated streamflow and sediment loads for the annual, monthly and daily time-series were not significantly different at the 95% level of confidence (95PPU) for the iteration with the Nash–Sutcliffe (NSE) coefficient of efficiency objective function. Model validation was therefore undertaken in SWAT-CUP based on the iteration with the NSE objective function with behavioral threshold at 0.01 for the period 2004-2013.

5.4 Validating the White Volta SWAT Model

Model validation refers to a process of re-running a calibrated model for a different time period or location using a different set of input data but maintaining the calibrated parameter values. The purpose of validating the model was to establish whether the model has the ability to predict the observed monthly streamflow and sediment loads at Nawuni for a different time period.

The monthly and daily streamflow and sediment loads time-series data from 2004 to 2013 were used to perform temporal validation of the model at Nawuni. Additionally, data collected during this study between September 2012 and December 2013 for Nasia and Pwalugu within the White Volta Basin were also used for spatial validation of the model. As with the calibration, the five above-mentioned goodness-of-fit measures were calculated for the model performance and efficiency at Nawuni for the selected validation period and the time-series plots also inspected. For the spatial validation, the coefficient of determination (R^2), the Nash–Sutcliffe (NSE) coefficient of efficiency and the index of agreement (IA) were used to evaluate the model performance.

The validated model predictive performance for the White Volta Basin at Nawuni for the period 2004-2013 is summarized in Table 5-8 and the time series plot of measured and best simulated monthly and daily streamflow and sediment loads presented in Figure 5-12 through 5-15. As can be observed in Table 5-8, the model predictive efficiencies were generally above 50% for all the performance evaluation coefficients indicating a good agreement between the observed and simulated time-series data for the validation period at Nawuni. The R-factor (thickness of the 95PPU band) was rather found to depart significantly from the desired value of 1 for the daily validation indicating a high model uncertainty for the validation period.

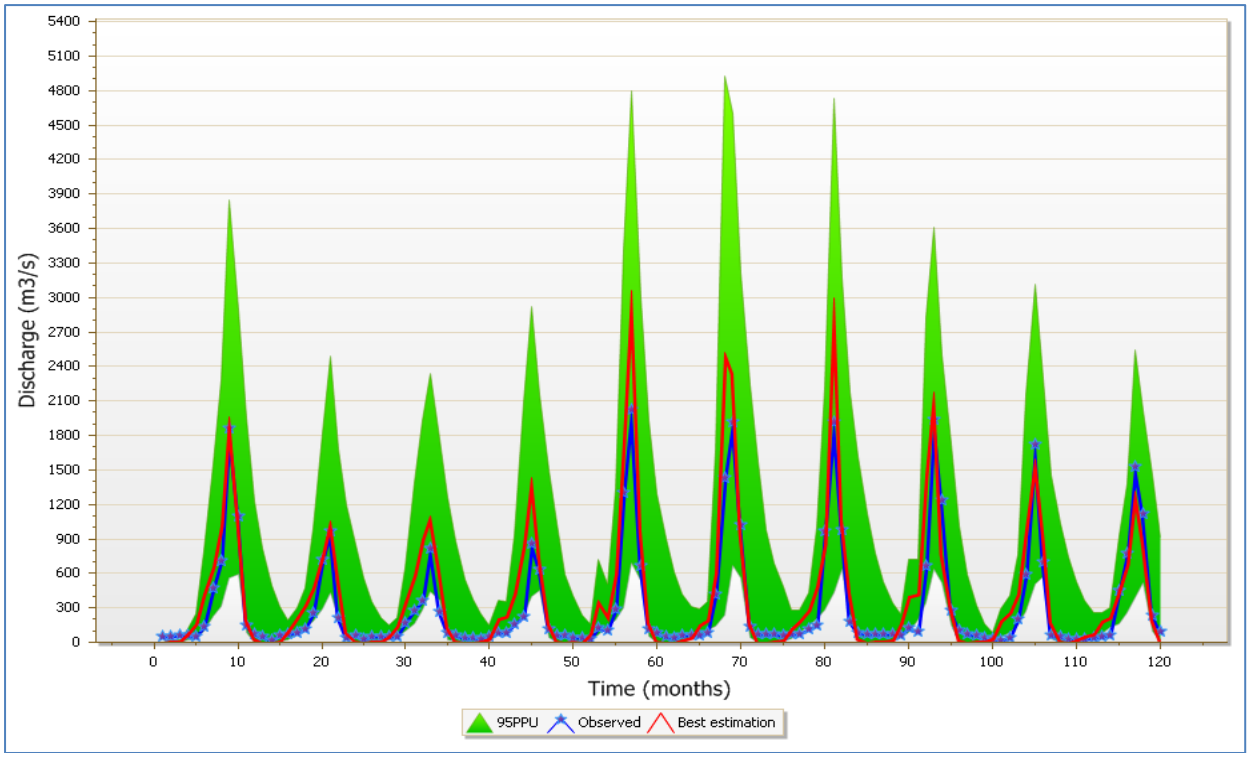

Figure 5-12: 95PPU (shaded green) derived by SUFI-2 with NS objective function for the monthly streamflow during the validation period (2004-2013).

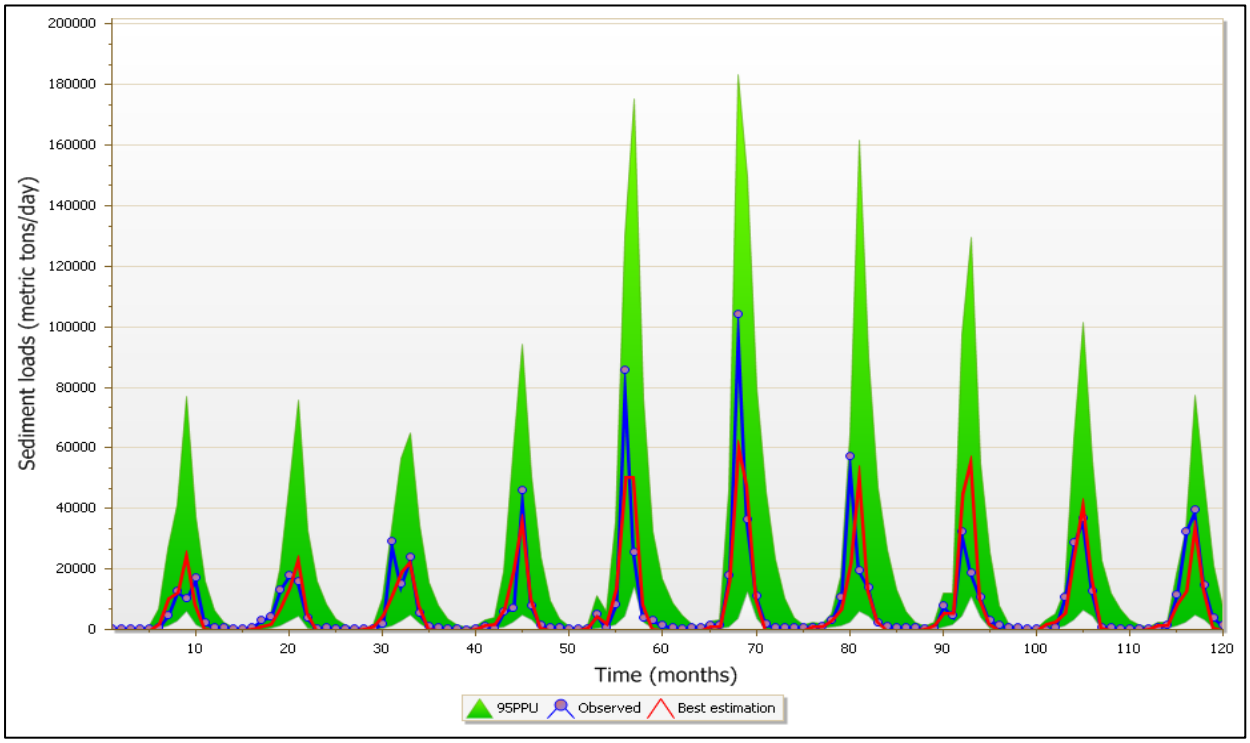

Figure 5-13: 95PPU (shaded green) derived by SUFI-2 with NS objective function for the monthly sediment loads during the validation period (2004-2013).

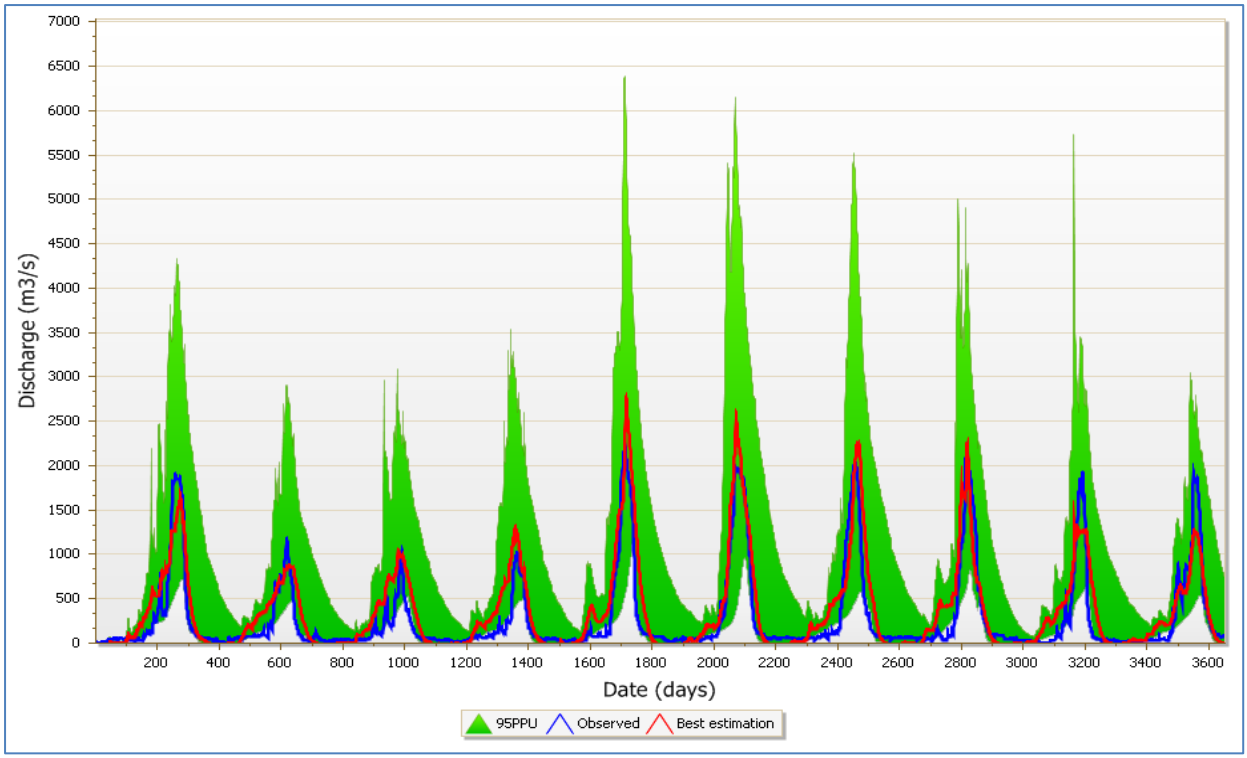

Figure 5-14: 95PPU (shaded green) derived by SUFI-2 with NS objective function for the daily streamflow during the validation period (2004-2013).

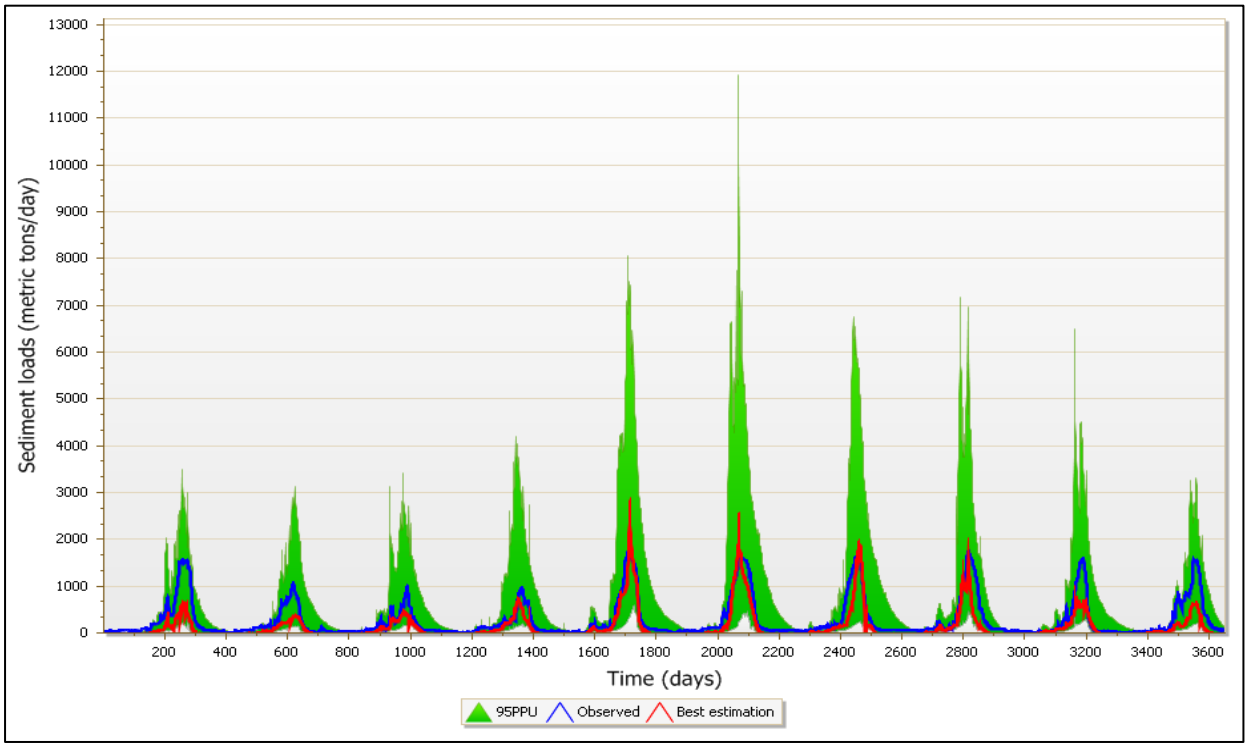

Figure 5-15: 95PPU (shaded green) derived by SUFI-2 with NS objective function for the daily sediment loads during the validation period (2004-2013).

Table 5-8: Model performance evaluation statistics for monthly streamflow validation at Nawuni (2004-2013) in the White Volta Basin.

Monthly	Goal type=Nash Sutcliff No. of simulations=500 Best simulation no.=449 Best goal=0.70					
	Variable	P-factor	R-factor	R^2	NSE	bR^2	PBIAS
	Streamflow	0.87	1.22	0.88	0.73	0.7382	-29.1
	Sediment Load	0.93	1.66	0.68	0.68	0.5000	4.4
Daily	Goal type=Nash-Sutcliff No. of simulations=500 Best simulation no.=82 Best goal=0.71					
	Variable	P-factor	R-factor	R^2	NSE	bR^2	PBAIS
	Streamflow	0.85	2.16	0.83	0.70	0.7830	-22.9
	Sediment Load	0.75	2.04	0.74	0.63	0.5252	45.9

The results of the monthly validation of the streamflow presented in Figure 5-12 and summarized in Table 5-8 can be classified as very good considering the P-factor and R-factor. From Table 5-8, the streamflow was found to be 87% bracketed by the 95PPU (P-factor) with an R-factor of 1.22, which are very close to the suggested values of 100% and 1 respectively. The model performance can therefore be considered as excellent according to Abbaspour, *et al.*, (2007). The R^2 and NSE of 0.88 and 0.73 respectively can also be classified as very good according to the general performance ratings recommended statistics for monthly time step by Moriasi *et al.*, (2007). The PBIAS of -29.1% indicates an overestimation of the peak flows and can be classified as unsatisfactory according to Moriasi *et al.*, (2007). Additionally, the validation of the streamflow displayed a 29.8% difference between the observed and simulated average monthly streamflow. The overestimation of the mean streamflow at Nawuni can be attributed to high intensity rainfall recoded between 2008 and 2010 for which the model overreacts to underlying extreme rainfall amounts of over 350 per month. It should be noted that the mean monthly streamflows are derived from mean daily streamflows which are computed from river stages read manually three times daily. The SWAT model however computes mean daily streamflow from daily climate data.

The results of the monthly validation of the sediment loads presented in Figure 5-13 and also summarized in table 5-8 shows that 93% of the sediment load is bracketed by the 95PPU (P-factor) with a R-factor value of 1.66 which can be classified as very good according to Abbaspour *et al.*, (2007). The R^2 and NSE of 0.68 can also be classified as very good according to the general performance ratings recommended statistics for monthly time step by Moriasi *et al.*, (2007). In contrast to the streamflow, the PBIAS of 4.4% for the sediment load indicates a very good agreement between the observed and simulated sediment

loads according to Moriasi *et al*., (2007). Generally, the model simulated the peak loads very well except in 2008 and 2009 were the model underestimated the peak loads. This could be attributed to overestimation of the sediment loads by the turbidity-suspended sediment concentration rating curve used in deriving the sediment loads.

For the validation of the daily streamflow, R^2, NSE and PBIAS were found to be 0.83, 0.70 and -22.9% respectively and can be classified as satisfactory according to the recommendation for validating streamflow by Moriasi *et al.*, (2007). The daily observed streamflow, as presented in Figure 5-14 and summarized in Table 5-8, was also found to be 85% bracketed by the 95PPU (P-factor) with an R-factor of 2.16 indicating a large uncertainty. This high level of uncertainty could be attributed to the high degree of uncertainty in the rainfall pattern due to the high spatial and temporal rainfall variability in the Volta Basin. Additionally, the onset of the raining season and the rainfall distribution in the basin are erratic with the annual precipitation occurring within one rainy season (Kasei, 2009). Similarly, the validation of the daily sediment load, as presented in Figure 5-15 and summarized in Table 5.-8, also showed a large level of uncertainty with 75% of the observed daily sediment loads bracketed by the 95PPU (P-factor) and an R-factor of 2.04. The results in Table 5-8 also showed that the model prediction of the peak loads was unsatisfactory, according to the recommendations in Moriasi *et al.*, (2007), with a PBIAS of 45.9.

The results of the daily validation showed slightly large prediction uncertainties compared to the monthly prediction considering the R-factor values. This may be due to averaging of the uncertainties in the daily time series into the monthly time series. The large levels of uncertainties can also be accounted for due to errors in filling-in gaps for missing data, sediment concentration overestimation by the sediment rating curves, some errors in data input sources and parameterization. Furthermore, the uncertainties may also result from human and instrumental errors during data processing. Another source of uncertainty is the fact that, the White Volta catchment has a high population density that is largely dependent on agricultural activities and as a result several ponds and dams have been constructed in the basin for dry season farming. This ponds and dams, which could serve as sediment detention ponds, were not incorporated into the model because of insufficient data availability.

Validation of the model was also extended to other locations within the basin without re-calibration at these locations. The model was validated at Pwalugu by applying the calibrated model from the Nawuni watershed over two time periods (July 1994-March 1995 and September 2012-December 2013). The Pwalugu watershed outlet is the second hydrometric gauging station on the main White Volta River downstream of the Bagre Dam in

Burkina Faso and provides an opportunity to analyze the performance of the model on the main river channel as that of Nawuni. The flows at Pwalugu, however, highly correlates with that of Nawuni with a correlation coefficient of 0.73 indicating that Pwalugu does not provide an independent check on the calibrated model. Although the Pwalugu gauge station does not fully satisfy the requirements for spatial validation, it provided a means to perform a consistency check on the calibration results at two different time frames.

Similar to Nawuni, Pwalugu has a short historical suspended sediment concentration data which was collected from July 1994 to March 1995 as well as other sporadic measurements for various projects which largely fall outside the calibration period. Additionally, as part of this study, sediment data was collected from the field between September 2012 and December 2013.

Simulated streamflows and sediment loads at the outlet of the Pwalugu watershed were extracted for the calibrated model for the two time frames of July 1994 to March 1995 and September 2012 to December 2013 and compared with the observed time-series of the same period. Results of the performance evaluation statistics are summarized in Table 5-9 and the plots of the observed and simulated monthly streamflow and sediment loads presented in Figures 5-16 through 5-19.

Table 5-9: Model performance evaluation coefficients for monthly time-series validation at Pwalugu in the White Volta Basin

Period	Variable Name	Mean		Difference (%)	Goodness-of-fit Indicators			
		Observed	Simulated		R^2	PBIAS	NSE	IA
Sep 2012 – Dec 2013	Streamflow	89.53	83.19	7	0.78	7.08	0.72	0.94
	Sediment load	3.23	2.46	24	0.87	24.18	0.83	0.95
Jul 1994 - Mar 1995	Streamflow	159.45	179.62	36	0.98	11.23	0.45	0.78
	Sediment load	6.89	3.71	46	0.94	46.21	0.66	0.87

From Table 5-9, the results of the model validation for the streamflow and sediment loadings at Pwalugu for the period July 1994 to March 1995 displays a R^2 value of 0.98 and 0.94 as well as an IA value of 0.78 and 0.87 respectively. This shows a strong correlation between the observed and simulated time series and can be explained by the fact that, the spatial validation at Pwalugu occurred within the same period as the calibration at Nawuni. Additionally, the streamflow at the outlet of the Pwalugu watershed highly correlates with that of Nawuni. The model efficiency however displayed a satisfactory agreement between

the simulated and observed streamflow and sediment loadings with NSE of 0.45 and 0.66 respectively. The model generally underestimated the peak flows with a PBIAS of 11.23% and 46.21% for the streamflows and sediment loads respectively. Although the model efficiency during the validation process at Pwalugu was found to be less than that of the calibrated model at Nawuni, it should be noted that the model parameters were changed during the calibration to fit the observed time series at Nawuni which includes contributions from other significant sub-watershed such as the Kulpawn, Sissili, Nasia and Nabogo.

From Figure 5-16 through 5-19, it can be observed that the model generally underestimates the streamflow and sediment loads at Pwalugu during the spatial validation process. This can be attributed to the quality and reliability of sediment data at Pwalugu for the 1994/95 period where the highest streamflow was recorded. Furthermore, it has been shown that sediment simulations are not only directly linked to the runoff simulations, but are also very sensitive to the calibration and parameter settings (Qiu, et al., 2012) which was performed at a different location. During the model sensitivity analysis at the Nawuni watershed, it was observed that the model was not sensitive to the CH_ROD (channel erodibility factor) and CH_COV (Channel cover factor) which play important roles in channel erosion in the main river channel. This implies that channel and bank erosion in the White Volta Basin is not significantly high enough to contribute to the sediment load at the watershed outlet at Nawuni. The model was however found to be sensitive to the parameters in the sediment transport equation, SPCON and SPEXP (see Table 5-3 for definitions). These parameters are not well defined physically and no measurements were available to estimate these parameters. However, calibration of the sediment component at the Nawuni watershed outlet was achieved by adjusting the SPCON, SPEXP, USLE_P (USLE equation support (USLE practice factor)) and CH_N2 (Manning's "n" value for the main channel).

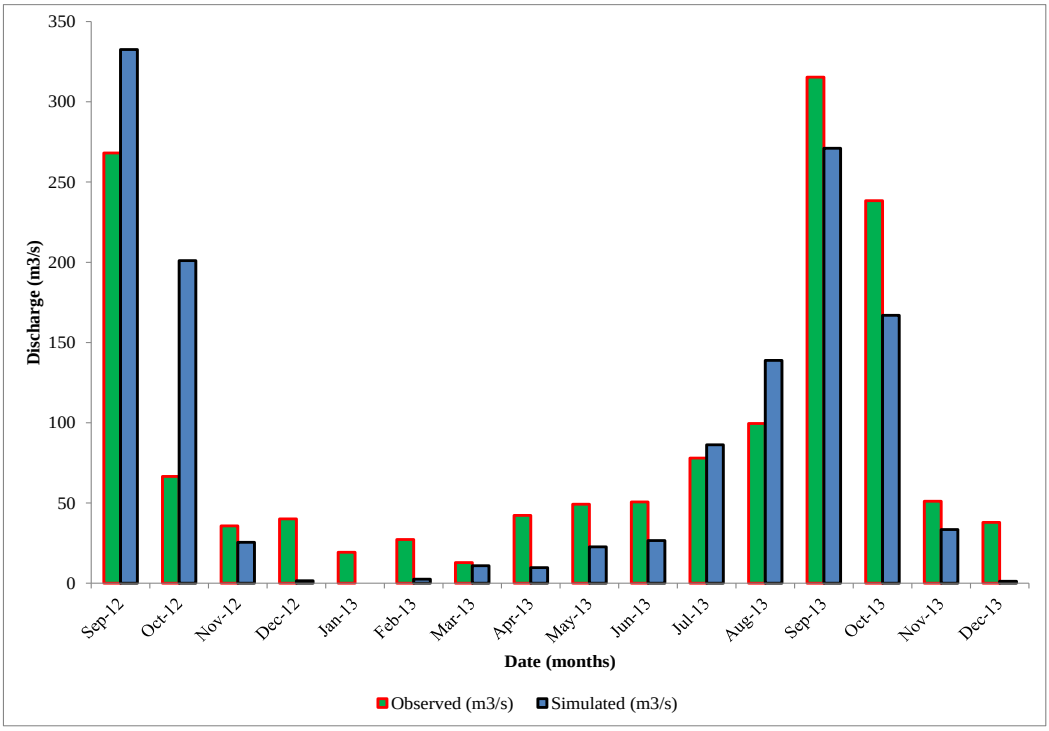

Figure 5-16: Plot of Best-fit simulation and observed monthly streamflow for the model validation at Pwalugu (September 2012 - December 2013).

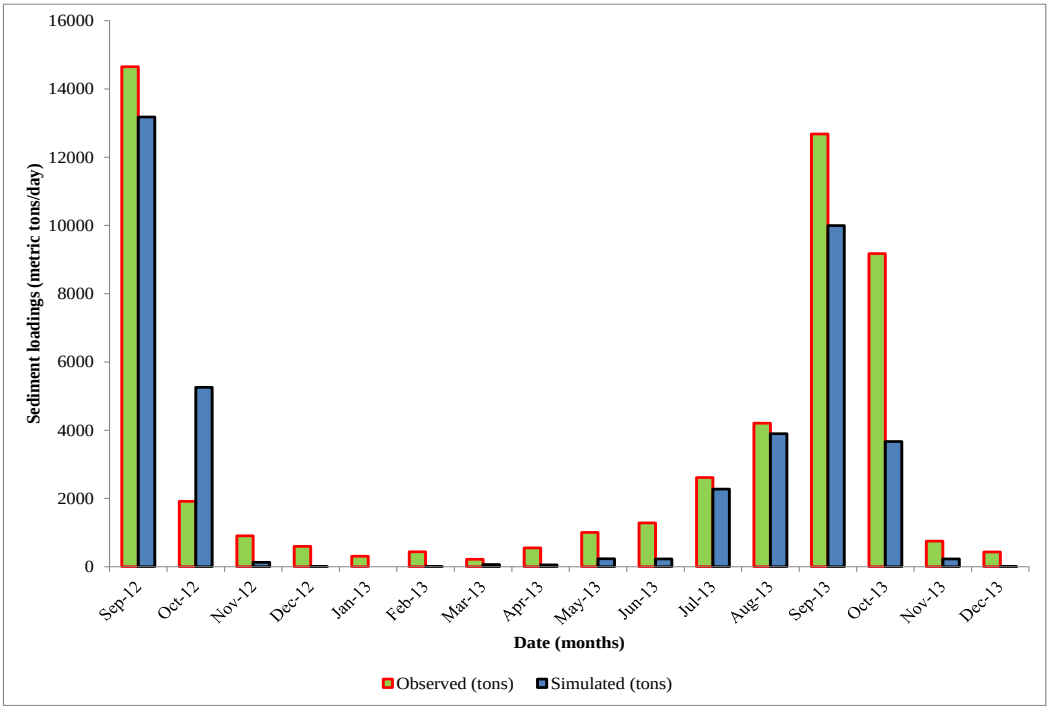

Figure 5-17: Plot of Best-fit simulation and observed monthly sediment loadings for the model validation at Pwalugu (September 2012 - December 2013).

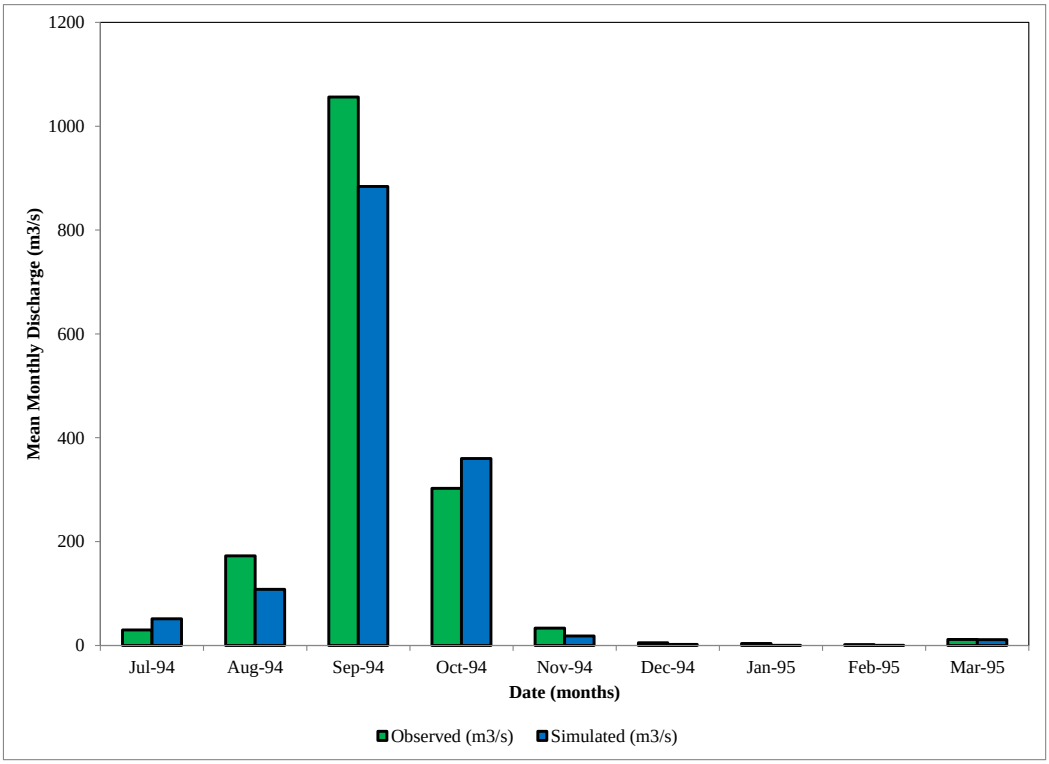

Figure 5-18: Plot of Best-fit simulation and observed monthly streamflow for the model validation at Pwalugu (July 1994-March 1995).

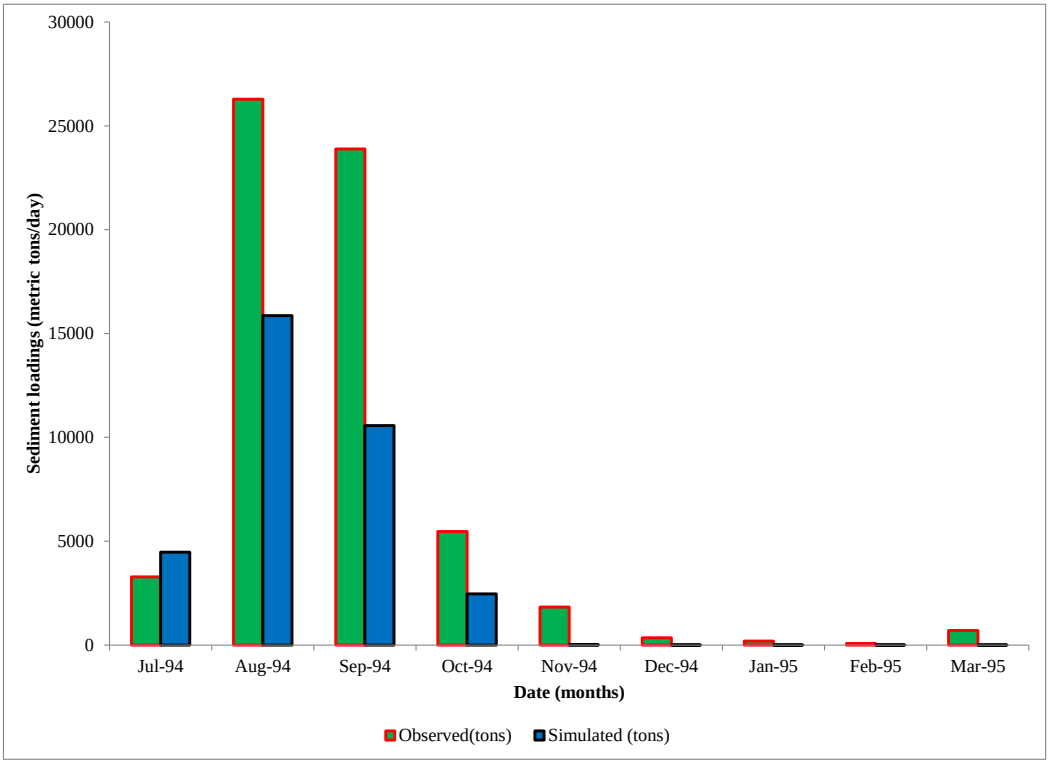

Figure 5-19: Plot of Best-fit simulation and observed monthly sediment loadings for the model validation at Pwalugu (July 1994-March 1995).

Validation of the White Volta SWAT model was also performed by spatial consideration of another sub-watershed within the basin but not directly on the main river channel as Nawuni and Pwalugu. Nasia, a tributary of the White Volta River downstream of Pwalugu and upstream of Nawuni was selected for the spatial model validation of the White Volta SWAT model. Similar to Pwalugu, the Nasia watershed is not hydrologically independent of the White Volta Basin since it has approximately similar climatic, soils, and land use conditions. This is also evident in the correlation coefficient of 0.94 in the mean annual flows between Nasia and Nawuni. This approach however became necessary in order to allow validation of the calibrated model within the sub-watersheds of the White Volta Basin. Other SWAT studies have reported the use of split-location calibration and validation approaches (e.g., Van Liew and Garbrecht, 2003; Cao et al., 2006; and Parajuli et al., 2009).

Although Nasia has a long-term time-series of mean daily streamflows, sediment data was collected during this study covering the period (Sept. 2012 - Dec. 2013). Similar to the spatial validation process at Pwalugu, the model was not recalibrated at Nasia. Simulated streamflows and sediment loads at the outlet of the Nasia watershed were extracted from the validated model and compared with the observed time-series. For the hydrological component, monthly streamflows for the period January 2004 to December 2013 were compared whereas for the sediment loads, the period of comparison was September 2012 to December 2013. Results of the performance evaluation statistics are summarized in Table 5-10 and the plots of the observed and simulated monthly streamflow and sediment loads shown in Figure 5-20 and 5-21 respectively.

Table 5-10: Model performance evaluation coefficients for monthly time-series validation at Nasia in the Nasia sub-catchment.

Variable Name	Mean		Difference (%)	Goodness-of-fit Indicators			
	Observed	Simulated		R^2	PBIAS	NSE	IA
Streamflow (2004–2013) (m^3/s)	21.76	21.10	0.03	0.64	3.02	0.63	0.89
Sediment load (Sept. 2012 – Dec 2013) (10^3 metric tons/day)	0.48	0.39	0.19	0.99	18.56	0.97	0.99

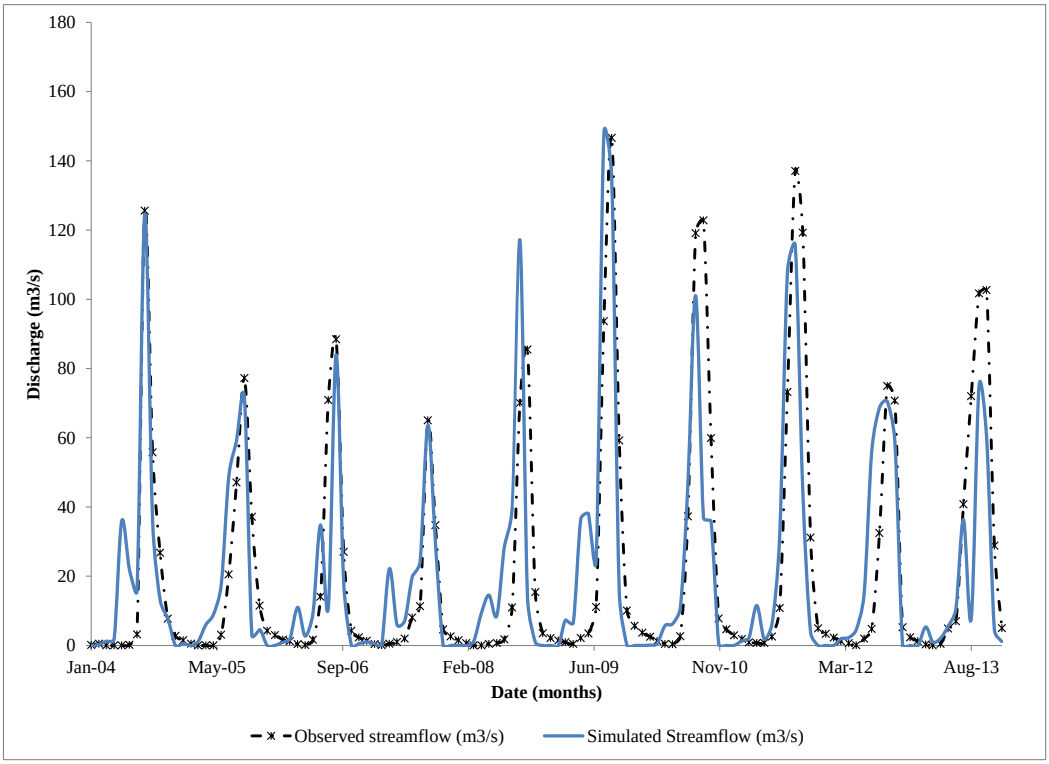

Figure 5-20: Plot of Best-fit simulation and observed monthly streamflow for the model validation at Nasia (January 2004-December 2013).

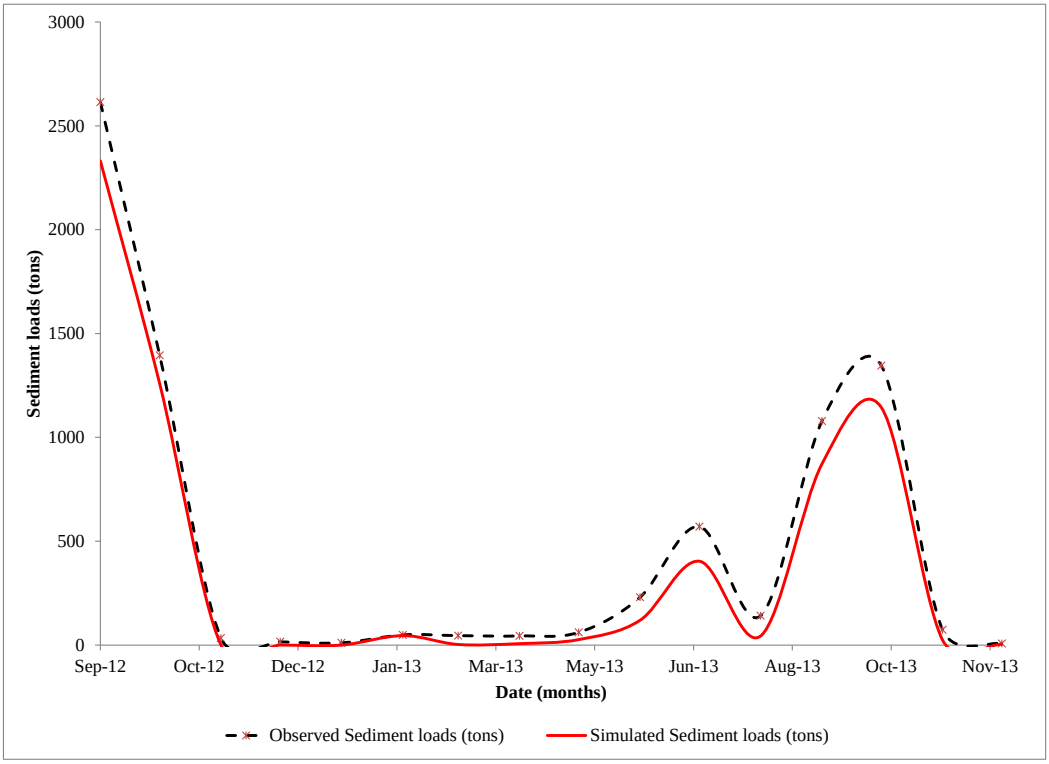

Figure 5-21: Plot of Best-fit simulation and observed monthly sediment loads for the model validation at Nasia (September 2012-December 2013).

Figure 5-20 shows a plot of the simulated and observed monthly streamflow at the outlet of the Nasia watershed for the spatial validation. The simulation performed using the Nawuni watershed calibrated model produced an NSE value of 0.73 and a PBIAS of -29.1% respectively for the Nasia watershed. The PBIAS of -29.1% is considered unsatisfactory for monthly streamflow validation according to the classification suggested by Moriasi *et al.*, (2007). As shown in Figure 5-20, the model generally overestimated the peak flows with additional minor peaks that were not present in the observed streamflow time-series. Similarly, Figure 5-21 presents a plot of the monthly simulated and observed sediment loads for the Nasia watershed during the validation period. In contrast to the streamflow, the calculated PBIAS of 4.4 for the sediment loads displayed a very good agreement according to the classification suggested by Moriasi *et al.*, (2007) with the NSE of 0.68 in the good category. Although, as shown in Figure 5-21, the model underestimated the peak sediment loads, the PBIAS value of 4.4 suggests a good agreement between the observed and simulated peak loads. Generally, the efficiencies were found to be lower for the validation period at the Nasia watershed than for the calibration period at the Nawuni watershed but are nevertheless satisfactory on the basis of the criteria suggested by Moriasi *et al.*, (2007).

The model performance evaluation coefficients for the calibration and validation periods shown in this study can be considered reasonably satisfactory and that the SWAT model is capable of predicting streamflows and sediment loads in the White Volta Basin with limited data availability. This indicates that the selected model parameters values during the calibration period are representative of the basin's parameters. This therefore implies that the calibrated SWAT model for the White Volta Basin can realistically reproduce the hydrological regime and sediment yields in the White Volta Basin and hence can be utilized for future impact studies.

5.5 Model Water Balance

The mean annual water balance for the White Volta Basin was analyzed for the calibrated and validated periods. Results of selected water balance components of the White Volta are presented in Table 5-11 and 5-12 while Table 5-13 summarized similar result of other studies in the basin. It can be observed in Table 5-11 and 5-12 that the mean annual water balance components of the model for the two periods were slightly different.

From Table 5-116 and 5-12, it can be seen that the mean annual precipitation during the validation period exceeds that of the mean annual precipitation during the calibration period by a margin of over 7%. For the calibration period (Table 5-116), it can be seen that about 84% of the mean annual precipitation that occurs in the study area evapotranspires, while for the validation period (Table 5-12) about 85% evapotranspires. The annual water yield and the surface runoff components of the water balance for the calibration period (Table 5-11) was estimated to be 13.10% and 4.90% respectively of the annual precipitation for the study area. For the validation period (Table 5-12), the simulated annual water yield and surface runoff were estimated to be 14% and 6% respectively of the annual rainfall.

Similar to the mean annual rainfall for the study area, the annual sediment loads during the validation period (Table 5-12) exceed the calibration period (Table 5-11) by 29%. From Table 5-11, the simulated mean annual sediment load for the White Volta Basin at Nawuni for the calibration period was estimated at 5.68×10^6 tons per annum which is consistent with reported studies in the study area. According to Milliman and Syvitski (1992), the mean annual sediment load of the Volta Basin prior to the construction of the Volta Lake was estimated to be 19×10^6 t/yr. Akrasi, 2005, also reported a sediment load of 4×10^6 ton per annum for the White Volta Basin and 17×10^6 t/yr for the Volta Basin.

Table 5-11: Mean annual water balance values for the White Volta Basin during the calibration period (1994-2003).

Parameter	Mean Value at Calibration	% of Precipitation	CV
Precipitation	861.27	-	0.08
Water Yield	112.84	13.10	0.20
Surface Runoff (mm)	42.20	4.90	0.34
Actual Evapotranspiration (mm)	726.70	84.37	0.05
Sediment loads (10^6 t/yr)	5.68	-	0.36

Table 5-12: Mean annual water balance values for the White Volta Basin during the validation period (2004-2013)

Parameter	Mean Value at Validation	% of Precipitation	CV
Precipitation	929.06	-	0.10
Water Yield	132.83	14.30	0.24
Surface Runoff (mm)	51.13	5.50	0.49
Actual Evapotranspiration (mm)	787.43	84.76	0.08
Sediment loads (10^6 t/yr)	6.90	-	0.49

Table 5-13: Reported annual mean values of the water balance for the White Volta Basin

Parameter	Reported Literature				
	a	b	c	d	e
Precipitation (mm)	-	1002	-	805.4	1045
Water Yield (mm)	-	-	-	-	-
Surface Runoff (mm)	91*	60	-	25.81	73
Actual Evapotranspiration (mm)	-	893	-	606.8	777
Sediment loads (10^6t/yr)	19*	-	17* 4!	-	-

(a): Milliman and Syvitski (1992); (b): Friesen et al., 2005; (c): Akrasi, 2011; (d): Obuobie, 2008; (e) Kasei, 2009. * - Volta Basin, ! – White Volta Basin

The water balance statistics indicate that, for both the calibration and validation periods, the sediment load and surface runoff reported the highest annual variability with a coefficient of variation of 0.36 and 0.34 for the calibration period (Table 5-11) and 0.49 for both components in the validation period (Table 5-12). The annual variations in rainfall and actual evapotranspiration were however slightly low. The annual amounts of the actual evapotranspiration, surface runoff and precipitation were found to be similar to the values reported for the White Volta Basin by other researchers (e.g. Friesen *et al.*, (2005), Obuobie, (2008), Kasei, (2009) and Akrasi, (2011)).

5.5.1 **Rainfall and Actual Evapotranspiration Dynamics**

As already indicated in Chapter 2, the White Volta basin has a mono modal rainfall pattern starting in April and peaking in August. Spatial distribution of the mean annual rainfall amount and actual evapotranspiration generally declines from south to north (Figure 5-22(a) and (b)). From Figure 5-22(a) and (b) it can be seen that the spatial dynamics of the mean annual rainfall amount and actual evapotranspiration in the White Volta basin as simulated by the SWAT model are consistent with the general trend in the entire Volta basin (see Figure 2-3).

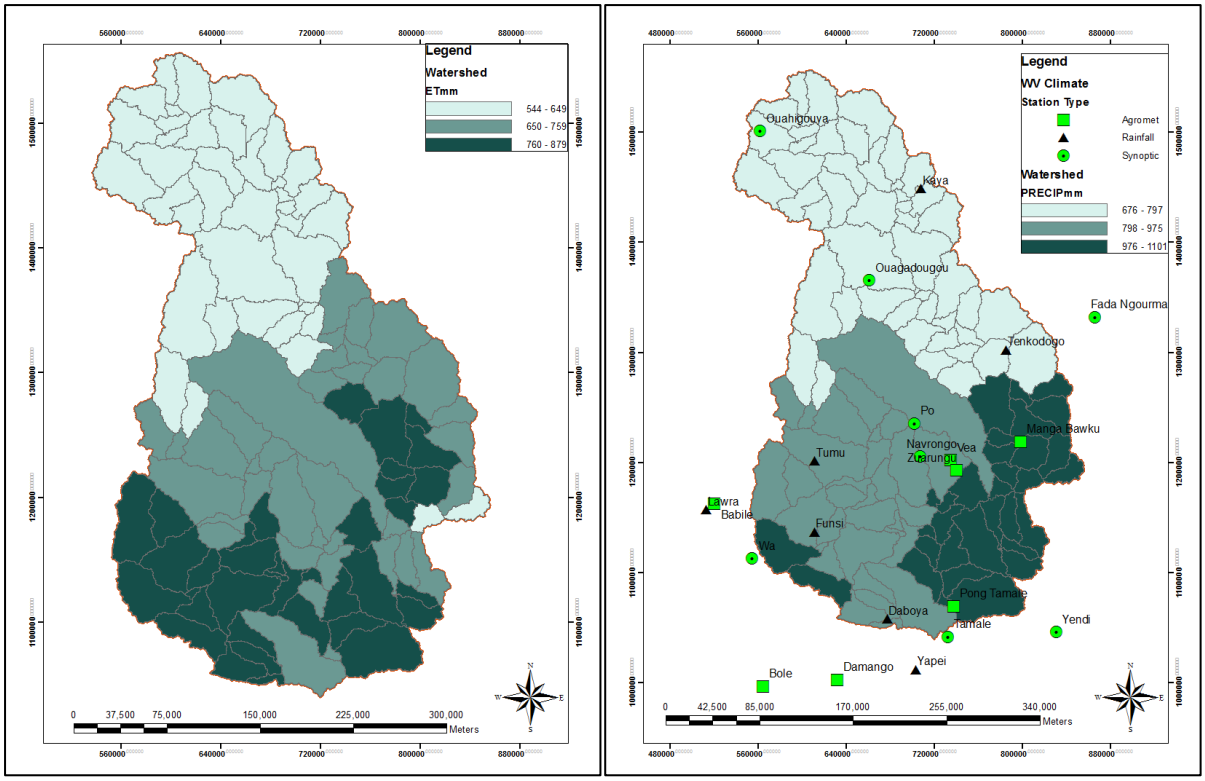

Figure 5-22: Spatial distribution of mean annual rainfall (a) and actual evapotranspiration (b) in the White Volta (1991-2013).

The temporal dynamics of the mean monthly rainfall and potential evapotranspiration were found to be consistent with the general trend in the entire Volta Basin as reported by Amsigo, (2004) (Figure 5-23). It can be observed in Figure 5-23 that except for the 4 wettest months of June, July, August and September, the mean monthly PET exceeds precipitation. The high levels of PET in the basin, notably in the driest months, imply groundwater losses to evapotranspiration instead of to baseflow. This means that the recession flow in streams cannot be used as a good determinant of groundwater recharge and storage (Amsisgo, 2004). Furthermore, with a high ETP in basin in most part of the year, most streams will dry up making them unreliable sources of water resources for domestic, agriculture, transport and industrial water use. This has resulted in the construction of numerous ponds and dams which incidentally serves as sediment traps in the basin.

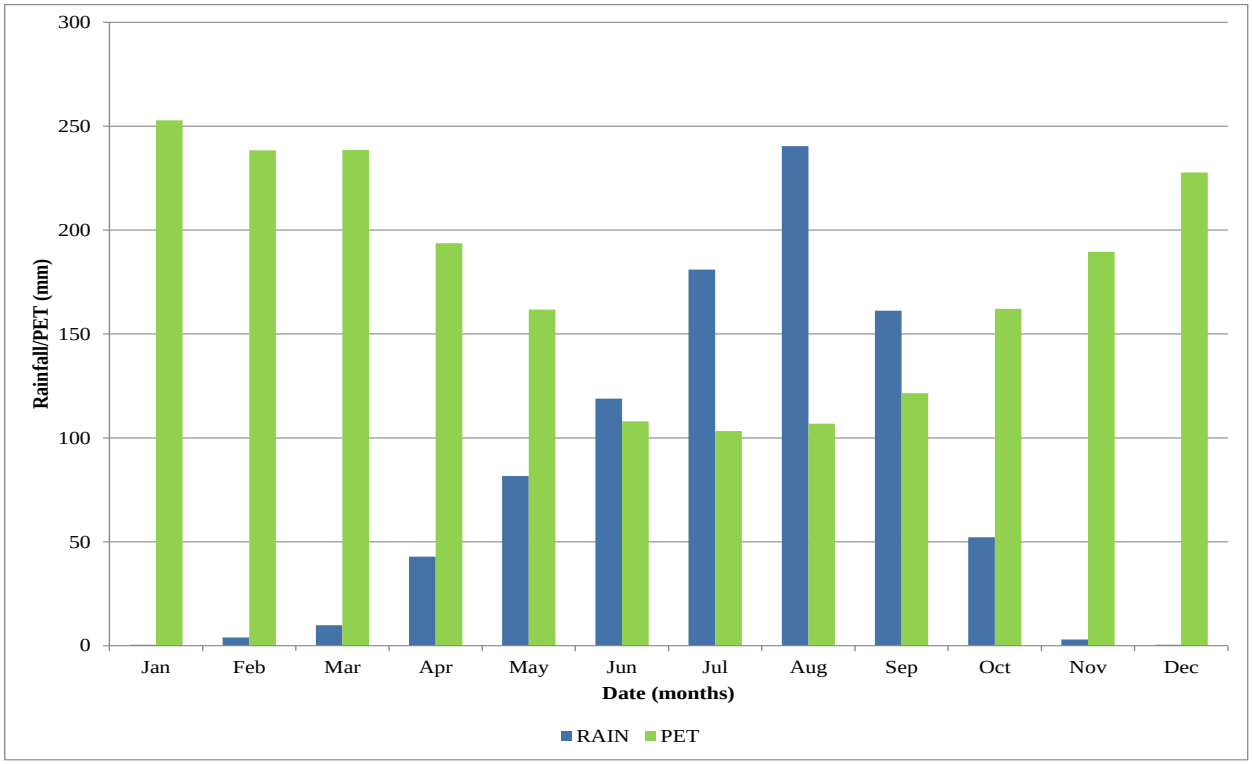

Figure 5-23: Temporal dynamics of long-term mean monthly rainfall and potential evapotranspiration (PET) in the White Volta Basin (1991-2013)

5.5.2 Surface Runoff and Sediment loads Distribution

The spatial distribution of the mean annual surface runoff and sediment loads was simulated for the study area using the calibrated SWAT model and presented in Figure 5-24 (a) and (b). From Figure 5-24 (a) it can be observed that surface runoff in the basin generally increases from north to south with the south-eastern part recording the largest range. Most of the surface runoff in the southern part of the basin could be attributed to the combine effects of rainfall and potential evapotranspiration. Surface runoff was also observed to be significantly low in the extreme north-eastern part of the basin which is similar to the trend observed in the rainfall and evapotranspiration. This could be attributed to the land use type in the area which is predominantly croplands mixed with vegetation forming 51% of the land use in the area. Another exception to the general trend is observed in the south-western parts of the basin where the surface runoff was found to be significantly low. This could also be attributed to the land use type in the area which is predominantly shrublands (51%) and Open broadleaved deciduous forest (21%) resulting in more runoff interceptions.

Similarly, as surface runoff is directly linked to erosion and sediment transport the spatial distribution of sediment loads in the basin follows the same pattern (Figure 5-24b) with some few exceptions. Clearly, the sediment load is also significantly low in the north-

eastern part of the basin as was the case with surface runoff. The watershed outlet at Nawuni recorded the highest sediment load compared to the rest of the catchment. The simulated mean annual sediment load for the entire watershed for the period 1991-2013 was $1.11x10^7$ metric tonnes per year while the sediment load transported out of the watershed at Nawuni was $5.55x10^6$ metric tonnes per year. This implies that approximately 50% of the sediment load generated in the basin reaches the watershed outlet with the remaining being deposited within the basin.

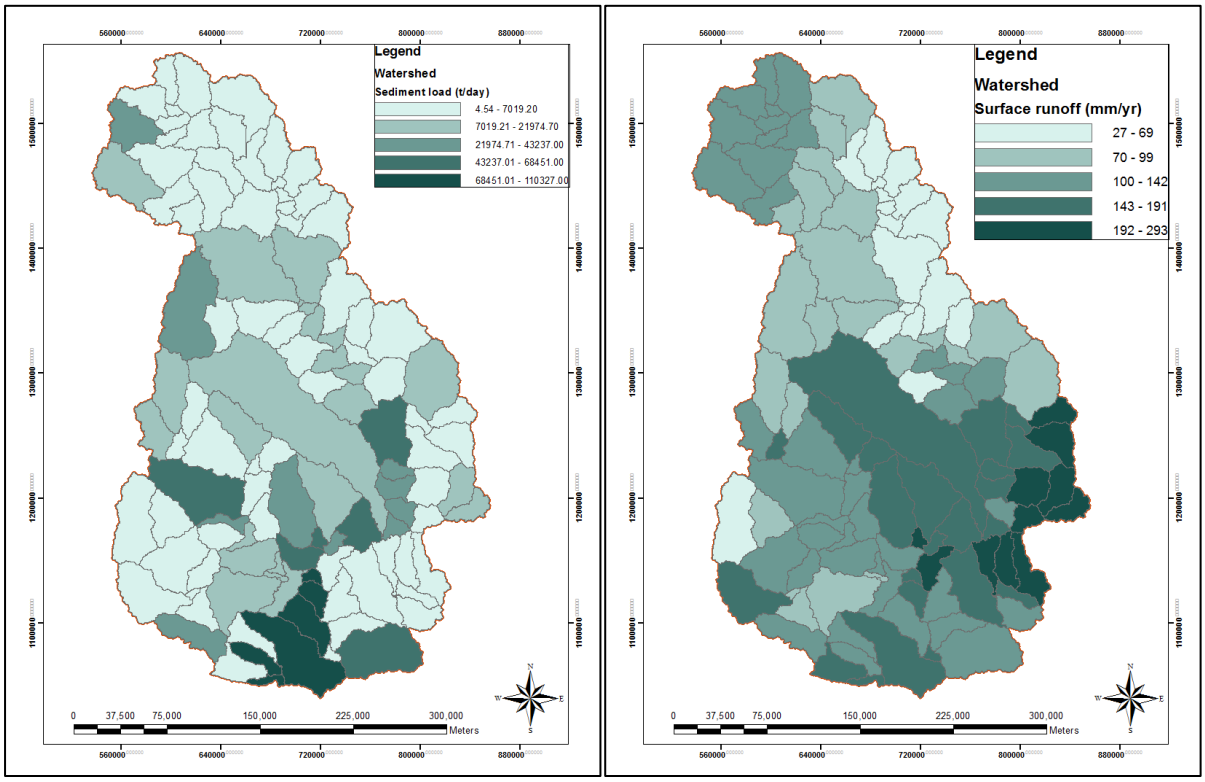

Figure 5-24: Spatial distribution of surface runoff (a) and sediment load (b) at the Nawuni watershed outlet of the White Volta Basin

5.6 Conclusion

The Soil and Water Assessment Tool (SWAT) was calibrated and validated at Nawuni for the periods of 1991–2003 and 2004–2013 respectively. Spatial validation was also performed at Pwalugu and Nasia for the periods 1994-1995 and 2012-2013 respectively. Key considerations in the SWAT model calibration were the overall water balance, the peak-flows to low-flow distribution and seasonal variation.

The calibrated White Volta SWAT model showed a good performance in reproducing the annual, monthly and daily streamflow and sediment loads of the basin. Generally, the

streamflow calibration shows a better agreement between the simulated and observed time series than that of the sediment loads calibration. The monthly streamflow calibration shows the best agreement between the observed and simulated with a NSE of 0.82, followed by annual and daily with NSE of 0.80 and 0.76 respectively. In the case of the sediment load calibration the daily sediment loads shows the best agreement between the simulated and observed with NSE of 0.77, followed by the monthly and annual with NSE of 0.74 and 0.67 respectively. Generally, the model overestimated the streamflow and underestimated the sediment loads during the model calibration. Similarly, the model performed better during the monthly streamflow validation process at Nawuni with a NSE of 0.88 (daily-NSE=0.70). The validation of the sediment loads follows the same trend with the monthly validation having a NSE of 0.68 (daily-NSE=0.63).

The simulated water balance of the White Volta Basin reveals that approximately 85% of the mean annual rainfall actually evapotranspired with over 13% contributing to the mean annual water yield. The mean annual sediment load that is transported out of the White Volta Basin watershed outlet at Nawuni is estimated to be over $5x10^6$ metric tonnes per annum.

In conclusion, the results from the model calibration and validation showed that, the SWAT model can reliably predict the streamflow and sediment loads with satisfactory results and can therefore be used as a tool for analysing the hydrological processes and sediment transport in the White Volta Basin under a changing climate.

Chapter 6

6 CLIMATE CHANGE IMPACT ANALYSIS

6.1 Introduction

In this chapter, the results of downscaling the future projected climate by the three (3) RCM-GCMs under the frame work of the Coordinated Regional Climate Downscaling Experiment (CORDEX) (Giorgi et al., 2009) are presented. The results of the evaluation of the RCM-GCMs performances, the trends in the future projected climate in its impact on the hydrology of the White Volta Basin are also presented.

6.2 Climate Change Projections, Downscaling and Bias Correction

Results of downscaling the future climate by the three (3) RCMs under the frame work of CORDEX-Africa (Giorgi et al., 2009) are presented in this section. To improve the biases associated with the future projection of climate variables by the RCMs as reported by Owusu and Klutse (2013) and Gbobaniyi et al., (2014), the Quantile Mapping (QM) downscaling technique (Boe et al., 2007) was applied to minimise the RCMs model bias in the projected future climate series. Having obtained the outputs of the three RCM-GCMs spanning the period (1950-2100) and applying the QM technique as described by Sarr et al., (2015) using the historical observed precipitation and minimum and maximum air temperatures as the control run (1991-2010), statistical analysis and comparison plots were evaluated.

.

6.2.1 Evaluation of Climate Change Scenarios

According to Lo *et al.*, (2008), precipitation is a model diagnostic field which is more difficult to simulate. This section therefore focuses on the performance of the three RCMs and their ensemble mean in simulating precipitation and temperature for the White Volta Basin.

Statistical analysis such as the mean, maximum, minimum and the coefficient of variation were computed and presented in Table 6-1 and 6-2 for the RCP4.5 and 8.5 respectively. The results in Table 6-1 and 6-2 generally show a good agreement between the control periods mean precipitations of all the RCM-GCMs forced by the RCP4.5 and RCP8.5 scenarios respectively and that of the historical observed precipitation for the same period.

However, the difference between the future mean precipitations of all the RCM-GCMs based on both RCP scenarios was high with RACMO22T-EARTH having the highest mean precipitation of 77.4 mm/day and CCLM-MPI-ESM reporting the least mean future mean precipitation of 68.0 mm/day.

Table 6-1: Computed statistics for precipitation for the control period (1991-2010) and future (2031-2050) based on the RCP4.5 scenario for the White Volta Basin.

RCM-GCMs	Precipitation (mm) Control Period (1991-2010)				Precipitation (mm) Future (2031-2050)			
	Mean	Max	Min	Median	Mean	Max	Min	CV
HISTORICAL OBS	74.4	356.8	0.0	41.0				
CCLM_MPI-ESM	72.6	580.1	0.0	35.2	68.0	648.8	0.0	37.7
HIRHAM5-EARTH	70.5	437.5	0.0	37.3	76.6	443.2	0.0	38.1
RACMO22T-EARTH	72.6	351.1	0.0	40.2	77.4	326.6	0.0	48.9
RCM-GCMS ESM	71.5	313.0	0.0	44.7	74.0	362.7	0.2	50.1

Table 6-2: Computed statistics for precipitation for the control period (1991-2010) and future (2031-2050) based on the RCP8.5 scenario for the White Volta Basin.

RCM-GCMs	Precipitation (mm) Control Period (1991-2010)				Precipitation (mm) Future (2031-2050)			
	Mean	Max	Min	Median	Mean	Max	Min	Median
HISTORICAL OBS	74.4	356.8	0.0	41.0				
CCLM_MPI-ESM	71.4	462.3	0.0	35.3	65.9	531.3	0.0	32.8
HIRHAM5-EARTH	70.5	437.5	0.0	37.3	80.2	496.6	0.1	44.7
RACMO22T-EARTH	71.8	361.1	0.0	39.2	79.2	337.0	0.0	47.9
RCM-GCMS ESM	71.3	316.5	0.0	41.1	75.1	379.2	0.3	49.0

The results also showed that, the RCM-GCMs showed a wide difference between the maximum daily precipitations for the control period for both RCP scenarios. The CCLM-MPI-ESM reported the highest maximum rainfall intensity of 580.1 mm/day for the control period whereas the RCM-GCMs-ESM showed the least maximum precipitation of 313.0 mm/day under the RCP4.5 scenario. The overestimation of the precipitation by the CCLM-MPI-ESM can be attributed to its overestimation of the pre- and post-monsoon precipitation as reported by Akinsanola et al., (2015). Similarly, a wide gap was also observed between the RCM-GCMs simulated maximum daily precipitation for the future with the CCLM-MPI-ESM and RCM-GCMs-ESM projecting a maximum daily rainfall intensity of 648.8 and

362.7 mm/day respectively for the period (2031-2050) under the RCP4.5 scenario. Similar trend is observed in the RCM-GCMs simulated precipitation based on the RCP8.5 scenario.

Generally, the results shows that RACMO22T-EARTH simulations of the long-term mean and maximum daily precipitation, under both RCP forcing, for the study area was comparable to that of the historical observations. Overall, the results presented in Table 6-1 and 6-2 indicate that the downscaled precipitations for the model scenario runs based on the RCP forcing are consistent with the RCM-GCMs outputs during the control runs after the QM bias correction.

As expected, the results presented in Table 6-3 and 6-4 for the RCP4.5 and RCP8.5 scenarios respectively did not show a wide range of variability in the maximum air temperature between the selected RCM-GMCs Ensembles indicating that the downscaled temperature for the model scenario runs based on the RCP forcing are consistent with the RCM-GCMs outputs during the control runs after the QM bias correction.

Table 6-3: Computed statistics for maximum daily air temperature for the control period (1991-2010) and future (2031-2050) based on the RCP4.5 scenario for the White Volta.

RCM-GCMs	TMax (°C) Control Period (1991-2010)				TMax (°C) Future (2031-2050)			
	Mean	Max	Min	Median	Mean	Max	Min	Median
HISTORICAL OBS	35.2	39.9	30.5	35.2				
CCLM_MPI-ESM	35.3	40.9	29.9	35.5	37.2	42.0	31.3	37.4
HIRHAM5-EARTH	35.3	40.3	30.5	35.3	36.4	41.3	31.2	36.6
RACMO22T-EARTH	35.3	40.7	29.7	35.2	36.6	41.6	31.4	36.6
RCM-GCMS ESM	35.3	40.1	30.5	35.2	36.7	41.5	31.9	36.6

Table 6-4: Computed statistics for maximum daily air temperature for the control period (1991-2010) and future (2031-2050) based on the RCP8.5 scenario for the White Volta.

RCM-GCMs	TMax (°C) Control Period (1991-2010)				TMax (°C) Future (2031-2050)			
	Mean	Max	Min	Median	Mean	Max	Min	Median
HISTORICAL OBS	35.2	39.9	30.5	35.2				
CCLM_MPI-ESM	35.3	41.0	29.9	35.4	37.7	43.3	31.5	38.1
HIRHAM5-EARTH	35.3	40.3	30.5	35.3	36.6	42.0	31.4	36.7
RACMO22T-EARTH	35.3	40.6	29.7	35.2	37.0	42.2	31.4	36.9
RCM-GCMS ESM	35.3	39.7	30.5	35.2	37.1	41.7	32.0	37.1

The difference between the mean of the historical observations of the maximum daily air temperature and that of all the RCM-GCMs simulations forced by both RCPs is 0.1 °C for

the control period. It can also be observed in Table 6-3 and 6-4 that, all the RCM-GCMs however, generally projects a future (2031-2050) rise in the maximum daily air temperature ranging from 1.1 °C by HIRHAM5-EARTH to 1.8 °C by CCLM-MPI-ESM under the RCP4.5 scenario. Likewise, the RCM-GCMs under the RCP8.5 scenario also show a rise in the maximum daily air temperature with a wide margine, generally more than 1°C (Table 6-4). Similar trend is observed in the RCM-GCMs simulated minimum daily air temperature. The results of the RCM-GCMs simulated minimum daily air temperature are presented in Appendix B for the RCP4.5 and RCP8.5 scenarios respectively.

The long-term mean monthly precipitation and temperature for the control period were also plotted and analyzed. Additionally, the reliability of the RCM-GCMs-simulated climate series was further analyzed by comparing with the observed basin-wide areal temperature and precipitation for the control period (1991-2010). Model performance was also checked for each RCM-GCM using the correlation coefficient, (Pearson's r) (Equation 3.2.4), the mean absolute error (MAE) (Equation 3.2.12) and percent bias (PBIAS) (Equation 3.3.30).

The long-term mean monthly precipitation for the control period (1991-2010) was generally well simulated by the RCM-GCMs (Figure 6-1). A plot of all the RCM-GCMs simulated precipitation (Figure 6-2) for the control period did not show any discernable trend. The plot however shows that the CCML-MPI-ESM generally overestimates the extreme precipitation despite the bias correction. The r, MAE and PBIAS (Table 6-5) for the RCM-GCMs-Ensemble mean were found to be 0.91, 2.92 and 3.93.9% respectively. An r of 0.91 indicates a very good correlation between the observed precipitation and that of the RCM-GCMs Ensemble mean simulated precipitation. A MAE of 2.92 and a PBIAS of 3.93% can be classified as very good according to Moriasi *et al.*, (2007) who recommended a PBIAS range of ±25%. A PBIAS of 3.93% indicates underestimation of the observed precipitation.

Table 6-5: RCM-GCMs model performance statistics for precipitation in the White Volta Basin for the control period (1991-2010)

RCM-GCMs	r	MAE	PBIAS
Observed			
CCLM-MPI-ESM	0.79	1.76	2.36
HIRHAM5-EARTH	0.82	3.91	5.25
RACMO22T-EARTH	0.85	1.79	2.41
RCM-GCMs-ESM	0.91	2.92	3.93

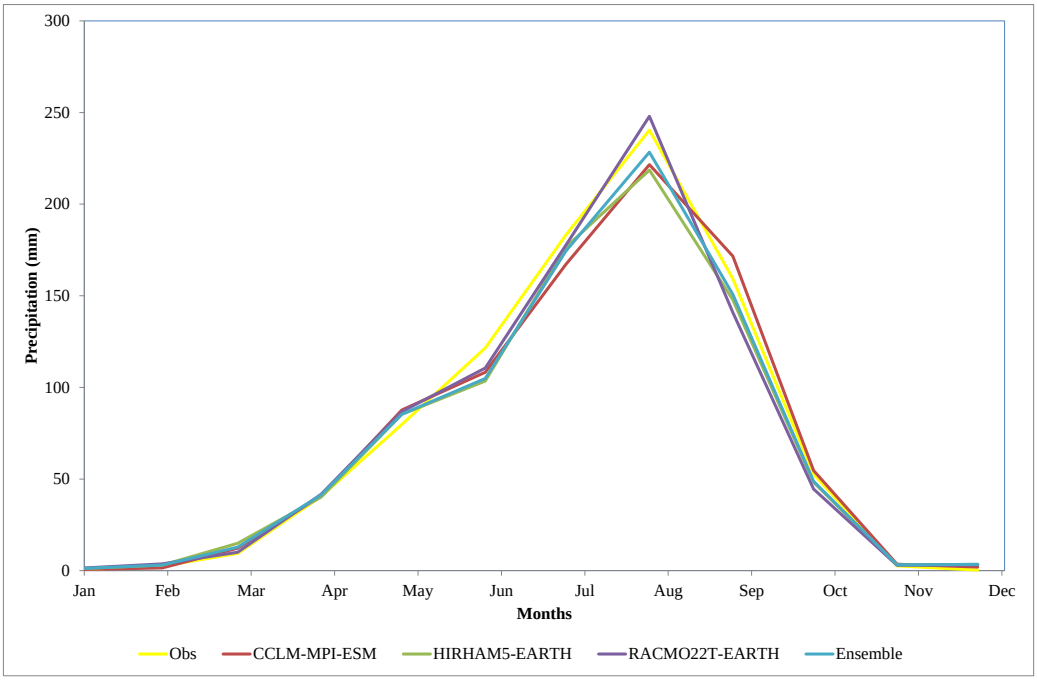

Figure 6-1: The RCM-GCMs simulated long-term monthly mean precipitation compared to the observed for the control period (1991-2010) for the White Volta Basin.

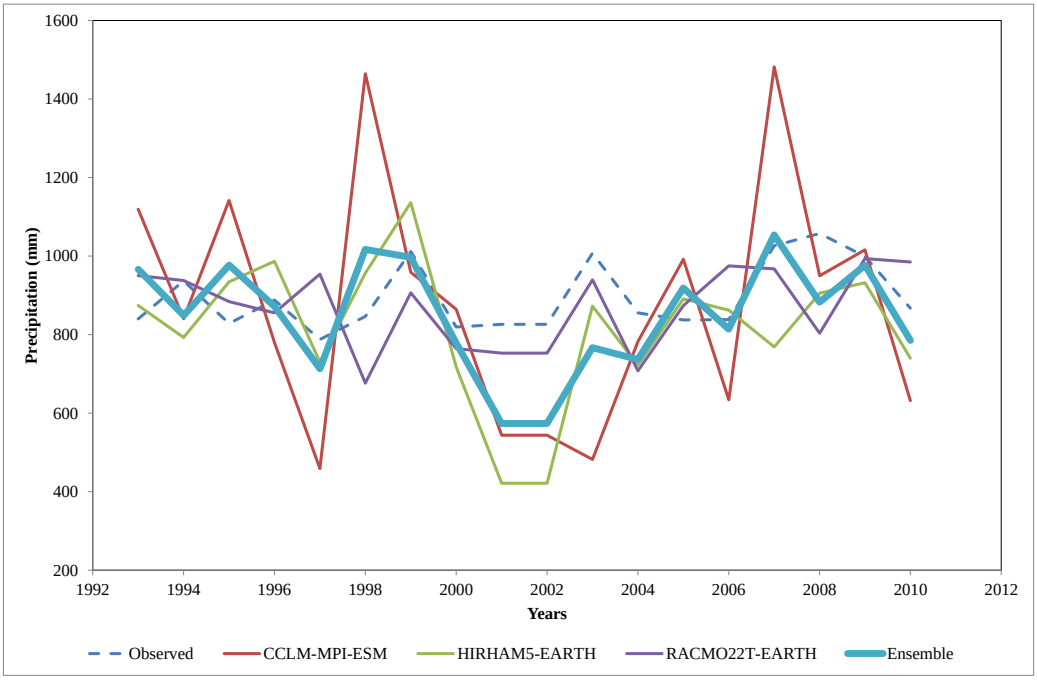

Figure 6-2: A trend analysis plot of all the RCM-GCMs simulated precipitation for the control period (1991-2010) for the White Volta Basin.

Similarly, the long-term mean monthly air temperature for the control period (1991-2010) was generally well simulated by the RCM-GCMs (Figure 6-3). A graphical plot of all the RCM-GCMs simulated mean air temperature (Figure 6-4) for the control period shows a

rising trend of temperature in the study area. The r, MAE and PBIAS (Table 6-6) for the RCM-GCMs-model Ensemble mean were found to be 0.89, 0.15 and -0.51% respectively. An r of 0.89 indicates a very good correlation between the observed mean air temperature and that of the RCM-GCMs-model ensemble mean simulated temperature. A MAE of 0.15 and a PBIAS of -0.51% can be classified as very good according to Moriasi *et al.*, (2007) who recommended a PBIAS range of ±25%. A PBIAS of -0.51% indicates an overestimation of the observed mean air temperature.

Overall, the RCM-GCMs Ensemble mean shows a better correlation between the model simulated and the observed climate variables in the study area during the control period. The CCLM-MPI-ESM has the least correlation with the observed climate variables for the control period.

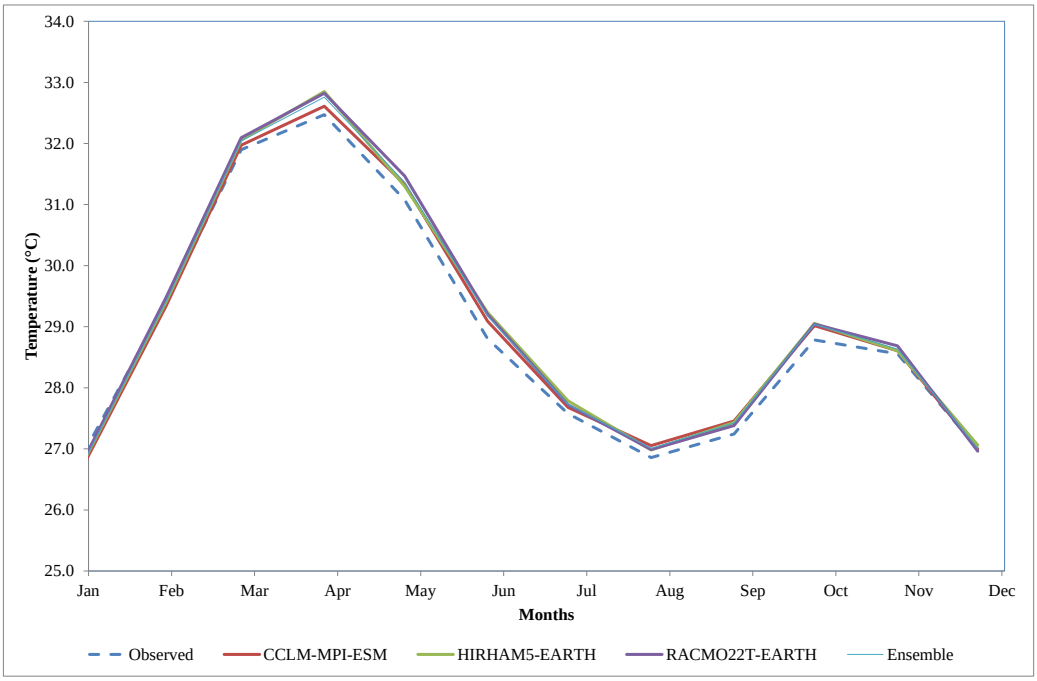

Figure 6-3: The RCM-GCMs simulated long-term monthly mean temperature compared to the observed for the control period (1991-2010) for the White Volta Basin.

Figure 6-4: A trend analysis plot of all the RCM-GCMs simulated mean air temperature for the control period

Table 6-6: RCM-GCMs model performance statistics for mean air temperature in the White Volta Basin for the control period (1991-2010)

RCM-GCMs	r	MAE	PBIAS
CCLM-MPI-ESM	0.85	0.11	-0.37
HIRHAM5-EARTH	0.86	0.16	-0.57
RACMO22T-EARTH	0.88	0.17	-0.60
RCM-GCMs ENSEMBLE mean	0.89	0.15	-0.51

6.2.2 **Trends in Future Climate**

As indicated Section 3.4.2.3, a plot of the RCM-GCMs simulated mean monthly precipitation against the mean temperature for the study area can provide a statistical means of detecting which RCM-GCM is predicting a future warmer/colder and drier/wetter climate scenarios. This effect can be observed in Figures 6-5 and 6-6 for the RCP4.5 and 8.5 respectively.

The scattered plots of the RCM-GCMs simulated mean temperatures and mean monthly precipitation, as observed in Figures 6-5 and 6-6, show a general cluster of scenarios around the temperature axis. This indicates that the RCM-GCMs generally project an increase in future temperature, with reference to the historical observations, ranging between 2.2 to 2.4 °C and 2.5 to 2.8 °C for the RCP4.5 and RCP8.5 scenarios respectively. On the contrarily, the RCM-GCMs simulations of the future precipitation are widely spread around

the precipitation axis with no clusters for both scenarios. This suggests that the three (3) selected RCM-GCMs generally disagree in the simulation of the future precipitation in the White Volta Basin.

The deviation of the RCM-GCMs simulation of the future precipitation, with reference to the historical observation, ranges from a decrease of 8.6% of rainfall by CCLM-MPI-ESM to an increase of 4.0% of rainfall by RACMO22T-Earth for the RCP4.5 scenario (Table 6-7). Similarly, for the RCP8.5 scenario, the CCLM-MPI-ESM predicts a future reduction in precipitation by 11.4% whereas HIRHAM5-Earth predicted the highest increase in precipitation by 7.8% (Table 6-7). The use of precipitation as a model diagnostic field, as pointed out by Lo *et al.*, (2008), can therefore pose a problem in predicting the trend in future climate change when only one RCM is applied for impact studies.

Table 6-7: Projected change in temperature and precipitation between the historical observations for the control period (1991-2010) and the RCM-GCMs simulations of future climate (2031-2050) under the RCPs scenario

RCM-GCMs	ΔTemperature (°C)		Change Trend	ΔPrecipitation (%)		Change Trend
	RCP4.5	RCP8.5		RCP4.5	RCP8.5	
CCLM-MPI-ESM	2.4	2.8	↑↑	-8.6	-11.4	↓↓
HIRHAM5-EARTH	2.2	2.5	↑↑	2.9	7.8	↑↑
RACMO22T-EARTH	2.3	2.8	↑↑	4.0	6.5	↑↑
RCM-GCMs-ESM	2.3	2.7	↑↑	-0.6	0.9	↓↑

Where ↑↓ represents the direction of the climate change signal (Δ).

Further examination of the individual points in the scatter plots (Figures 6-5 and 6-6) can indicate whether the future climate will be warmer/colder and drier/wetter as simulated by the individual RCM-GCMs under the two RCPs. As can be observed in Figures 6-5 and 6-6 the CCLM-PMI-ESM predicts a warmer and drier future climate, with reference to the historical observations, whereas RACMO22T-Earth and HIRHAM5-Earth both predicts a warmer but wetter future climate under both RCPs. The RCM-GCMs- model ensemble means however shows a slight reduction in precipitation, with reference to the historical observations, for the RCP4.5 scenario and a marginal increase for that of the RCP8.5 scenario.

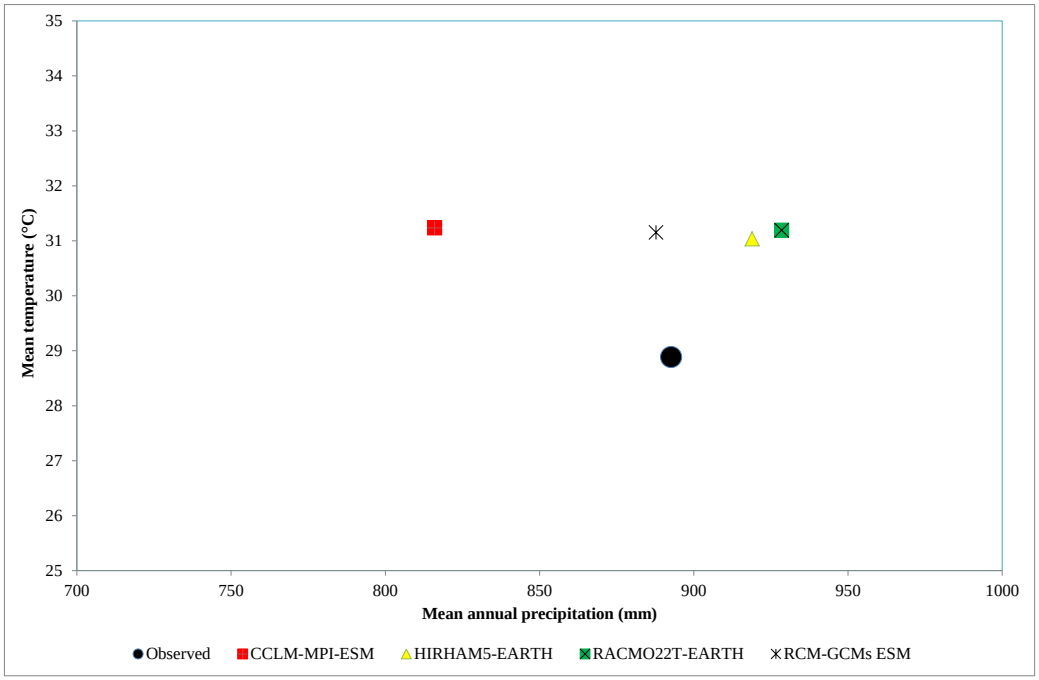

Figure 6-5: A plot of RCM-GCMs simulated mean temperature against mean monthly precipitation for the RCP4.5 scenario for the future period (2031-2050).

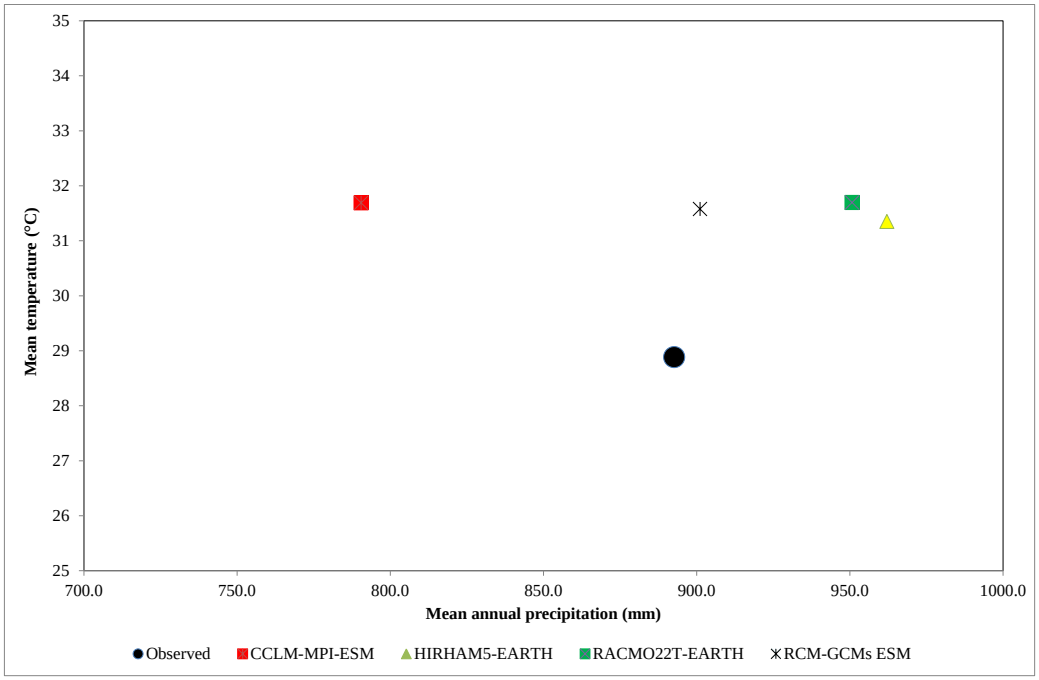

Figure 6-6: A plot of RCM-GCMs simulated mean temperature against mean monthly precipitation for the RCP8.5 scenario for the future period (2031-2050).

The RCM-GCMs simulated precipitation and temperature for the control period and the projected future climate driven by the RCPs scenario were used to examine the projected future behavior of the individual RCM-GCMs using Equation 3.4.2 and presented in Table 6-8 and 6-9 respectively.

Table 6-8: Projected change in precipitation between the RCM-GCMs control period (1991-2010) and the future (2031-2050) based on the RCPs scenario

RCM-GCMs	Annual Precipitation (mm)			Relative Change (%)		Climate Change Trend
	Control Period	RCP4.5	RCP8.5	ΔRCP4.5	ΔRCP8.5	
CCLM-MPI-ESM	884.6	825.7	791.9	-6.7	-10.5	↓↓
HIRHAM5-EARTH	855.9	936.3	976.4	9.4	14.1	↑↑
RACMO22T-EARTH	880.6	936.2	952.8	6.3	8.2	↑↑
RCM-GCMs Ensemble Mean	865.8	899.4	907.0	3.9	4.8	↑↑

Where ↑↓ represents the direction of the climate change signal (Δ).

Table 6-9: Projected mean air temperature change between the RCM-GCMs control period (1991-2010) and the future (2031-2050) based on the RCPs scenario

RCM-GCMs	Temperature (°C)			Relative Change (%)		Climate Change Trend
	Control Period	RCP4.5	RCP8.5	ΔRCP4.5	ΔRCP8.5	
CCLM-MPI-ESM	29.0	31.2	31.7	7.7	9.3	↑↑
HIRHAM5-EARTH	29.0	31.0	31.4	6.8	7.9	↑↑
RACMO22T-EARTH	29.1	31.2	31.7	7.3	9.1	↑↑
RCM-GCMs Ensemble Mean	29.0	31.2	31.6	7.3	8.8	↑↑

Where ↑↓ represents the direction of the climate change signal (Δ).

Similar to the comparison of the projected future climate with the historical observations, Table 6-9 shows that all the RCM-GCM models forced by the RCPs points to a rising temperature. The CCLM-MPI-ESM predicts that, projected future (2031-2050) temperature could rise by as much as 9.3% with reference to the control period (1991-2010). However, in the case of the precipitation simulations, the Earth-GCM driven RCMs (HIRMAN5 and RACMO22T) in addition to the RCM-GCM Ensembles Means points to an increase in precipitation whereas the CCLM-MPI-ESM points to a reduction in future precipitations (Table 6-8).

The results of this analysis could potentially affect the water resources of the White Volta Basin in the immediate future. There is therefore the urgent need to develop impact based adaptation strategies to mitigate this potential threat. After downscaling and analyzing three RCMs under the framework of CORDEX-Africa, the two driving parameters of the

hydrological cycle, precipitation and temperature, were used as inputs in a hydrological model, SWAT to study the impact of climate change on the streamflows and sediment loads of the White Volta Basin.

6.3 Impact of Climate Change on Streamflows and Sediment Loads

In this section, the results of the assessment of the impact of climate change on the streamflows and sediment loads in the White Volta Basin using the calibrated SWAT model driven by the RCM-GCMs downscaled temperature and precipitation time series under the RCPs forcing are presented.

The output of the SWAT simulations for the control period using the climate series from the historical observations and the RCM-GCMs simulated series forced by RCP4.5 were compared. The results of the SWAT simulation using the historical and all the RCM-GCMs downscaled climate series for the control period are summarized in Table 6-10. A comparison of the long-term mean monthly streamflow and sediment loads are presented in Figure 6-7 and 6-8 respectively.

The results can be generally classified as satisfactory considering the P-factor and R-factor according to Abbaspour, et al., (2007). From Table 6-10, the streamflow was found to be 40% and 39% bracketed by the 95PPU (P-factor) with an R-factor of 0.47 and 0.41 for the CCLM-PMI-ESM and RCM-GCMs Ensemble mean respectively. A perfect fit is achieved when the P- and R-values are 100% and 1 respectively (Abbaspour, et al., 2007). The R^2 and NSE of 0.44 and -0.01 respectively for the CCLM-MPI-ESM is however classified as unsatisfactory according to the general performance ratings recommended statistics for monthly time step by Moriasi et al., (2007). The PBIAS of -0.2% indicates an overestimation of the peak flows and can be classified as very good according to Moriasi et al., (2007). On the other hand, the R^2 and NSE of 0.70 and 0.55 respectively for the RCM-GCMs Ensemble mean is classified as satisfactory according to Moriasi *et al*., (2007). A PBIAS of 24.5% indicates an underestimation of the peak flows and can also be classified as satisfactory according to Moriasi *et al*., (2007).

Similar to the streamflow, the SWAT simulation of the sediment loads can be generally classified as satisfactory considering the P-factor and R-factor according to Abbaspour, *et al.,* (2007). From Table 6-10, the sediment load was found to be 51% and 66% bracketed by the 95PPU (P-factor) with an R-factor of 2.21 and 0.44 for the CCLM-PMI-ESM and RCM-GCMs Ensemble mean respectively. The R^2 of 0.31, NSE of -4.54 and a

PBIAS of -104.1% for the CCLM-MPI-ESM is however classified as unsatisfactory according to the general performance ratings recommended statistics for sediment loads by Moriasi *et al*., (2007). On the other hand, the R^2 of 0.49, NSE of 0.48 and a PBIAS of 51.6% for the RCM-GCMs Ensemble mean is classified as satisfactory according to Moriasi *et al*., (2007) for simulated sediment loads at a monthly time step.

The comparison plot of the long-term mean monthly streamflow and sediments loads (Figures 6-7 and 6-8) show that the CCLM-MPI-ESM generally overestimates the streamflow and sediment loads for the wet season i.e. from May to October with pronounced difference between the historical observations and the SWAT-simulated time series in the peak rainfall months of July to September (JAS). SWAT unsatisfactory simulation of the streamflow and sediment loads peaks based on the input from the CCLM-MPI-ESM downscaled climate series can be directly linked to the amounts and intensities of extreme climatic events as presented in Figure 6-2.

Table 6-10: SWAT performance evaluation statistics for the control period (1990-2010) using downscaled climate series as inputs

RCM-GCMs	Variable	P-factor	R-factor	R^2	NSE	PBIAS
HISTORICAL	Streamflow	0.44	0.49	0.88	0.64	-43.3
OBSERVATIONS	Sediment Load	0.60	1.72	0.54	0.44	7.7
CCLM-MPI-ESM	Streamflow	0.40	0.47	0.44	-0.01	-0.2
	Sediment Load	0.51	2.21	0.31	-4.54	-104.1
HIRHAM5-EARTH	Streamflow	0.52	0.37	0.63	0.59	24.5
	Sediment Load	0.65	1.17	0.47	0.31	-10.8
RACMO22T-EARTH	Streamflow	0.46	0.39	0.54	0.52	22.2
	Sediment Load	0.63	1.22	0.34	0.31	-31.7
RCM-GCM ESM	Streamflow	0.39	0.41	0.70	0.55	24.5
Mean	Sediment Load	0.66	0.44	0.49	0.48	51.6

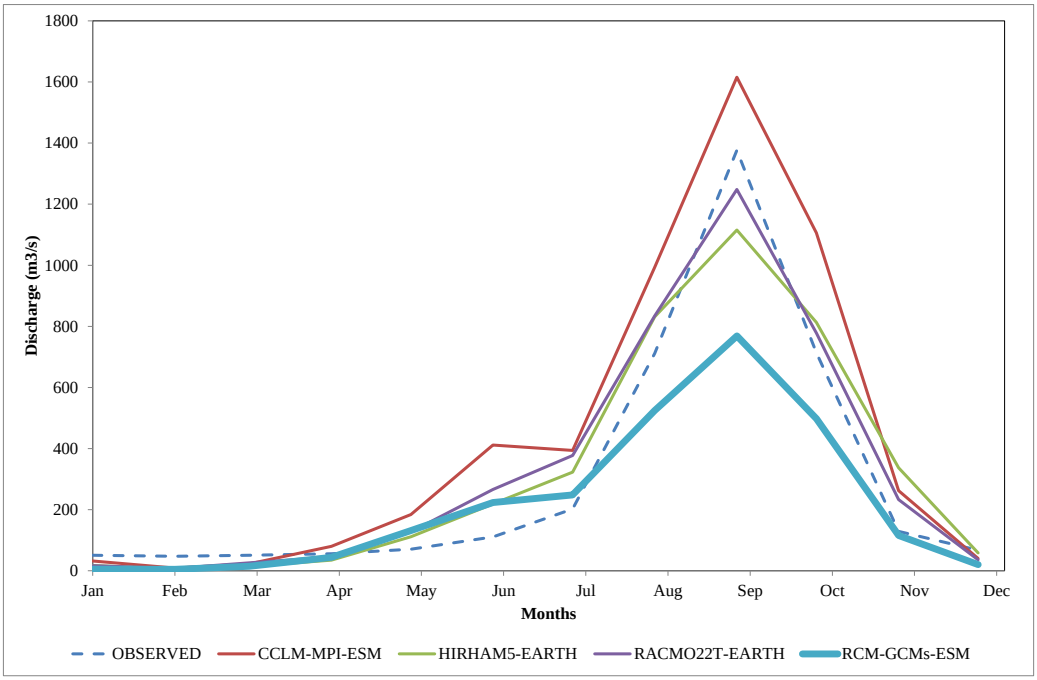

Figure 6-7: SWAT-simulated long-term monthly mean streamflow based on the RCM-GCMs climate inputs compared to the observed for the control period (1991-2010).

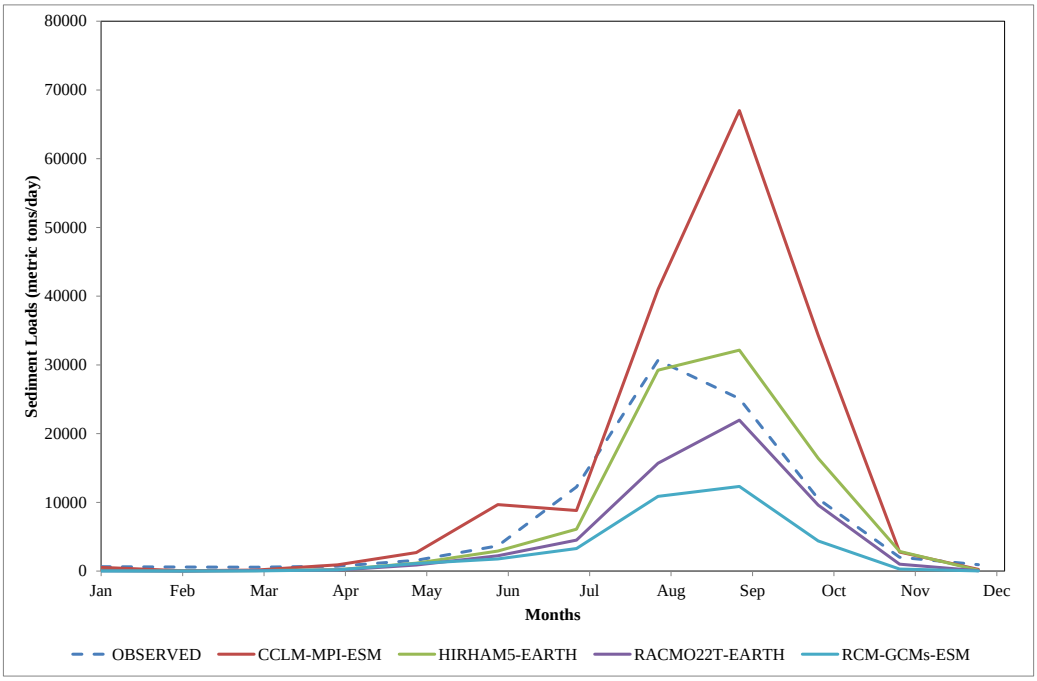

Figure 6-8: SWAT-simulated long-term monthly mean sediment loads based on the RCM-GCMs climate inputs compared to the observed for the control period (1991-2010).

The PBIAS was however considered to be very good due to the fact the CCLM-MPI-ESM generally overestimate the extreme high and low rainfalls. In contrast to the CCLM-MPI-ESM, the SWAT simulation of the streamflows and sediment loads in the study area

using temperature and precipitation from the RCM-GCMs Ensemble mean was found to underestimate the streamflow and sediment loads, particularly for the rainy months of July, August and September (JAS). The underestimation of the peak streamflow and sediment loads is due to the effect of averaging the RCM-GCMs outputs without considering effects of possible mismatch of dry and wet days. SWAT simulation of streamflow based on inputs from RACMO22T-EARTH was however found to be satisfactory (Figure 6-7). Likewise inputs from HIRHAM5-EARTH resulted in satisfactory simulation of sediment loads in the study area by SWAT (Figure 6-8).

Comparable to the SWAT simulation of the streamflows, the simulated sediment loads based on the CCLM-MPI-ESM and the RCM-GCMs-ESM (Figure 6-8) downscaled climate series also performed poorly by respectively overestimating and underestimating the extreme events compared to that of the RCMs driven by the EARTH-GCM. This can be generally attributed to the fact that the generation and transport of sediment loads in the study area directly correspond to the high intense rainfall amounts and subsequent generation of runoff in the study area as explained in Section 5.5.2.

6.3.1 **Trends in Future Hydrology**

In other to assess the impact of the projected changes in the RCM-GCMs downscaled precipitation and temperature on streamflow and sediment loads in the study, the downscaled future (2031-2050) climate data was applied as inputs into the hydrological model, SWAT to simulate the impact of climate change on the hydrology of the White Volta Basin relative to the baseline period (1991-2010). The trend in the projected future hydrology (streamflow, surface runoff, actual evapotranspiration, AET, potential evapotranspiration, PET and sediment loads) of the study area was computed using Equation 3.4.2 and presented in Table 6-11. The mean annual values are presented in Apendix B.

The results of the projected future (2031-2050) water balance shows a general increase in the mean annual rainfall, surface runoff and actual evapotranspiration by all the RCM-GCMs, except the CCLM-MPI-ESM (Table 6-11) which shows a decline in all the components except the PET and sediment loads.

Similar to the precipitation projections, the surface runoff and actual evapotranspiration projections based on the RCM-GCMs simulated inputs showed mixed results. The effect of climate change on precipitation under scenario RCP4.5 and its impact on surface runoff and sediment loads is illustrated in Figure 6-9.

Table 6-11: Projected change in future (2031-2050) water balance components with reference to the control period (1991-2010) for the White Volta

Water Balance Parameters	CCLM-MPI-ESM		HIRHAM5-EARTH		RACMO22T-EARTH		RCM-GCMs_ESM	
	ΔRCP4.5 (%)	ΔRCP8.5 (%)	ΔRCP4.5 (%)	ΔRCP8.5 (%)	ΔRCP4.5 %)	ΔRCP8.5 (%)	ΔRCP4.5 %)	ΔRCP8.5 (%)
Precipitation	-6.7	-10.5	+9.4	+14.1	+6.3	+8.2	+3.9	+4.8
Water Yield	-11.6	-7.5	+56.5	+76.7	+39.7	+47.4	+31.2	+41.4
Surface Runoff	-4.3	-7.1	+49.3	+54.8	+29.8	+40.4	+32.3	+36.3
AET	-7.1	-11.5	+0.3	+3.8	+0.7	+2.1	-0.1	+1.1
PET	+5.6	+6.9	+4.5	+4.6	+5.2	+6.8	+5.2	+6.1
Sediment loads	+15.5	+11.3	+51.7	+52.9	+5.5	+15.4	+36.0	+32.0

Where + indicates an increase and – shows a decline.

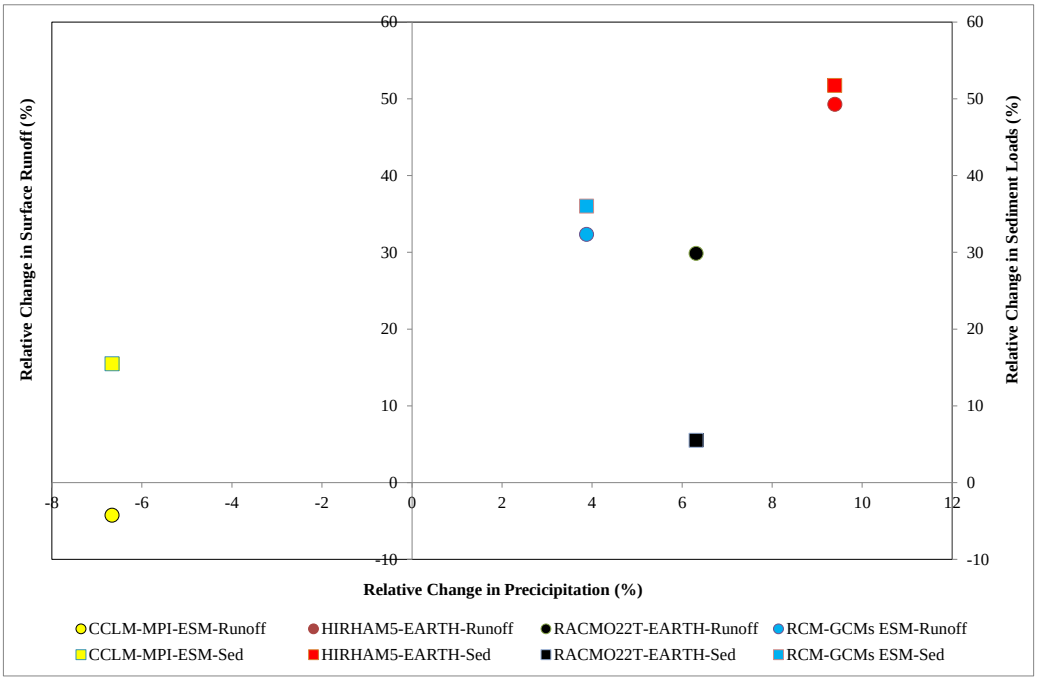

Figure 6-9: Impact of relative change in future (2031-2050) precipitation on surface runoff and sediment loads under RCP4.5. (Runoff – Surface Runoff and Sed–Sediment loads)

From Figure 6-9 it can be observed that an increase in future (2031-2050) precipitation, relative to the baseline (1991-2010), results in an increase in surface runoff and sediment loads for all the RCM-GCMs, except the CCLM-MPI-ESM. The CCLM-MPI-ESM projects a 6.7% decline in precipitation and a corresponding decline in surface runoff and evapotranspiration by 4.3% and 7.1% respectively under the RCP4.5 scenario. Sediment loads under the same scenario is however projected to increase by 15.5% in contrast to the current conditions whereby sediment loads in the study area directly relates to surface runoff.

Similarly, under the RCP8.5 scenario, surface runoff and evapotranspiration are projected to decline by 7.1% and 11.5% respectively whereas sediment loads are projected to increase by 11.3%. This contrasting relationship could be attributed to the fact that, the CCLM-MPI-ESM generally projects the extreme precipitation for (both wet and dry conditions), which may result in flooding and draughts. Draughts may potentially cause soils to become very dry, loose and easily erodible. Subsequent rainfall in the study area will convey the loss soils into the channel network.

Remarkably, the magnitude of change in the future (2031-2050) PET is similar for all the RCM-GCMs based simulations. All the RCM-GCMs showed an average increase of over 5% for the RCP4.5 scenario and 6% for the RCP8.5 scenario except HIRHAM5-EARTH in which PET increased by 4.5 and 4.6 for the RCP4.5 and RCP8.5 scenarios respectively. The less visible variation in the magnitude of change between the RCM-GCMs-SWAT simulated PET can be directly attributed to the bias correction of temperature which resulted in a temperature difference of 0.1 °C between the RCM-GCMs-simulated temperatures for the control period. The projected future temperature also showed less variation between the RCM-GCM models with a projected difference of 0.2 °C for the RCP4.5 scenario (Table 6-9).

Again, just as in the case of the precipitation projections by HIRHAM5-EARTH, RACMO22T-EARTH, and the RCM-GCMs-Ensemble mean, surface runoff and the corresponding sediment loads are projected to increase by 49.3% and 51.7% (HIRHAM5-EARTH), 29.8% and 5.5% (RACMO22T-EARTH), and 32.3% and 36% (RCM-GCMs-Ensemble mean) respectively under the RCP4.5 scenario (Table 6-11 and Figure 6-9). HIRHAM5-EARTH projects the highest rise in surface runoff and sediment loads by as much as 54.8% and 52.9% respectively under the RCP8.5 scenario whereas RACMO22T-EARTH forced by RCP4.5 scenario projects the least increase in surface runoff and sediment loads. The effect of climate change on precipitation under scenario RCP8.5 and its impact on surface runoff and sediment loads are presented in Appendix A.

The effect of climate change on precipitation under scenario RCP4.5 and its impact on surface runoff, actual evapotranspiration, AET, potential evapotranspiration, PET and sediment loads for all the RCM-GCMs are illustrated in Figure 6-10. The results for scenario RCP8.5 is presented in Appendix A.

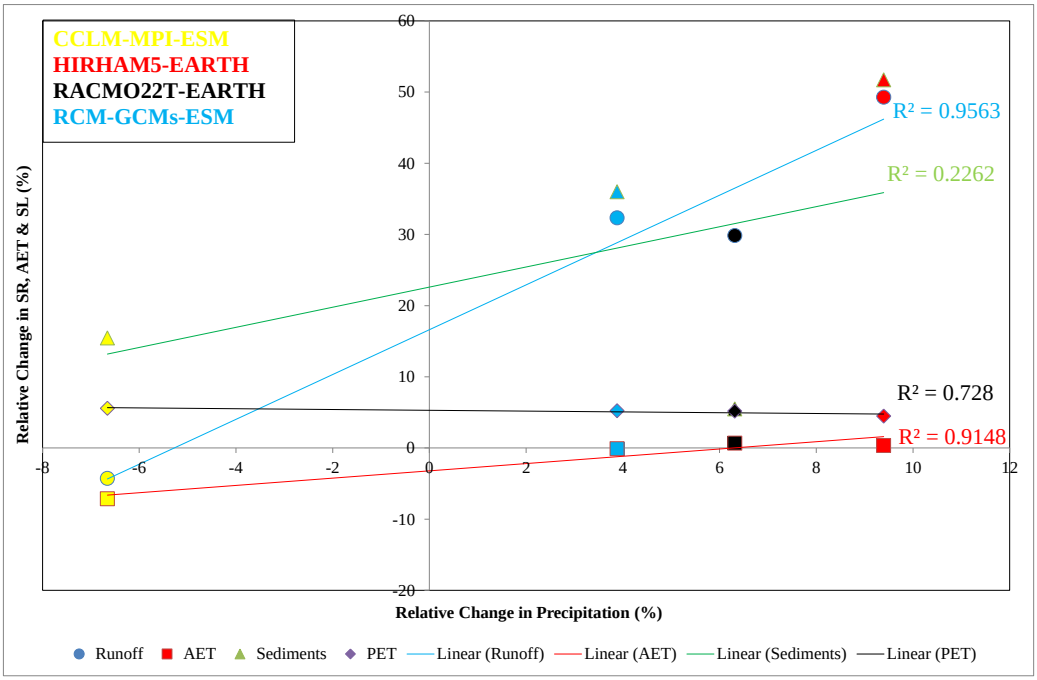

Figure 6-10: Impact of relative change in future (2031-2050) precipitation on surface runoff, actual evapotranspiration and sediment loads under RCP4.5. (Different symbols represent different water balance variables and different colors represent different RCM-GCMs).

From Figure 6-10 it can be observed that there is a proportional correlation between changes in precipitation with changes in surface runoff and actual evapotranspiration as projected by all the RCM-GCMs, albeit at different scales. The results show that, irrespective of the characteristics of the RCM-GCMs, there is over 90% likelihood that an increase in precipitation by 6% will result in a marginal increase in actual evapotranspiration by 0.7% whereas surface runoff is expected to increase by over 30% for the same level of change in precipitation. Similarly, sediment load is expected to increase by approximately 30% if precipitation increases by 6% in the future, although with a lesser certainty (less than 25%) of that occurring. Contrary to the surface runoff, AET and sediment loads, the results presented in Table 6-11 and Figure 6-10 shows that the basin's response to change in future PET by all the RCM-GCMs do not significantly correspond to changes in the precipitation irrespective of the RCM-GCM being applied for climate projection in the study area.

Generally, sediment loads in the study area is projected, based on all the RCM-GCMs simulated inputs, to increase by an average of 24.7% equivalent to 9.36×10^6 metric tons/yr under the RCP4.5 scenario and 26.3% equivalent to 9.49×10^6 metric tons/yr.

6.4 Conclusion

The results obtained in this chapter shows that due to climate change, temperature in the basin is projected to rise by 2.3 °C or 2.7 °C depending on the direction of the representative concentration pathways, RCPs. Precipitation is also projected to increase on average by 3.2% and 4.0% based on the RCP4.5 and RCP8.5 scenarios and consequently surface runoff is also projected to increase by 23.8% and 27.8% respectively. Actual evapotranspiration, AET in the basin is however projected to decline by 1.5% and 1.1% based on RCP4.5 and 8.5 respectively.

Finally, the results showed that due to climate change, future (2031-2050) projection of mean annual sediment loads in the White Volta Basin will increase by on average by 24.7% and 26.3% respectively based on RCP4.5 and RCP8.5 scenarios with reference to the baseline time period (1990-2010).

Chapter 7

7 ANALYSIS OF EXTREME PRECIPITATION

7.1 Introduction

The impact of climate change on sediment loads can be directly linked to the intensities of extreme precipitation in the study area. This is generally due to the fact that the generation of runoff, and consequently sediment loads, in the catchment is highly influenced by the intensities and amounts of precipitation. This chapter therefore focuses on analyzing the exceedance probabilities (or return periods) of extreme rainfall amounts by fitting a probability distribution to the long-term maximum daily rainfall for the peak months of July, August and September (JAS) at each climate station in the study area. The return levels of extreme precipitation precipitations for some selected return periods are then analyzed with regards to changes in the future climate.

7.2 Maxima Precipitation for July, August and September (JAS)

The annual rainfall amounts in the study area usually occur between May and October and peaking in August and/or September. The application of the peak-over threshold (POT) method results in the selection of at least 60 and at most 90 highest rainfall amounts for the JAS in the historical observations. Similarly, the maximum daily rainfall amounts for the months of JAS extracted from the RCM-GCMs-simulated precipitation for the present (1981-2010) and future (2031-2060) periods under the RCP4.5 scenario resulted in 90 maximum rainfall values extracted per station for each period and RCM-GCM ensemble.

7.3 Homogeneity Test

The homogeneity tests for the peak rainfall amounts for the historical observations for the Babile climate station is presented in Figure 7-1. The test for the other climate stations showed similar trend (see Appendix A). From Figure 7-1, it can be observed that the time series fluctuates around the mean value of 49 mm implying that there is no systematic pattern in the deviations and the time series can be considered to be homogeneous and independent. The p-value was also estimated to be 0.48 which is greater than the set significance level of 0.05.

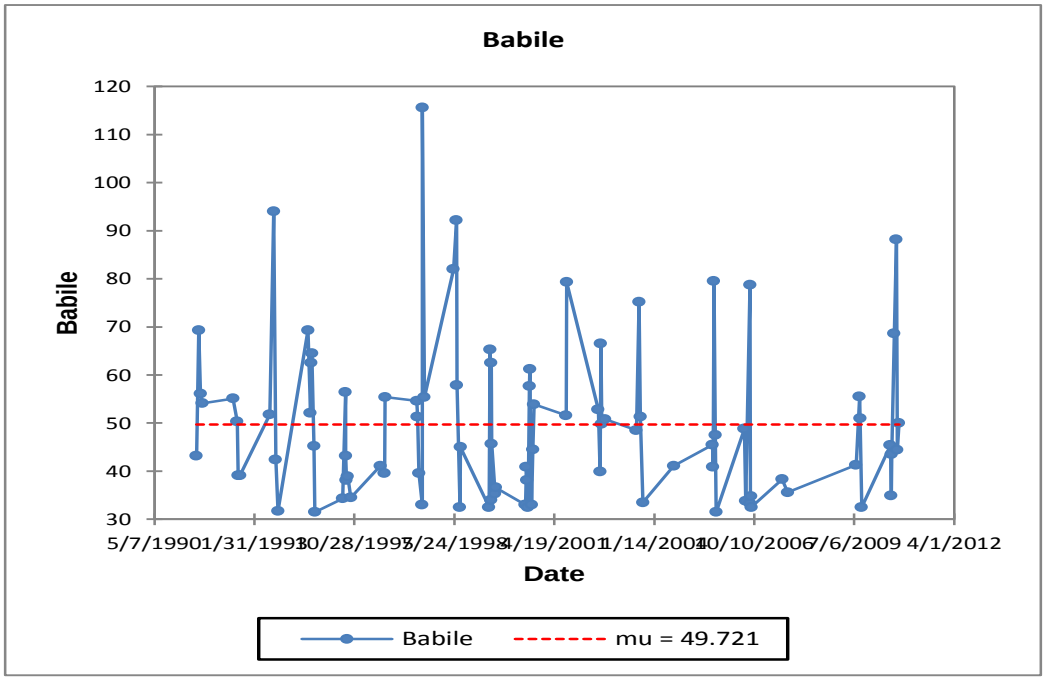

Figure 7-1: Homogeneity test for the historical extreme precipitation for JAS at the Babile climate station in the White Volta.

7.4 Fitting the Generalized Extreme Value, GEV Distribution

This section presents the results of fitting the four 3-parameter probability distributions namely; the generalized extreme value, GEV, the Pearson Type III, the Log-Logistic (3) and Lognormal (3P) functions to the annual extreme precipitation of the historical and the RCM-GCMs projected extreme precipitation for JAS in the selected climate stations.

The results of the best fitted probability distribution function based on the Anderson-Darling test statistic for the historical observations and the corresponding estimated parameters for each climate station in the study area is summarized in Table 7-1. The results in Table 7-1 show that the Log-Logistic (3P) is the best fitted distribution for majority of the climate stations in the study area.

The Q-Q plot for the best fitted probability distribution (Log-Pearson 3) for the historical observations for the Babile climate station is presented in Figure 7-2. It can be observed in Figure 7-2 that the Log-Pearson Type III distribution fits well the historical extreme precipitations for the JAS months. Similar trends, albeit with different distributions were observed for the other stations (see Appendix A). The results in Table 7-1 and e.g. Figure 7-2 shows that all the fitted probability distributions based on the Anderson-Darling test at the significance level of 0.05 were acceptable as the best fitted probability distributions

for the climate stations in the study area. The extreme value analysis, EVA was also performed for all the RCM-GCMs-simulated maximum daily precipitation for the JAS for the present (1981-2010) and the future (2031-2060) under the RCP4.5 scenario.

Table 7-1: Fitted probability distributions for the control (1991-2010) run of CCLM-MPI-ESM under RCP4.5 in the White Volta

Station	Distribution	Anderson-Darling Test	Parameters
Babile	Log-Pearson 3	0.311	a=-9.14 b=0.099 g=2.96
Bui	Gen. Extreme Value	0.474	k=0.213 s=11.2 m=37.0
Fada	Gen. Extreme Value	0.495	k=0.045 s=10.7 m=38.7
Manga	Log-Pearson 3	0.436	a=7.55 b=0.138 g=2.92
Navrongo	Log-Pearson 3	0.274	a=52.1 b=-0.048 g=6.38
Ouaga	Log-Logistic (3P)	0.304	a=4.23 b=29.4 g=8.4
Ouahi	Gen. Extreme Value	0.181	k=0.042 s=9.96 m=36.7
Pong	Log-Logistic (3P)	0.279	a=4.66 b=44.2 g=4.86
Tamale	Gen. Extreme Value	0.195	k=-0.041 s=16.0 m=41.5
Vea	Log-Logistic (3P)	0.459	a=3.98 b=32.9 g=11.9
Zuarungu	Log-Logistic (3P)	0.822	a=6.73 b=61.0 g=-13.2

Anderson-Darling test critical value for the null hypothesis to be rejected = 2.5 at α=0.05 significance level

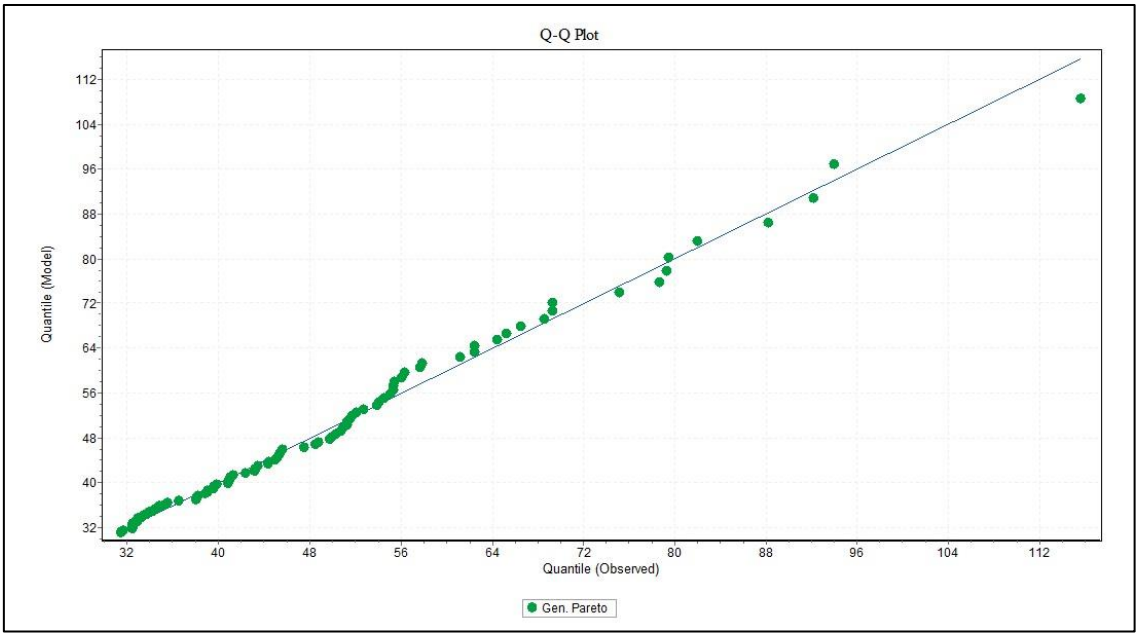

Figure 7-2: Q-Q plot of the Log-Pearson III distribution fitted to the maximum daily rainfall for JAS in historical observations, Babile climate station.

7.5 Exceedance Probability (Return Period) and Climate Scaling Factor

After determining the best fitted probability distribution for the selected climate stations in the study area, the probability of occurrence, which is defined as the probability of an event of a specified magnitude being equaled or exceeded during the specified period was computed and the results presented in Table 7-2 and 7-3 and Appendix B. The return levels of rainfall events estimated for return periods (2-200 years) from the historical observations (1991-2010) and the RCM-GCMs-simulated precipitation forced by the RCP4.5 scenario for the present (1981-2010) and future (2031-2050) are presented in Table 5-15 and 5-16 for the historical observations and the CCLM-MPI-ESM forced by RCP4.5 respectively.

Table 7-2: Computed return levels for selected return periods based on extreme rainfall events (JAS) for the control period (1991-2010) of the historical observations.

Return Period	Return Levels (mm)										
	Babile	Bui	Fada	Manga	N'go	Ouaga	Ouahi	Pong	T'le	Vea	Z'ngu
2	45.2	41.3	42.7	50.2	48.1	37.8	40.4	49.1	47.3	44.8	47.8
5	61.8	56.8	55.3	70.7	63.7	49.2	52.1	64.4	64.7	58.5	61.8
10	73.0	69.3	64.1	87.0	73.2	57.9	60.2	75.7	75.8	69.0	71.4
20	83.0	83.3	72.7	105.0	81.7	67.4	68.2	88.0	86.1	80.8	81.3
30	88.5	92.7	77.9	116.0	86.5	73.8	73.0	96.1	92.1	88.7	87.6
50	94.7	105.0	84.3	131.0	92.0	82.2	78.9	107.0	99.0	99.3	95.6
100	103.0	124.0	93.3	154.0	99.3	95.6	87.2	123.0	108.0	116.0	108.0
200	110.0	147.0	103.0	179.0	106.0	111.0	95.8	143.0	117.0	136.0	121.0

Table 7-3: Computed return levels for selected return periods based on extreme rainfall events (JAS) for the present period (1981-2010) for CCLM-MPI-ESM forced by RCP4.5.

Return Period	Return Levels (mm)										
	Babile	Bui	Fada	Manga	N'go	Ouaga	Ouahi	Pong	T'le	Vea	Z'ngu
2	25.4	31.9	42.5	38.0	40.2	33.3	34.4	39.5	39.2	39.4	43.4
5	45.2	57.7	59.4	62.3	65.2	51.2	52.3	66.9	63.2	57.7	60.8
10	60.3	75.0	69.0	80.8	83.2	64.0	63.4	87.0	79.0	68.1	71.7
20	76.4	91.9	77.3	101.0	102.0	77.1	73.5	108.0	94.2	76.9	82.3
30	86.7	102.0	81.7	114.0	113.0	85.1	79.2	121.0	103.0	81.7	88.6
50	99.6	114.0	86.7	130.0	127.0	95.1	85.7	137.0	114.0	86.9	96.4
100	119.0	131.0	92.9	155.0	148.0	110.0	94.3	162.0	128.0	93.5	108.0
200	141.0	148.0	98.5	183.0	170.0	125.0	102.0	188.0	143.0	99.4	119.0

Manga=Manga Bawku, Fada=Fada Ngourma, N'go=Navrongo, Ouaga=Ouagadougou, Ouahi=Ouahigouya, Pong=Pong Tamale, T'=Tamale and Z'ngu=Zuarungu

The climate scaling factor (Sanderson, 2010), which was adopted and applied to the estimated extreme return levels of rainfall for the selected return periods was computed and

evaluated in this section. The results generally show that, as the return period increases, the magnitude of extreme precipitation amounts is also expected to increase. This trend was observed at all the climate stations for all the RCM-GCMs simulated extreme precipitation values for the selected return periods. The results obtained for the future change in return levels for selected return periods are presented in Figure 7-3 for the Babile climate station. The other climate stations in the study area generally showed similar trends to the Babile climate station. It can be observed in Figure 7-3 that the magnitude of extreme rainfall depths generally increased for return periods compared to what currently pertains in the study area. The CCLM-MPI generally showed the least change in the future return levels for a given return period. For example, the 1 in 100 year return period at Babile which currently yields a return level of 103.0 mm is projected by the CCLM-MPI-ESM to increase to 105.6 mm (Figure 7-3) for the same return period. This represents a 3% increase in the future extreme precipitation amount for the same recurrence interval as at the present period. Similarly, the HIRHAM5-EARTH and RAMCO22T-EARTH projects an increase in the future extreme precipitation depth by as much as 17% and 8% respectively for all the recurrence intervals at the Babile climate station.

The projected changes in the magnitude and frequency of extreme rainfall events in the study area have direct impact on the generation and transport of sediment loads. For instance, whereas CCLM-MPI-ESM projects a decline in future precipitation and runoff by 6.7% and 4.3% respectively (Table 6-11), sediment loads are projected to increase by 15.5%. This can be explained by the fact that, high intensity rainfall events with short duration have the potential to increase soil erosion in the basin. Consequently, a projected decline in annual rainfall amount by CCLM-MPI-ESM, coupled with a projected increase in the magnitude of extreme rainfall events for the same recurrence interval as pertains presently implies that more water will be expected in the future for a relatively shorter interval. This high intensity but short duration rainfall events can potentially cause an increase the erosion of soils resulting in an increase of sediment loads in the study area.

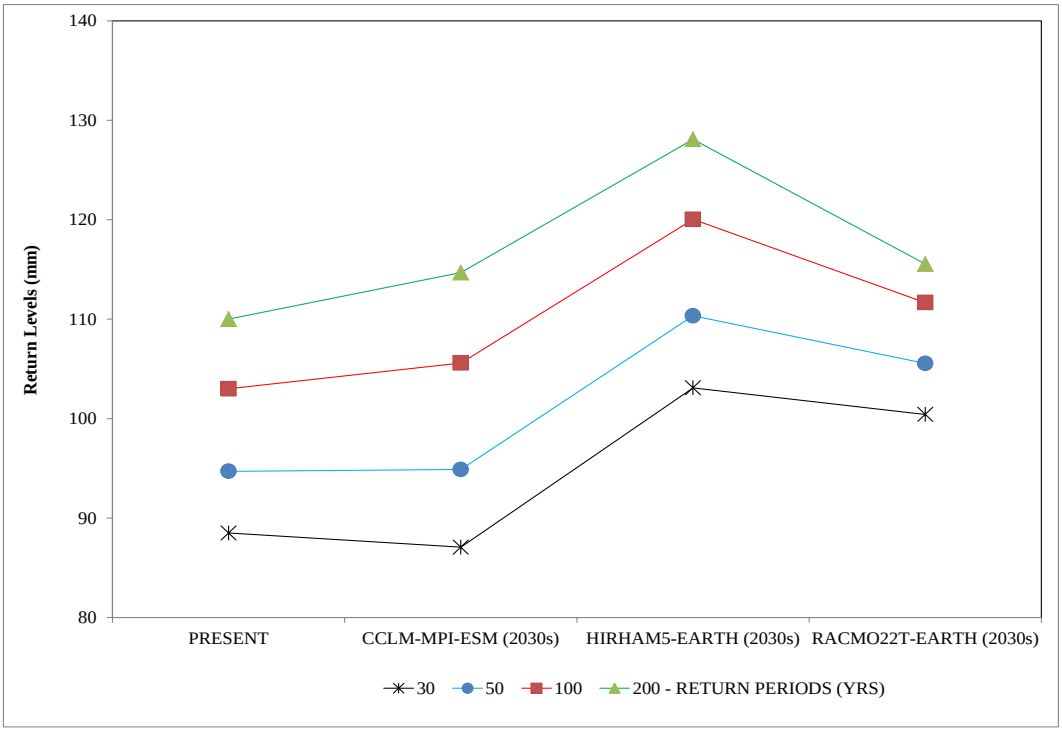

Figure 7-3: Future changes in the JAS extreme return levels for selected return periods at Babile climate station.

7.6 Spatial Distribution of Changes in Return Levels

A second analysis of the changes in the future projected extreme precipitation amounts was performed to evaluate the spatial variability of the changes in the return periods in the study area. Spatial analysis of the changes can provide detail information about the patterns and direction of the future extreme rainfall events and its impact on sediment loads in the study area. The spatial distribution of the 30-year return period was analyzed by taking the relative difference between the return levels as projected by the RCM-GCMs and that of the historical observations using Equation 3.4.2. The spatial pattern of the future changes in return levels for the 30-year return period as projected by the RCM-GCMs was analyzed by performing a simple kriging.

The results of the spatial distribution of the projected changes in the return levels and the corresponding impact on the future changes in the watershed parameters such as actual evapotranspiration, streamflow and sediment loads for the CCLM-MPI-ESM, HIRHAM5-EARTH and RACMO22T-EARTH are presented in Figures 7-4, 7-5 and 7-6 respectively.

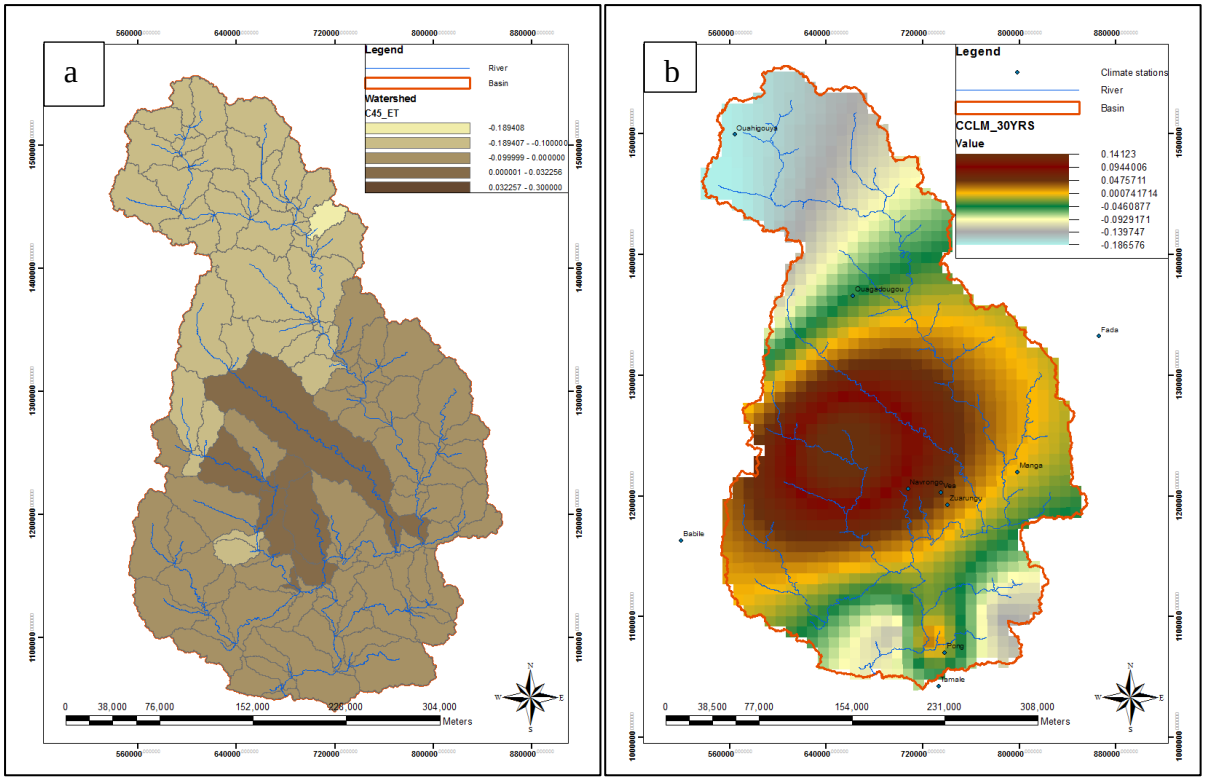

Figure 7-4: Spatial distribution of future change in (a) extreme rainfall events and (b) AET for a 1 in 30 year return period based on CCLM-MPI-ESM simulations forced by RCP4.5.

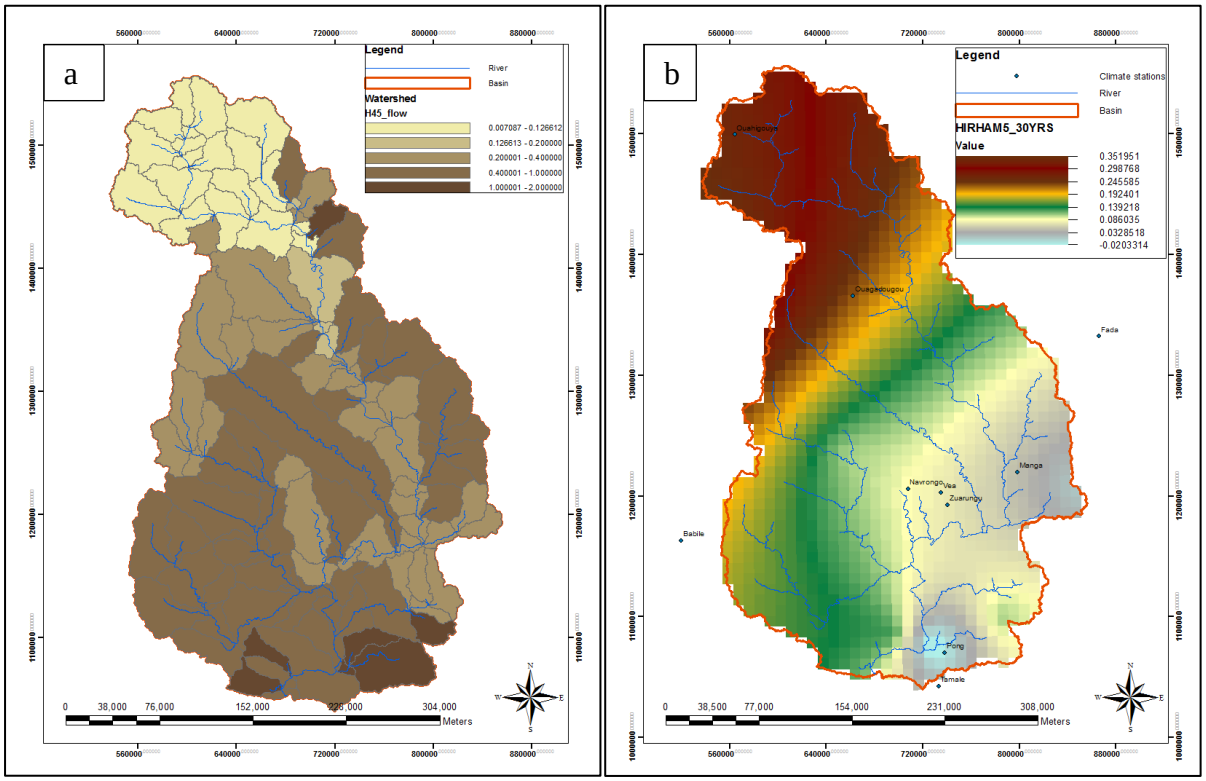

Figure 7-5: Spatial distribution of future change in (a) extreme rainfall events and (b) streamflow for a 1 in 30 year return period based on HIRHAM5-EARTH simulations forced by RCP4.5.

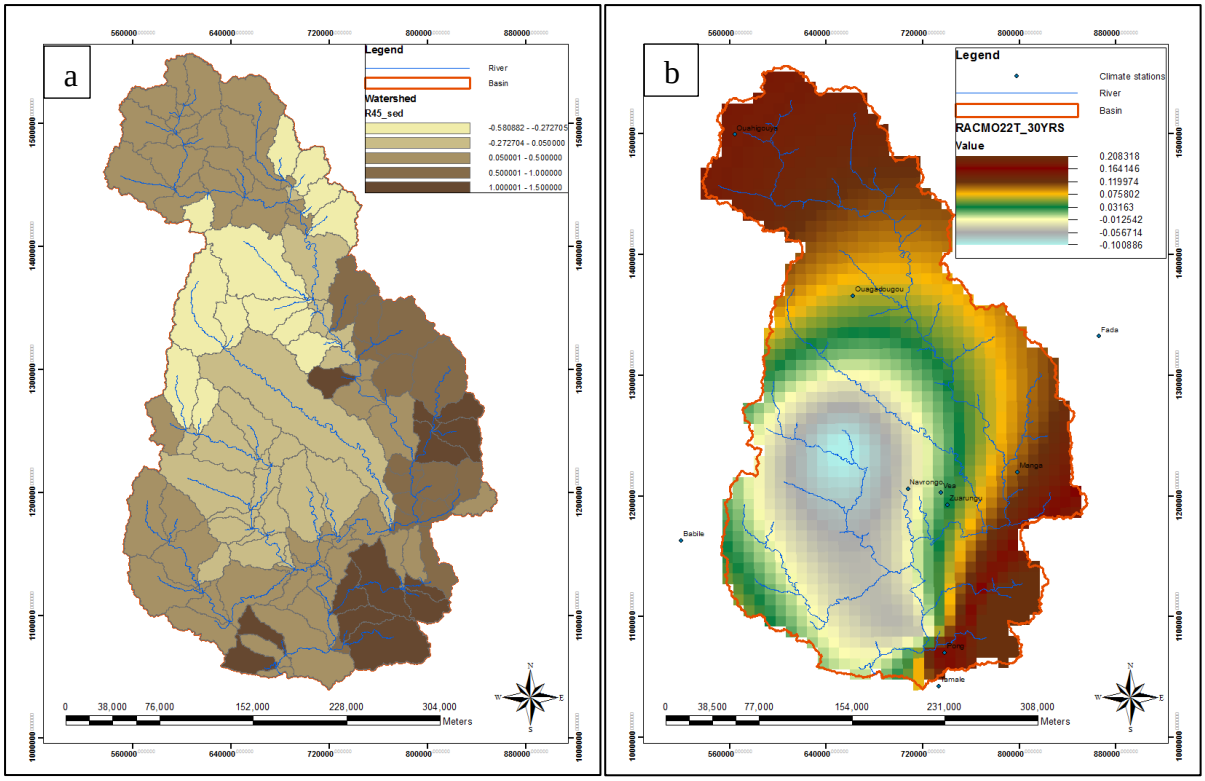

Figure 7-6: Spatial distribution of change in (a) extreme rainfall events and (b) sediment loads for a 1 in 30 year return period based on RACMO22T-EARTH simulations forced by RCP4.5.

The results of the spatial analysis of the distribution of changes in the future return levels, actual evapotranspiration, streamflows and sediment loads generally showed similar patterns. For the purposes of analysis, the results for the projected changes in the future extreme rainfall events by all the RCM-GCMs forced by RCP4.5 are presented here. However, only actual evapotranspiration, streamflows and sediment loads for the CCLM-MPI-ESM, HIRHAM5-EARTH and RACMO22T-EARTH all forced by RCP4.5 are respectively presented here. The other results are presented in Appendix A.

The pattern of relative change in the future extreme precipitation depths for the 30-year return period as projected by HIRHAM5-EARTH under the RCP4.5 (Figure 7-5) shows increasing return levels roughly along the southeast to the northwest direction and this is reflected in the spatial distribution of streamflows in the basin except at the extreme north. Although, HIRHAM5-EARTH forced by RCP4.5 projects a future increase in the annual precipitation amount by 9.4% (Table 6-11) and coupled with a projected increase in extreme rainfall events, the streamflows in the extreme north will marginally change due to the fact that the area is mostly made up of rivulets which generally dry up a few hours after a major rainstorm event.

The patterns of the change in the future extreme rainfall events for the 30-year return period as projected by CCLM-MPI-ESM and RACMO22T-EARTH (Figure 7-4 and 7-6 respectively) are rather complex. Whereas CCLM-MPI-ESM projection shows a pronounced rise in the magnitude of the extreme rainfall events in the central part of the basin for the 1 in 30-years return period, RACMO22T-EARTH projection shows a decline in the magnitude of the return levels for the mid-sections of the basin. This is directly reflected in the spatial distribution of future actual evapotranspiration and sediment loads in the basin.

As can be observed in Figure 7-6(a), RACMO22T-EARTH projects an increase in the magnitude of extreme rainfall events for the 30-year return period in the extreme north and south-eastern part of basin. This has clearly influenced the change in future distribution of sediment loads (Figure 7-6(b)) in the basin which follows a similar pattern indicating a direct linkage between the changes in extreme precipitation and sediment loads.

Similarly, it can be observed in Figure 7-4 (a) and (b) that except in the mid-sections of the basin, extreme rainfall events and actual evapotranspiration are projected by CCLM-MPI-ESM to decline as earlier observed in Section 6.3.1.

7.7 Conclusion

Extreme value analysis of maximum precipitation for the wet months of July, August and September showed that the magnitude of extreme rainfall events are likely to increase in the future with direct consequence for the generation of streamflow and soil erosion in the basin. For example, the 1 in 100 year return period at Babile which currently yields a return level of 103.0 mm is projected by the CCLM-MPI-ESM to increase to 105.6 mm (Figure 5.13) for the same return period. This represents a 3% increase in the future extreme precipitation amount for the same recurrence interval as at the present period. Similarly, the HIRHAM5-EARTH and RAMCO22T-EARTH projects an increase in the future extreme precipitation depth by as much as 17% and 8% respectively for all the recurrence intervals at the Babile climate station.

Chapter 8

8 GENERAL CONCLUSIONS AND RECOMMENDATIONS

8.1 Introduction

This chapter presents a general discussion relating all the findings of the study, stating the significance of the results to decision making and policy formulation, drawing conclusions and making recommendations for future studies and for informed decision making.

The White Volta Basin is one of the major subbasin of the Volta Basin and plays a pivotal role in the socio-economic development of the people who are predominantly rural and relies heavily on the water resources of the basin. Many socio-economic trends in the basin suggest that the pressure on the natural resources is likely to grow over the coming years. The most notable are: fast population growth and urbanization; growing demand for food; growing demand for water for agriculture, energy and households; high dependence of biofuels for energy, and; rapid growth in livestock numbers. These factors are likely to combine with climate change to pose a real threat to sustainable development of the basin and the integrity of its natural resources. Implementing adaptation measures such as water and soil conservation and reduction in the rate of deforestation as well as adapting appropriate watershed management practices will play a pivotal role in managing the impacts of climate change on streamflow and sediment loads in the basin.

8.2 Correction Factor for Correcting Surface Dip Underestimation

The effects of underestimating suspended-sediment concentration obtained from a suspended-sediment sample collected from the water surface using the surface dip method of sampling can be corrected by applying a correction factor obtained through depth integrated sampling. In this study, suspended-sediment samples were simultaneously collected by using a depth integrated sampler and the surface dip method. A correction factor for the study area was then determined by computing the ratio of the average concentration of cross-section samples (depth-integrated samples) to the average concentration of surface dip samples. An average correction factor that can be applied to account for underestimation due to sampling by the surface dip method in the White Volta Basin was found to be 1.34 (i.e. 34%).

The surface dip method of sampling will likely continue to be deployed as the major method of sampling suspended-sediment concentration in the study area due to the fact that

the White Volta Basin is shared between two developing countries, Ghana and Burkina Faso where there is computing demands for scarce resources. A correction factor of 34% can therefore be applied to correct underestimation of suspended-sediment concentration in the White Volta Basin whenever the surface dip method of sampling is deployed.

8.3 Deriving Long-Term Sediment Loads from Turbidity

The cost of collecting sediment data in a developing country can be a daunting task with very limited resources in terms of human, financial and technology. However, the collection and analysis of suspended-sediment data are a very necessary part of investigations to evaluate impact of climate change on suspended-sediment loads in the White Volta Basin.

The collection of suspended-sediment data in the White Volta Basin in particular and the Volta Basin in general has been sporadic and at best project/program demand driven. The use of the surrogate methods of generating long-term suspended-sediment data using turbidity and/or river discharge was therefore explored. Continuous turbidity data collected by GWCL as part of their water quality assessment requirement was calibrated with measured SSC data and used to estimate long-term time-series of suspended sediment loads for the White Volta Basin at Nawuni. A simple linear regression, SLR model relating turbidity and the measured SSC data was derived.

With the challenge of developing sustainable and continuous SSC sampling due to lack of resources, sediment rating curves based on continuously monitored turbidity by GWCL provides a better option of computing long-term suspended-sediment loads in the country. The developed sediment rating curves can be bi-annually updated with detailed sampling of SSC. Based on the analysis of the SLR and NMR models, the simple-linear regression, SLR model was selected for the White Volta Basin on the basis of the relationship between the base-10 logarithmic transformation of turbidity and SSC.

The mean annual suspended sediment load for the White Volta Basin at Nawuni was estimated to be 5.68×10^6 metric tonnes per annum. Although the estimated sediment loads for the White Volta Basin can be considered to be relatively low compared with other rivers, the results provide a valuable basis for assessing the potential impact of climate change on sedimentation of the Volta Lake.

8.4 Streamflow and Sediment Load Modeling using SWAT

The Soil and Water Assessment Tool (SWAT) was calibrated at Nawuni and validated at Nasia, Pwalugu and Nawuni in the White Volta Basin. The calibration and validation of the model at Nawuni focused on the periods of 1991–2003 and 2004–2013, respectively. Spatial validation was performed at Pwalugu and Nasia for the periods 1994-1995 and 2012-2013. Calibration and validation were completed by comparing time-series model results to observed daily and monthly mean streamflows and sediment loads. Key considerations in the SWAT model calibration were the overall water balance, the peak-flows to low-flow distribution and seasonal variation. Five model performance criteria for goodness of fit were used to evaluate the model performance during calibration and validation. The criteria used to evaluate the performance of the SWAT model includes graphical comparison, coefficient of determination, R^2, the index of agreement, *IA*, Nash-Sutcliffe efficiency, *NSE* and percent bias, *PBIAS*.

The calibrated White Volta SWAT model showed a good performance in reproducing the annual, monthly and daily streamflow and sediment loads of the basin. The calibration of SWAT for the White Volta at Nawuni and the validation processes for the two sub-catchments of the basin at Pwalugu on the main White Volta and Nasia, a tributary reveal a realistic simulation of the hydrology of the watershed.

Generally, the streamflow calibration shows a better agreement between the simulated and observed time series than that of the sediment loads calibration. The monthly streamflow calibration shows the best agreement between the observed and simulated with a *NSE* of 0.82, followed by annual and daily with *NSE* of 0.80 and 0.76 respectively. In the case of the sediment load calibration the daily sediment loads shows the best agreement between the simulated and observed with *NSE* of 0.77, followed by the monthly and annual with *NSE* of 0.74 and 0.67 respectively. Generally, the model overestimated the streamflow and underestimated the sediment loads during the model calibration.

Similarly, the model performed better during the monthly streamflow validation process at Nawuni with a NSE of 0.88 (daily-NSE=0.70). The validation of the sediment loads follows the same trend with the monthly validation having a NSE of 0.68 (daily-NSE=0.63). Contrary to the validation process at Nawuni, the spatial validation of the model at Pwalugu and Nasia had a better agreement between the simulated and observed sediment loads than the streamflow. The NSE for the streamflow validation at Pwalugu was found to be 0.72 and that of Nasia 0.63. On the other hand the NSE for the sediment loads was found to be 0.83 and 0.97 for Pwalugu and Nasia respectively.

The simulated water balance of the White Volta Basin reveals that approximately 85% of the mean annual rainfall actually evapotranspired with over 13% contributing to the mean annual water yield. The mean annual sediment load that is transported out of the White Volta Basin watershed outlet at Nawuni is estimated to be over $5x10^6$ metric tonnes per annum.

The application of models in general has several limitations. However, models can serve as a means of understanding the underlying processes that are oftentimes difficult if not impossible to measure. The results from the model calibration and validation showed that, the SWAT model can reliably predict the streamflow and sediment loads with satisfactory results and can therefore be used as a tool for analysing the hydrological processes and sediment transport in the White Volta Basin.

8.5 Impact of Climate Change on Streamflow and Sediment Load

The White Volta Basin is one of the major tributaries of the Volta Basin and plays a pivotal role in the socio-economic development of Ghana and Burkina Faso whose people are predominantly rural and relies heavily on the water resources of the basin. Many socio-economic factors put pressure on the natural resources of the basin and would likely increase over the coming years. These factors are likely to combine with climate change to pose a real threat to sustainable development of the basin and the integrity of its natural resources.

The simulated water balance of the White Volta Basin reveals that approximately 85% of the mean annual rainfall actually evapotranspired with over 13% contributing to the mean annual water yield. However due to climate change, temperature in the basin is projected to rise by 2.3 °C or 2.7 °C depending on the direction of the representative concentration pathways, RCPs. Precipitation is also projected to increase on average by 3.2% and 4.0% based on the RCP4.5 and RCP8.5 scenarios and consequently surface runoff is also projected to increase by 23.8% and 27.8% respectively. Actual evapotranspiration, AET in the basin is however projected to decline by 1.5% and 1.1% based on RCP4.5 and 8.5 respectively.

The mean annual sediment load that is transported out of the White Volta watershed outlet at Nawuni is estimated to be over $5x10^6$ metric tonnes per annum. The results of the future (2031-2050) climate change projection showed that the mean annual sediment loads in the White Volta Basin will increase by 24.7% and 26.3% respectively based on RCP4.5 and RCP8.5 scenarios with reference to the baseline time period (1990-2010).

8.6 Impact of Extreme Rainfall on Streamflow and Sediment Load

Extreme value analysis of maximum precipitation for the wet months of July, August and September showed that the magnitude of extreme rainfall events are likely to increase in the future with direct consequence for the generation of streamflow and soil erosion in the basin. For example, the 1 in 100 year return period at Babile which currently yields a return level of 103.0 mm is projected by the CCLM-MPI-ESM to increase to 105.6 mm (Figure 5.13) for the same return period. This represents a 3% increase in the future extreme precipitation amount for the same recurrence interval as at the present period. Similarly, the HIRHAM5-EARTH and RAMCO22T-EARTH projects an increase in the future extreme precipitation depth by as much as 17% and 8% respectively for all the recurrence intervals at the Babile climate station.

The differences in the results of the climate projections by all the selected RCM-GCMs used in this study and also based on other reported research conducted in the Volta Basin requires a holistic approach in adopting and/or developing a climate model that best describes the physical dynamic of climate in this region.

8.7 Other studies in the Volta Basin

The results presented in this study differs from Kwabena Kankam-Yeboah *et al.* (2013) who used SWAT coupled with an ensemble of two global climate models (ECHAM4/CSIRO) based on the IPCC SRES A1FI projections to estimate the impact of climate change on streamflow in the White Volta. Kwabena Kankam-Yeboah *et al.* (2013) reported a reduction in the mean annual rainfall for the 2020s (2006–2035) and 2050s (2036–2065) of 12.3% and 19.6%, respectively relative to the baseline (1961–1990) and a corresponding reduction in the mean annual streamflow by 22% and 50% for the 2020s and 2050 respectively. They also reported an increase of 0.6 and 1.9% in the mean annual temperature for the 2020s and 2050s respectively relative to the baseline (1961-1990).

Significantly, the results of this study which project an increment in rainfall and streamflow is in agreement with Awotwi *et al.* (2015). Awotwi *et al.* (2015) in their study, predicting hydrological response to climate change in the White Volta Catchment, used SWAT also driven by downscaled climate series from ECHAM4 using REMO. They reported an increase in future (2030-2043) precipitation and temperature of 8% and 1.7% respectively, with a corresponding 26% and 24% increase in surface runoff and baseflow respectively (Awotwi *et al.*, 2015).

The results from this study predict a projected future (2031-2050) increase in streamflow of 23.8% and 27.8% for a corresponding marginal increase of 3.2% and 4.0% in mean annual rainfall based on the RCP4.5 and RCP8.5 scenarios respectively. This prediction is reasonable considering the fact that ET is projected to decline by 1.5% and 1.0% for the RCP4.5 and RCP8.5 respectively. The decline in ET agrees with Kasei (2009) who also predicted a decrease of 4% and 7% using WaSiM coupled with REMO for the A1B and B1 scenarios respectively. According to Martin (2005), ET in the White Volta Basin is estimated to range between 70-87% of the total mean annual rainfall (Martin, 2005). This can partly be attributed to availability of more water and high temperatures in the basin. With projected decline in ET it is expected that any marginal increase in rainfall will result in excess surface runoff volumes in the basin.

The projected future (2031-2050) increase in sediment loads in the study area is quite significant for the development and management of reservoirs in the basin. Milliman and Syvitski (1992) estimated the sediment loads for the entire Volta Basin prior to the construction of the Akosombo hydro-electric dam to be $19x10^6$ metric tonnes per annum. Similar to Akrasi (2005), who estimated sediment loads in the White Volta Basin to be $4x10^6$ metric tonnes per annum, the sediment loads in the present study for the baseline period (1990-2010) was estimated to be $8.20x10^6$ metric tons/yr.

8.8 Recommendations

Suspended sediment can have adverse impact on domestic and irrigation water supply, aquatic life, recreation, flood control, transportation, and hydro-power generation in the White Volta Basin. Accurate estimation of suspended sediment in the basin is therefore very important for sustainable planning, development and management of the water resources in the basin.

In this study, effort was made to develop a coefficient/correction factor to correct underestimation associated with surface dip in the White Volta Basin. The depth integrated sampling data used in developing the coefficient/correction factor, although covered the entire range of the hydrograph, were few for all the stations. It is therefore recommended that more samples using depth integrated method of sampling suspended-sediment should be collected simultaneously with the surface dip sampling for a more accurate estimation of the surface dip correction factor.

Currently, the opportunity exists in the White Volta Basin to compute long-term suspended sediment based on the fact that GWCL is continuously monitoring the turbidity of the White Volta Basin at Nawuni. It is therefore recommended that SSC measurements should be undertaken at least twice a year to continuously update the sediment rating curve.

The quality of the output of any hydrological model depends largely on the inputs driving the model and the measured variables used in the calibration of the model. The quality of the outputs from the calibrated White Volta SWAT model depends on the quality of the input climate data and the quality of the discharge measurement in the basin. Except the rainfall input data and to some extent the temperature stations, which were fairly distributed in the basin, the other inputs e.g. wind speed, solar radiation and relative humidity where available in only a few of the climate stations. Furthermore, climate data from some of the climate stations have missing records and were therefore filled by the weather generator in SWAT. The White Volta Basin also has several discharge stations but records from these stations are mostly unreliable and have several gaps ranging from one day to a decade. Due to competing demands for resources, it is recommended that priority selected stations in the basin should be equipped and maintained to obtain accurate and continuous records rather than spreading the limited resources thin to collect data from several stations that cannot be meaningfully used.

Finally, with the projected climate change scenarios pointing to increases in mean annual rainfall and surface runoff in the White Volta Basin and a corresponding increase of over 70% of sediment loads, managers of the White Volta Basin should begin to draw out strategies and action plans that will mitigate these challenges for sustainable utilization of the water resources in the basin. This involves the development of climate change adaptation policies gear towards the adaption of innovative technologies. The following recommendations are made for the management of the White Volta Basin and further research:

1. Currently there is no legislation or regulatory framework on sediments at the local, national, or trans-boundary levels. Generally, sediment issues in the basin are mostly classified as a water quality and/or water degrading agent in most water resources related frameworks. Inadequate attention to the sustainable management of sediments in the basin due to the cursory inclusion of sediments in a generic policy and legislation can present unintended cost implications to the riparian countries and the environment. With current concomitant effects on climate and land use changes on

sediments in the basin, there is the urgent need to develop a comprehensive legislation and regulatory framework for the sustainable management of sediments in the basin.

2. The variability of land use/land cover is known to play a vital role in the hydrology and sediment transport of a watershed. However, the impact of land use change on the streamflows and sediment loads in the White Volta Basin was not investigated. Furthermore, future scenarios on the impact of climate change on the streamflows and sediment loads were conducted with current land use/land cover maps, and this could lead to errors in projections. It is therefore recommended that projected simulations of the combine effects of climate and land use/land cover change in the basin should be desirable for sustainable management and development of the water resources in the basin.
3. The impact of the Bagre dam and the proposed Pwalugu dam in Ghana should be investigated in conjunction with the effects of climate change on the streamflows and sediment loads in the White Volta basin. Additionally, the impact of the Bagre dam on river bank erosion coupled with the impact of climate cange and land use changes should be investigated.
4. The results of the extreme rainfall analysis under the impact of climate projections in this study suggest that designers of hydraulic structures in the basin should consider the impact of climate change in their designs due to rising extreme events and declining recurrence intervals observed in this research.

REFERENCE

Abbaspour, K.C. Rouholahnejad E., Vaghefi S., Srinivasan R., Klöve B., (2014) Modeling hydrology and water quality of the European Continent at a subbasin scale: calibration of a high - resolution large - scale SWAT model. Journal of Hydrology, 524:733-752. http://www.sciencedirect.com/science/article/pii/S0022169415001985.

Abbaspour, K.C., Yang J., Maximov I., Siber R., Bogner K., Mieleitner J., Zobrist J., and R. Srinivasan. (2007). Modeling hydrology and water quality in the pre-alpine/alpine Thur watershed using SWAT. J. Hydrol. 333(2-4): 413-430.

Agyare, W. A. (2004). Soil characterization and modeling of spatial distribution of saturated hydraulic conductivity at two sites in the Volta Basin of Ghana. Doctoral thesis. Ecology and Development Series No. 17, 2004. www.fachschaft-agrar.uni-bonn.de.

Ajayi, A. E., Vlek, P. L. G., Denich, M., Martius, C., van de Giesen, N., (2004). Surface runoff and infiltration processes in the Volta Basin, West Africa: Observation and modeling. Ecology and Development Series No. 18, 2004. p2.

Akhavan, S., (2010). Application of SWAT model to investigate nitrate leaching in Hamadan-Bahar Watershed, Iran, Agriculture, Ecosystems and Environment.

Akinsanola, A. A., Ogunjobi K. O., Gbode I. E. and Ajayi V. O., (2015). Assessing the capabilities of three Regional Climate Models over CORDEX-Africa in simulating West African Summer Monsoon Precipitation. Advances in Meteorology, vol 2015. hppt://dx.doi.org/10.1155/2015/935431.

Akrasi, S. A., (2005). The assessment of suspended sediment inputs to Volta Lake. Lakes & Reservoirs: Research and Management 10: 179–186.

Akrasi, S.A., (2011). Sediment Discharges from Ghanaian Rivers into the Sea. W. African J. of Applied Ecology.ISSN:0855-4307. www.ajol.info/index.php/wajae/article/view/70320.

Alansi. AW, M.S.M. Amin, G. Abdul Halim, Shafri, H.Z.M, Thamer A.M, A.R.M, Waleed, W. Aimrun and M. H. Ezrin. (2009). The Effect of Development and Land Use Change on Rainfall-Runoff and Runoff-Sediment Relationships Under Humid Tropical Condition: Case Study of Bernam Watershed MalaysiaEuropean Journal of Scientific Research ISSN 1450-216X Vol.31 No.1 (2009), pp. 88-105.

Amisigo B. A. and Akrasi S. A. (1996) Suspended Sediment Rating Curves for Selected Rivers in the Volta Basin of Ghana. Water Resources Research Institute, Accra, Ghana.

Amisigo, B. A., (2005). Modeling Riverflow in the Volta Basin of West Africa: A Data-Driven Framework, ZEF- Ecology and Development Series No 34, 73.

Andah, E.I, van de Giesen N, Biney CA, (2003). Water, climate, food, and environment in the Volta Basin. Adaptation strategies to changing environments. Contribution to the ADAPT project. http://www.weap21.org/downloads/ADAPTVolta.pdf

Andah, Winston E.I. (ed.) 2005. Volta River Basin: Enhancing Agricultural Water Productivity Through Strategic Research. Technical Report No. 8, Challenge Program onWater and Food, P.O. Box 2075, Colombo, Sri Lanka.

Anderson, C.W., (2005). Turbidity: U.S. Geological Survey Techniques of Water-Resources Investigations, book 9, chaps. A6.7, http://pubs.water.usgs.gov/twri9A.

Andreini, M, van de Giesen N, (2001). The GLOWA Volta Project. Sustainable Water Use in the Volta Basin. http://www.glowavolta.de/publications/printed/IHDP_andreini.htm

Andreini, M., N. van de Giesen, A. van Edig, M. Fosu, W. Andah, (2000). Volta Basin Water Balance, ZEF – Discussion Papers on Development Policy No. 21, Center for Development Research, Bonn, pp. 29.

Andrews, E. D., (1981). Measurement and Computation of Bed-Material Discharge in a shallow sand-bed stream, Muddy Creek, Wyoming. Water Resources Research, Vol. 17, No. 1, pp.131-141.

Arabi, M., Govindaraju R.S., Engel B. and Hantush M., (2007), Multiobjective sensitivity analysis of sediment and nitrogen processes with a watershed model, Water Resour. Res., 43, W06409, doi:10.1029/2006WR005463

Arino, O., Perez R., Julio J., Vasileios K., Sophie B., Pierre D., Van Bogaert E., (2012). Global Land Cover Map for 2009 (GlobCover 2009).© European Space Agency (ESA) & Universitécatholique de Louvain (UCL), doi:10.1594/PANGAEA.787668..

Arnold, J. G., and J. R. Williams. (1987). Validation of SWRRB: Simulator for water resources in rural basins. J. Water Resour. Plan. Manage. ASCE 113(2): 243-256.

Arnold, J.G., and Allen P.M., (1996). Estimating hydrologic budgets for three Illinois watersheds. J. Hydrol. 176(1-4): 57-77.

Arnold, J.G., and N. Fohrer. (2005). SWAT2000: Current capabilities and research opportunities in applied watershed modeling. Hydrol. Processes 19(3):563–572. doi:10.1002/hyp.5611.

Arnold, J.G., Kiniry J.R., Srinivasan R., Williams J.R., Haney E.B., and S.L. Neitsch (2012). Soil and Water Asssessment Tool Input/Output Documentation. Texas Water Resources Institute: 650

Arnold, J.G., Muttiah R.S., Srinivasan R., and Allen P.M. (2000). Regional estimation of base flow and groundwater recharge in the upper Mississippi basin. J. Hydrol. 227(1-4): 21-40.

Arnold, J.G., R. Srinivasan, R.S. Muttiah and J.R. Williams, (1998). Large area hydrologic modeling and assessment part I: model development. Journal of the American Water Resources Association. 34(1): 73-89.

Arnold, J.G., Srinivasan R., Muttiah R.S., Allen P.M., and Walker C. (1999). Continental-scale simulation of the hydrologic balance. J. American Water Resour. Assoc. 35(5): 1037-1052.

Arnold, J.G., Williams J.R., and D. R. Maidment. (1995). Continuous-time water and sediment-routing model for large basins. J. Hydrol. Eng. ASCE 121(2): 171-183.

ASCE. (1993). Criteria for evaluation of watershed models. J. Irrigation Drainage Eng. 119(3): 429-442.

Asselman, N.E.M., (2000). Fitting and Interpretation of Sediment Rating Curves. Journal of Hydrology, 234, pp.228-248.

ASTM International. (1997). Standard test method for determining sediment concentration in water samples. ATM Designation D3977-97, ASTM International, West Conshohocken, PA.

Awotwi A, Kumi M, Jansson PE, Yeboah F, Nti IK (2015) Predicting Hydrological Response to Climate Change in the White Volta Catchment, West Africa. J Earth Sci Clim Change 6: 249. doi:10.4172/2157-7617.1000249.

Baguis P., Boukhris O., Ntegeka V., Roulin E., Willems P., Demaree G., (2008). Climate change impact on hydrological extremes along rivers and urban drainage systems. I. Literature review, Belgian Science Policy-SSD Research Programme, Technical report CCI-HYDR project by K.U.Leuven – Hydraulics Section & Royal Meteorological Institute of Belgium, 57p.

Barry, B., Obuobie E., Andreini M., Andah W., and Pluquet M., (2005). Comprehensive Assessment of Water Management in Agriculture - Comparative study of river basin development and management. www.iwmi.cgiar.org/assessment/files_new/research_projects/River_Basin_Development_and_Management/VoltaRiverBasin_Boubacar.pdf

Beasley, D.B., Huggins, L.F. and dan Monke, E.J. (1980), ANSWERS: A model for watershed planning. Transaction of the American Society of Agricultural Engineers, 23, 938-944.

Betrie, G.D., Mohamed, Y.A., van Griensven, A., Srinivasan, R., (2011). Sediment management modeling in the Blue Nile Basin using SWAT model. Hydrol. Earth Syst. Sci. 15(3), 807-818.

Beven, K.J., and A.M. Binley, (1992). The future of distributed models: Model calibration and uncertainty prediction, Hydrol. Processes, 6, 279–298, doi:10.1002/hyp.3360060305.

Bharati, L, C. Rodgers, T. Erdenberger, M. Plotnikova, S. Shumilov, P. Vlek, N. Martin, (2008). Integration of economic and hydrologic models: Exploring conjunctive irrigation water use strategies in the Volta Basin. Agricultural water management 95, 925–936.

Boe, J., Terray, L., Habetsb, F., and Martinc, E. (2007). Statistical and dynamical downscaling of the seine basin climate for hydro-meteorological studies. International Journal of Climatology, 27.

Boiten, W., (2008). Boiten W. Hydrometry 3rd edition: A comprehensive introduction to the measurement of flow in open channels. CrC press/Balkema ISBN 0415467632. 2008.

Boorman, D.B. (2003). Climate, Hydrochemistry, and Economics of Surface-water Systems (CHESS): Adding a European dimension to the catchment modeling experience developed under LOIS. Sci. Total Environ. 314-316: 411-437.

Borah, D.K., Yagow G., Saleh A., Barnes P.L., Rosenthal W., Krug E.C., and Hauck L.M., (2006). Sediment and nutrient modeling for TMDL development and implementation. Trans. ASABE 49(4): 967-986.

Boukhris, O., Willems P., Vanneuville W., Van Eerdenbrugh K., (2008). Climate change impact on hydrological extremes in Flanders: regional differences. WL Rapporten, 706/13. Flanders Hydraulics Research/KU Leuven: Antwerpen, Belgium. 99p.

Boukhrissa, Z; Khanchoul, K; Bissonnais, Y and Tourki, M., (2013). Prediction of sediment load by sediment rating curve and neural network (ANN) in El Kebir catchment, Algeria", Journal of Earth System Science.

Bouraoui, F., Galbiati L., and Bidoglio G., (2002). Climate change impacts on nutrient loads in the Yorkshire Ouse catchment (UK). Hydrol. Earth System Sci. 6(2): 197-209.

Bourg, L. and P. Etanchaud, The AMORGOS MERIS CFI (Accurate MERIS Ortho Rectified Geo-location Operational Software), Software User Manual and Interface Control Document, PO-ID-ACR-GS-003, February 2007.

Buishand, T. A. (1982). Some methods for testing the homogeneity of rainfall records. Journal of Hydrology, (58): 11-27.

Cao, W., Bowden W.B., Davie T., and A. Fenemor, (2006). Multi-variable and multi-site calibration and validation of SWAT in a large mountainous catchment with high spatial variability. Hydrol. Proc. 20(5): 1057-1073.

CCAFS and FAO, (2012). Training Guide-Gender and climate change research in agriculture and food security for rural development. www.fao.org/climatechange/micca/gender/en.

CEAP. (2007). Conservation Effects Assessment Project. Washington, D.C.: USDA Natural Resources Conservation Service. www.nrcs.usda.gov/technical/NRI/ceap/

Clesceri, L.S., Greenberg A.E and Eaton A.D. (eds) (1994). Standard methods for the examination of water and wastewater. 2o ed. American Public Health Association, Washington, DC.

Chekol, D.A., (2006). Modeling of Hydrology and Soil Erosion of Upper Awash River Basin. PhD Thesis, University of Bonn: 233pp.

Chicco, G., Cocina V., Di Leo P., Spertino F., and Massi P.A. (2016). Error assessment of solar irradiance forecasts and AC power from energy conversion model in grid-connected photovoltaic systems. Energies (19961073).

Choi, J.Y., Engel B.A., and H.W. Chung (2002). Daily streamflow modeling and assessment based on the curve-number technique, Hydrol. Processes, 16, 3131–3150.

Chong-yu, X., (1999). Climate change and hydrologic models: A review of existing gaps and recent research developments. Water Resources Management 13(5):369-382.

Christensen, J.H., K. Krishna Kumar, E. Aldrian, S.-I. An, I.F.A. Cavalcanti, M. de Castro, W. Dong, P. Goswami, A. Hall, J.K. Kanyanga, A. Kitoh, J. Kossin, N.-C. Lau, J. Renwick, D.B. Stephenson, S.-P. Xie and T. Zhou, (2013): Climate Phenomena and their Relevance for Future Regional Climate Change. In: Climate Change 2013: The Physical Science Basis. Contribution of Working Group I to the Fifth Assessment Report of the Intergovernmental Panel on Climate Change [Stocker, T.F., D. Qin, G.-K. Plattner, M. Tignor, S.K. Allen, J. Boschung, A. Nauels, Y. Xia, V. Bex and P.M. Midgley (eds.)]. Cambridge University Press, Cambridge, United Kingdom and New York, NY, USA

Christensen, V.G., Jian, Xiaodong, and Ziegler, A.C., (2000). Regression analysis and real-time water-quality monitoring to estimate constituent concentrations, loads, and yields in the Little Arkansas River, south-central Kansas, 1995–99: U.S. Geological Survey Water-Resources Investigations Report 00–4126, 36 p.

Cigizoglu H K (2002). Suspended sediment estimation and forecasting using artificial neural networks; Turk. J. Eng. Environ. Sci. 26 15–25.

Conan, C., Bouraoui F., Turpin N., de Marsily G., and Bidoglio G., (2003). Modeling flow and nitrate fate at catchment scale in Brittany (France). J. Environ. Qual. 32(6): 2026-2032.

Coyne et Bellier, (1993). White Volta Development Scheme – Prefeasibility Study. Volta River Authority. Chapter 2.

De Roo, A.P.J. and Offermans, R.J.E. (1995) LISEM: A physically-based hydrologie and soil erosion model for basin scale water and sediment management: sensitivity analysis, calibration and validation. In: Modeling and Management of Sustainable Basin-Scale Water Resource Systems (ed. by S.P. Simonovic, Z. Kundzewicz, D. Rosbjerg & K. Takeuchi) (Proc. Boulder Symp., July 1995), 399-407. IAHS Publ. no. 231.

de Vries, M. (1993). Use of models for river problems. IHP- Project M-3-5(a) UNESCO (IHP-IV), 7, ISBN 92-3-102861-8.

Di Luzio, M., Srinivasan R., and Arnold J.G.. (2002). Integration of watershed tools and SWAT model into BASINS. J. American Water Resour. Assoc. 38(4): 1127-1141.

Dosio, A. and Panitz H-J., (2015). Dynamically downscaling of CMPI5 CGMs over CORDEX-Africa with COSMO-CLM: analysis of the climate change signal and differences with the driving GCMs. Clim Dyn. doi:10.1007/s00382-015-2664-4.

Druyan, L. M., Fulakeza M., Lonergan P., and E. Noble (2009). Regional climate model simulation of the AMMA Special Observing Period #3 and the pre-Helene easterly wave Meteorol Atmos Phys (2009) 105:191–210.

Duan, Naihua, (1983), Smearing estimate-A nonparametric retransformation method: Journal of the American Statistical Association, v. 78, no. 383, p. 605–610.

Edwards, T. K., and Glysson, G. D., (1999). Field Methods for Measurement of Fluvial Sediments. In: U.S. Geological Survey Techniques of Water-Resources Investigations, Book 3, Chapter C2, U.S. Geological Survey, Information Services, Reston, Virginia.

Fadil, A., Rhinane H., Kaoukaya Ab., Kharchaf A. and Bachir O.A. (2011). Hydrologic modeling of the Bouregreg watershed (Morocco) using GIS and SWAT model. Journal of Geographic Information System

FAO, (1997). Irrigation potential in Africa: A basin approach. FAO Land and Water Bulletin 4.

FAO/UNESCO, (2003). WRB (World reference Base for Soil Resources) Map of World Soil Resources, 1:25,000,000. (http://www.fao.org/AG/agL/agll/wrb/soilres.stm.

FAO-UNESCO (1994) Soil map of the world - Revised Legend. Technical paper 20. Roma: FAO; ISRIC. www.fao.org/fileadmin/user_upload/soils/doc/isricu_i9264_001.pdf

Ferguson, R.I. (1986). River loads underestimated by rating curves. Water Resources Research, 22(1), 74–76.

FitzHugh, T.W. and Mackay D.S., (2000). Impacts of input parameter spatial aggregation on an agricultural nonpoint-source pollution model. J. Hydrol. 236(1-2): 35-53.

Fowler, H.J., Kilsby C.G., (2007). Using regional climate model data to simulate historical and future river flows in northwest England. Clim Chang 80:337-367.

Friesen, J., Andreini M., Andah W., Amisigo B., van de Giesen N., (2005). Storage capacity and long-term water balance of the Volta Basin, West Africa. IAHS Publication no. 296: 138-145.

Garde, R.J. and Ranga-Raju, K. G. (2000). Mechanics of Sediment Transport, New Age International Publishers.

Gassman, P.W., Reyes M.R., Green C.H. and Arnold J.G.. (2007). "The Soil and Water Assessment Tool: Historical Development, Applications, and Future Directions." Trans. ASABE 50(4): 1211-1250.

Gbobaniyi E., Sarr A., Sylla M. B., Diallo I., Lennard C., Dosio A., Dhié-diou A., Kamga A., Klutse NAB, Hewitson B., Nikulin G., Lamptey B., (2014). Climatology, annual cycle and interannual variability of precipitation and temperature in CORDEX simulations over West Africa. Int J Climatol 34(7):2241–2257.

Ghosh, S., and Misra, C., (2010). Assessing Hydrological Impacts of Climate Change: Modeling Techniques and Challenges. The Open Hydrology Journal, 2010, 4, 115-121.

Gikas, G.D., Yiannakopoulou T., and Tsihrintzis V.A., (2005). Modeling of nonpoint-source pollution in a Mediterranean drainage basin. Environ. Model. Assess. 11(3): 219-233.

Giorgi, F., Jones C. and Asrar G., (2009). Addressing climate information needs at the regional level: the CORDEX framework. World Meteorological Organization (WMO) Bulletin, vol 58, pp. 175-183.

Govender, M., and C. S. Everson. (2005). Modeling streamflow from two small South African experimental catchments using the SWAT model. Hydrol. Process. 19(3): 683-692.

Govers, G., and Loch, R. (1993). 'Effects of initial water content and soil mechanical strength on the runoff erosion resistance of clay soils.' Australian Journal of Soil Research, 31, 549-566.

Gray, J.R. (Ed.) (2005). Proceedings of the Federal Interagency Sediment Monitoring Instrument and Analysis Research Workshop, Flagstaff, Arizona, 9–11 September, U.S. Geol. Surv. Circ., 1276, 46 pp. http://pubs.usgs.gov/circ/2005/1276/.

Gray, J.R., and Gartner, J.W. (2010a). Surrogate technologies for monitoring suspended-sediment transport in rivers, in Poleto, Cristiano, and Charlesworth, Susanne, eds., Sedimentology of Aqueous Systems, London, Wiley-Blackwell, Chapter 1, pp 3-45.

Gray, J.R., and Gartner, J.W. (2010b). Overview of selected surrogate technologies for high temporal resolution suspended-sediment monitoring. 2nd Joint Federal Interagency Conference, Las Vegas, NV, June 27 - July 1, 2010 pp.

Gray, J.R., and Simões, F.J.M., (2008). Estimating sediment discharge, in Garcia, Marcelo, ed., Sedimentation engineering-processes, measurements, modeling, and practice: American Society of Civil Engineers Manual 110, Appendix D, p. 1,067–1,088.

Gray, J.R., Glysson, G.D., and Edwards, T.E., (2008). Suspended-sediment samplers and sampling methods, in Garcia, Marcelo, ed., Sedimentation engineering—Processes, measurements, modeling, and practice: American Society of Civil Engineers Manual 110, chap. 5.3, p. 320–339.

Gubareva, T. S., and Gartsman B. I., (2010). Estimating distribution parameters of extreme hydrological characteristics by L-moment method. Water Resources, 2010, Vol. 37, No. 4, pp. 437-445.

Gupta, H.V., Sorooshian S., and P.O. Yapo. (1999). Status of automatic calibration for hydrologic models: Comparison with multilevel expert calibration. J. Hydrologic Eng. 4(2): 135-143.

Haan, C.T., B.J. Barfield, and J.C. Hayes, (1994). Design Hydrology and Sedimentology for Small Catchments. Academic Press, San Diego, California, USA. 588 pp.

Hansen, D and Bray D.I. (1993). Single-station estimates of suspended sediment loads using sediment rating curves. Canadian Journal of Civil Engineering 20: 133–143.

Hao, F.H., Zhang X.S., and Yang Z.F.. (2004). A distributed nonpoint-source pollution model: Calibration and validation in the Yellow River basin. J. Environ. Sci. 16(4): 646-650.

HAP, (2008). Hydrological assessment of the Northern Regions of Ghana: A bibliographical review of selected papers. CIDA, WRC, SNC-LAVALIN International.

Hargreaves, G.L., Hargreaves G.H., and J.P. Riley. (1985). Agricultural benefits for Senegal River basin. J. Irrig. Drain. Eng. 108(3): 225-230.

Helsel, D.R., and Hirsch, R.M., (2002). Statistical methods in water resources-hydrologic analysis and interpretation: USGS Techniques of Water-Resources Investigations, book 4, chap. A3, 510, www.pubs.usgs.gov/twri/twri4a3/Helsel_Hirsch.pdf.

Heuvelmans, G., Garcio-Qujano J.F., Muys B., Feyen J., and Coppin P., (2005). Modeling the water balance with SWAT as part of the land use impact evaluation in a life cycle study of CO_2 emission reduction scenarios. Hydrol. Process. 19(3): 729-748.

Holtschlag DJ. (2001). Optimal estimation of suspended-sediment concentrations in streams. Hydrological Processes 15: 1133–1156.

Horowitz A.J., Elrick K.A., Smith J.J., (2001). Estimating suspended sediment and trace element fluxes in large river basins: methodological considerations as applied to the NASQAN programme. Hydrological Processes 15: 1107–1132.

Horowitz, A.J. (2003). An evaluation of sediment rating curves for estimating suspended sediment concentrations for subsequent flux calculations. Hydrol. Process. 17, 3387–3409 (2003).

Hosking, J.R.M., and Wallis, J.R. (1997). Regional frequency analysis. Cambridge University Press: Cambridge, UK.

Huisman, J.A., Breuer L., and Frede H.G.. (2004). Sensitivity of simulated hydrological fluxes towards changes in soil properties in response to land use change. Phys. Chem. Earth 29(11-12): 749-758.

IPCC (2007a), Climate Change (2007): Impacts, Adaptation and Vulnerability. Contribution of Working Group II to the Fourth Assessment Report of the Intergovernmental Panel on Climate Change, Cambridge University Press, Cambridge.

IPCC (2007b), (Intergovernmental Panel on Climate Change), (2007). Climate change: the physical science basis. Contribution of Working Group I to the Fourth Assessment

Report of the Intergovernmental Panel on Climate Change. Cambridge, UK: Cambridge University Press.

IPCC (2014). Climate Change 2014: Impacts, adaptation, and vulnerability. Part B: Regional aspects. Contribution of working group II to the fifth assessment report of the intergovernmental panel on climate change (p. 688). Cambridge, United Kingdom and New York, NY, USA: Cambridge University Press.

IPCC (2016). Climate Change 2014 Synthesis Report Fifth Assessment Report. http://ar5-syr.ipcc.ch/topic_futurechanges.php

ISRIC, (2016). World Soil Information. http://www.isric.org/about-soils/world-soil-distribution/

IUCN, (2008), http://www.iucn.org/about/work/.../wp_our_work_vrb/

Izaurralde, R.C., Williams J.R., McGill W.B., Rosenberg N.J., and M.C. Quiroga Jakas. (2006). Simulating soil C dynamics with EPIC: Model description and testing against long-term data. Ecol. Model. 192(3-4): 362-384.

Jain, M.K., and Das, D., (2010). Estimation of Sediment Yield and Areas of Soil Erosion and Deposition forWatershed Prioritization using GIS and Remote Sensing. Water Resources Management, 24: pp.2091–2112.

Jastram, J. D., Zipper, C. E., Zelazny, L. W., & Hyer, K. E. (2009). Increasing precision of turbidity-based suspended sediment concentration and load estimates. Journal of Environmental Quality, 39, 1306-1326.

Jha, M., Arnold J.G., Gassman P.W., Giorgi F., and Gu R.. (2006). Climate change sensitivity assessment on upper Mississippi river basin streamflows using SWAT. J. American Water Resour. Assoc. 42(4): 997-1015.

Jha, M., Gassman P.W., and Arnold J.G.. (2007). Water quality modeling for the Raccoon River watershed using SWAT2000. Trans. ASABE 50(2): 479-493.

Johnson, B.E., Julien, P.Y., Molnar, D.K., and Watson, C.C., (2000). The two-dimensional-upland erosion model CASC2D-SED. J. of the AWRA, 36(1), 31-42.

Kasai, M., Brierley, G.J., Page, M. J., Marutani, T and Trustrum, N. A, (2005). Impacts of land use change on patterns of sediment flux in Weraamaia catchment, New Zealand. Catena 64, 27-60.

Kasei R., (2009). Modeling impacts of climate change on water resources in the Volta Basin, West Africa. Doctoral thesis, Rheinische Friedrich Wilhelms Universität, Bonn/ Germany, http://www.glowavolta.

Khan M.S., Coulibaly P., and Dibike Y., (2006). Uncertainty analysis of statistical downscaling methods. Journal of Hydrology 319:357 – 382.

Khanchoul, K., Benslama, M., and Remini, B., (2010). Regressions on Monthly Stream Discharge to Predict Sediment Inflow to a Reservoir in Algeria. Journal of Geography and Geology, Vol. 2, No.1; pp.36 – 47.

Kim, J., Waliser D. E., Matttmann C. A., Goodale C. E., Hart A. F., Zimdars P. A., Crichton D. J., Jones C., Nikulin G., Hewitson B., Jack C., Lennard C., Favre A., (2014). Evaluation of the CORDEX-Africa multi-RCM hindcast: systematic model errors. Clim Dyn, 42:1189–1202DOI10.1007/s00382-013-1751-7

Kim, N.W., and Lee, J., (2008). Temporally weighted average curve number method for daily runoff simulation, Hydrological Processes, 22, 4936-4948.

Kinnell, P.I.A., and Risse L.M., (1998). USLE-M: Empirical modeling rainfall erosion through runoff and sediment concentration. Soil Sci. Soc. Am. J. 62, 1667-1672.

Kisi, Özgür, (2007). Development of Streamflow-Suspended Sediment Rating Curve Using a Range Dependent Neural Network. International Journal of Science & Technology Volume 2, No 1, 49-61.

Klein, C., Bliefernicht, J., Heinzeller, D. Kunstmann, H. (2014): WRF model performance and sensitivity to model physics in a medium- and high-resolution downscaling experiment for West Africa, http://meetingorganizer.copernicus.org/EGU2014/EGU2014-6376.pdf

Klutse N. A. B., Sylla M. B., Diallo I., Sarr A., Dosio A., Diedhiou A., Kamga A., Lamptey B., Ali A., Gbobaniyi E. O., Owusu K., Lennard C., Hewitson B., Nikulin G., Panitz H-J, Bucher M., (2014). Daily characteristics of West African summer monsoon precipitation in CORDEX simulations. Theor Appl Climatol. DOI 10.1007/s00704-014-1352-3.

Knisel, W. G. (Ed.). (1980). CREAMS: a field scale model for chemicals, runoff and erosion from agricultural management systems, USDA Conservation Research Report No. 26.

Kunstmann, H. and G. Jung, (2005). Impact of regional climate change on water availability in the Volta basin of West Africa. In: Regional Hydrological Impacts of Climatic Variability and Change. IAHS Publ. 295.

Kwabena Kankam-Yeboah, Emmanuel Obuobie, Barnabas Amisigo & Yaw Opoku-Ankomah (2013) Impact of climate change on streamflow in selected river basins in

Ghana, Hydrological Sciences Journal, 58:4, 773-788, DOI: 10.1080/02626667.2013.782101

Lane, L. J., Hernandez, M., and Nichols, M., (1997). Processes Controlling Sediment Yield from Watersheds as functions of Spatial Scale, Environmental Modeling and Software, Vol.12, No.4, pp.355 - 369.

Laprise R., Hernandez-Diaz L., Tete K., Sushuma L., Separovic L., Martynov A., Winger K. and Valin M. (2012). Climate projection over the CORDEX Africa domain using the fifth generation Canadian Regional Climate Model (CRCM5). Climate Dynamics 41, 3219-3246.

Lawler, D.M., Petts, G.E., Foster, I.D.L. and Harper, S. (2006) Turbidity dynamics and hysteresis patterns during spring storm events in an urban headwater system: the Upper Tame, West Midlands, UK. Sci. Total Environ. 360, 109–126.

Lee, C.J., Rasmussen, P.P., and Ziegler, A.C. (2008). Characterization of suspended-sediment loading to and from John Redmond Reservoir, east-central Kansas, 2007–08, USGS Scientific Investigations Report 2008–5123, 25 p.

Leemhuis, C., Jung, G., Kasei, R., and J. Liebe, 2009. The Volta Basin Water Allocation System: Assessing the Impact of Small-Scale Reservoir Development on the Water Resources of the Volta basin, West Africa. Adv. Geosci., 21, 57–62, 2009.

Legates, D.R., and G.J. McCabe. (1999). Evaluating the use of "goodness-of-fit" measures in hydrologic and hydroclimatic model validation. Water Resources Res. 35(1): 233-241.

Leh, M., Bajwa, S., Chaubey, I., (2011). Impact of Land use Change on Erosion Risk: An Integrated Remote Sensing, Geographic Information System and Modeling Methodology. In Land Degradation & Development. DOI: 10.1002/ldr.1137. Assessed on 15th July, 2014.

Lewis, Jack, (1996). Turbidity controlled suspended sediment sampling for runoff event load estimation: Water Resources Research, v. 32, no. 7, p. 2,299–2,310.

Lo, J.C.F., Yang Z.L., and R.A. Pielke Sr. (2008). Assessment of three dynamical climate downscaling methods using the Weather Research and Forecasting (WRF) model, J. Geophys. Res., 113, D09112, doi:10.1029/2007JD009216.

Loch R.J. and Rosewell C.J. (1992) Laboratory methods for measurement of soil erodibility (K factors) or the Universal Soil Loss Equation. Australian Journal of Soil Research 30, 233–248.

Lorente-Plazas R., García-Díez M., Jimenez-Guerrero P., Fernández J., and Montavez J. P., (2014). On the added value and sensitivity of WRF to driving conditions over CORDEX-Africa domain. Geophysical Research Abstracts Vol. 16, EGU2014-10889, 2014 EGU General Assembly.

Lorz, C., Volk M., and Schmidt G., (2007). Considering spatial distribution and functionality of forests in a modeling framework for river basin management. For. Ecol. Mgmt. 248(1-2): 17-25.

Ma, L., Ascough II J.C., Ahuja L.R., Shaffer M.J., Hanson J.D., and K.W. Rojas. 2000. Root Zone Water Quality Model sensitivity analysis using Monte Carlo simulation. Trans. ASAE 43(4): 883-895.

Martin N., (2005). Development of a water balance for the Atankwidi catchment, West Africa - A case study of groundwater recharge in a semi-arid climate. PhD thesis; Georg-August-Universität-Göttingen,Germany, http://www.glowavolta.de/fileadmin/template/Glowa/Downloads/thesis_martin.pdf.

Martin, N. and van de Giesen, N. (2005). Spatial Distribution of Groundwater Production and Development Potential in the Volta River basin of Ghana and Burkina Faso. Water International, Volume 30, Number 2, Pages 239–249.

Mausbach, M.J., and Dedrick A.R.. (2004). The length we go: Measuring environmental benefits of conservation practices. J. Soil Water Cons. 59(5): 96A-103A.

Mearns LO, the NARCCAP Team. (2006). Overview of the North American Regional Climate Change Assessment Program. In NOAA RISA-NCAR Meeting, Tucson, AZ, March 2006.

Merritt, W.S., Letcher, R.A. and Jakeman, A.J., (2003). A review of erosion and sediment transport models. Environmental modelling and software. 18, 761-799.

Miller, S.N., Kepner W.G., Mehaffey M.H., Hernandez M., Miller R.C., Goodrich D.C., Devonald K.K, Heggem D.T., and Miller W.P., (2002). Integrating landscape assessment and hydrologic modeling for land cover change analysis. J. American Water Res. Assoc. 38(4): 915-929.

Milliman, J.D., and Syvitski, J.P.M., (1992). Geomorphic/Tectonic Control of Sediment Discharge to the Ocean : The Importance of Small Mountainous Rivers', *The Journal of Geology*. 100, 525-544.

Monteith, J. L. (1965). Evaporation and the environment. In The State and Movement of Water in Living Organisms, Proc. 19th Symp. Swansea, U.K.: Society of Experimental Biology, Cambridge University Press.

Morgan, R.P.C., Quinton J.N., Smith R.E., Govers G., Poesen J.W.A., Auerswald K., Chisci G., Torri D. and Styczen M. E., (1998). The European Soil Erosion Model (EUROSEM): A dynamic approach for predicting sediment transport from fields and small catchments. Earth Surf. Process. Landforms 23, 527–544 (1998). http://gruenland.wzw.tum.de/fileadmin/auerswald/1998_Morgan-ESPL.pdf

Moriasi, D. N., Arnold, J. G., Liew, M. W. V., Bingner, R. L., Harmel, R. D., and Veith, T. L. (2007). Model Evaluation Guidelines for Systematic Quantification of Accuracy in Watershed Simulations, T. ASABE, 50, 885–900.

Moss, R., Edmonds, J., Hibbard, K., Manning, M., Rose, S., van Vuuren, D., Carter, T., Emori, S., Kainuma, M., Kram, T., et al. (2010). The next generation of scenarios for climate change research and assessment. Nature, 463(7282):747–756.

Moshe, Inbar (1982). Measurement of fluvial sediment transport compared with lacustrine sedimentation rates: the flow of the River Jordan into Lake Kinneret, Hydrological Sciences Journal, 27:4, 439-449, DOI: 10.1080/02626668209491125

Nangia, V., Wymar, P., and Klang, J., (2010). Evaluation of a GIS-based watershed modeling approach for sediment transport. International Journal of Agricultural and Biological Engineering, Vol. 3, No.3, pp. 43-53.

Nash, J.E., and J.V. Sutcliffe. (1970). River flow forecasting through conceptual models: Part 1. A discussion of principles. J. Hydrology 10(3): 282-290.

Nearing, M. A., Lane L. J., and Lopes V.L., (1994). Modeling soil erosion. pp 127-156. In: Lal, R.: Soil erosion research methods. Second Ed. Soil and Water Conservation Society and St. Lucie Press, FL.

Nearing, M.A. and Harisine, P.B. (2011) The future of soil erosion modelling, Morgan, R.P.C. and Nearing, M.A. (eds) Handbook for erosion modelling, Blackwell Publishing Ltd., pp 389-397.

Neitsch, S.L., Arnold, J.G., Kiniry J.R, Williams, J.R. (2005). Soil and Water Assessment Tool, Theoretical Documentation: Version. Temple, TX. USDA Agricultural Research Service and Texas A&M Blackland Research Center, 2005.

Neitsch, S.L., Arnold, J.G., Kiniry, J.R., and Williams, J.R., (2011). Soil and Water Assessment Tool Theoretical Documentation Version 2009, Grassland, Soil and

Water Research Laboratory, Agricultural Research Service and Blackland Research Center, Texas Agricultural Experiment Station, College Station, Texas, 2011.

Nichols, M. H., (2006). Measured Sediment Yield Rates from Semiarid Rangeland Watersheds. Rangeland Ecology & Management, 59(1), pp.55-62.

Nii Consult (2007). Water Audit Volta Basin. Project for Improving Water Governance in the Volta River Basin. Final report. IUCN/BRAO, Ouagadougou, August 2007.

Nikulin, G., Jones, C., Giorgi, F., Asrar, G., Büchner, M., Cerezo-Mota, R., Christensen, O.B., Déqué, M., Fernandez, J., Hänsler, A., van Meijgaard, E., Samuelsson, P., Sylla, M.B., Sushama, L., (2012). Precipitation Climatology in an Ensemble of CORDEX-Africa Regional Climate Simulations. J. Clim. 25, 565 6057–6078. doi:10.1175/JCLI-D-11-00375.1

Nolan, K. Michael, John R. Gray, and G. Douglas Glysson, (2005), Introduction to Suspended-Sediment Sampling, U.S. Geological Survey, Scientific Investigations Report 2005-5077.

Obuobie E., (2008). Estimation of groundwater recharge in the context of future climate change in the White Volta River Basin. Doctoral thesis, Rheinische Friedrich Wilhelms Universität, Bonn/ Germany, http://www.glowavolta.

Opoku-Ankomah, Y. and Amisigo, B.A., (1997). Surface Water Resources; Volta Basin system, Information Building Block: Ghana Water Resources Management Study. WRRI, Accra

Opoku-Ankomah, Y., (2000). Impacts of Potential Climate Change on River Discharge inClimate Change Vulnerability and Adaptation Assessment on Water Resources of Ghana.Water Research Institute (CSIR), Accra. Ghana.

Owusu, K., Browne and Klutse N. A. B., (2013). Simulation of the rainfall regime over Ghana from CORDEX. Int. Jou. of Geosc., 785-791. http://dx.doi.org/10.4236/ijg.2013.44072.

Paeth, H., Hall, N. M. J., Gaertner, M. A., Alonso, M. D., Moumouni, S., Polcher, J., Ruti, P. M., Fink, A. H., Gosset, M., Lebel, T., Gaye, A. T., Rowell, D. P., Moufouma-Okia, W., Jacob, D., Rockel, B., Giorgi, F., Rummukainen, M., (2011). Progress in regional downscaling of west African precipitation. Atmospheric Sci. Lett. 12, 75–82. doi:10.1002/asl.306.

Parajuli, P.B., Nelson N.O., Frees L.D., and K.R. Mankin. (2009). Comparison of AnnAGNPS and SWAT model simulation results in USDA-CEAP agricultural watersheds in south-central Kansas. Hydrol. Proc. 23(5): 748-763.

Photius, C., (2004). Ghana Rivers and Lakes. www.photius.com/countries/ghana/geography/ghana_geography_rivers_and_lakes.html

Porterfield, George, (1972). Computation of fluvial-sediment discharge: U.S. Geological Survey Techniques of Water-Resources Investigations, book 3, chap. C3, 66 p.

Priestly, C.H.B., and R.J. Taylor. (1972). On the assessment of surface heat flux and evaporation using large-scale parameters. Monthly Weather Rev. 100(2): 81-92.

Qiu, L., Zheng, F., and R. Yin, (2012). SWAT-based runoff and sediment simulation in a small watershed, the loessial hilly-gullied region of China: capabilities and challenges. International Journal of Sediment Research, Vol. 27, No. 2, 2012, pp. 226–234.

Rasmussen, P.P., Gray, J.R., Glysson, G.D., and Ziegler, A.C., (2009). Guidelines and procedures for computing time-series suspended-sediment concentrations and loads from in-stream turbidity-sensor and streamflow data: U.S. Geological Survey Techniques and Methods, book 3, chap. C4, 52 p.

Renard, K.G., Foster G.R., Weesies G.A., and Porter J.P. (1991). RUSLE - Revised universal soil loss equation. Journal of Soil and Water Conservation. Jan.-Feb. 1991. pp 30-33.

Renard, K.G., Foster G.R., Yoder D.C., and McCool D.K., (1994). RUSLE revisited: Status, questions, answers, and the future. J. Soil Water Conserv. 49(3): 213-220.

Roberts G. (1997). The influence of sampling frequency on streamflow chemical loads. Journal of the Chartered Institution of Water and Environmental Management 11: 114–118.

Rodgers C, van de Giesen N, Laube W, Vlek PLG, Youkhana E (2007) The GLOWA Volta project: A framework for water resources decision-making and scientific capacity building in a transnational West African Basin. In: E. Craswell, M. Bonell, D. Bossio, S. Demuth, and N. van de Giesen (Editors). Integrated assessment of water resources and global change (A north-south analysis). Springer, p.295-313.

Rodgers, C., van de Giesen, N., Laube, W., Vlek, P. L. G., Youkhana, E. (2006): The GLOWA Volta project: A framework for water resources decision-making and scientific capacity building in a transnational West African Basin. Water Resources Management, 21(1), 295-313. http://link.springer.com/10.1007/s11269-006-9054-y doi: 10.1007/s11269-006-9054-y

Rooseboom A. & Annandale G. W. (1981). Techniques applied in determining sediment loads in South African rivers. In: Erosion and sediment transport measurement (ed. D. E. Walling) pp. 219–24. Proceedings of the Florence (Italy) Symposium on

Erosion and Sediment Transport Measurement; 22–26 Jun 1981, Florence, Italy. IAHS Press, London.

Ryan, P.J., McKenzie, N.J., 1997. Digital terrain attributes and erosion modelling for forests. In: Erosion in Forests Workshop, Cooperative Research Centre for Catchment Hydrology, CSIRO, 4 – 6 March 1997.

Sanderson, M., (2010). Changes in the frequency of extreme rainfall events for selected towns and cities. Met Office, UK.

Santhi, C., Arnold J.G., Williams J.R., Dugas W.A., Srinivasan R., and L.M. Hauck. (2001). Validation of the SWAT model on a large river basin with point and nonpoint sources. J. American Water Resources Assoc. 37(5): 1169-1188.

Sarr, M. A., Seidou O., Tramblay Y. and El Adlouni S., (2015). Comparison of downscaling methods for mean and extreme precipitation in Senegal. Journal of Hydrology: Regional Studies 4, 369-385.

Schmengler, A.C., (2011). Modeling soil erosion and reservoir sedimentation at hillslopeand catchment scale in semi-arid Burkina Faso. University of Bonn, PhD Dissertation, http://hss.ulb.uni-bonn.de/diss_online.

Schuol J., Abbaspour K.C., Yang H., Srinivasan R. and Zehnder A.J.B., (2008b). Modeling blue and green water availability in Africa. WATER RESOURCES RESEARCH, VOL. 44, W07406, doi:10.1029/2007WR006609, 2008.

Schuol, J., Abbaspour K.C, Srinivasan R., Yang H., (2008a). Estimation of freshwater availability in the West African sub-continent using the SWAT hydrologic model Journal of Hydrology. 2008(352):30-49.

Setegn Shimelis G., Ragahavan Srinivasan, Bijan Dargahi (2008). Identification of Erosion Potential Areas in Lake Tana Catchment, Ethiopia, Proceedings of American Water Resources Association (AWRA) 2008 GIS and Water Resources V Conference, March 17-19, 2008, San Mateo, California USA, 2008/TPS-08-1, ISBN 1-882132-76-9.

Sharpley, A.N. and Williams J.R., (1990). EPIC-Erosion/Productivity Impact Calculator. Model Documentation. U.S. Dept Agric. Tech. bull. No. 1768.

Sichingabula, H.M. (1998). Factors controlling variations in suspended sediment concentration for single-valued sediment rating curves, Fraser River, British Columbia, Canada. Hydrological Processes 13: 1035–1050.

Singh, K. P., and Dugunoğlu, A., (1989). Developing accurate and reliable stream sediment yields. Sediment and the Environment (Proceedings of the Baltimore Symposium), IAHS Publ. No. 184, pp.193-199.

Sintondji L., (2005). Modelling of process rainfall-runoff in the Upper Quémé catchment area (Terou) in a context of climate change: extrapolation from the local scale to a regional scale. PhD Thesis. Shaker Verlag, Aachen, Germany.

Slaymaker, O., (2003). The sediment budget as conceptual framework and management tool. Hydrobiologia 494, 71-82.

Sloan, P.G. and Moore, I.D., (1984). Modeling subsurface stormflow on steeply sloping forested watersheds,*Water Resour. Res., 20, 1815-1822.*

Sloan, P.G., Moore, I.D., Coltharp, G.B., and Engel, J.D., (1983). Modeling surface and subsurface stormflow on steeply-sloping forested watershed. Lexington. University of Kentucky. 142pp.

Smith, R.E., Goodrich, D.C., Woolhiser, D.A., and Unkrich, C.L., (1995), KINEROS – A kinematic runoff and erosion model. Chap. 20 of Computer Models of Watershed Hydrology, Singh, V.J., Ed., *Water Resources Pub., Highlands Ranch, Colo*., pp. 697-732.

Stephens, M.A., (1974). EDF statistics for goodness of fit and some comparisons, *Journal of the American Statistical Association*, 69, pp. 730-737, DOI: 10.1080/01621459.1974.10480194

Summer, W., Klaghofer, E., Abi-zeid, I. & Villeneuve, J.P. (1992) Critical reflections on long term sediment monitoring programs demonstrated on the Austrian Danube. In: Erosion and Sediment Transport Monitoring Programs in River Basins. *Proc. Oslo Symp., IAHS*, 210, 255–262.

Taylor K. E., Stouffer R. J., Meehl G. A., (2012). An overview of CMIP5 and the experiment design. *Bull Am Meteorol Soc* 93(4):485-498. Doi: 10.1175/BAMS-D-11-00094.1.

Thomas, R. B., (1985). Estimating Total Suspended Sediment Yield with Probability Sampling. *Water Resources Research,* Vol. 21, No. 9, pp.1381-1388.

Trzaska, S. and Schnarr E., (2014). A review of downscaling methods for climate change projections (African and Latin American Resilience to Climate Change (ARCC)). http://www.ciesin.org/documents/Downscaling_CLEARED_000.pdf

UNFCCC (2011). Fact sheet: Climate change science–the status of climate change science today. www.unfccc.int/files/press/backgrounders/application/pdf/press_factsh_science.pdf.

USEPA. (2006). Better Assessment Science Integrating Point and Nonpoint Sources. Washington, D.C.: U.S. Environmental Protection Agency. www.epa.gov/waterscience/BASINS/

van de Giesen, N.C., Stomph T. J. and de Ridder N. (2000). Scale effects of Hortonian overland flow and rainfall-runoff dynamics in a West African catena landscape. Hydrological Processes 14 (1): 165-175.

van Griensven, A., (2005). Sensitivity, auto-calibration, uncertainty and model evaluation in SWAT2005. Unpublished report.

van Griensven, A., Popescu I., Abdelhamid M.R., Ndomba P.M, Beeyers L., and Betrie G.D., (2013). Comparison of sediment transport computations using hydrodynamic versus hydrologic models in the Simiyu River in Tanzania. Physics and Chemistry of the Earth Parts A/B/C.

van Griensven A., and T. Meixner. (2006). Methods to quantify and identify the sources of uncertainty for river basin water quality models. Water Sci. Tech. 53(1): 51-59.

van Griensven, A., and Bauwens W., (2003). Multi-objective auto-calibration for semi-distributed water quality models. Water Resour. Res. 39(12): SWC 9.1- SWC 9.9.

Van Liew, M.W., Arnold J.G., and J.D. Garbrecht. (2003). Hydrologic simulation on agricultural watersheds: Choosing between two models. *Trans. ASAE* 46(6): 1539-1551.

Van Lee, M.W., and Garbrecht J., (2003). Hydrologic simulation of the Little Washita River experimental watershed using SWAT. *J. American Water Resour. Ass.* 39(2): 413-426.

Van Rijn, L.C., (1993). Principles of sediment transport in rivers, estuaries and coastal seas. *Aqua Publications*, Amsterdam, The Netherlands. www.aquapublications.nl.

Veith, T.L. and L.T. Ghebremichael. (2009). How to: applying and interpreting the SWAT Auto-calibration tools. In: Fifth International SWAT Conference Proceedings. August 5-7, 2009 (Proceedings).

Verstraeten, G., and Poesen, J., (2001). Factors controlling sediment yield from small intensively cultivated catchments in a temperate humid climate. Geomorphology, 40, pp.123–144.

Vlugter, H. (1962). Sediment transportation by running water and the design of stable channels in alluvial soils. Bouwn-en Waterbouwn-kunde. De Ingenieur 74(36), 227-231.

Volta-HYSCOS Project, (2006). Volta-Hycos Project – A Sub-Component of The AOC-HYCOS Project. www.whycos.org/whycos/projects/under-implementation/volta-hycos.

Vries, M. de (1993). Use of models for river problems. Studies and reports in hydrology 51, UNESCO [ISBN 92-3-102861-8]

Vuuren, D., et al. (2011). The representative concentration pathways: An overview. Clim Change, 109(1), 5-31.

Wagner, R.J., Boulger, R.W., Jr., Oblinger, C.J., and Smith, B.A., (2006). Guidelines and standard procedures for continuous water-quality monitors—station operation, record computation, and data reporting: U.S. Geological Survey Techniques and Methods 1–D3, 51 p., 8. http://pubs.water.usgs.gov/tm1d3.

Walling D.E. and Webb B. W. (1981) Patterns of sediment yield. In: Background to Palaeohydrology (ed. K. J. Gregory) pp. 69–100. Wiley, Chichester.

Walling, D.E. (1977). Assessing the accuracy of suspended sediment rating curves for a small basin. Water Resources Research 12: 1869–1894.

Walling, D.E., (1983). The sediment delivery problem. Journal of Hydrology 65, 209-237.

White, K.L. and Chaubey I., (2005). Sensitivity analysis, calibration, and validations for a multisite and multivariable SWAT model. J. American Water Resour. Assoc. 41(5): 1077-1089.

Wicks, J. M., Bathurst J. C. (1996). SHESED: a physically based, distributed erosion and; yield component for the SHE hydrological modeling system, J. Hydrology, 1996, 175 (1-4): 213-238.

Willems, P., and Vrac M., (2011). Statistical precipitation downscaling for small-scale hydrological impact investigations of climate change. Journal of Hydrology 402, 193-205pp.

Williams, J.R. & Berndt, H.D., 1977. Sediment yield prediction based on watershed hydrology. Trans. ASAE 20(6): 1100-1104.

Williams, J.R. (1975). Sediment routing for agricultural watersheds. Water Resources Bulletin. 11(5):965-974.

Williams, J.R. (1990). The erosion productivity impact calculator (EPIC) model: A case history. Phil. Trans. R. Soc. London 329(1255): 421-428.

Williams, J.R. (1995). The EPIC Model. In: V.P. Singh, editor, Computer models of watershed hydrology. Water Resources Publ., Littleton, CO. p. 909–1000.

Williams, J.R. and R.W. Hann. (1973). HYMO: Problem oriented computer language for hydrologic modeling. USDA ARS-S-9. 76 pp.

Willmott, C.J., (1981). On the validation of models. Physical Geography 2: 184-194.

Wischmeier, W. H. and Smith, D. D. 1978. Predicting Rainfall Erosion Losses, USDA Agricultural Handbook No. 537.

Wischmeier, W.H., and D.D. Smith. (1978). Predicting rainfall erosion losses - a guide to conservation planning. The USDA Agriculture Handbook No. 537.

WMO-No. 168., (2008). Guide to Hydrological Practices (Data acquisition and processing, analysis, forecasting and other applications). www.wmo.int/en/resources/library/guide-hydrological-practices-wmo-no168.

Woolhiser, D.A., Smith R.E., and Goodrich D.C.. (1990). KINEROS, A Kinematic Runoff and Erosion Model: Documentation and User Manual. ARS-77. Tucson, Ariz.: USDA-ARS Southwest Watershed Research Center. www.tucson.ars.ag.gov/kineros.

WRC, (2008). White Volta Integrated Water Resources Management Plan, www.wrc-gh.org.

WRI (2003). Watersheds of Africa Water Resources eAtlas Land Cover and Use Variables: A19 Volta. WRI. www.earthtrends.wri.org/pdf_library/maps/watersheds/af26.pdf.

WRI, (2000). Water Research Institute. Csir-water.com/Annual_Report

Wu, K., and Xu Y.J, (2006). Evaluation of the applicability of the swat model for coastal watersheds in southeastern Louisiana. Journal of the American water resources association 42 (5), 1247 – 1260.

Xu, C.Y., Singh, V.P., (2004). Review on regional water resources assessment models under stationary and changing climate. Water Resources Management 18, 591e612.

Yang, J., K. C. Abbaspour, P. Reichert, and H. Yang. (2008). Comparing uncertainty analysis techniques for a SWAT application to Chaohe basin in China. J. Hydrol. 358(1-2): 1-23.

Yenigun K., Gumus V., Bulut H., (2008). Trends in streamflow of Euphrates Basins, Turkey, ICE Water Management 161 (4): 189-198.

Young, R.A., Onstad C.A., Bosch D.D., and Anderson W.P. (1989). AGNPS: A nonpoint-source pollution model for evaluating agricultural watersheds. Journal of Soil and Water Conservation 44(2): 168-73.

Zhang, J., Tisdale, T. S. and Wagner, R. A., (1995). A watershed phosphorous loading model for Taylor Creek Basin, Florida. Proceedings of the International Symposium on

Water Quality Modeling, April 2-5, 1995, American Society of Agricultural Engineers, Orlando, FL.

Zhang, X. K., Xu, J. H., Lu, X. Q., Deng, Y. J. & Gao, D. W. (1992). A study on the soil loss equation in Heilongjiang Province. Bulletin of Soil and Water Conservation, 12, 19.

Appendix A (List of Additional Figures)

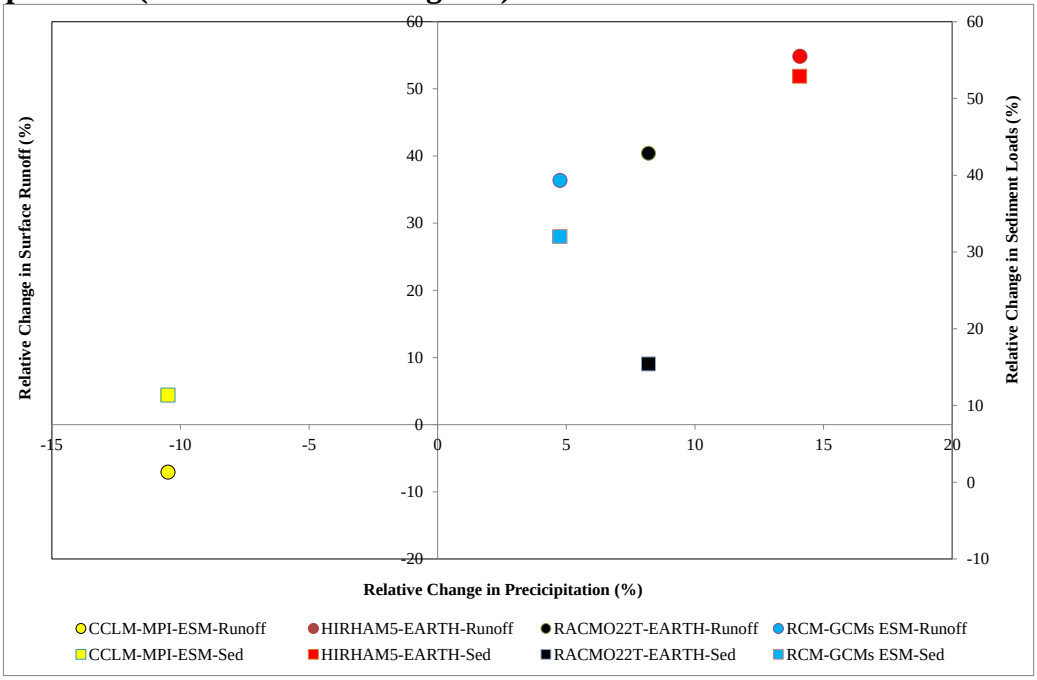

Figure A.0-1: Impact of relative change in future (2031-2050) precipitation on surface runoff (Runoff) and sediment loads (Sed) under RCP8.5

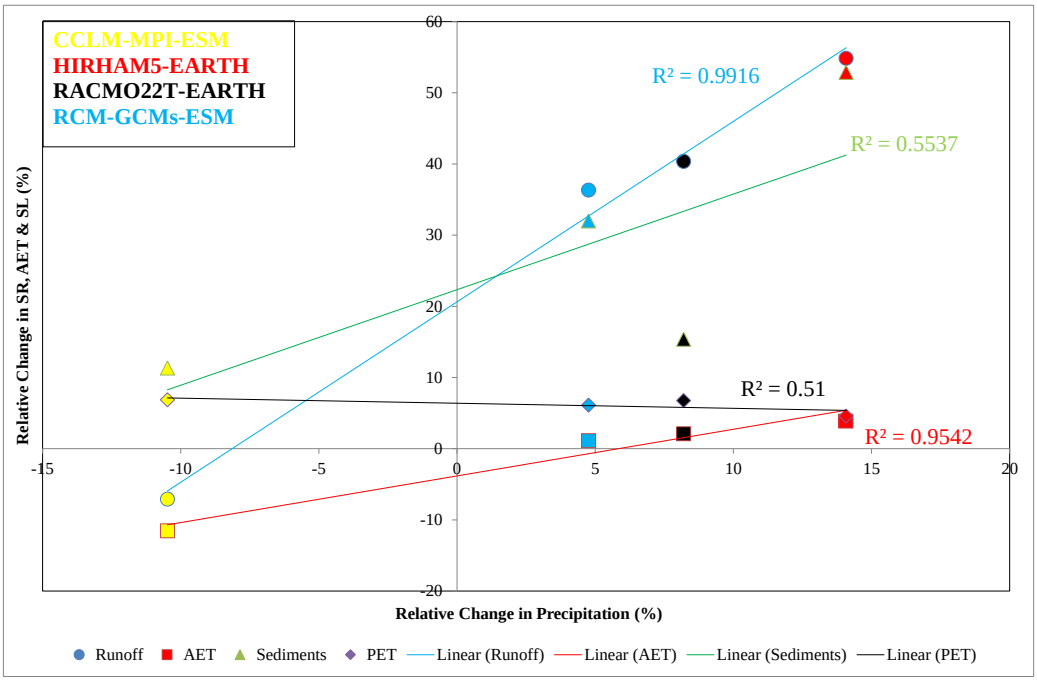

Figure A.0-2: Impact of relative change in future (2031-2050) precipitation on surface runoff, actual evapotranspiration, potential evapotranspiration and sediment loads under RCP8.5. (Different symbols represent different water balance variables and different colors represent different RCM-GCMs).

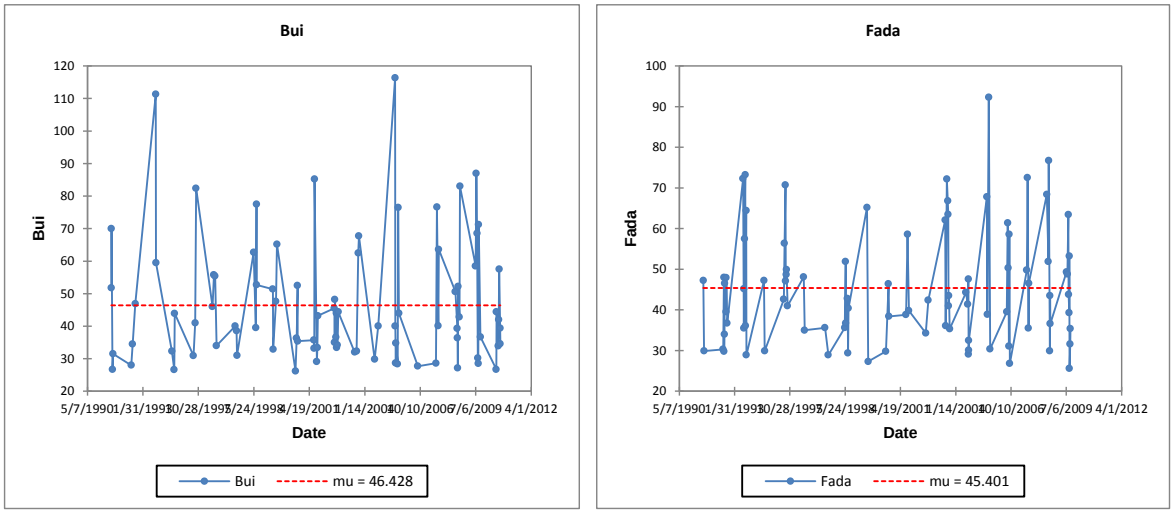

Figure A.0-3: Homogeneity test for the historical extreme precipitation for JAS at the Bui and Fada Ngouma climate stations.

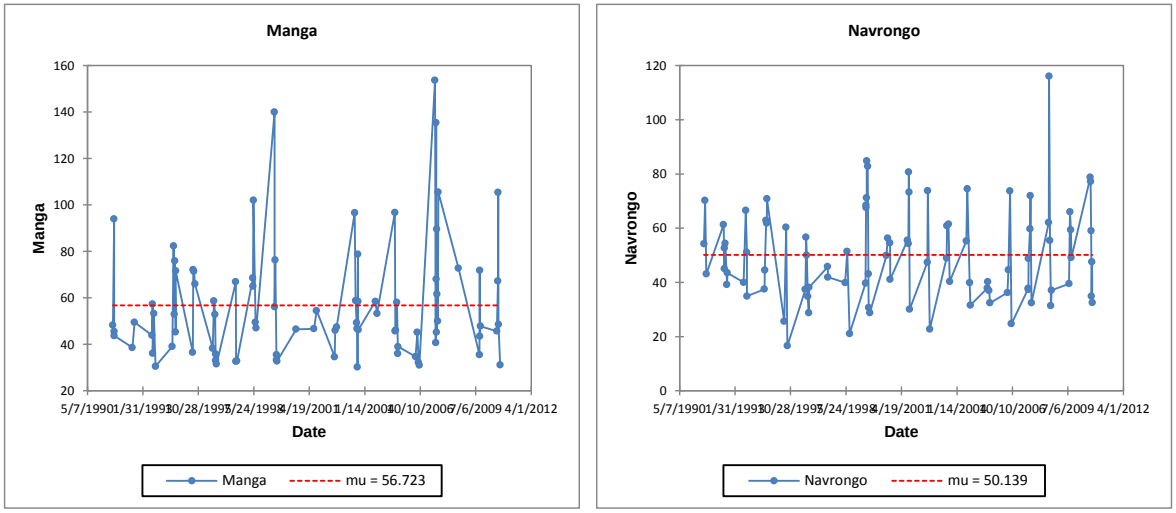

Figure A.0-4: Homogeneity test for the historical extreme precipitation for JAS at the Manga Bawku and Navrongo climate stations.

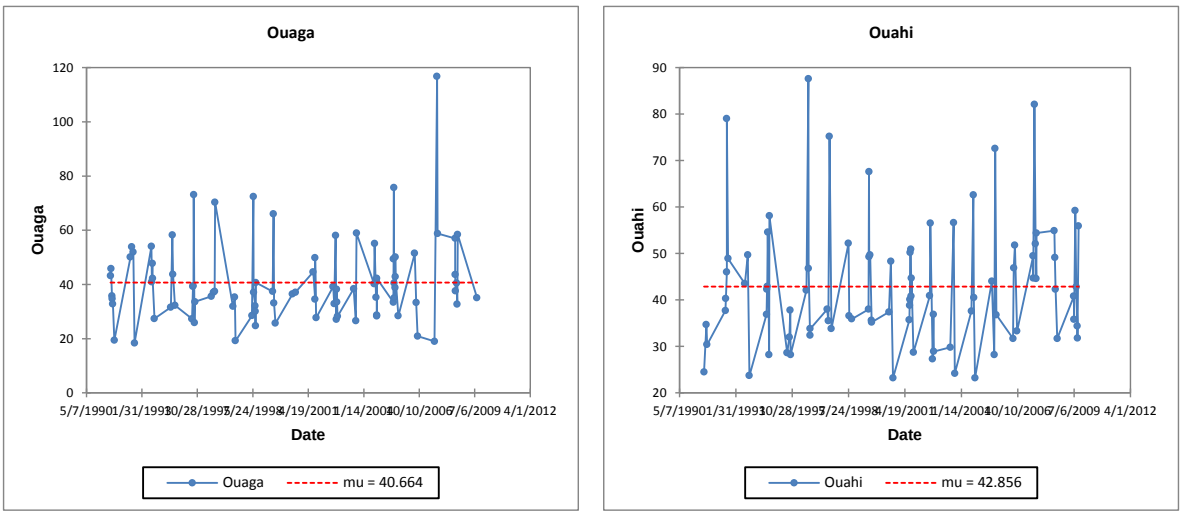

Figure A.0-5: Homogeneity test for the historical extreme precipitation for JAS at the Ouagadougou and Ouahigouya climate stations.

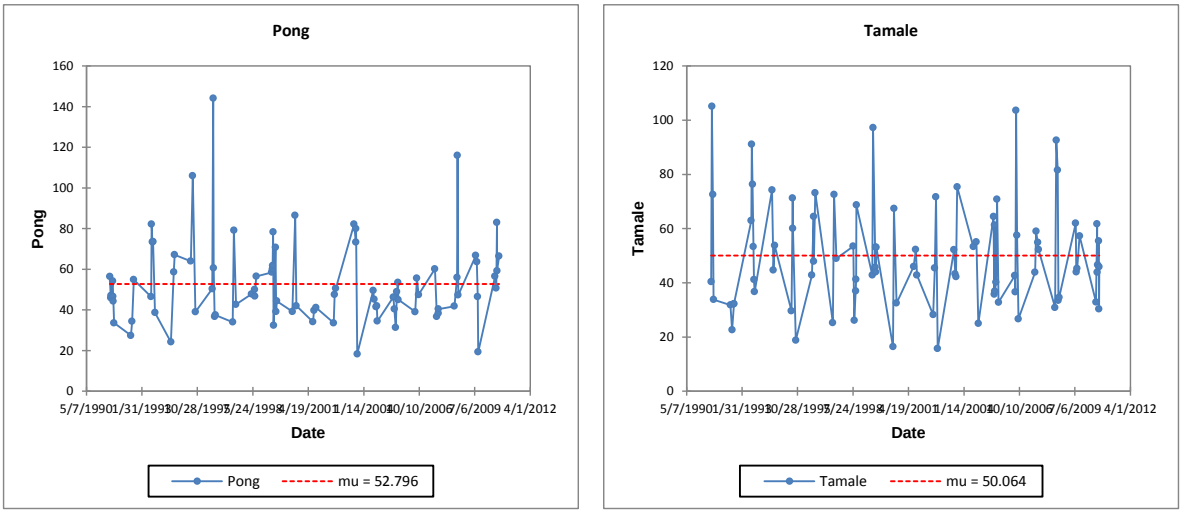

Figure A.0-6: Homogeneity test for the historical extreme precipitation for JAS at the Pong Tamale and Tamale climate stations.

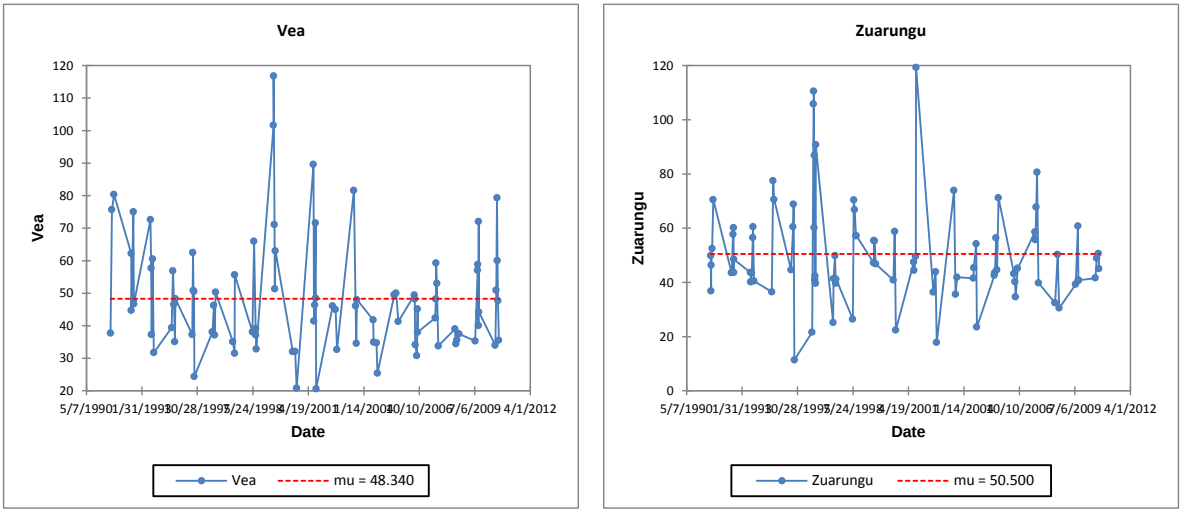

Figure A.0-7: Homogeneity test for the historical extreme precipitation for JAS at the Vea and Zuarungu climate stations.

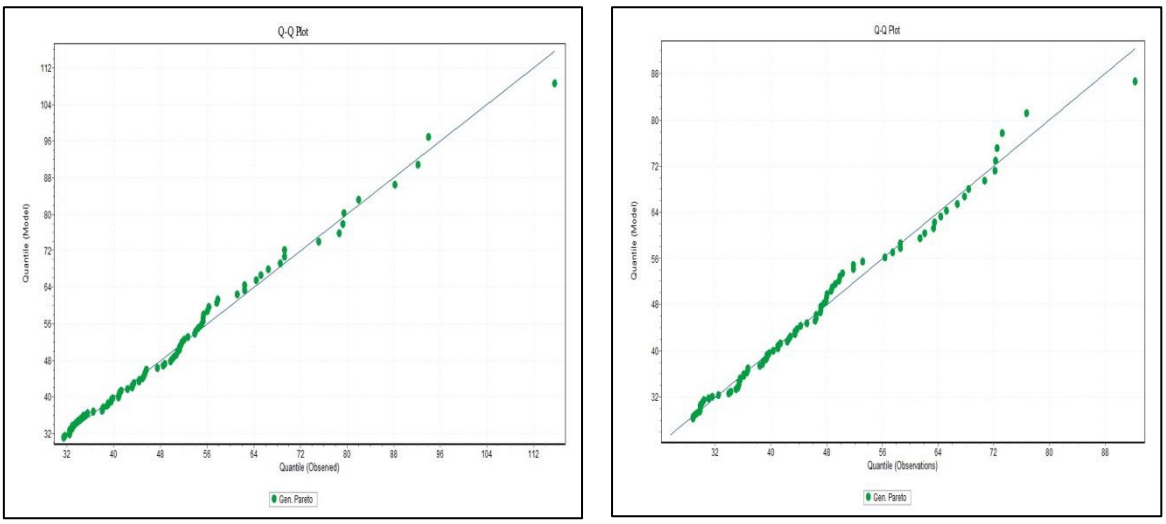

Figure A.0-8: Q-Q plot of the fitted probability distribution to the maximum daily rainfall for JAS in historical observations at Bui and Fad Ngouma climate stations.

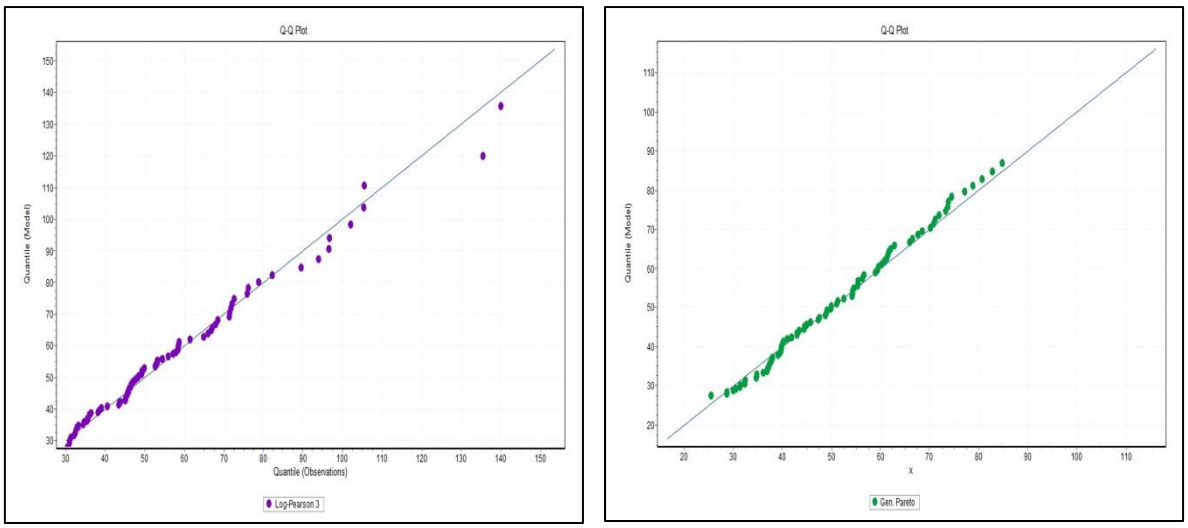

Figure A.0-9: Q-Q plot of the fitted probability distribution to the maximum daily rainfall for JAS in historical observations at Manga Bawku and Navrongo climate stations.

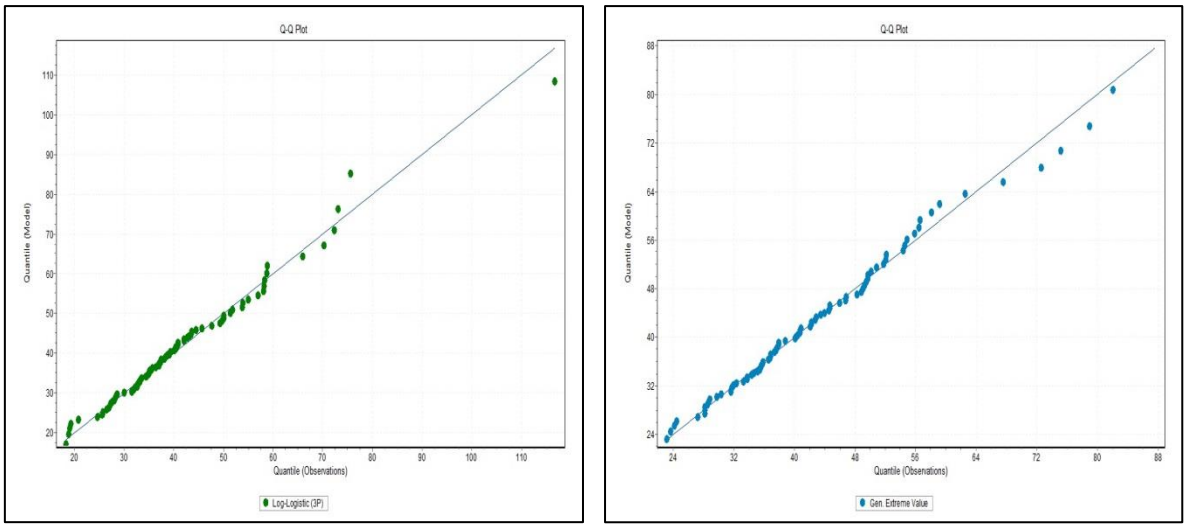

Figure A.0-10: Q-Q plot of the fitted probability distribution to the maximum daily rainfall for JAS in historical observations at Ouagadougou and Ouahigouya climate stations.

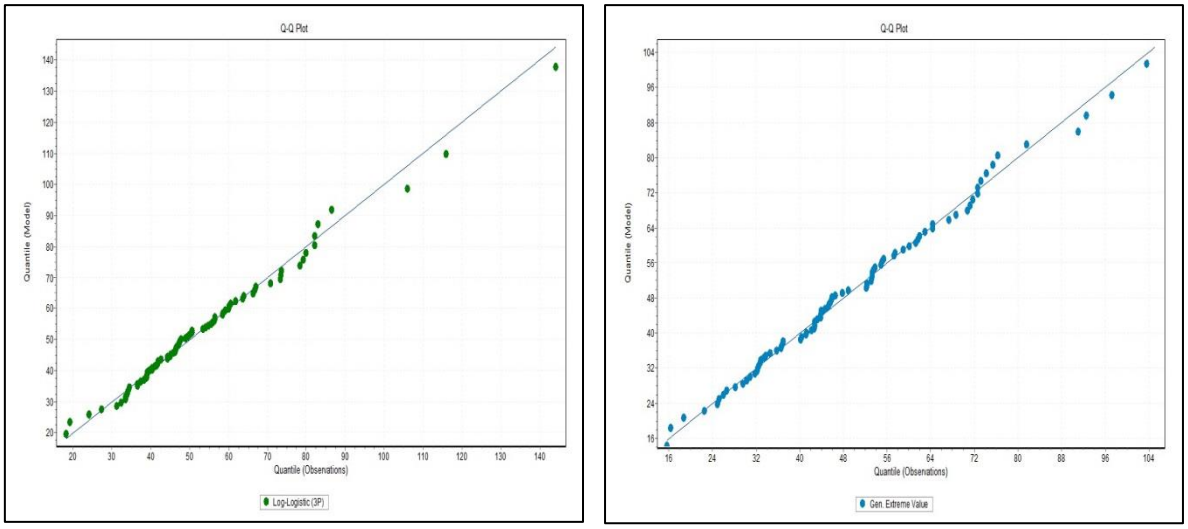

Figure A.0-11: Q-Q plot of the fitted probability distribution to the maximum daily rainfall for JAS in historical observations at Pong Tamale and Tamale climate stations.

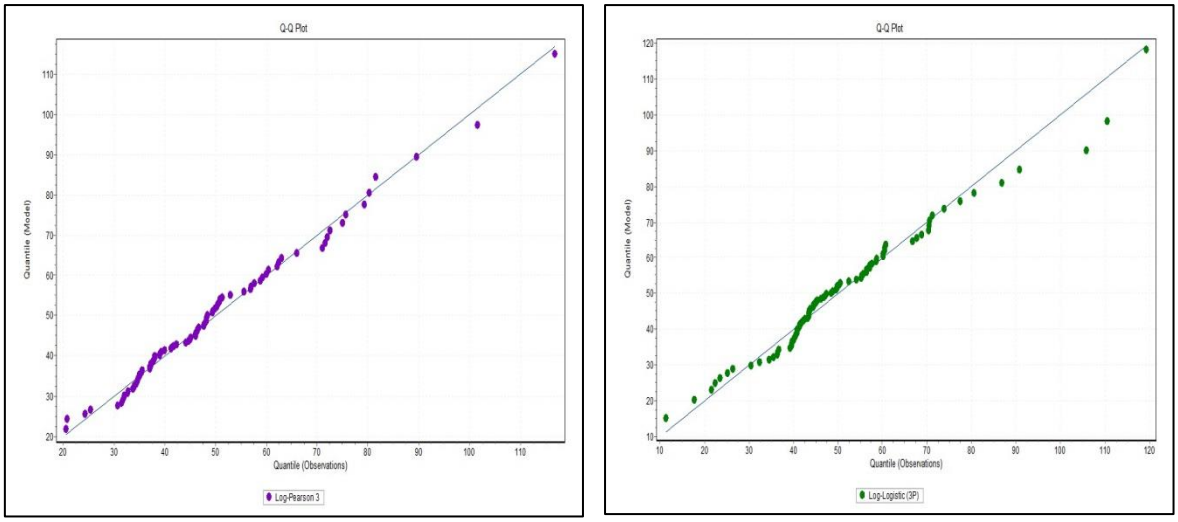

Figure A.0-12: Q-Q plot of the fitted probability distribution to the maximum daily rainfall for JAS in historical observations at Vea and Zuarungu climate stations.

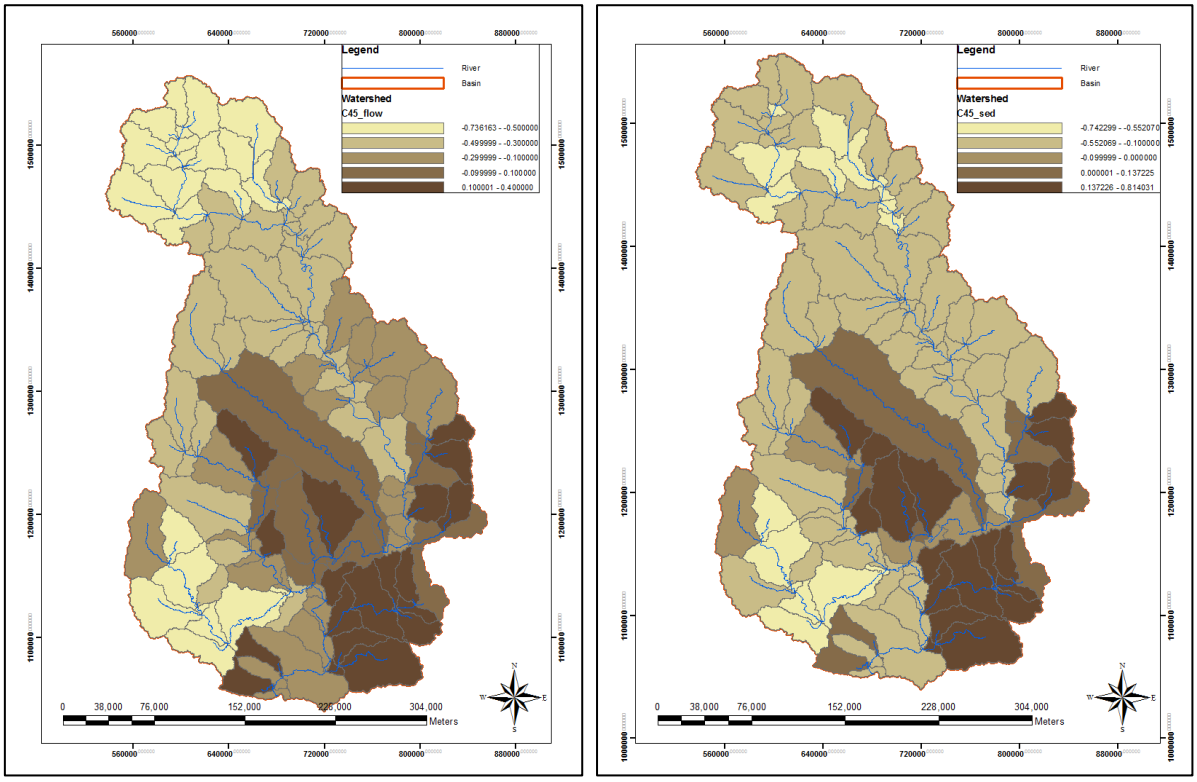

Figure A.0-13: Spatial distribution of future change in streamflows and sediment loads for a 1 in 30 year return period based on CCLM-MPI-ESM simulations forced by RCP4.5.

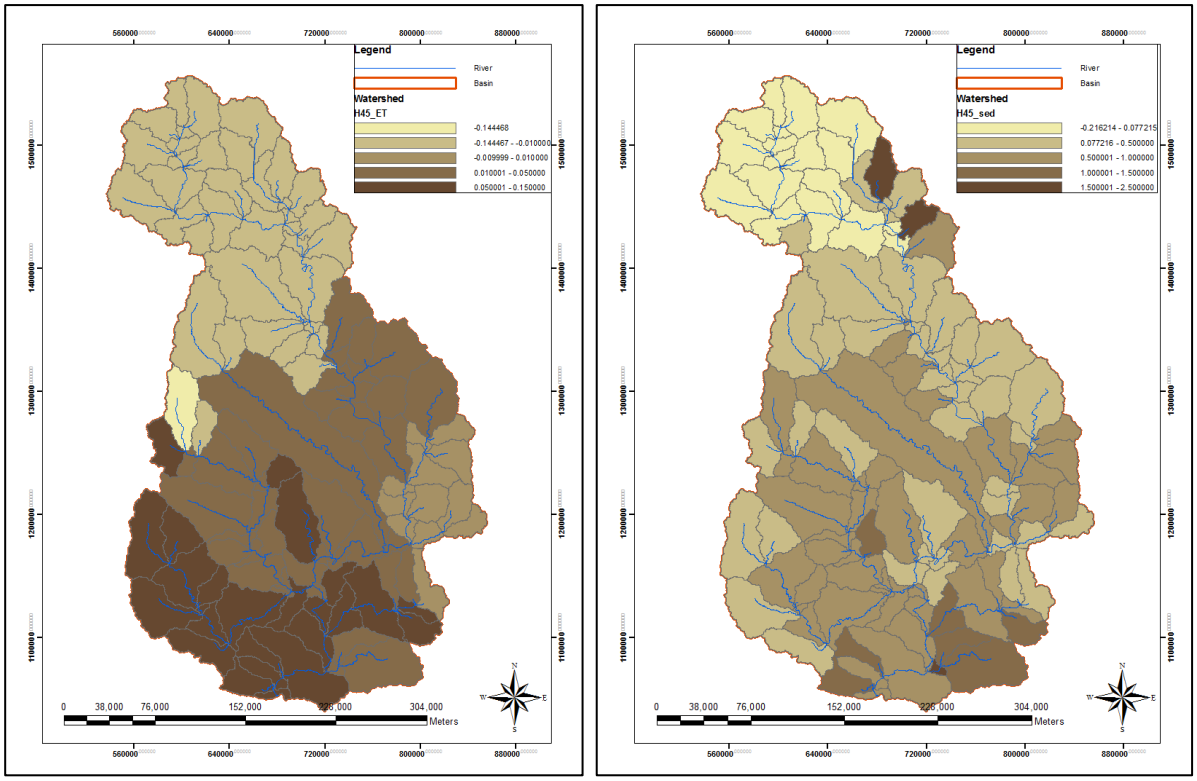

Figure A.0-14: Spatial distribution of future change in AET and sediment loads for a 1 in 30 year return period based on HIRHAM5_EARTH simulations forced by RCP4.5.

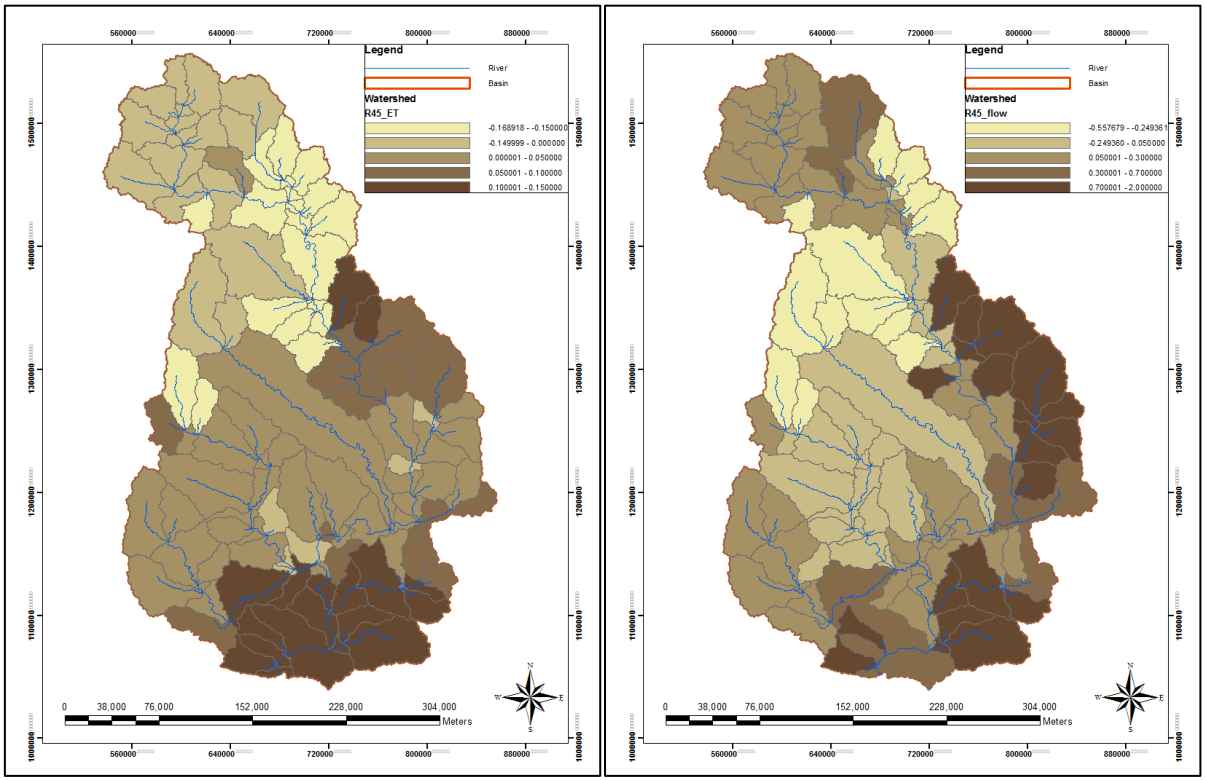

Figure A.0-15: Spatial distribution of future change in AET and streamflows for a 1 in 30 year return period based on HIRHAM5_EARTH simulations forced by RCP4.5.

Appendix B (List of Additional Tables)

Table B-0-1: List of selected meteorological stations used in downscaling.

No.	STATION	Latitude	Longitude
1	Babile	-2.820	10.520
2	Bui	-2.280	8.280
3	Fada	0.360	12.030
4	Manga	-0.270	11.020
5	Navrongo	-1.100	10.900
6	Ouaga	-1.510	12.350
7	Ouahigouya	-2.410	13.560
8	Pong	-0.830	9.670
9	Tamale	-0.880	9.420
10	Vea	-0.850	10.870
11	Zuarungu	-0.800	10.780

Table B-0-2: Computed statistics for minimum daily air temperature for the control period (1991-2010) and future (2031-2050) based on the RCP4.5 scenario for the White Volta Basin.

RCM-GCMs	TMin (°C) Control Period (1991-2010)				TMin (°C) Future (2031-2050)			
	Mean	Max	Min	Median	Mean	Max	Min	Median
HISTORICAL OBS	22.5	27.3	17.0	22.7				
CCLM_MPI-ESM	22.7	28.5	16.7	22.9	25.3	31.0	20.3	24.8
HIRHAM5-EARTH	22.8	28.2	17.4	23.0	25.7	31.1	20.6	25.1
RACMO22T-EARTH	22.8	28.4	16.9	22.9	25.8	31.2	21.3	25.1
RCM-GCMS ESM	22.7	27.7	17.3	22.9	25.6	30.9	21.4	24.9

Table B-0-3: Computed statistics for minimum daily air temperature for the control period (1991-2010) and future (2031-2050) based on the RCP8.5 scenario for the White Volta Basin.

RCM-GCMs	TMin (°C) Control Period (1991-2010)				TMin (°C) Future (2031-2050)			
	Mean	Max	Min	Median	Mean	Max	Min	Median
HISTORICAL OBS	22.5	27.3	17.0	22.7				
CCLM_MPI-ESM	22.6	28.4	17.0	22.8	25.6	31.5	18.6	25.2
HIRHAM5-EARTH	22.8	28.2	17.4	23.0	26.1	31.5	21.0	25.6
RACMO22T-EARTH	22.8	29.4	16.9	22.9	26.4	31.4	21.6	25.6
RCM-GCMS ESM	22.8	27.6	17.3	23.0	26.0	30.7	20.7	25.4

Table B-0-4: Mean annual water balance components simulated by SWAT based on inputs from all the RCM-GCMs simulations {Baseline (1990-2010) and (RCP4.5 and RCP8.5 (2031-2050)}

Water Balance Parameters	CCLM-MPI-ESM			HIRHAM5-EARTH			RACMO22T-EARTH			RCM-GCMs_ESM		
	Baseline	RCP4.5	RCP8.5	Baseline	RCP4.5	RCP8.5	Baseline	RCP4.5	RCP8.5	Baseline	RCP4.5	RCP8.5
Precipitation (mm)	884.6	825.7	791.9	855.9	936.3	976.4	880.6	936.2	952.8	865.8	899.4	907
Water Yield (mm)	150.6	133.1	139.3	112.6	176.2	199.0	117.1	163.5	172.6	99.61	130.7	140.9
Surface Runoff (mm)	105.5	101.0	98.0	85.0	126.9	131.6	87.7	113.9	123.1	31.18	41.3	42.5
AET (mm)	674.7	626.6	596.9	691.1	693.4	717.7	706.6	711.4	721.5	707.9	707.2	715.9
Sediment loads (10^6 t/yr)	9.71	11.22	10.82	8.71	13.22	13.32	9.11	9.61	10.52	2.50	3.4	3.3

Table B-0-5: Computed return levels for selected return periods based on extreme rainfall events (JAS) for the future period (2031-2060) for CCLM-MPI-ESM forced by RCP4.5

Return Period	Return Levels (mm)										
	Babile	Bui	Fada	Manga	Navrongo	Ouaga	Ouahi	Pong	Tamale	Vea	Zuarungu
2	22.8	22.9	38.9	34.8	37.9	28.3	27.8	38.2	38.4	40.2	40.5
5	42.1	45.0	55.4	55.1	60.0	48.0	43.5	62.2	62.2	59.3	61.2
10	57.4	60.1	65.0	70.3	74.9	64.4	52.4	77.1	76.4	69.6	72.8
20	74.3	75.2	73.4	86.9	89.4	83.8	59.8	90.6	89.1	77.8	82.5
30	85.3	84.2	77.9	98.0	97.9	97.4	63.8	98.2	96.1	82.1	87.7
50	99.8	95.3	82.9	113.0	108.0	116.0	68.2	107.0	104.0	86.7	93.3
100	122.0	111.0	89.3	136.0	123.0	147.0	73.6	119.0	114.0	92.2	100.0
200	147.0	127.0	95.1	162.0	137.0	186.0	78.5	130.0	124.0	96.8	107.0

Table B-0-6: Computed return levels for selected return periods based on extreme rainfall events (JAS) for the present period (1981-2010) for HIRHAM5-EARTH forced by RCP4.5

Return Period	Return Levels										
	Babile	Bui	Fada	Manga	Navrongo	Ouaga	Ouahi	Pong	Tamale	Vea	Zuarungu
2	31.7	38.2	45.8	46.5	46.4	36.6	35.2	50.5	51.4	42.4	48.9
5	54.5	64.5	61.8	70.8	70.4	53.2	51.1	70.4	73.1	59.4	70.5
10	70.6	80.4	71.2	87.3	86.2	63.9	61.7	80.7	85.2	69.0	83.4
20	87.0	94.6	79.4	103.0	101.0	73.8	72.3	88.8	95.3	77.1	94.7
30	97.0	103.0	83.9	113.0	110.0	79.6	79.0	93.0	101.0	81.5	101.0
50	109.0	112.0	89.1	125.0	121.0	86.4	87.3	97.3	106.0	86.4	108.0
100	127.0	124.0	95.8	141.0	136.0	95.5	99.5	102.0	114.0	92.4	117.0
200	146.0	135.0	102.0	157.0	150.0	104.0	113.0	107.0	120.0	97.7	126.0

Table B-0-7: Computed return levels for selected return periods based on extreme rainfall events (JAS) for the future period (2031-2060) for HIRHAM5-EARTH forced by RCP4.5

Return Period	Return Levels (mm)										
	Babile	Bui	Fada	Manga	Navrongo	Ouaga	Ouahi	Pong	Tamale	Vea	Zuarungu
2	36.3	48.0	50.6	52.2	50.4	38.0	35.9	57.7	61.9	46.0	50.3
5	63.2	77.5	66.8	79.0	75.9	57.8	56.5	79.1	83.3	59.3	70.3
10	82.1	94.2	75.0	96.9	94.0	70.2	73.6	90.2	99.1	67.7	81.9
20	101.0	108.0	81.4	114.0	112.0	81.7	94.0	99.0	116.0	75.7	92.1
30	113.0	116.0	84.6	125.0	124.0	88.2	108.0	104.0	128.0	80.6	97.7
50	127.0	124.0	87.9	137.0	138.0	95.7	128.0	108.0	142.0	86.5	104.0
100	148.0	135.0	91.8	155.0	158.0	106.0	161.0	114.0	166.0	95.0	112.0
200	170.0	144.0	95.0	172.0	179.0	115.0	203.0	119.0	192.0	104.0	119.0

Table B-0-8: Computed return levels for selected return periods based on extreme rainfall events (JAS) for the present period (1981-2010) for RACMO22T-EARTH forced by RCP4.5

Return Period	Return Levels (mm)										
	Babile	Bui	Fada	Manga	Navrongo	Ouaga	Ouahi	Pong	Tamale	Vea	Zuarungu
2	42.5	38.2	44.1	42.0	44.8	40.9	37.8	47.8	48.1	48.2	44.8
5	56.1	66.9	59.9	63.8	64.4	56.7	52.0	67.0	66.6	64.8	57.6
10	68.6	90.9	69.1	80.4	77.0	66.6	60.1	79.0	77.8	73.8	66.5
20	80.6	119.0	77.0	98.2	88.9	75.6	67.0	89.9	87.7	81.0	75.6
30	87.6	139.0	81.2	110.0	95.7	80.8	70.8	96.0	93.3	84.8	81.4
50	96.0	167.0	86.1	124.0	104.0	86.8	74.9	103.0	99.6	88.9	88.7
100	107.0	212.0	92.2	146.0	115.0	94.8	80.1	113.0	108.0	94.0	99.8
200	119.0	270.0	97.9	171.0	125.0	103.0	84.8	122.0	115.0	98.3	112.0

Table B-0-9: Computed return levels for selected return periods based on extreme rainfall events (JAS) for the future period (2031-2060) for RACMO22T-EARTH forced by RCP4.5

Return Period	Return Levels (mm)										
	Babile	Bui	Fada	Manga	Navrongo	Ouaga	Ouahi	Pong	Tamale	Vea	Zuarungu
2	47.9	43.3	52.2	54.5	49.7	37.2	41.8	61.0	57.5	51.8	53.6
5	69.0	70.4	68.3	83.3	67.8	53.1	55.2	74.7	79.2	63.9	67.2
10	81.8	87.9	77.7	103.0	78.1	61.8	64.1	80.4	95.0	71.0	76.4
20	93.1	104.0	86.4	122.0	86.7	68.8	72.9	84.3	112.0	77.6	85.9
30	99.4	114.0	91.5	133.0	91.3	72.5	78.4	86.0	123.0	81.4	91.9
50	107.0	125.0	97.4	146.0	96.3	76.5	85.3	87.6	137.0	85.9	99.4
100	116.0	141.0	106.0	164.0	103.0	81.3	95.3	89.3	159.0	92.0	111.0
200	125.0	156.0	114.0	182.0	108.0	85.5	106.0	90.5	184.0	98.1	123.0